Feasibility study, Dynamic modeling, Optimization, and Implementation of Low-cost communication systems for Remote DC microgrids in Nigeria

By

©Ndukwe Cherechi Izuchukwu, BSc, MSc

A thesis submitted to the School of Graduate Studies
In partial fulfillment of the requirements for the degree of
Doctor of Philosophy in Electrical Engineering.

Electrical and Computer Engineering Department
Faculty of Engineering and Applied Science
Memorial University of Newfoundland
St. John's, NL, Canada

October 20, 2022

DEDICATION

This work is dedicated to the Almighty God for making the whole study process possible, my dear wife Aruoriwoghene Ndukwe (my main support), who left no stones unturned to guide me even when I was getting discouraged. She will always say “BABE” it’s study time. And to my children, Bernice Udochinyere and Nathan Chukwuemeka, who were there with me and for me throughout my studies. I would also like to sincerely appreciate my parents, Prof Israel Chukwuemeka and Mrs. Clementina Ndukwe, and my parents-in-law, Mr. Felix and Mrs. Caroline Uduoborie, for their continuous support even during the hard times. Finally, to all my siblings and friends for their unalloyed support during this period.

ABSTRACT

Renewable energy-based microgrids are important contributors toward meeting the growing global energy needs in remote communities. In designing such microgrids, Supervisory Control and Data Acquisition (SCADA) systems and their communication methods are very crucial towards achieving reliable parameter control for optimal performance. A hierarchical microgrid is, in general, divided into three control levels: primary, secondary, and tertiary. Research over the years showed that control of the primary control level could be achieved without communication systems using control schemes such as droop control and other modified communication-less control schemes. On the other hand, the secondary and tertiary control levels are mostly achieved using communication systems for data transfer between the controllers. This, therefore, entails that a reliable and robust communication system that meets the requirements of each control level supported by a SCADA system is essential in achieving the optimum performance of a remote microgrid.

The first part of this thesis presents a techno-economic sizing of AC and DC microgrids for a remote rural community in West Africa. In the first research, an AC microgrid was sized in Homer to meet the energy requirements of the community. Being that the community was a peasant community, it had low amount of electrical equipment and as such had lower energy needs. Further, due to the low energy requirement, a DC microgrid was sized for the same community after analysing the community. The sized DC microgrid also met the energy needs at a low financial cost. The result of the sizing showed that when the traditional AC equipment was switched to DC, the community energy needs were reduced and well met with a DC microgrid. Finally in this part of the research the sized DC microgrid was simulated in MATLAB and the control schemes were employed to observed the dynamic performance of the DC microgrid.

The second part proposes a LoRa-based wireless communication system for data transfer in DC microgrids at the secondary control level. The proposed method allows the connection of multiple sensors to the LoRa transceivers and enables the data collection from various units within a microgrid. Chapter 4 and Chapter 6 focused on communications at the secondary communication level of the microgrid between local controllers

of each distributed generation (DG) unit and the microgrid central controller due to the possibility of using low-bandwidth communication systems. The data transfer process and management scheme for priority data transfer in a microgrid are analyzed. Furthermore, the data transmisson time, and control action transmission between the central microgrid and the local microgrids are assessed.

The third part presents an open-source, low-cost Internet of Things (IoT) based SCADA system that uses the Chirpstack IoT platform to achieve SCADA functions. The proposed system is an improvement to the existing IoT solutions by eliminating cloud-based IoT platforms and introducing an all in one system where the IoT gateway and platform are installed on one machine. This solution increases systems reliability by reducing the number of components and at the same time, reducing the costs involved. This solution eliminates the requirement for the internet for data transfer. The proposed system prototype consists of voltage and current sensors, Arduino Uno microcontroller, and Raspberry Pi. The sensors acquire data from the monitored unit. The Arduino Uno receives and processes the data for transmission to the Raspberry Pi using LoRa communication. At the Raspberry Pi, the local Chirpstack platform processes and displays the measured data using the Grafana dashboard for real-time data monitoring. The information is stored in an InfluxDB database. For system validation purposes, the prototype is designed, developed, and set up to monitor a set of solar photovoltaic (PV) panel voltages, currents, and battery voltages. The results obtained from the test setup are compared with the physical point measurements. The proposed system is featured as a low-cost, open-source, scalable, and interoperable system. This, therefore, makes the proposed SCADA system an alternative for commercial SCADA systems, especially for remote renewable energy-based microgrid applications. The system proposed in this research can be deployed for large industrial systems with appropriate upgrades and customization.

The main contributions of this work are:

- Design of a renewable energy-based microgrid for a remote location in Nigeria.
- Design of an all-DC remote microgrid for a remote community in Nigeria..
- Design of a low-power wireless communication system for microgrids.
- Design of LoRa-based communication and SCADA system for remote microgrids.
- Analysis of LoRa transmission delay effect on the dynamic performance of a DC microgrid.

ACKNOWLEDGEMENTS

I want to express my gratitude to my supervisors: Prof Tariq Iqbal, Dr. Mohsin Jamil, and Dr. Jahangir Khan, for their mentorship in all facets of this study: academic, career, and my personal development. I am also thankful for their unalloyed support alongside research and time management mentorship. I would also like to extend my gratitude to Dr. X. Liang, who started with me in this research but left due to other work engagements. I sincerely appreciate your contributions to my studies. I want to also thank my senior colleagues and mentors from the Federal University of Technology Owerri: Dr. Peter Eze, Dr. Uchenna Diala, Dr. Oliver Ozioko, and Mrs. Uchechi Iwuchukwu for all your mentorship during my studies and your contributions towards making resources available for me to carry out my research. I would also like to thank my friends: Lawrence Aghenta, Mr. Charles Chilaka and family, Justin Irechukwu, Jeffery Odianosen, Amagh Nduka (jnr), and many others too numerous to mention.

Table of Contents

List of Figures

List of Tables

List of Acronyms

AC	Alternating Current
ADPMS	Adaptive Dynamic Power Management Strategy
ASCII	American Standard Code for Information Interchange
AWGN	Additive white Gaussian noise
BW	Bandwidth
COE	Cost of Energy
CPLs	Constant Power Load
CSI	Current Source Inverter
CSS	Forward Error Correction
DBMS	Database Management System
DBS	DC Bus Signalling
DC	Direct Current
DERs	Distributed Energy Resources
DG	Distributed Generation
ESSs	Energy Storage Systems
FEC	Forward Error Correction
FIDs	Field Instrumentation Devices
GSM	Global System for Mobile communication
GPIO	General-Purpose Input/Output
HDG	High Droop Gain
IDE	Integrated Development Environment
IEDs	Intelligent End Devices
IoT	Internet of Things
IP	Internet Protocol
ISM	Industrial, Scientific, and Medical
ISOP	Input-Series-Output-Parallel
LAN	Local Area Network
LED	Light Emitting Diode

LoRa	Long Range
LoRaWAN	Long Range Wide Area Network
LPWAN	Low Power Wide Area Network
LTE	Long Term Evolution
MAC	Media Access Control
MGCC	Microgrid Central Controller
MPPT	Maximum Power Point Tracking
MQTT	MQ Telemetry Transport
MTUs	Master Terminal Unit
MUN	Memorial University of Newfoundland
NASA	National Aeronautics and Space Administration
NPC	Net Present Cost
OEM	Original Equipment Manufacturer
OSI	Open Systems Interconnection
PDR	Packet Delivery Ratio
PDC	Polynomial Droop Curve
PDCVC	Polynomial Droop Curve with Voltage Compensation
PI	Proportional Integrator
PLCs	Programmable Logic Controllers
PMUs	Phasor Measurement Units
PV	Photovoltaic
RFID	Radio Frequency Identification
RMS	Root Mean Square
RTUs	Remote Terminal Units
SCADA	Supervisory Control and Data Acquisition
SF	Spreading Factor
SoC	State of Charge
TCP	Transmission Control Protocol
VSC	Voltage Source Converter
WANs	Wide Area Networks

Chapter 1

Introduction and Literature Review

1.1 Introduction

Most rural areas in developing countries have no electrical supply from the main power grid. This is mainly attributed to the lack of access to these areas, because of the high cost of transmission and distribution infrastructure. Worldwide, an estimated 1.5 billion people lack access to electricity [1]. These communities have therefore resorted to the use of local methods to meet their lighting, heating, and cooking needs. Often this has a detrimental effect on the socio-economic sectors, environment, and quality of life. Surprisingly, many of these areas have abundant renewable energy resources such as wind, solar and hydro that can be harnessed as a cost-effective and clean energy solution. To this end, renewable energy-based microgrids can play a critical role.

Depending on the power being fed, microgrids can be of two types: AC or DC microgrids. At present, rural communities in developing countries have a very low need for AC loads. AC loads can also easily be replaced by DC appliances such as LED bulbs, televisions, and radios. Furthermore, more and more consumer electronics are being used by the end-users, increasing the share of DC loads. This has, therefore, made deploying a DC microgrid a more suitable option than the AC power system, especially for remote rural communities. The driving factors are easy integration with renewable energy sources and storage [1,2], the recent proliferation of DC loads [3,4], loss reduction due to a lower number of conversion stages [5], low cost of distribution network, and low system complexity [6].

Renewable energy-based microgrids with distributed energy resources (DERs), such as wind and solar generation, can operate in either grid-connected or islanded mode [7] [8]. In the grid-connected mode, the grid defines the microgrid's voltage and frequency; hence the DERs are controlled to produce the desired power [8]. In the island mode, the DERs are required to supply the microgrid's load demand and to regulate

the line voltage and supply frequency within acceptable limits [9], [10]. In this context, isolated microgrids in remote communities permanently operate in islanded mode.

To achieve proper control and operation of a microgrid, each DG unit should be updated with information pertaining to the microgrid's operating mode [11]. This entails real-time power measurement of the grid, loads, and DGs, as well as the state of charge (SoC) of battery storage systems [12]. The RMS value, phase angle, frequency of the voltage, and active and reactive power at specific points in the microgrid can also serve as monitoring signals for the microgrid control systems [13]. Furthermore, instantaneous values of voltages at the DG terminals and the feeder are needed for synchronizing the DG units within the microgrid [14]. It is expected that in the near future, automated operation of microgrids can be achieved [15][16] by monitoring the system through various sensors, and by analyzing the collected sensor data, and integrating the results into advanced control schemes that pass the control commands back to the nodes [17]. To achieve automation, a fast and reliable communication system for data and command transfer at every control level within the microgrid is a fundamental requirement [18].

1.2 Background

Further background on three key aspects of this research is presented in the following sections: DC microgrid, data transfer, and LoRa communication technology.

1.2.1 DC Microgrid

DC microgrid is an attractive modern technology solution as it offers easy integration with renewable energy sources and reduces the number of energy losses. The DC microgrid system is made up of mostly renewable energy sources that deliver the energy to the components of the microgrid in direct current form. Various components of a DC microgrid are connected directly to the sources through the system bus with no need for intermediate conversion. Figure 1.1 shows a block diagram architecture of a DC microgrid.

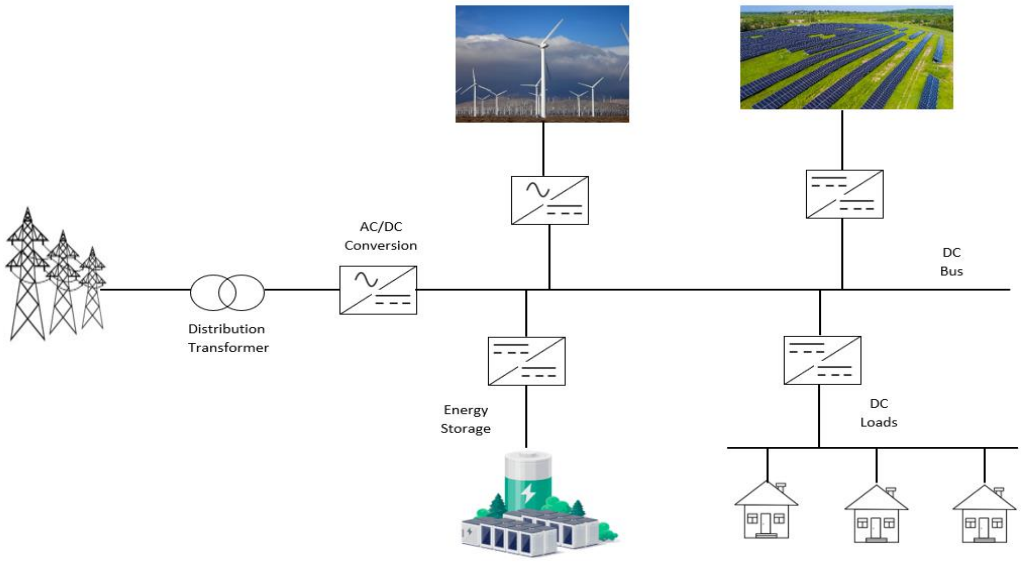

Figure 1. 1. Schematic diagram of a grid-connected DC microgrid

1.2.1.1 Justification for DC microgrids

The main advantages of a DC microgrid are outlined and discussed as follows:

- **Seamless integration with renewable energy sources and storage**

Most renewable energy sources such as the PV, small wind turbines, micro-hydro, and biomass systems produce power in the direct current form. This, therefore, eliminates the need to incorporate converters for power conditioning. Energy storage systems are employed to supply energy to the loads in times of low power generation and are also used to stabilize the system against fluctuations that may occur as a result of variations in the renewable energy sources [1]. Most storage systems such as batteries, fuel cells, and super-capacitors are all DC systems by design, which deliver DC power. Although the flywheels are mechanical energy storage systems, they are mostly coupled to a permanent magnet synchronous machine that can be integrated into the system through a DC link [2].

- **DC load**

Most consumer electronic products and appliances such as televisions, laptops, phones, microwave ovens, and lighting fixtures run using DC power [3]. Most recently, residential lighting systems use LED bulbs, which are also powered using direct current [4]. In current literature, many heating, ventilation, and air

conditioning systems, fans, variable speed motors for pumps, and industrial systems such as the DC electric arc furnace and the electrochemical industries also use DC power or a DC intermediate stage during power conversion [5-6].

- **Loss Reduction**

According to work in [19], the relationship between AC and DC cable resistance is as given by.

$$R_{ac} = \frac{\pi.r^2}{\pi.r^2 - \pi(r-\delta)^2}.R_{dc} \qquad (1.1)$$

Where R_{ac} and R_{dc} are the resistance of AC and DC cables, respectively, r is the Conductor radius, and δ is the Conductor Skin Depth. From (1), it can be observed that the cable AC resistance will always be higher than its corresponding DC resistance. So, the losses in the AC system would be more, and the current-carrying capacity would be less compared to its corresponding DC system. This entails that the employment of the DC system will reduce the amount of losses in the system.

- **Low Cost of Energy Distribution**

Firstly, the reduction in the conversion stages in electricity distribution in a DC system already accounts for the lower number of components which results in low overall cost. Various losses (skin effect, eddy losses, hysteresis) unique to AC systems are not present in DC systems [6]. Consequently, the losses and costs are reduced as smaller conductors can be used in DC systems when compared to AC systems

- **Low System Complexity**

At the microgrid level, it can also be envisioned that the design and operational complexity of a DC system will be reduced. This is particularly important as, unlike AC systems, there is no need for reactive power control, frequency regulation, and phase synchronization [6].

1.2.1.2 DC Microgrid Control Schemes

To achieve efficient operation and guaranteed stability of the DC microgrid, effective control strategies need to be implemented. Various converters interfaced in the DC microgrid play various key roles in the proper operation of the DC microgrid. They perform such functions as a proper local operation, and they also enable coordinated interconnection between different units of a DC microgrid. With increasing energy,distributed generation, and nonlinear loads, the DC microgrid control structure is a very important factor for consideration. The main control objectives of the DC microgrid system include [20-25].

- Efficient voltage and current control in all operating modes.
- Coordination among different Distributed Energy Resources (DERs) and Energy Storage Devices.
- Smooth transition between various operation modes of the DC microgrid.
- Power flow control within the DC microgrid.
- Maximum utilization of the potential of DERs.

DC microgrid control schemes can be classified into two main categories: Basic control and multilevel control strategies.[26]. The basic control is normally achieved through either centralized, decentralized, or distributed control, while the multilevel control scheme is achieved through different levels of control in the hierarchy. In the hierarchical scheme, each of the control levels then employs either of the basic control schemes [26]. A diagrammatic representation of the various control schemes is shown in Figure 1.2.

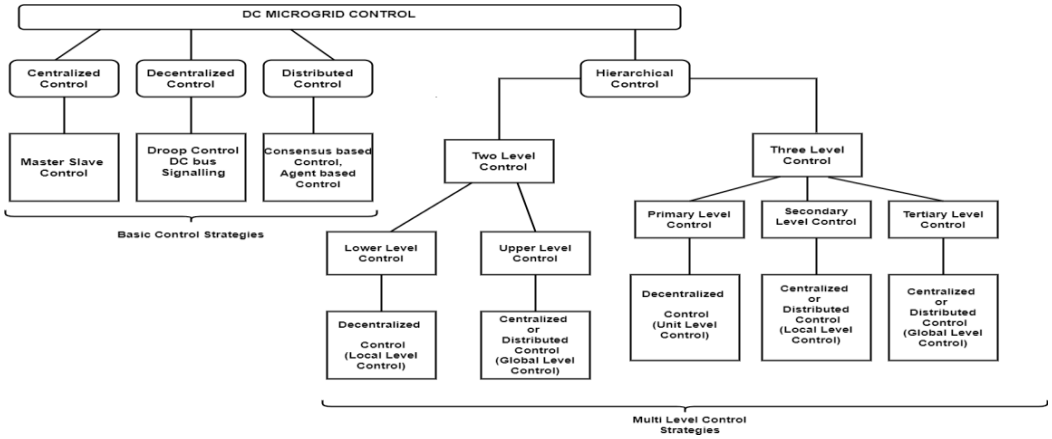

Figure 1. 2. A diagrammatic representation of the various control schemes .

1.2.1.2.1 Basic Control Strategies

Centralized control. This scheme features a control scenario where the distributed units are controlled by a central controller [26]. This entails that data is collected from the distributed units by local controllers and transmitted to the central controller for processing, and commands are transmitted back using digital communication links. The centralized control scheme has a very high dependence on communication systems. The communication strategy presents advantages which include a high level of system observability and controllability, with its main disadvantage being a single point of failure and scalability. This, therefore, makes the control strategy suitable for small-sized DC microgrids [27-30]. The schematic configuration of the centralized control scheme is presented in Figure 1.3

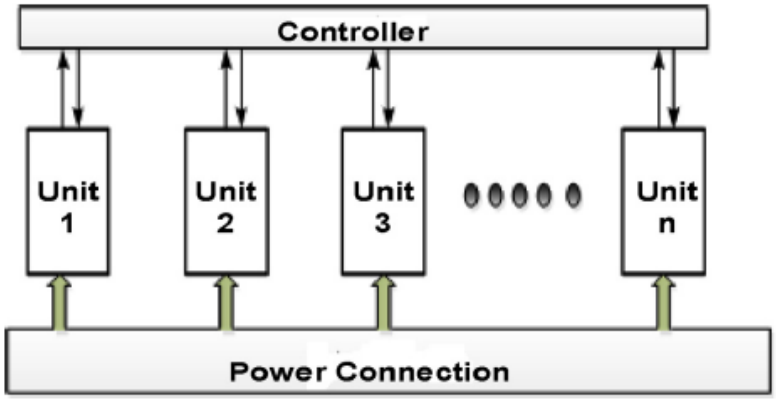

Figure 1. 3. Schematic Configuration of the Centralized control Scheme.

A typical example of the centralized control scheme is the Master-slave control strategy, as shown in Figure 1.4 [31].

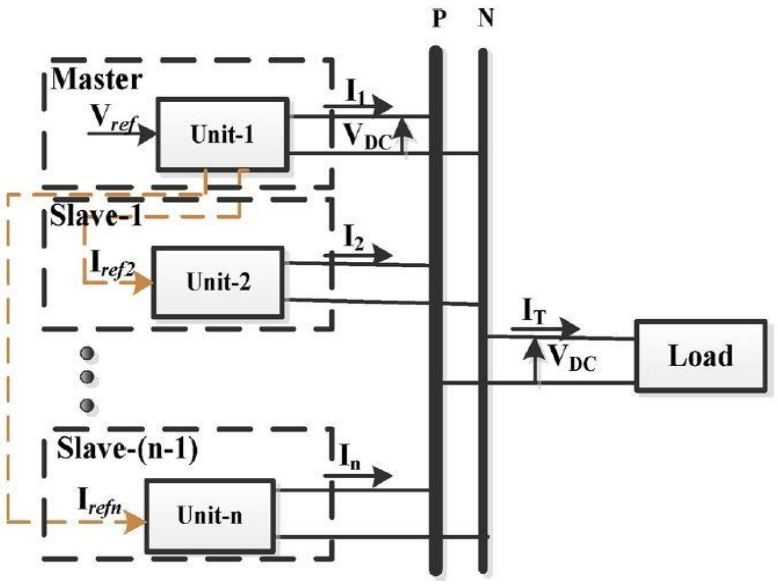

Figure 1. 4. Master-slave control

This control strategy presents a scheme where one converter operates as the master and functions as a Voltage Source Converter (VSC) and is responsible for the DC bus voltage regulation with others working as the Current Source Inverter (CSI) following the pattern of the master converter. This control strategy is mainly achieved by the employment of High Bandwidth communication [32]. Being a type of centralized control, the main disadvantage of this strategy is the single point of failure, which adversely affects the operation of the system.

Decentralized control. This control strategy does not require communication links because the distributed units are controlled by independent controllers using their local variables. The basic configuration of the decentralized control scheme is presented in Figure 1.5. This control scheme has some performance limitations due to insufficient unit information, but it is considered the most reliable control strategy due to its communication independence between the various units. A well-known decentralized control scheme is the droop control strategy shown in Figure 1.6 [31].

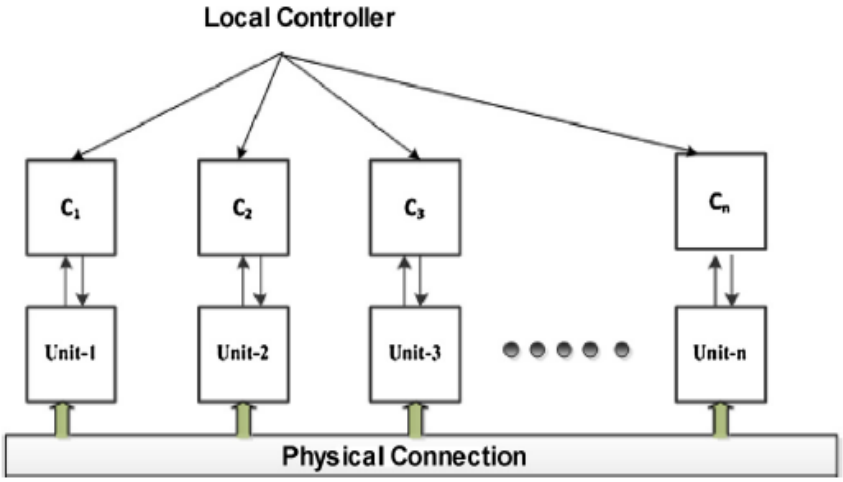

Figure 1. 5. Schematic diagram of the decentralized control scheme

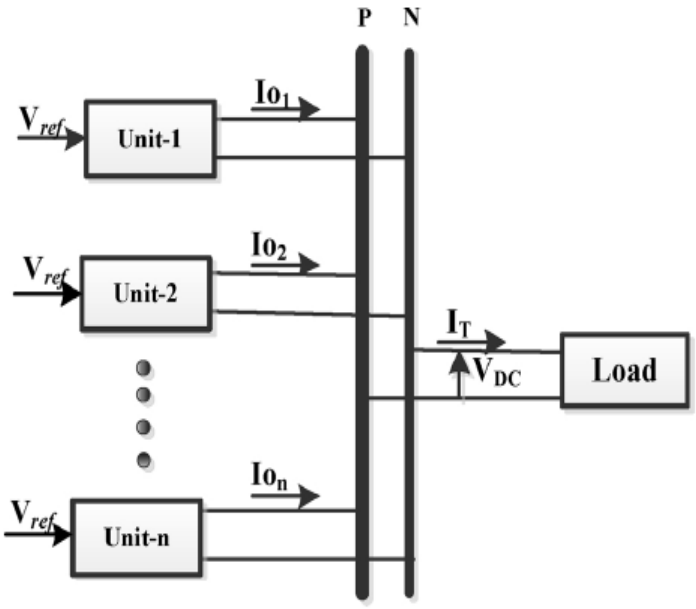

Figure 1. 6. Voltage droop control.

In this strategy, the converters are connected in parallel with the DC microgrid. The droop technique is usually employed to avoid circulating currents between the various converters without the employment of communication links. Mainly, the output power or the output current is fed back as droop feedback for the purpose of system control. In this strategy, the output power is mainly used as a feedback control signal in Constant Power Loads (CPLs), while the output current feedback signal is used in other load scenarios.

Diagrammatic representation of the droop principle for power droops and current droops are shown in Figure 1.7, and their characteristics are represented by equations (1.2) and (1.3).

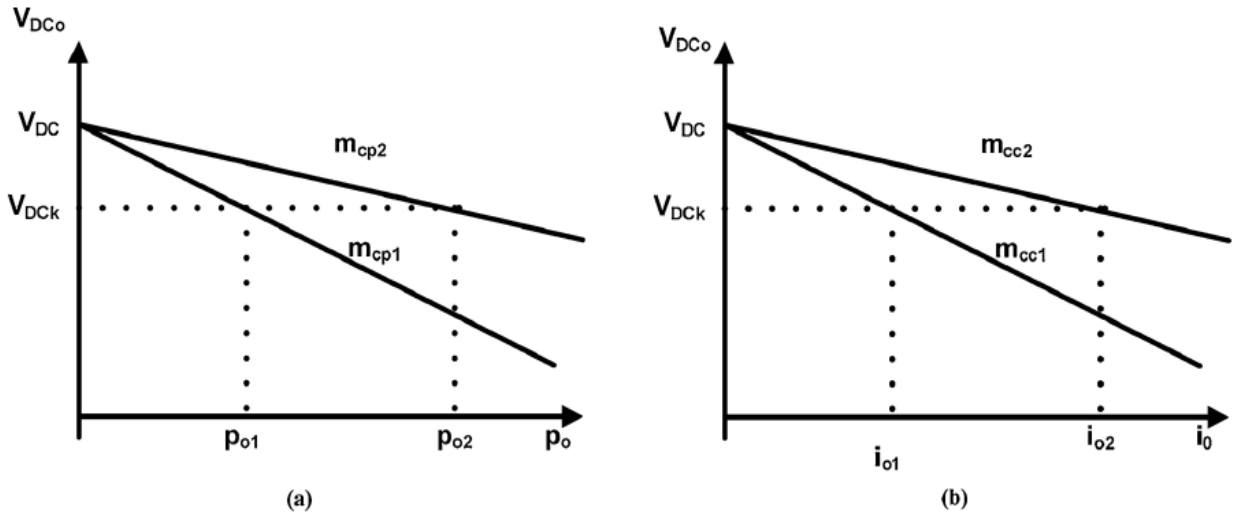

Figure 1. 7. Droop Curves (a) Power Droops (b) Current Droops

$$V_{DCK} = V_{DC} - m_{cp}p_{ok} \tag{1.2}$$

$$V_{DCK} = V_{DC} - m_{cc}i_{ok} \tag{1.3}$$

Where, V_{DCK} is the reference value of output voltage of the kth converter, V_{DC} is the DC bus voltage, m_{cp} and m_{cc} are defined as the power and current droop coefficients of the converter, respectively. i_{ok} and p_{ok} are the output current and power of the kth converter. From the equations, it is observed that the current sharing and system stability are well affected by the droop coefficients, and as such, a higher droop current coefficient increases the system damping and therefore increases current sharing and accuracy [33]. On the other hand, this causes voltage deviation. This, therefore, entails that employing this technique requires a tradeoff between system accuracy, current sharing, and voltage deviation. Considering the absence of a communication system in this control technique, the system is assumed to be very reliable and flexible. However, it suffers drawbacks such as load dependence, i.e., the voltage of the common bus, changes with the load (mainly in islanded mode) [34], poor transient performance, and voltage deviations.

Distributed control. This control technique employs some advantages of centralized and decentralized control. In this control scheme, there are limited communication links, and the controllers employ these links to transfer data between neighboring controllers to achieve control objectives such as voltage restoration, current sharing, and proportional load power-sharing. [35]. In cases where implementation of centralized control seems difficult, distributed control is normally employed. The diagrammatic representation of the distributed control is shown in Figure 1.8.

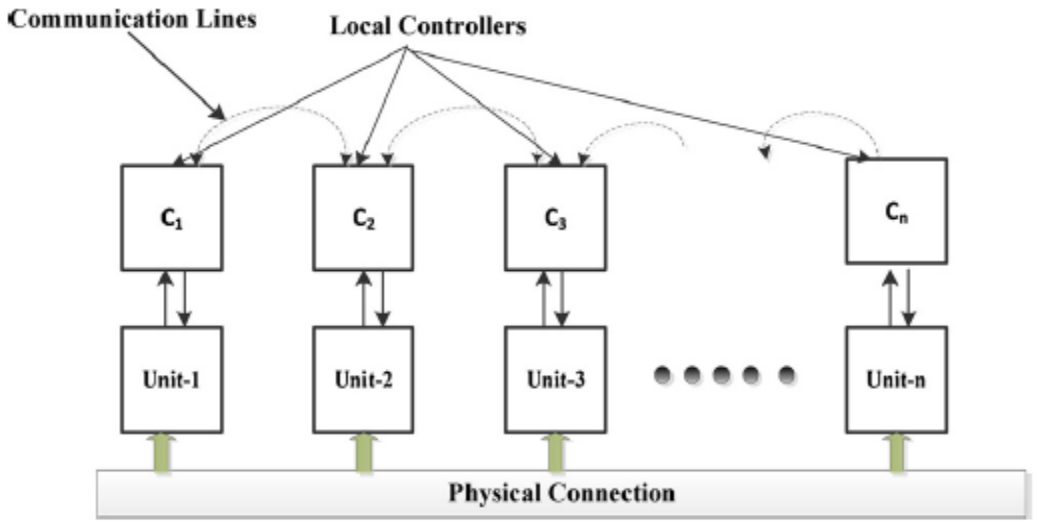

Figure 1. 8. Diagrammatic representation of distributed control scheme

The main advantage of this scheme is its immunity to the single point of failure, as the system can function fully even with the failure of some of the communication links. Complexity, power tracking error, and voltage deviation are the main drawbacks of this control scheme [36]. The main examples of distributed control are agent-based and consensus-based control strategies.

In consensus strategy, the algorithm is an interaction protocol that specifies the information exchange between neighboring units. This approach is normally employed for the solution of distributed optimization problems by offering a flexible control [37]. This algorithm is normally used to achieve agreement between units. [38] and [39] presented works that proposed a consensus algorithm for DC microgrids.

The agent-based control strategy is another well-known distributed control applied in DC microgrids. In this strategy, every unit is considered an agent. There are many agents in the DC microgrid, which gives it the name multi-agent system control. [40] proposed two schemes based on the agent-based distributed control for distributed energy storage systems for power exchange decisions by distributed energy storage systems under the cyber-attack scenario. [41] presented a survey on the application of agent-based control technology for industrial processes. The main focus of the survey was on the automation of continuous industrial processes.

1.2.1.2.2 Hierarchical (multi-level) control

Various power system control objectives such as voltage control, current control, and power control alongside advanced objectives such as power-sharing between DGs, power quality control, participation in energy markets and minimizing operating cost, can only be achieved by the application of higher intelligent control systems. It will be very difficult to achieve these objectives through single-level controls such as the centralized and distributed schemes discussed in the preceding sections [42]. Modern power systems such as the DC microgrid require these multilevel control strategies to be able to carry out various control functions according to their levels of complexity and latency requirements.

In recent times, developments in communication technologies have made the employment of multi-level control strategy more preferred in DC microgrids. This level of control has enhanced the degree of independence between the various control levels towards achieving systems stability. This improves the overall system reliability because even in the event of failures in the upper control levels, the lower levels continue the system operation until the problem is rectified [27,43,44].

In order to develop a system that is suitable for all types of DC microgrid, for optimum performance in all operating modes, a combination of the above-mentioned control strategies into the hierarchical control framework will be important [45,46-49]. In the hierarchical control framework, the microgrid control functions are divided by different levels in the hierarchy. In general, there are three hierarchical control levels

with their respective functions. These various control levels with their functions and time frame are shown in Figure 1.9. The control levels are discussed in the following subsections.

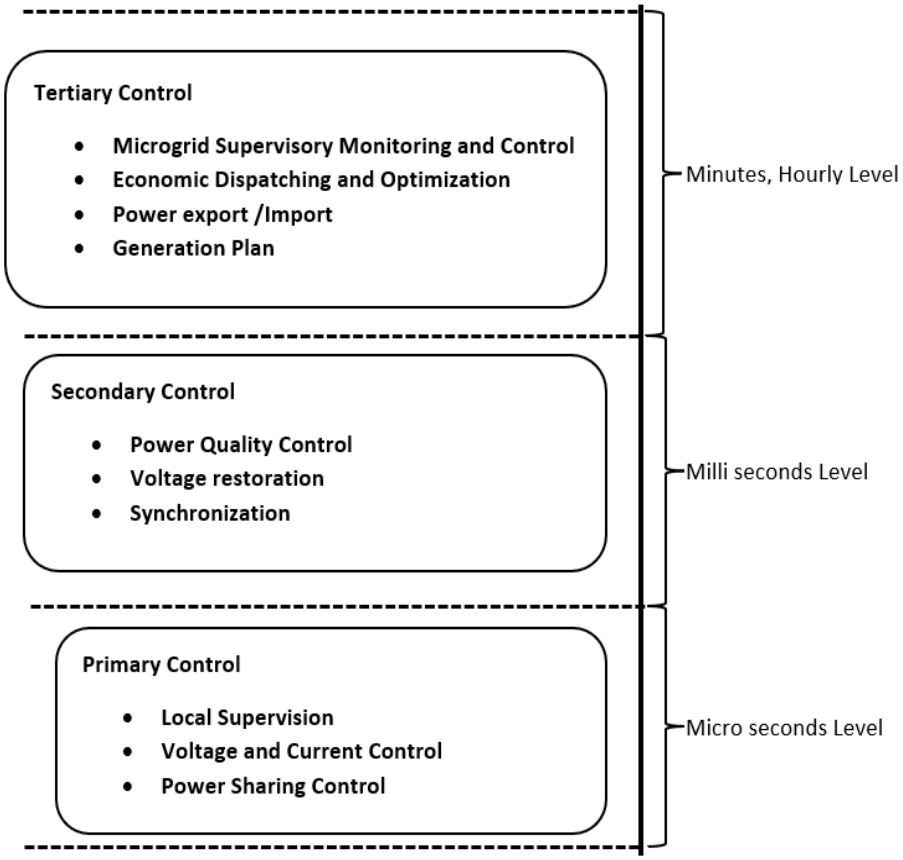

Figure 1. 9. Hierarchical Control: Functions and timeframe

Primary (local) control level: The primary control level is the first layer of control in a hierarchical control structure. This level is responsible for the current and voltage control of the microgrid. Furthermore, the primary control level damps the oscillations created by the constant power loads (CPLs) in the DC microgrid. Sometimes, proper power management is achieved in the microgrid by employing decentralized load-sharing schemes. The popular primary control level methods are the Droop Control, Fuzzy Logic Control, and DC Bus Signalling (DBS) control method.

The droop control method offers one of the manageable non-feedback paralleling schemes that require no communication system for data transfer. This makes the droop control most widely employed because it offers

a good level of voltage and current regulation [50, 51]. The basic droop control method employs a linear approach toward the reduction of the DC voltage concerning the increase in output current [52]. Equation (1.4) expresses the conventional droop control method.

$$V_{dck} = V_{dc}^{*} - I_{dck} * R_{dk} \tag{1.4}$$

Where V_{dck} is the output voltage of *kth* converter, V_{dc}^{*} is the reference DC output voltage, I_{dck} is the output current, R_{dk} is the virtual resistance (VR) and k = 1,2, 3…. [53]. This relationship normally results in voltage deviation and asymmetric line drop. This is, therefore, one of the main flaws of the conventional droop control technique.

Research has shown that line impedance has a very critical effect on the performance of the conventional droop control technique. The droop system can be applied in linear and also in a non-linear approaches. Considering the adverse effect of line impedance over the linear droop control technique, a modification to the non-linear droop control approach has been employed. The non-linear droop control technique reduces the trade-off between voltage regulation and current sharing. Furthermore, various researchers have developed various modifications to the conventional droop control technique to mitigate the various drawbacks posed by the conventional droop control technique.

In [54], an inverse-droop control is presented for the achievement of power-sharing, including voltage sharing and output current for input-series-output-parallel (ISOP) DC-DC converters. By employing the inverse-droop control, the output voltage reference is increased with increased load. [55] presented a non-linear droop control in which the droop control gain is a function of the DC/DC converter output current. This proposed method can increase the droop resistance when the load is increased, thus solving the trade-off in the conventional droop method. [56] proposed three novel non-linear droop control algorithms; high droop gain (HDG) methods, Polynomial droop curve (PDC), and polynomial droop curve with voltage compensation (PDCVC). From the three proposed droop control techniques in the work, the HDG offers the best voltage regulation but performs badly in power-sharing at light load conditions. On the other hand, the PDCVC

provides the best performance in heavy load conditions. The PDC technique offers good load sharing and fair voltage regulation under all load conditions. [57,47] investigated a droop-controlled DC microgrid with the integration of energy storage systems. This work proposed a dead-band droop characteristic for the battery energy storage system to introduce a standby working mode. This avoids the unnecessary repetition of charging and discharging. The work in [58] presents a novel droop technique that controls the nominal voltage to achieve good load sharing. The drawback of this technique is that it only considers load sharing among sources with the same rating and, as such, does not take sources with different capacities into consideration. [59] proposes a State of Charged (SoC) based adaptive droop control to achieve dynamic SoC balancing and appropriate power-sharing. [60] presents a decentralized power-sharing approach that takes the line impedance into account in low voltage DC microgrids consisting of PV, and battery. The work discussed the droop gains while considering both the grid-connected and islanded modes.

Secondary control level: The secondary control level plays a very important role in DC microgrid by functioning as an intermediary between the primary and tertiary control levels. As mentioned in the preceding subsection, the main drawbacks of the primary control level are voltage deviation and poor current sharing among the converters due to the line impedance. The secondary control level has the responsibility of overcoming the aforementioned problem by providing a voltage set point for the primary level controllers and proportional load sharing. This control level employs the functions of the voltage and current regulators. Furthermore, the secondary control level is responsible for power flow management within the microgrid and in a microgrid cluster environment [61]. The secondary control level can be employed as a centralized, decentralized, or distributed configuration. The main function of the secondary control level is to provide a voltage and current reference point for the local controllers. This function further enhances the performance of the primary controllers during voltage and current sharing; thus, improving the overall power quality of the microgrid by the enhancement of the power-sharing capacity of the microgrid.

In a centralized configuration, the microgrid central controller is connected to the various Distributed Energy Resources (DERs) local controllers through communication links. The central controller generally measures the common bus voltage at which all loads are assembled and creates a set point as the DC bus voltage. This set point is then sent to the voltage controller. As earlier mentioned as the advantages of the centralized control configuration, it features high precision control and high flexibility but has a high drawback due to its high dependence on communication [62, 63, 64].

In decentralized secondary control, there is very little to no requirement for a communication system. This is because this configuration performs local regulation based on available local variables from the various individual modules by employing various strategies such as the droop-based feedforward control for terminal voltage reference and proportional controller for cable impedance balancing. The decentralized configuration offers simplified implementation, which also enhances reliability. However, due to the unavailability of global data of the system at the decentralized control units, the error correction term provided by this configuration does not match exactly with the required compensation term, and as a result, there is a deterioration of the system optimization. [62, 63].

The distributed secondary control configuration normally requires a distributed communication network and distributive control approach for execution on locally available variables. This configuration features the ability to be fully functional even with the failure of some communication links, provided the communication link is connected. This increases the immunity of this configuration to a single point of failure [65]. In contrast to the centralized secondary control, the information directly exchanged between local controllers contains only locally available variables. This, therefore, entails that if two units are not directly connected by the communication link, data and information sharing will not be very possible, resulting in the limitation of the system observation. In order to mitigate this drawback, the distributed secondary control configuration can be categorized into three: average current or voltage sharing scheme [34,35,66], dc bus signaling scheme [67,36], and cooperative control scheme [68-70].

Considering DC microgrid secondary control level, various investigations have displayed high interest in the analysis and possible employment of low-bandwidth communication systems for data transfer in communication-based hierarchical DC microgrid control. The authors in [34] employed the use of low bandwidth communication systems to achieve good voltage regulation and accurate load sharing using droop control. The work employed the low bandwidth communication system mainly for system monitoring and set point validations. This reduction in the parameters measured allowed for adequate bandwidth for data transfer and control. The works presented in [35,65] achieved a decentralized control scheme using the low-bandwidth communication system for transfers of data and set point control between the constituent controllers in a DC microgrid. Similar to the work in [34], the authors also employed low-bandwidth communication alongside an improved droop control technique to achieve improved current sharing and system voltage restoration simultaneously. In [71], a distributed secondary power-sharing approach with a low bandwidth communication network was proposed for low voltage DC microgrids. In this work, the proposed control system carried out the current value of the other converters to achieve accurate current sharing and suitable voltage regulation as well. The secondary controller is realized locally while employing the low-bandwidth communication network for transferring dc currents values. This, therefore, made it possible for the employment of low-bandwidth communication. The secondary controller, therefore, regulated the average voltage by only using the current data transfers.

Chapters 4 and 6 of this thesis focus on the proposal of a low bandwidth communication system for data and control transfer for a centralized secondary control layer of the DC microgrid.

Tertiary control level: The tertiary control level is considered as the third and last layer of control in a hierarchical control structure. The tertiary control level manages the power flow among the microgrid and the utility grid or other neighboring microgrids. The main role of the tertiary controller is the overall management of power and energy with determining objectives such as energy storage devices coordination, minimization of operation costs, and reduction of power flow losses [18, 72,73]. The tertiary control can be implemented

in a hierarchical control structure as centralized or distributed fashion. In contrast to the primary and secondary control levels, the tertiary control scheme can extend its operational area beyond the microgrid. This, therefore, makes the tertiary control level a mandatory tool for achieving proper power and energy management in a microgrid system. Notwithstanding the difference in size between a microgrid and the utility grid or other microgrids, the need for power flow control and energy management is essential for the improvement of overall system efficiency. The tertiary control level employs simple calculation techniques and algorithms. This makes this control level slower and with reduced effectiveness because it deals with complex calculations and covers the whole microgrid system. [74,75]. Before any control scheme is employed, the reliability, economic feasibility, and optimal state of the system should be considered. From the above-mentioned parameters to be considered, the tertiary control level is employed to meet the economic and the system optimal state functions.

The main optimization schemes employed at the tertiary control level, among others, are the Genetic algorithm, and the consensus algorithm.

The genetic algorithm concept emerged from the Darwinian theory. [76-78]. This algorithm generates good results than the random search option and provides a better optimal solution, given any additional knowledge of the problem [78]. This algorithm has the capability of searching and obtaining an appropriate solution for highly complex computational issues. The genetic algorithm is a process that was developed from biological processes, employs some biological terms such as chromosome, population, and fitness function, and also adheres to some basic biological processes towards the achievement of the optimal solution. The basic steps to be taken in this algorithm are as follows.

i) Generate a random population of chromosomes.

(ii) Calculation of chromosome fitness in the population.

(iii) As long as the new population is not available, the steps given below should be repeated.

(a) According to fitness level, parents are selected from the population. Better fitness creates a higher chance of becoming a parent.

(b) Crossover action is performed to create new offspring.

(c) The mutation is performed.

(iv) Further steps are executed on the new population instead of the first population.

(v) Repeat step (ii) [75, 77, 79].

The genetic algorithm is normally implemented by the execution of three primary genetic operators: reproduction, crossover, and mutation. The initialization of the genetic algorithm starts with randomly selecting members. These members are treated as the first population. This is then followed by the selection of fittest members for reproduction. This makes the selected members the parents of the future generation. Furthermore, to enhance the fitness of the upcoming generation, both parents exchange their genes in a process known as crossover. The next genetic mutation operator helps to manage genetic diversity from one generation of members to the upcoming generation [75,79]. To produce better optimization results, researchers have made various modifications to the genetic algorithm. [75] presents a work that employed a genetic algorithm to obtain controlled switching laws for a full-bridge power converter in order to achieve wide-range operational characteristics. [80] employed genetic algorithm to achieve voltage regulation along with State of Charge balancing in a power system.

The consensus algorithm employs the distributive computation method to find out the solution to a consensus problem. The consensus is an understanding of the agreement of an equal amount which depends on the status of all the agents, and after implementing mathematical analysis, everyone tries to converge at one point [81,82]. The consensus theory employs many tools such as graph theory, matrix theory, and control theory. Generally, the neighboring rule has been taken to exchange information between nodes. The network topology having multiple agents is represented as a directed graph $G = (V, E)$. Here, V represents a set of nodes $V =$

$V_1, V_2, V_3, \ldots \ldots, V_n$ and E represents a set of edges for data exchange between nodes. The directed or diagraph is known to be balanced if

$$\sum_j a_{ij} = \sum_j a_{ji} \tag{1.5}$$

Here nodes only exchange data with neighboring nodes. An adjacency matrix $\boldsymbol{A} = [a_{ij}]$ shows the weight of information exchange between nodes i and j . When employing the graph theory, the Laplacian matrix emerges as the best approach for consensus protocols and has been deeply researched in recent times. The Laplacian matrix is defined as $\boldsymbol{L} = \boldsymbol{D} - \boldsymbol{A}$, where $\boldsymbol{D}$ represents the diagonal matrix and $\boldsymbol{A}$ represents the adjacent matrix.

1.3 Data Transfer in Microgrids

Data transfer between various components of a microgrid is a critical factor in maintaining the optimum performance of the microgrid. This entails that a very reliable and consistent communication system is required for timely and accurate transfer of data for monitoring and control purposes. Data transfer in the microgrid is present at various levels, such as primary, secondary, and tertiary levels. To achieve proper operation of the microgrid, the following data transfer requirements will have to be met.

- **Data Latency**

Data Latency is defined as the amount of time taken by a message to get to its destination through a communication channel. The messages and commands communicated between the various components of a microgrid may consist of different network latency requirements. For instance, the protection information and commands exchanged between intelligent electronic devices will require low network latency [83]. This entails that the messages be delivered as soon as possible to their destination. The SCADA messages between sensors and meters may take higher latency than the protection messages [84]. Hence, the communication system is meant to meet various latency requirements associated with each component of the microgrid. Table 1.1 shows the latency requirements of various messages in a microgrid.

Table 1. 1: Delay requirements for different microgrid functions[85]

Microgrid Messages	**Delay Requirements(millisec)**
Protection information	4 ms
Monitoring information	1 s
Control information	16 ms – 100 ms
Operation and maintenance information	1 s
Messages requiring immediate actions at the receiving IEDs	20 ms – 100 ms
Continuous data streams from IEDs	3 ms or 10ms
Synchronization messages	(Accuracy)

The latency of the message is determined by the path through which the message reaches its destination. This means the number of hops the message must go through to get to the destination [85] is an important consideration. In addition, the data rate supported by the communication system is a determining factor for the message latency [85].

- **Data Delivery Criticality**

Data delivery criticality implies the levels of importance associated with various data sent in for system operation. There are three possible data criticality levels in the microgrid: (a) 'high' is employed where the confirmation of end-to-end data delivery is compulsory, and the absence of confirmation is always followed by a reply [85] normally employed for SCADA control commands; (b) 'medium' is used mostly for situations where confirmation is not required but data losses can be detected by the receiver [85] - e.g., measured current and voltage values; and (c) 'non-critical' is always used where data loss is acceptable to the receiver - normally employed in periodic data for monitoring purpose [85].

- **Reliability**

Considering the high dependence of a microgrid on the communication system for sending and delivery of critical messages to maintain the microgrid stability, it is therefore critical to have a reliable communication system in the grid. The communication network reliability is affected by a number of possible failures that include time-out failures, network failures, and resource failures [85]. A time-out failure occurs if the time spent in detecting, assembling, delivering, and action in response to a control message exceeds the time requirement. A network failure occurs when there is a failure in one of the communication protocols [85]. A resource failure means a failure of the end node that initiates communications or receives messages [85].

- **Time synchronization**

Some of the devices on a microgrid may need to be synchronized in time. The requirements for time synchronization of various devices are dependent on the criticality of the application [86]. Intelligent end devices (IEDs) are very strict with regard to tolerance and resolution requirements for time synchronization, especially as they are employed in areas of sensitive data processing. For instance, phasor measurement units (PMUs) need strict time synchronization as they provide geo-referenced real-time measurements of electrical quantities (voltage and current) for analysis, measurement, and control [86].

Communication technologies for data transfer in a microgrid can be categorized into wired and wireless communication. A wired communication for data transfer within microgrids may include ModBus, ProfiBus, power line communication, and Ethernet. On the other hand, wireless communication technologies include Zig-Bee, Wi-Fi, WiMax, and cellular. Table 1.2 shows various wireless communication systems currently being employed for microgrid communication.

Table 1. 2: Wireless communication systems presently employed in microgrids

Family	Data rate	Coverage	Advantages	Disadvantages
Zig-Bee	256 kbps	10-50 m	• Very low power consumption • Low-cost equipment • Suitable for SCADA systems	• Low bandwidth • Do not scale to large networks
Wi-Fi	Up to 54 Mbps	300 m outdoors	• Low-cost network deployments • High flexibility, suitable for different use cases	• High interference • High power consumption • Simple quality-of-service
WiMAX	Up to 100 Mbps	0-10 km	• Suitable for thousands of simultaneous users • Longer distance than Wi-Fi	• Complex network management • High cost of terminal equipment • Use of licensed spectrum
Cellular	14.4 Mbps – 500 Mbps	Up to 50 km	• Able to support tens of millions of devices • Low power consumption of terminal equipment • High flexibility suitable for different use cases	• High cost of usage (licensed spectrum) • High delay in transmission of data related to distance and number of users.

1.4 LoRa communication technology

Long Range Wide Area Network (LoRaWAN) is a low power wide area network (LPWAN) technology developed by the Semtech Corporation [87]. LoRa employs a star topology in which the end device (node) has direct communication with a few gateways in a single hop approach. The gateway then forwards the obtained data packets to a central network. The gateway communicates with the end devices using different

frequency channels and data rates which have an effect on the range and data transfer duration. LoRa has, in recent years, attracted significant interest for its application in sensor monitoring systems and various other IoT applications due to its ability to efficiently trade communication range for high data rates [88]. The LoRa protocol stack is shown in Figure 1.10.

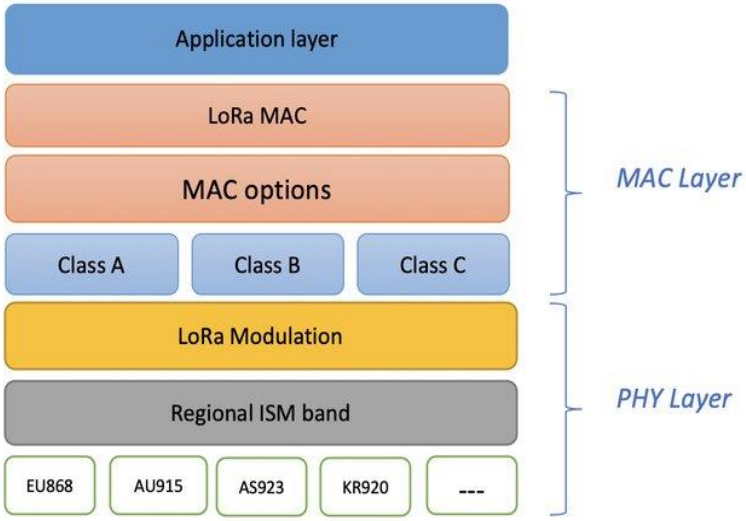

Figure 1. 10. LoRa Protocol Stack

1.4.1 LoRa Physical Layer

At the physical layer, LoRa employs the Chirp Spread Spectrum (CSS) modulation with the integration of the Forward Error Correction (FEC) [88]. This design reduces interference between end devices that are using different data rates. At this level, LoRa operates over multiple channels, which has an increasing effect on the network capacity. LoRa physical layer operates in the unlicensed Industrial, Scientific, and Medical (ISM) frequency band, which is 902-928 MHz for North America with the center frequency of 915 MHz. LoRa can transfer data in three usable bandwidths: 125 kHz, 250 kHz and 500 kHz. The data transmission time generally reduces with an increase in the bandwidths. This entails that for applications where data latency is very important and affects system performance, the high transmission bandwidths should be considered. Furthermore, a spreading factor and coding rate must be decided on for data to be transferred. These parameters have various effects on robustness, interference immunity, and transmission delay. LoRa employs

an orthogonal spreading factor, which allows for the transfer of multiple data packets with different spreading factors over the same channel simultaneously, which improves system efficiency and throughput. Generally, LoRa allows packet transmission in spreading factors between 7 and 12.

1.4.2 LoRa Modulation and Demodulation

LoRa employs the Chirp Spread Spectrum modulation for data transfer. In this subsection, a review of the Chirp Spread Spectrum modulation and demodulation will be presented.

1.4.2.1 Chirp Spread Spectrum Modulation

The CSS modulation employed by LoRa converts each data symbol into a chirp [89]. This is a signal whose frequency increases or decreases linearly with time. A chirp can also be referred to as a sweep signal [89]. A CSS symbol sweeps through the bandwidth once. Once the instantaneous frequency of the CSS signal reaches the highest, it wraps over and starts from the lowest frequency [89]. The spreading factor (SF) can be referred to as the most relevant parameter of the CSS system. In CSS modulation, the modulation order is given as $M = 2^{SF}$, this means that every CSS symbol carries SF number of bits. At baseband, each CSS symbol contains M complex samples, which are transmitted at a rate with same value as the signal bandwidth (BW). This therefore shows that the transmission time of a CSS symbol is given by $T_{sym} = {}^{M}/_{BW}$ (sec). The rate at which the frequency of the CSS signal changes over time is referred to as the chirp rate and this is defined as [89].

$$\mu = \frac{BW}{T_{sym}} = \frac{BW^2}{M}(\text{Hz/s}). \tag{1.6}$$

CSS modulation produces different chirps based on the basic chirp. The basic chirp can be defined as a chirp that starts at the lowest chirp (-BW/2), sweeps through the entire bandwidth and then stop at the highest frequency (BW/2) [89]. This therefore means that the basic chirp at the baseband is centered at zero frequency and is given by the continuous- time waveform:

$$x_0(t) = exp\left\{\underbrace{j2\pi\left(\frac{\mu t}{2} - \frac{BW}{2}\right)t}_{\emptyset_0(t)}\right\}, 0 \le t \le T_{sym} \qquad (1.7)$$

Where $\emptyset_0(t)$ is the phase function of the basic chirp. The instantaneous frequency of the signal at time t is the phase slope of the signal at the moment. The phase function can be differentiated over time to obtain the slope,

$$\frac{\partial \emptyset_0(t)}{\partial t} = 2\pi\left(\mu t - \frac{BW}{2}\right) \text{ (rads/s)} \qquad (1.8)$$

This corresponds to a frequency of

$$f(t) = \left(\mu t - \frac{BW}{2}\right) \text{ (Hz)} \qquad (1.9)$$

An observation of equations (1.6) and (1.9), it can be deduced that a) the frequency of the signal sweeps through the entire bandwidth (BW) over the period of T_{sym} and b) the center frequency is 0 Hz which means that the signal is at baseband. Therefore, the base chirp can be denoted as 0. The next symbol in this case symbol 1 can be obtained by cyclically time-shifting symbol 0 by an amount of 1/BW, and so on. Since overall, there are M different symbols, they are therefore collectively defined as.

$$x_m(t) = x_o\left(\left(t - m\frac{T_{sym}}{M}\right) \; mod \; T_{sym}\right), t \in [0, T_{sym}] \qquad (1.10)$$

Since each baseband chirp is bandlimited to BW/2, it can be sampled at a sampling rate of $F_{samp} = BW$ without any loss of information. Therefore, each continuous-time baseband symbol $x_m(t)$ can be represented by M values that are samples of $x_m(t)$ taken at rate $F_{samp} = BW$ over the symbol duration. Particularly, the baseband discrete-time (digital) samples of the basic chirp are given as

$$x_0[n] = x_0(t)|_{t=nT_{samp}}$$

$$= exp\left\{j2\pi\left(\frac{\mu n T_{samp}}{2} - \frac{BW}{2}\right)nT_{samp}\right\}$$

$$= exp\left\{j2\pi\left(\frac{n^2}{2M} - \frac{n}{2}\right)\right\}; n = 0,1, \dots, M-1. \quad (1.11)$$

Furthermore, it is simple to show that digital samples of the *mth* chirp can be obtained by cyclically shifting the digital chirp by m samples. The digital basic chirp repeats itself after every M sample, i.e., $x_0[n+M] = x_0[n], \forall n$. This therefore means that the *mth* digital chirp at the baseband can also be written mathematically as $x_m[n] = x_0[n+m]$. The explained property of the digital chirp is a very important parameter employed for modulation and demodulation of CSS signals.

1.4.2.2 Chirp Spread Spectrum Demodulation

Considering that LoRa signals have a narrow bandwidth (500 kHz and below), the channel can be considered as having a constant power gain across the bandwidth [89]. Therefore, the received signal after being down converted to digital baseband can be expressed as

$$y_m[n] = exp(j\psi)x_m[n] + w[n], n = 0,1, \dots, M-1. \quad (1.12)$$

In equation (1.12), ψ is defined as a random phase rotation caused by the fact that the oscillators at the transmitter and receiver are not phase-locked, and $w[n]$ is AWGN noise sample with zero mean and variance N_0. In this input/output model, it is easy to observe that the signal-to-noise ratio (SNR) is given as $SNR = \left({}^{1}/_{N_0}\right)$.

De-chirping is normally carried out on every received symbol by the multiplication with the complex conjugate of the basic chirp. For instance, if the basic chirp is an up-chirp, its conjugate is a down-chirp with the same chirp rate, and vice versa. This therefore entails that de-chirping unwinds the second phase function applied on the transmitted signal. This then leaves only the constant and linear phase terms as shown in the expressions below:

$$v_m[n] = y_m[n]x_0^*[n]$$

$$= \left[exp(j\psi) exp\left\{ j2\pi \left(\frac{(n+m)^2}{2M} - \frac{n+m}{2} \right) \right\} + w[n] \right] \times exp\left\{ -j2\pi \left(\frac{n^2}{2M} - \frac{n}{2} \right) \right\}$$

$$= exp(j\psi) exp\left\{ j2\pi \left(\frac{2nm + m^2}{2M} - \frac{m}{2} \right) \right\} + \widehat{w}[n]$$

$$= \underbrace{exp\left\{ j\psi + j2\pi \left(\frac{m^2}{2M} - \frac{m}{2} \right) \right\}}_{Constant\ Phase} \underbrace{exp\left\{ \frac{j2\pi nm}{M} \right\}}_{Linear\ Phase} + \widehat{w}[n] \qquad (1.13)$$

Where $\widehat{w}[n] = w[n]x_0^*[n]$ is also an AWGN noise sample with zero mean and variance N_0. Thus, in the absence of noise, the CSS signal after de-chirping is a pure sinusoid with a frequency of *m/M* (cycles/sample). Denote the constant phase term as $\psi_m = \psi + 2\pi \left(\left[{}^{m^2}/_{2M} \right] - \left[{}^{m}/_{2} \right] \right)$, then the symbol demodulation can be carried out by performing *M*-point DFT on the de-chirped signal to obtain

$$V_m[k] = \frac{1}{\sqrt{M}} \sum_{n=0}^{M-1} v_m[n] exp\left\{ \frac{-j2\pi nk}{M} \right\}$$

$$= \frac{1}{\sqrt{M}} \sum_{n=0}^{M-1} exp\{j\psi_m\} exp\left\{ \frac{j2\pi nm}{M} \right\} exp\left\{ \frac{-j2\pi nk}{M} \right\} + \underbrace{\frac{1}{\sqrt{M}} \sum_{n=0}^{M-1} \widehat{w}[n] exp\left\{ \frac{-j2\pi nk}{M} \right\}}_{W[k]}$$

$$= \frac{exp\{j\psi_m\}}{\sqrt{M}} \sum_{n=0}^{M-1} \widehat{w}[n] exp\left\{ \frac{j2\pi n(m-k)}{M} \right\} + W[k]$$

$$= \begin{cases} \sqrt{M} exp\{j\psi_m\} + W[m], & if\ k = m \\ W[k], & otherwise \end{cases} \qquad (1.14)$$

1.5 Supervisory Control and Data Acquisition

Supervisory Control and Data Acquisition (SCADA) is a technology that allows for the collection of data from one or a variety of facilities at various locations for monitoring and control purposes. SCADA can be employed to any system, such as energy generation systems, water purification systems, waste management

systems etc. The SCADA system acquires data from system devices such as valves, pumps, actuators, etc., while providing control from a remote SCADA host platform [90, 91]. SCADA systems have increased the level of automation in various systems since they make the permanent placement of personnel at sites very unnecessary and they also drastically reduce the rate of personnel visits to plants located in very remote environments for inspection and monitoring purposes. Since its inception in the 1950s, SCADA has greatly developed from the very first structure of employing telephone relay systems and minicomputers [90]. The early SCADA systems achieved data acquisition using panel meters, lights, and strip chart recorders, while supervisory control was carried out by manual operation of various knobs by the personnel. These forms of early SCADA systems are still being employed for use in some plants around the world today [90 - 95].

1.5.1 SCADA Architectural Evolution

The SCADA system has evolved over time. This evolution has made the SCADA system to go through several generations. These generations are as described below [92].

- **First Generation- Monolithic SCADA**

The main feature of the first-generation SCADA system is its standalone abilities with no connectivity. This was due to the absence of networks during the time of its existence. This generation of SCADA systems were implemented using two mainframe systems where Wide Area Networks (WANs) communicated with the Remote Terminal Units (RTUs) only. The monolithic architecture employed only proprietary software.The first-generation SCADA architecture is as shown in Figure 1.11.

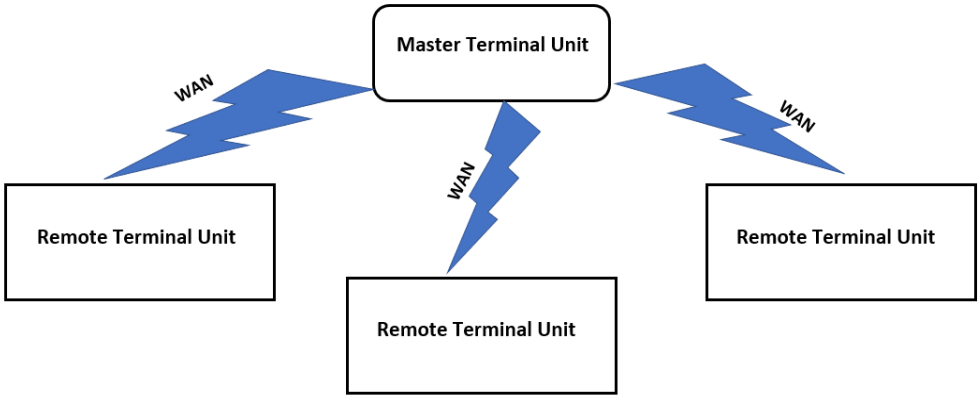

Figure 1. 11. Monolithic SCADA Architecture .

- **Second Generation – Distributed SCADA**

This generation of SCADA systems employed the Local Area Network (LAN) communication technology for system process and function distribution. This generation presented cheaper systems and, at the same time, featured miniature systems, with an overall reduced size from the first generation. This system, to a great extent, allowed for real-time information circulation across all the components of the network. The distributed nature of this SCADA generation allowed for an overall increase in system reliability, triggered by high processing power and redundancy. The main limitation of this SCADA architecture was its inability to reach components that were outside the confinement of the local network. Furthermore, the LAN protocols employed were mainly proprietary and, as a result, could not allow for better mixing of system components. The distributed SCADA architecture is shown in Figure 1.12.

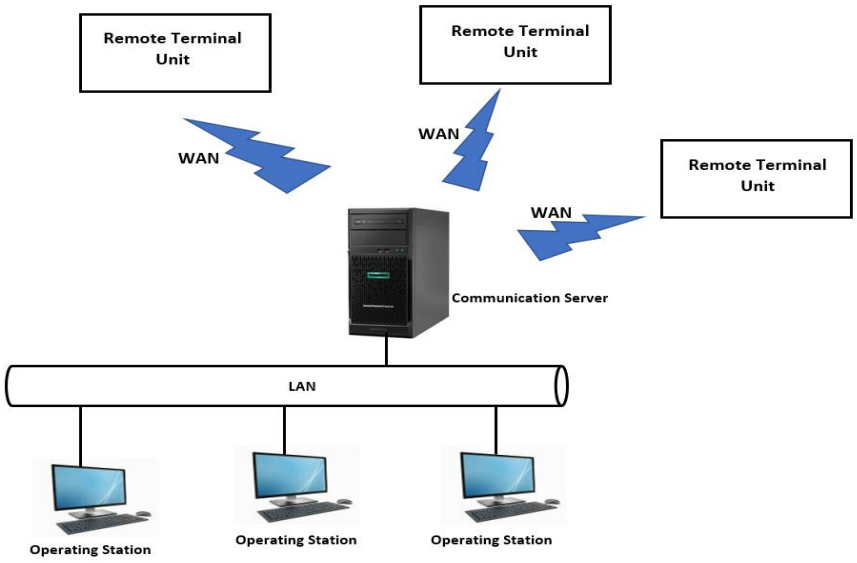

Figure 1. 12. Distributed SCADA architecture.

- **Third Generation – Networked SCADA**

This generation of SCADA systems became more versatile than the earlier generations. This was mainly because it employed open system architecture. In this architecture, the SCADA system allows for multiple networked systems to communicate over WANs, sharing master station functions. This architecture mostly employed PLCs for monitoring and control purposes. This generation shares a great resemblance to the second-generation SCADA because it allows WAN communication. However, it differs from that generation because of its ability to connect to the internet and other third-party peripherals using the Internet Protocol (IP). The third generation SCADA architecture is mainly still being employed for process monitoring and control functions in various factories and plants. The Third generation SCADA architecture is shown in Figure 1.13.

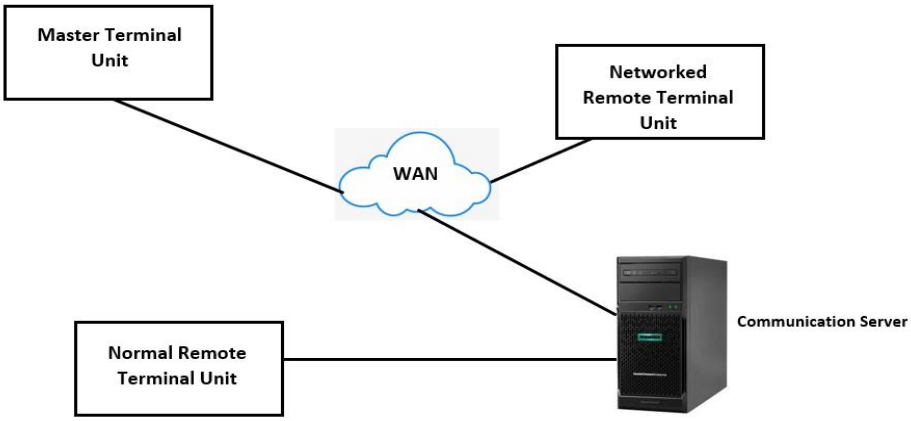

Figure 1. 13. Networked SCADA Architecture

- **Fourth Generation -Internet of Things (IoT) SCADA**

With the advance in technology, SCADA systems now employ very advanced software with very high-performance microprocessors with the ability to connect wirelessly to the cloud and, via the cloud, have very multiple connections to various other devices located at very distant places. This most recent development in the SCADA system became the Internet of Things SCADA architecture. This SCADA architecture eliminates the need for PLCs to monitor and control process systems. This is because the architecture combines the conventional SCADA with cloud capabilities which involves the use of data modelling and complex algorithms to achieve increased data accessibility, flexibility, scalability, and availability while reducing system cost. The SCADA system presented in a later chapter in this thesis was developed on the IoT SCADA architecture. The Internet of Things SCADA architecture is shown in Figure 1.14.

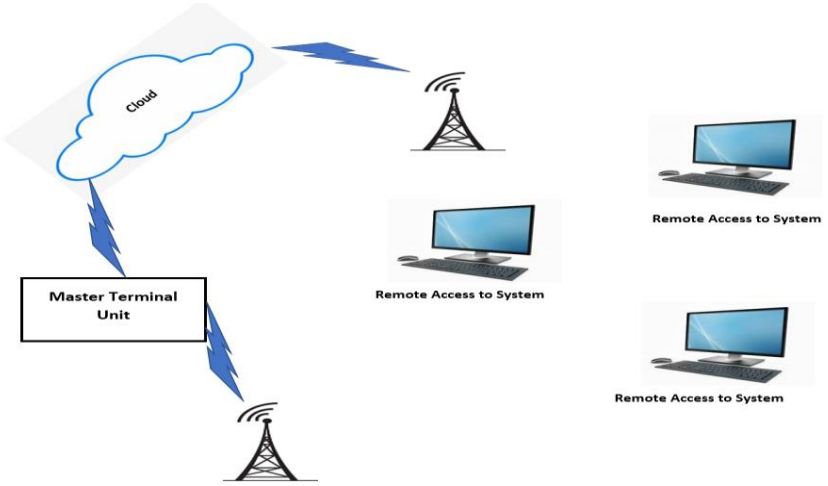

Figure 1. 14. Internet of Things (IoT) based SCADA Architecture [92].

1.5.2 SCADA System Components

The SCADA system is made up of four main components. These components also allow for the level classification of the SCADA system [90,91]. The components are explained as follows:

- **Field Instrumentation Devices (FIDs):** The field Instrumentation Devices are comprised of devices that are directly connected to the monitored or controlled process. They include the sensors, actuators, transmitters, etc. These devices are used to collect or measure data from the equipment and transmit it to the central SCADA systems. Other devices such as the actuators and pumps are normally employed to carry out control actions on the system.
- **Remote Terminal Units (RTUs):** The RTUs are generally small, computerized units, micro-controllers, microprocessors (this includes Programmable Logic Controllers (PLCs)), deployed in the field at specific sites and locations, and they help to collect the control information locally from the field instrumentation devices, process the information and parse them on to the master station for human interactions.
- **Master Terminal Units (MTUs):** The MTU serves as the heart of the SCADA. The master terminal unit is made up of larger computer consoles or servers. This unit is mainly in charge of data collection,

storage, and control command transmission to the FIDs through the RTUs. The Master Terminal unit places the host to the various SCADA software that is employed for system monitoring and control.

- **Communication Networks:** This is basically the mode through which data and control commands are transmitted between the RTUs and the MTU, which are usually located remotely from the plants or process facilities. The main communication protocols that are currently employed for SCADA systems are Wi-Fi, Fieldbus, Modbus, Profibus, etc.

1.5.3 Features of SCADA

For effective employment of SCADA for system monitoring and control, the SCADA system should possess some features which will make the system suitable for such application. The desired features of a SCADA system include [96]:

- **Low Power Consumption**: This is a very important feature SCADA system. SCADA systems are supposed to work 24/7 towards effective monitoring and control of the processing facility, and as such, power consumption is a very important factor to consider. Therefore, a SCADA system should have very low power consumption capabilities to be able to operate for such a long time without energy wastage.
- **Reliability and Availability**: Considering the importance of system monitoring towards achieving optimum system performance in any area, a SCADA system should depict a high level of reliability as a failure in the SCADA system can have a problematic effect on the overall system performance. SCADA system failures have mainly been observed to occur when an operator is unable to obtain measured data from the RTUs. This is mainly due to communication problems as having been seen in various kinds of literature [97, 98].
- **Ease of Installation/Use**: Easy deployment and usage have been shown to be one of the most important features of any SCADA system. This means that for effective use of a SCADA system for

monitoring and control functions, it should exhibit a high level of user-friendliness and, at the same time, be easy to deploy with minimal training of the personnel. Furthermore, various components of the SCADA system should be able to be installed with ease.

- **Redundancy**: A SCADA system with a high level of redundancy shows a great feature for high reliability.
- **Scalability:** SCADA systems are not supposed to be static. This is because various systems continue to increase in size and capacity, and a good SCADA system is supposed to also scale up and down as the case may be. This, therefore, means that various components of the SCADA system should be able to display plug-and-play capabilities where components can be added to the system without complicated processes.
- **Security:** The security of a SCADA system is very important both from the operational and economic points of view. This, therefore, entails that for proper and effective transfer of data between the various components of the SCADA system, the security of the SCADA infrastructure is of very high importance towards the protection of the integrity of the transmitted data and controls.

1.5.4 Classes of SCADA Systems

Generally, SCADA systems employed for supervisory monitoring and control in process facilities are categorized into two classes:

1.5.4.1 Proprietary (traditional) SCADA

SCADA systems such as the Simatic WinCC (Siemens), Clear SCADA (Schneider Electric), Ovation SCADA (Emerson), Micro SCADA (Allen Bradley), ABB Ability SCADA, Experion SCADA (Honeywell), HMI SCADA (General Electric), fall in this classification. This class is made up of SCADA systems whose major components are mainly manufactured by one manufacturer. Furthermore, the standards for the operation of the SCADA system are developed and controlled by the specific manufacturer [93]. This,

therefore, entails that all the responsibilities of operating the SCADA system, such as security, training, and parts replacements, are solely those of the manufacturer. This has a very high amount of negative effect on the proper functioning of the SCADA system as events such as part replacement might take a longer time due to the single manufacturer factor. Furthermore, any effect on the supplier, such as going out of market or end of production of such system, normally has an adverse operational effect on the customer. Considering the monopoly of the proprietary SCADA manufacturers on the systems, these SCADA systems are generally expensive both for sale and after-sale services and, as such, can only be used by highly financially capable customers leaving customers of lower financial levels without any option for system monitoring.

1.5.4.2 Open-Source SCADA

The open-source SCADA class offers a high level of system flexibility as it allows for a user to "mix and match" components [93]. This allows the user to choose the most suitable components for a proposed SCADA system from various vendors. This, therefore, entails that since the open-source SCADA system is not manufactured by a single manufacturer, hence the operations and efficiency of the system are not the sole responsibility of a single vendor. Currently, various components that are employed for the development of SCADA systems have been built by the manufacturers towards a general standard; as the systems get operational, various parts can be changed with parts from the various vendor. This flexibility has also had a very positive economic impact on the customers as the competition between component vendors has caused a reduction in the price of the components and after-sale service provided by the vendors. One of the main SCADA systems in this classification is the Internet of Things-based SCADA system.

Internet of Things was a communication concept that was a coined in 1999 by a member of the Radio Frequency Identification (RFID) [99] and has become very relevant to the world of data communication and cloud computing [100]. Internet of Things facilitated the connections of up to billions of objects for sensing, communication, and sharing of information towards improvement in analysis, management, and system control [100]. Internet of Things can be categorized into three categories: (1) people to people, (2) People to

machine/Things, and (3) Machine to Machine by interaction through the internet. The main goal of IoT is to enable the continuous connectivity of systems at all times and places.

The desired characteristics of the Internet of Things include:

- Interconnectivity
- Things-related services
- Heterogeneity
- Dynamism
- Scalability
- Security
- Accessibility

The IoT architecture consists of various layers of technologies that work together toward the proper achievement of the IoT system.

- **Sensors**

The sensors are the lowest layer in the IoT architecture, made up of various smart devices integrated to enable the interconnections between the physical world to the digital world through real-time data measurement, sharing, and processing. Various sensors employed for IoT applications vary in their functionalities depending on their areas of application. These sensors have the capability to collect data such as temperature, electricity parameters, human health vitals, and renewable energy resources values. The sensors also possess conversion ability; hence the measured physical parameters are converted into digital signals for transmission. Connectivity is required between the sensors and the IoT gateway. The main communication systems for this purpose include Wi-Fi, Zigbee, LoRa, Bluetooth, GSM, and LTE for direct connection to servers and applications. In recent times Wireless Sensor Networks are gaining popularity due to their ability to accommodate the high number of sensor nodes with lower power consumption.

- **Gateways and Networks**

Considering the massive volume of data generated by the sensors, a robust network infrastructure for data transmission is of very high importance to guarantee the reliability and integrity of the generated data. With the increasing need to serve a wider range of IoT services like real-time updates of energy generations systems, and real-time high-volume e-commerce transactions, multiple networks, technologies, and access protocols are required to cooperate towards achieving a heterogeneous configuration. These networks can exist as private, public, or hybrid network systems built to meet various criteria such as latency, bandwidth, and security.

- **Management Service Layer**

The processing of the transmitted data is handled here at the management service layer. Services such as analytics, security controls, and device management are carried out in this layer. One of the main features of this layer is the business and process rule engine [99]. The rule engine normally supports the formulation of decision logic which triggers interactive and automated processes from the processing of the measured data to the achievement of a responsive system.

- **Application Layer**

This layer covers the smart environment spaces in various domains such as Energy generation, City automation, Healthcare, Supply chains, etc.

Various systems have been developed by various researchers and companies for monitoring and control of small process plants, such as small renewable energy generation systems. In [101], the authors proposed and developed a prototype low-cost, open-source SCADA system for solar photovoltaic system monitoring. The work implemented a system that comprises sensors that measure electrical parameters of a PV system, and the data is transferred to a locally installed EMMON CMS server for monitoring and control actions. The communication system implemented for data transfer in this work was Wi-Fi. The work in [102] implemented

a web-based monitoring and control system for real-time electrical data measurement of a hybrid power system using a web-based inTouch system for the graphical user interface. The research in [103] describes the functions of a LoRa-based SCADA system. This work focused only on the security of the communication system employed, such as the data encryption algorithm and security of LoRa – in the context of communication in microgrids. In [104], a low-cost SCADA system was implemented for CO_2-enhanced oil recovery, which uses sensors and actuators connected to the wellhead and data stored in the MYSQL database and displayed on a graphical user interface. Recently, researchers in [105] designed and developed a low-cost, open-sources IOT-based SCADA system using Thinger.IO and the ESP32 microcontroller board. This system has voltage and current sensors connected to a PV system. The electrical parameters were measured and parsed using the ESP32 microcontroller board. The data is then transferred to a Raspberry Pi that hosts the Thinger.IO server platform for data presentation, monitoring and control activities. This system also uses Wi-Fi as the communication for data transfer. Publications such as [100 -109] are also examples of various categories of IoT-based SCADA systems.

1.5.5 Areas of Application of SCADA Systems

SCADA has been employed widely in various industrial facilities for effective monitoring and control of the process in both the public and private sectors. A few areas in which SCADA has been continuously employed for system monitoring include [90]:

- **Energy Generation, transmission, and distribution**: SCADA has been employed in the energy industry for monitoring of various system parameters such as current flow and power production and to find faults in the systems from various measured parameters. In the renewable energy sector, where the energy generation has a high dependence on environmental factors, the SCADA system also includes measuring environmental factors such as the wind speed, solar irradiation, and flow rate for wind, solar and hydro systems, respectively.

- **Mass Transit:** City commuter systems now employ SCADA for fleet control. Furthermore, SCADA systems are employed to regulate the control of traffic lights and to find faulty transport components.
- **Buildings and Facilities:** SCADA has also been employed by real estate and facility managers for the control of various operational components such as the HVAC, refrigeration units, lighting, etc.
- **Water and Sewage Systems:** SCADA is also currently employed by the municipality councils in various cities for the monitoring of various processes such as water and sewage control. Here, SCADA is used to monitor and regulate parameters such as water flow and reservoir levels.

1.6 Research Problem

To improve the overall efficiency of the DC microgrid, this research mainly focuses on the applications of LoRa communications technology as a data transfer system in DC microgrids at the secondary control level where the microgrid functions as a communication base controlled microgrid and at the supervisory and control level for SCADA purposes. In doing this, the main research questions of concern are:

1. What are the parameters to be transferred in the DC microgrid?
2. What is the latency requirement for optimum performance of the DC microgrid?
3. What are the features of LoRa communication technology that makes it suitable for microgrid data transfer?
4. What effects does the employment of LoRa for data transfer in microgrids have on the dynamic performance of the DC microgrid?
5. How can the problems developed by LoRa employment be mitigated to allow LoRa employment for microgrid data transfer?

The above research questions were attempted to be answered by firstly designing AC and DC microgrids (Chapters 2 and 3) to understand how microgrids work and the best microgrid to employ in a particular

community in Nigeria. In chapters 4-6, the main research questions stated above were precisely covered through various studies and simulations focused on answering the questions.

1.7 Research Objectives

This research proposes to design, develop, and analyze the application of LoRa physical level communication for data transfer at the various control levels of a remote DC microgrid. To achieve this goal, the objectives of the research are:

1. Techno-economic feasibility study of AC microgrids for power generation and supply in rural communities in West Africa.
2. Design, dynamic modelling, and simulation of a standalone PV-based DC microgrid with a battery storage system for a remote community in Nigeria.
3. Development of a LoRa-based communication scheme for secondary control level data transfer in remote microgrids.
4. Design and development of a low-cost LoRa-Based SCADA system for monitoring small renewable energy generation systems.
5. Analysis of LoRa data transmission delay on the dynamic performance of the DC microgrid.

1.8 Research Contributions

The main contributions of this PhD thesis are:

1. Sizing, Design and development of AC and DC microgrids for a remote community. The designs depicted the relevance of DC microgrids for remote communities, especially those with no electrical equipments.

2. Design and development of a Low-cost LoRa-based SCADA system for monitoring of small renewable energy generating systems.
3. Investigating the employment of LoRa physical level communication for data and control transfer at the secondary control level of hierarchical DC microgrids. This contribution was achieved through a study, prototype design and the analysis of the LoRa transmission effect on the dynamic performance of the DC microgrid.

1.9 Thesis Outline/ Summary

This thesis adopted the manuscript-style format. A summary of the remaining parts of the thesis and each of the chapters is presented as follows:

Chapter 2 presents the optimal sizing and analysis of a small hybrid power system for a remote community in Nigeria. This chapter focused on data collections from the community, such as the amount of daily energy requirement of the community and the time periods during which electricity is needed more. Furthermore, the renewable energy resources of the community, such as wind and solar resources, were investigated. Using this data, a techno-economic feasibility study was carried out on Homer, and a hybrid AC microgrid with the lowest cost and best energy production was designed for the community. This work in this chapter helped to achieve research objective 1 of this thesis, as stated in Section 1.7. The work in this Chapter has been published in the **International Journal of Photoenergy**, Volume 2019, Article ID 6960191, 8 pages https://doi.org/10.1155/2019/6960191.

The work in Chapter 3 is a follow-up on the AC microgrid designed and developed in Chapter 2. The work in chapter 3 focuses on the sizing of a DC microgrid for the same community in Chapter 2. This work was carried out to observe the best microgrid that will be suited for the remote community. The sizing indicated that a DC microgrid would be more suitable for the community as they are normally farmers and civil servants. A switch to DC appliances will save them a lot of energy while reducing the cost of installation of the DC microgrid. Furthermore, the DC microgrid was then simulated in Matlab/Simulink to observe the dynamic

performance of the proposed DC microgrid by transferring the system sizing obtained from the Homer sizing. The simulation results showed that the system meets the energy requirements of the community. This work in this chapter helped to achieve research objective 2 of this thesis, as stated in Section 1.7. The work in this Chapter has been published in the **Journal of Energy Systems** Volume 3, Issue 2, 2019; Pages 67-85, DOI: 10.30521/jes.544710.

Chapter 4 presents the proposal of LoRa for microgrid data transfer. This work focused on the employment of LoRa for secondary-level data transfer in hierarchical microgrids. The proposed system in this work focuses on the communication between the microgrid local controllers and the central controller for control purposes. The work showcased a proof-of-concept testbed experiment illustrating a one-way communication ability of LoRa to send measurements between the LoRa nodes and the gateway. This work also showed the data coverage range of LoRa. This work showed that since the DC microgrid has fewer parameters to measure for control, LoRa can be employed for data transfer and control at the secondary control level. The work in this Chapter has been published in the **AIMS Electronics and Electrical Engineering,** 4(3): Pages 303–325. DOI: 10.3934/ElectrEng.2020.3.303.

In Chapter 5, an open-source LoRa-based, low-cost IoT platform for renewable energy generation unit monitoring and supervisory control was presented. In this work, an IoT-based SCADA system was designed and developed for monitoring and supervisory control of renewable energy systems. This system employed LoRa as the communication network. This, therefore, showed that the system did not depend on the internet for data transfer which is one of the key features of the designed low-cost system. This makes the system able to be deployed to remote areas where there is no communication infrastructure in existence. Furthermore, for better system security, the proposed SCADA system has all its components hosted on one machine, which eliminates the need for any cloud storage system and hence reduces the system's vulnerability to attacks. The work in this Chapter has been published in the **Journal of Energy and Power Technology** 2022, volume 4, issue 1 doi:10.21926/jept.2201007.

Chapter 6 analyzed the effect of employing LoRa for secondary control level data transfer in hierarchical DC microgrids. This study was carried out in MATLAB/Simulink to observe the effects of LoRa transmission delay on the dynamic performance of the DC microgrid during system control. This study considered the DC microgrid designed in Chapter 3. LoRa transmission delays were calculated for data and control signals transmitted between the local controllers and the microgrid central controller. The calculated delays were included in the simulation as transport delays, and the effects were observed on the DC bus voltage of the microgrid. To eliminate these variations, delay compensation techniques were proposed to show that the system can still perform at near-optimal capabilities even with the employment of a low bandwidth communication system such as LoRa. This work, in conclusion, showed that with proper system design of the DC microgrid, LoRa could be employed for data transfer at the secondary control level. The work in this Chapter has been published in the **Journal of Energy and Power Technology 2022,** volume 4, issue 2 doi:10.21926/jept.2202022.

Chapter 7 presents the conclusions and recommended future works of the thesis.

Appendix A presents the Arduino Codes used in the proof-of-concept development of the one-way LoRa communication system in Chapter 4.

Appendix B presents the Arduino Codes used in the Data Acquisition and Display Phase of the designed Low-cost SCADA system in Chapter 5.

Appendix C Presents the MATLAB/Simulink model of the DC microgrid studied in Chapter 6.

1.10 References

[1] L. Shaver, "Implementation of a DC Microgrid", Master's Degree, UNIVERSITY OF WISCONSIN-MADISON, 2017.

[2] A. Elsayed, A. Mohamed and O. Mohammed, "DC microgrids and distribution systems: An overview", *Electric Power Systems Research*, vol. 119, pp. 407-417, 2015.

[3] S. Ryu, J. Ahn, K. Cho and B. Lee, "Single-Switch ZVZCS Quasi-Resonant CLL Isolated DC-DC Converter for 32" LCD TV", *Journal of Electrical Engineering and Technology*, vol. 10, no. 4, pp. 1646-1654, 2015.

[4] B. Thomas, "Edison revisited: impact of DC distribution on the cost of LED lighting and distribution generation", *27th Annual IEEE Applied Power Electronics Conference and Exposition (APEC),*, pp. 588–593, 2010.

[5] K. Vijayaragavan, "Feasibility of DC Microgrids for Rural Electrification", Master's Degree, European Solar Engineering School, 2017.

[6] D. Kumar, F. Zare and A. Ghosh, "DC Microgrid Technology: System Architectures, AC Grid Interfaces, Grounding Schemes, Power Quality, Communication Networks, Applications, and Standardizations Aspects", *IEEE Access*, vol. 5, pp. 12230-12256, 2017.

[7] Planas E, Andreu J, Gárate JI, et al. (2015) AC and DC technology inmicrogrids: A review. *Renew Sustain Energy Rev* 43: 726–749

[8] Zhao J and Dörfler F (2015) Distributed control and optimization in DC microgrids. *Automatica* 61: 18–26.

[9] Das K, Nitsas A, Altin M, et al. (2017) Improved Load-Shedding Scheme Considering Distributed Generation. *IEEE T Power Deliver* 32: 515–524.

[10] Kim YS, Kim ES, Moon SI (2017) Distributed Generation Control Method for Active Power Sharing and Self-Frequency Recovery in an Islanded Microgrid. *IEEE T Power Syst* 32: 544–551.

[11] Jamian JJ, Illias HA, Gia Ing K, et al. (2016) Optimum distribution network operation considering distributed generation mode of operations and safety margin. *IET Renew Power Gen* 10: 1049–1058.

[12] Mahfouz MMA and El-Sayed MAH (2016) Smart grid fault detection and classification with multi-distributed generation based on current signals approach. *IET Gener Transm Distrib* 10: 4040–4047.

[13] Lin J, Yu W, Zhang N, et al. (2017) A Survey on Internet of Things: Architecture , Enabling Technologies , Security and Privacy , and Applications. *IEEE Internet Things J* 4: 1125–1142.

[14] Saleh SA, Ozkop E, Aljankawey AS (2016) The Development of a Coordinated Anti-Islanding Protection for Collector Systems with Multiple Distributed Generation Units. *IEEE Trans Ind Appl* 52: 4656–4667.

[15] Sendin A (2012) Communication Technologies, Networks, and Strategies for Practical Smart Grid Deployments: From Substations to Meters. *Communication and Networking in Smart Grids*, 241–275.

[16] Stojkoska BLR and Trivodaliev KV (2017) A review of Internet of Things for smart home: Challenges and solutions. *J Clean Prod* 140: 1454–1464.

[17] Liu Z, Su C, Hoidalen H, et al. (2017) A Multi-Agent System Based Protection and Control Scheme for Distribution System with Distributed Generation Integration. *IEEE T Power Deliv*er 32: 536–545.

[18] S. Moayedi and A. Davoudi, "Distributed Tertiary Control of DC Microgrid Clusters," in IEEE Transactions on Power Electronics, vol. 31, no. 2, pp. 1717-1733, Feb. 2016.

[19] A.W. Cirino, Hd. Paula, R.C. Mesquita, E. Saraiva, Cable parameter determination focusing on proximity effect inclusion using finite element analysis, COBEP' 09. *Brazilian P. Electronics Conf.* Bonito-Mato Grosso Do Sul (2009) 402–409.

[20] L. Herrera, W. Zhang and J. Wang, "Stability Analysis and Controller Design of DC Microgrids With Constant Power Loads," in *IEEE Transactions on Smart Grid*, vol. 8, no. 2, pp. 881-888, March 2017, doi: 10.1109/TSG.2015.2457909.

[21] L. Meng et al., "Review on Control of DC Microgrids and Multiple Microgrid Clusters," in IEEE Journal of Emerging and Selected Topics in Power Electronics, vol. 5, no. 3, pp. 928-948, Sept. 2017, doi: 10.1109/JESTPE.2017.2690219.

[22] A. Gupta, S. Doolla and K. Chatterjee, "Hybrid AC–DC Microgrid: Systematic Evaluation of Control Strategies," in *IEEE Transactions on Smart Grid*, vol. 9, no. 4, pp. 3830-3843, July 2018, doi: 10.1109/TSG.2017.2727344.

[23] Sen, S. and Kumar, V., 2018. Microgrid control: A comprehensive survey. *Annual Reviews in Control*, 45, pp.118-151.

[24] Z. Shuai, J. Fang, F. Ning and Z. Shen, "Hierarchical structure and bus voltage control of DC microgrid", *Renewable and Sustainable Energy Reviews*, vol. 82, pp. 3670-3682, 2018. Available:

10.1016/j.rser.2017.10.096.

[25] N. Eghtedarpour and E. Farjah, "Power Control and Management in a Hybrid AC/DC Microgrid," *in IEEE Transactions on Smart Grid*, vol. 5, no. 3, pp. 1494-1505, May 2014, doi: 10.1109/TSG.2013.2294275.

[26] Z. Shuai, J. Fang, F. Ning and Z. Shen, "Hierarchical structure and bus voltage control of DC microgrid", *Renewable and Sustainable Energy Reviews*, vol. 82, pp. 3670-3682, 2018. Available: 10.1016/j.rser.2017.10.096.

[27] S. Sahoo, A. Sinha and N. Kishore, "Control Techniques in AC, DC, and Hybrid AC–DC Microgrid: A Review", *IEEE Journal of Emerging and Selected Topics in Power Electronics*, vol. 6, no. 2, pp. 738-759, 2018. Available: 10.1109/jestpe.2017.2786588.

[28] A. Kaur, J. Kaushal and P. Basak, "A review on microgrid central controller", *Renewable and Sustainable Energy Reviews*, vol. 55, pp. 338-345, 2016. Available: 10.1016/j.rser.2015.10.141.

[29] A. G. Tsikalakis and N. D. Hatziargyriou, "Centralized Control for Optimizing Microgrids Operation," in *IEEE Transactions on Energy Conversion*, vol. 23, no. 1, pp. 241-248, March 2008, doi: 10.1109/TEC.2007.914686.

[30] C. Chen, S. Duan, T. Cai, B. Liu and G. Hu, "Smart energy management system for optimal microgrid economic operation", *IET Renewable Power Generation*, vol. 5, no. 3, p. 258, 2011. Available: 10.1049/iet-rpg.2010.0052.

[31] R. A. F. Ferreira, H. A. C. Braga, A. A. Ferreira and P. G. Barbosa, "Analysis of voltage droop control method for dc microgrids with Simulink: Modelling and simulation," *2012 10th IEEE/IAS International Conference on Industry Applications*, 2012, pp. 1-6, doi: 10.1109/INDUSCON.2012.6452563.

[32] B. Wang, M. Sechilariu and F. Locment, "Intelligent DC Microgrid With Smart Grid Communications: Control Strategy Consideration and Design," in *IEEE Transactions on Smart Grid*, vol. 3, no. 4, pp. 2148-2156, Dec. 2012, doi: 10.1109/TSG.2012.2217764.

[33] P. Huang, P. Liu, W. Xiao and M. S. El Moursi, "A Novel Droop-Based Average Voltage Sharing Control Strategy for DC Microgrids," in *IEEE Transactions on Smart Grid*, vol. 6, no. 3, pp. 1096-1106, May 2015, doi: 10.1109/TSG.2014.2357179.

[34] X. Lu, J. M. Guerrero, K. Sun and J. C. Vasquez, "An Improved Droop Control Method for DC Microgrids Based on Low Bandwidth Communication with DC Bus Voltage Restoration and Enhanced Current Sharing Accuracy," in *IEEE Transactions on Power Electronics*, vol. 29, no. 4, pp. 1800-1812, April 2014, doi:

10.1109/TPEL.2013.2266419.

[35] S. Anand, B. G. Fernandes and J. Guerrero, "Distributed Control to Ensure Proportional Load Sharing and Improve Voltage Regulation in Low-Voltage DC Microgrids," in *IEEE Transactions on Power Electronics*, vol. 28, no. 4, pp. 1900-1913, April 2013, doi: 10.1109/TPEL.2012.2215055.

[36] K. Sun, L. Zhang, Y. Xing and J. M. Guerrero, "A Distributed Control Strategy Based on DC Bus Signaling for Modular Photovoltaic Generation Systems with Battery Energy Storage," in *IEEE Transactions on Power Electronics*, vol. 26, no. 10, pp. 3032-3045, Oct. 2011, doi: 10.1109/TPEL.2011.2127488.

[37] M. Yazdanian and A. Mehrizi-Sani, "Distributed Control Techniques in Microgrids," in *IEEE Transactions on Smart Grid*, vol. 5, no. 6, pp. 2901-2909, Nov. 2014.

[38] D. Dam and H. Lee, "A Power Distributed Control Method for Proportional Load Power Sharing and Bus Voltage Restoration in a DC Microgrid," in *IEEE Transactions on Industry Applications*, vol. 54, no. 4, pp. 3616-3625, July-Aug. 2018.

[39] C. D. Persis, E. R. A. Weitenberg and F. Dorfler, “A power consensus algorithm for DC microgrids”, Elsevier, Automatica, Vol. 89, pp -364-375, March 2018.

[40] D. D. Sharma, S. N. Singh, J. Lin and E. Foruzan, "Agent-Based Distributed Control Schemes for Distributed Energy Storage Systems Under Cyber Attacks," in *IEEE Journal on Emerging and Selected Topics in Circuits and Systems*, vol. 7, no. 2, pp. 307-318, June 2017.

[41] M. Metzger and G. Polakow, "A Survey on Applications of Agent Technology in Industrial Process Control," in *IEEE Transactions on Industrial Informatics*, vol. 7, no. 4, pp. 570-581, Nov. 2011.

[42] J. Kumar, A. Agarwal and V. Agarwal, "A review on overall control of DC microgrids", *Journal of Energy Storage*, vol. 21, pp. 113-138, 2019. Available: 10.1016/j.est.2018.11.013.

[43] T. R. Oliveira, W. W. A. Gonçalves Silva and P. F. Donoso-Garcia, "Distributed Secondary Level Control for Energy Storage Management in DC Microgrids," in *IEEE Transactions on Smart Grid*, vol. 8, no. 6, pp. 2597-2607, Nov. 2017.

[44] L. Meng, T. Dragicevic, J. C. Vasquez and J. M. Guerrero, "Tertiary and Secondary Control Levels for Efficiency Optimization and System Damping in Droop Controlled DC–DC Converters," in *IEEE Transactions on Smart Grid*, vol. 6, no. 6, pp. 2615-2626, Nov. 2015.

[45] A. Bidram and A. Davoudi, "Hierarchical Structure of Microgrids Control System," in *IEEE Transactions on Smart Grid*, vol. 3, no. 4, pp. 1963-1976, Dec. 2012.

[46] J. Hu, J. Duan, H. Ma and M. -Y. Chow, "Distributed Adaptive Droop Control for Optimal Power Dispatch in DC Microgrid," in *IEEE Transactions on Industrial Electronics*, vol. 65, no. 1, pp. 778-789, Jan. 2018.

[47] C. Jin, P. Wang, J. Xiao, Y. Tang and F. H. Choo, "Implementation of Hierarchical Control in DC Microgrids," in *IEEE Transactions on Industrial Electronics*, vol. 61, no. 8, pp. 4032-4042, Aug. 2014.

[48] Q. Shafiee, T. Dragičević, J. C. Vasquez and J. M. Guerrero, "Hierarchical Control for Multiple DC-Microgrids Clusters," in *IEEE Transactions on Energy Conversion*, vol. 29, no. 4, pp. 922-933, Dec. 2014.

[49] X. Yu, X. She, X. Ni and A. Q. Huang, "System Integration and Hierarchical Power Management Strategy for a Solid-State Transformer Interfaced Microgrid System," in *IEEE Transactions on Power Electronics*, vol. 29, no. 8, pp. 4414-4425, Aug. 2014.

[50] A. Firdaus and S. Mishra, "Auxiliary signal-assisted droop-based secondary frequency control of inverter-based PV microgrids for improvement in power sharing and system stability", *IET Renewable Power Generation*, vol. 13, no. 13, pp. 2328-2337, 2019.

[51] W. Souza, M. Severo-Mendes and L. Lopes, "Power sharing control strategies for a three-phase microgrid in different operating condition with droop control and damping factor investigation", *IET Renewable Power Generation*, vol. 9, no. 7, pp. 831-839, 2015.

[52] E. Planas, A. Gil-de-Muro, J. Andreu, I. Kortabarria and I. Alegría, "Design and implementation of a droop control in d–q frame for islanded microgrids", *IET Renewable Power Generation*, vol. 7, no. 5, pp. 458-474, 2013.

[53] V. Mortezapour and H. Lesani, "Adaptive primary droop control for islanded operation of hybrid AC–DC MGs", *IET Generation, Transmission & Distribution*, vol. 12, no. 10, pp. 2388-2396, 2018.

[54] G. Xu, D. Sha and X. Liao, "Decentralized Inverse-Droop Control for Input-Series–Output-Parallel DC–DC Converters," in *IEEE Transactions on Power Electronics*, vol. 30, no. 9, pp. 4621-4625, Sept. 2015.

[55] F. Chen, R. Burgos, D. Boroyevich and W. Zhang, "A nonlinear droop method to improve voltage regulation and load sharing in DC systems," *2015 IEEE First International Conference on DC Microgrids (ICDCM)*, 2015, pp. 45-50.

[56] P. Prabhakaran, Y. Goyal and V. Agarwal, "Novel Nonlinear Droop Control Techniques to Overcome the Load

Sharing and Voltage Regulation Issues in DC Microgrid," in *IEEE Transactions on Power Electronics*, vol. 33, no. 5, pp. 4477-4487, May 2018.

[57] F. Gao, S. Yeoh, S. Bozhko and G. Asher, "Coordinated control of a DC electrical power system in the more electric aircraft integrated with energy storage," *2015 IEEE Energy Conversion Congress and Exposition (ECCE)*, 2015, pp. 5431-5438.

[58] Jung-Won Kim, Hang-Seok Choi and Bo Hyung Cho, "A novel droop method for converter parallel operation," in IEEE Transactions on Power Electronics, vol. 17, no. 1, pp. 25-32, Jan. 2002.

[59] X. Lu, K. Sun, J. M. Guerrero, J. C. Vasquez and L. Huang, "State-of-Charge Balance Using Adaptive Droop Control for Distributed Energy Storage Systems in DC Microgrid Applications," in IEEE Transactions on Industrial Electronics, vol. 61, no. 6, pp. 2804-2815, June 2014.

[60] H. Ho and K. Chen, "Improved Current Sharing Performance by Dynamic Droop Scaling Technique in Multiple Power Systems," 2007 IEEE Power Electronics Specialists Conference, 2007, pp. 189-193.

[61] P. Pinceti, M. Vanti, C. Brocca, M. Carnesecchi and G. Macera, "Design criteria for a power management system for microgrids with renewable sources", *Electric Power Systems Research*, vol. 122, pp. 168-179, 2015.

[62] A. Kwasinski, "Quantitative Evaluation of DC Microgrids Availability: Effects of System Architecture and Converter Topology Design Choices," in IEEE Transactions on Power Electronics, vol. 26, no. 3, pp. 835-851, March 2011.

[63] J. Shen and A. Khaligh, "A Supervisory Energy Management Control Strategy in a Battery/Ultracapacitor Hybrid Energy Storage System," in IEEE Transactions on Transportation Electrification, vol. 1, no. 3, pp. 223-231, Oct. 2015.

[64] U. Manandhar, A. Ukil and T. K. Kiat Jonathan, "Efficiency comparison of DC and AC microgrid," 2015 IEEE Innovative Smart Grid Technologies - Asia (ISGT ASIA), 2015, pp. 1-6.

[65] P. C. Loh, F. Blaabjerg, S. Peyghami-Akhuleh and H. Mokhtari, "Distributed secondary control in DC microgrids with low-bandwidth communication link," 2016 7th Power Electronics and Drive Systems Technologies Conference (PEDSTC), 2016, pp. 641-645.

[66] P. Wang, X. Lu, X. Yang, W. Wang and D. Xu, "An Improved Distributed Secondary Control Method for DC Microgrids With Enhanced Dynamic Current Sharing Performance," in IEEE Transactions on Power Electronics,

vol. 31, no. 9, pp. 6658-6673, Sept. 2016.

[67] J. Schonbergerschonberger, R. Duke and S. D. Round, "DC-Bus Signaling: A Distributed Control Strategy for a Hybrid Renewable Nanogrid," in IEEE Transactions on Industrial Electronics, vol. 53, no. 5, pp. 1453-1460, Oct. 2006.

[68] V. Nasirian, S. Moayedi, A. Davoudi and F. L. Lewis, "Distributed Cooperative Control of DC Microgrids," in IEEE Transactions on Power Electronics, vol. 30, no. 4, pp. 2288-2303, April 2015.

[69] T. Morstyn, B. Hredzak, G. D. Demetriades and V. G. Agelidis, "Unified Distributed Control for DC Microgrid Operating Modes," in IEEE Transactions on Power Systems, vol. 31, no. 1, pp. 802-812, Jan. 2016.

[70] L. Meng et al., "Distributed Voltage Unbalance Compensation in Islanded Microgrids by Using a Dynamic Consensus Algorithm," in IEEE Transactions on Power Electronics, vol. 31, no. 1, pp. 827-838, Jan. 2016.

[71] P. Prabhakaran, Y. Goyal and V. Agarwal, "A Novel Communication-Based Average Voltage Regulation Scheme for a Droop Controlled DC Microgrid," in IEEE Transactions on Smart Grid, vol. 10, no. 2, pp. 1250-1258, March 2019.

[72] M. Zaery, E. M. Ahmed and M. Orabi, "Consensus algorithm based distributed control for economic operation of islanded DC microgrids," 2016 Eighteenth International Middle East Power Systems Conference (MEPCON), 2016, pp. 854-859.

[73] L. Che and M. Shahidehpour, "DC Microgrids: Economic Operation and Enhancement of Resilience by Hierarchical Control," in IEEE Transactions on Smart Grid, vol. 5, no. 5, pp. 2517-2526, Sept. 2014.

[74] X. Li et al., "Flexible Interlinking and Coordinated Power Control of Multiple DC Microgrids Clusters," in IEEE Transactions on Sustainable Energy, vol. 9, no. 2, pp. 904-915, April 2018.

[75] K. Sundareswaran, V. Vigneshkumar and S. Palani, "Development of a hybrid genetic algorithm/perturb and observe algorithm for maximum power point tracking in photovoltaic systems under non-uniform insolation", *IET Renewable Power Generation*, vol. 9, no. 7, pp. 757-765, 2015.

[76] V. Verma and B. Singh, "Genetic-Algorithm-Based Design of Passive Filters for Offshore Applications," in IEEE Transactions on Industry Applications, vol. 46, no. 4, pp. 1295-1303, July-Aug. 2010.

[77] J. Zhao, T. Huang, F. Pang and Y. Liu, "Genetic Algorithm Based on Greedy Strategy in the 0-1 Knapsack Problem," 2009 Third International Conference on Genetic and Evolutionary Computing, 2009, pp. 105-107.

[78] R. Raj, C. Kamalakannan and R. Karthigaivel, "Genetic algorithm-based analysis of wind-driven parallel operated self-excited induction generators supplying isolated loads", *IET Renewable Power Generation*, vol. 12, no. 4, pp. 472-483, 2018.

[79] M. Mitchell, *An Introduction to Genetic Algorithms*. Cambridge: MIT Press, 1998.

[80] L. Meng, T. Dragicevic, J. Vasquez, J. Guerrero and E. R. Sanseverino, "Hierarchical control with virtual resistance optimization for efficiency enhancement and State-of-Charge balancing in DC microgrids," 2015 IEEE First International Conference on DC Microgrids (ICDCM), 2015, pp. 1-6.

[81] N. Rahbari-Asr, Y. Zhang and M. Chow, "Consensus-based distributed scheduling for cooperative operation of distributed energy resources and storage devices in smart grids", *IET Generation, Transmission & Distribution*, vol. 10, no. 5, pp. 1268-1277, 2016.

[82] F. Chen, M. Chen, Z. Xu, J. Guerrero and L. Wang, "Distributed noise-resilient economic dispatch strategy for islanded microgrids", *IET Generation, Transmission & Distribution*, vol. 13, no. 14, pp. 3029-3039, 2019.

[83] M, Adamiak, R. Patterson and J. Melcher. “Inter and Intra Substation Communications: Requirements and Solutions”. 2011.

[84] V. Skendzic and A. Guzma, "Enhancing Power System Automation Through the Use of Real-Time Ethernet," 2006 Power Systems Conference: Advanced Metering, Protection, Control, Communication, and Distributed Resources, 2006, pp. 480-495.

[85] W. Wang, Y. Xu and M. Khanna, "A survey on the communication architectures in smart grid", *Computer Networks*, vol. 55, no. 15, pp. 3604-3629, 2011.

[86] "IEEE Standard Communication Delivery Time Performance Requirements for Electric Power Substation Automation," in IEEE Std 1646-2004, vol., no., pp.1-36, 25 Feb. 2005.

[87] M. Ertürk, M. Aydın, M. Büyükakkaşlar and H. Evirgen, "A Survey on LoRaWAN Architecture, Protocol and Technologies", *Future Internet*, vol. 11, no. 10, p. 216, 2019.

[88] Haxhibeqiri, E. De Poorter, I. Moerman and J. Hoebeke, "A Survey of LoRaWAN for IoT: From Technology to Application", *Sensors*, vol. 18, no. 11, p. 3995, 2018.

[89] T. T. Nguyen, H. H. Nguyen, R. Barton and P. Grossetete, "Efficient Design of Chirp Spread Spectrum Modulation for Low-Power Wide-Area Networks," in IEEE Internet of Things Journal, vol. 6, no. 6, pp. 9503-9515, Dec. 2019.

[90] K. Stouffer, J. Falco and K. Kent, “Guide to Supervisory Control and Data Acquisition (SCADA) and Industrial Control Systems Security—Recommendations of the National Institute of Standards and Technology,” Special Publication 800-82, Initial Public Draft, Sept. 2006.

[91] White paper on SCADA Systems Overview, "Telemetry & Remote SCADA Solutions." Available Online: www.schneider-electric.com. Document Number TBUL00001-31, March 2012.

[92] A. Sajid, H. Abbas and K. Saleem, "Cloud-Assisted IoT-Based SCADA Systems Security: A Review of the State of the Art and Future Challenges,". IEEE Access, vol. 4, pp. 1375-1384, 2016.

[93] L. Abbey, "Telemetry / SCADA Open Systems vs Proprietary Systems," Available Online: https://www.abbey.co.nz/telemetry–scada-open-vs-proprietarysystems-2003.html.

[94] IDC Technologies, "Fundamentals of Instrumentation, Process Control, PLCs and SCADA for Plant Operators and Other Non-Instrument Personnel," Available Online:https://books.idc-online.com/book-categories/instrumentation/

[95] Mader Electric, "Automation & Controls,". Available Online:https://www.maderelectricinc.com/automation-electrical-controls.

[96] A. M. Grilo, J. Chen, M. Díaz, D. Garrido and A. Casaca, "An Integrated WSAN and SCADA System for Monitoring a Critical Infrastructure," in IEEE Transactions on Industrial Informatics, vol. 10, no. 3, pp. 1755-1764, Aug. 2014.

[97] A. G. Bruce, "Reliability analysis of electric utility SCADA systems," IEEE Transactions on Power Systems, vol. 13, no. 3, pp. 844-849, Aug. 1998.

[98] H. Guozhen, C. Tao, C. Changsong and D. Shanxu, "Solutions for SCADA system communication reliability in photovoltaic power plants," 2009 IEEE 6th International Power Electronics and Motion Control Conference, Wuhan, 2009, pp. 2482-2485.

[99] B. Chae, "The evolution of the Internet of Things (IoT): A computational text analysis", *Telecommunications Policy*, vol. 43, no. 10, p. 101848, 2019.

[100] P. de Arquer Fernández, M. Fernández Fernández, J. Carús Candás and P. Arboleya Arboleya, "An IoT open source platform for photovoltaic plants supervision", *International Journal of Electrical Power & Energy Systems*, vol. 125, p. 106540, 2021.

[101] L. O. Aghenta and M. T. Iqbal, "Development of an IoT Based Open Source SCADA System for PV System Monitoring," 2019 IEEE Canadian Conference of Electrical and Computer Engineering (CCECE), 2019, pp. 1-4.

[102] Li Wang and K. -H. Liu, "Implementation of a Web-Based Real-Time Monitoring and Control System for a Hybrid Wind-PV-Battery Renewable Energy System," 2007 International Conference on Intelligent Systems Applications to Power Systems, 2007, pp. 1-6.

[103] A. Iqbal and T. Iqbal, "Low-cost and Secure Communication System for Remote Micro-grids using AES Cryptography on ESP32 with LoRa Module," 2018 IEEE Electrical Power and Energy Conference (EPEC), 2018, pp. 1-5.

[104] X. Lu. "Supervisory Control and Data Acquisition System Design for CO2 Enhanced Oil Recovery", Master of Engineering Thesis, Technical Report No.UCB/EECS-2014-123. EECS Department, University of California at Berkeley, May 21, 2014.

[105] L. Aghenta and M. Iqbal, "Low-Cost, Open Source IoT-Based SCADA System Design Using Thinger.IO and ESP32 Thing", *Electronics*, vol. 8, no. 8, p. 822, 2019.

[106] N. P. Kumar and R. K. Jatoth," Development of cloud based light intensity monitoring system using raspberry Pi," 2015 International Conference on Industrial Instrumentation and Control (ICIC), Pune, 2015, pp. 1356-1361.

[107] V. Sandeep, K. L. Gopal, S. Naveen, A. Amudhan and L. S. Kumar," Globally accessible machine automation using Raspberry pi based on Internet of Things," 2015 International Conference on Advances in Computing, Communications and Informatics (ICACCI), Kochi, 2015, pp. 1144-1147.

[108] S. Chanthakit and C. Rattanapoka," MQTT Based Air Quality Monitoring System using Node MCU and Node-RED," 2018 Seventh ICT International Student Project Conference (ICT-ISPC), Nakhonpathom, 2018, pp. 1-5.

[109] J. C. B. Lopez and H. M. Villaruz," Low-cost weather monitoring system with online logging and data visualization," 2015 International Conference on Humanoid, Nanotechnology, Information Technology, Communication and Control, Environment and Management (HNICEM), Cebu City, 2015, pp. 1-6.

Chapter 2

Optimal Sizing and Analysis of a Small Hybrid Power System for Umuokpo Amumara in Eastern Nigeria

Co-authorship statement

This chapter achieves research objective 1 of this thesis as stated in Section 1.7. It presents the Optimal sizing and Analysis of a small hybrid power system for a remote community in Nigeria with focus on data collections from the community such as the amount of daily energy requirements of the community and the time periods during which electricity is needed more. The renewable energy resources of the community such as the wind, and solar resources were investigated. Using this data, a techno-economic feasibility study was carried out on Homer software and a hybrid AC microgrid with lowest cost and best energy production was designed for the community.

I (Ndukwe Cherechi Izuchukwu) am the principal author and contributed to Conceptualization, Methodology, Software Investigation, Writing of Original Draft and Editing of the research manuscript. The research in this chapter was supervised by Dr. Tariq Iqbal, Dr X. Liang and Dr. Jahangir Khan. The supervisors contributed to the conceptualization and methodology. They also supervised the entire chapter, reviewed and corrected the research manuscript. The work in this Chapter has been published in the **International Journal of Photoenergy**, Volume 2019, Article ID 6960191, 8 pages https://doi.org/10.1155/2019/6960191.

Abstract

Umuokpo Amumara is a village with an estimated population of 9,000 people and about 800 households located in the eastern region of Nigeria in West Africa. This village has no access to power grids for over a decade of existence. Umuokpo by virtue of its location 5°27'35.9"N 7°19'60.0"E, on the average receives about 6 hours of sunlight with a daily average irradiance of 6.12 kWh/m^2. The solar energy can be tapped and

harnessed to generate quality electricity for this small village. Since the wind speed is low (ranging between 3.0 m/s to 3.5 m/s), the wind resource cannot be incorporated into the design. The average load demand of the village is 9.422 MWh/day with a peak load of 1.3 MW. This paper aims to design a small hybrid power system that can generate sustainable electricity for the village from renewable energy sources. The design also considers a backup diesel generator and an energy storage system. The designed system consists of a 2,750 kW solar photovoltaic (PV), a 21,600 kWh battery storage, a 1,500 kW power electronic converter, and a 1,000 kW diesel generator. The simulation suggests that the proposed system can adequately meet electricity needs of the village. A sensitivity analysis is also carried out on the system to observe its behavior with varying levels of irradiation and load.

Keywords – microgrid, renewable energy, remote area electrification, solar energy, optimization, HOMER

2.1 Introduction

Many rural areas in the world lack electrical supply due their remote locations and consequent high cost of electrical infrastructure. Worldwide, more than 1.5 billion people lack access to electricity [1]. These communities have therefore, resorted to the use of local methods to meet their lighting, heating and cooking needs, which to a very large extent have a detrimental effect on the surrounding environment, economic development and quality of life. Most times, these areas have abundant renewable energy resources such as wind, solar and hydro. In principle, these resources can provide electricity – at least in part.

Renewable resources are intermittent in nature, which creates significant system design challenges [2,5]. To mitigate uncertainty caused by renewable energy sources, the combination of conventional and renewable power generation known as a hybrid power system appears to be effective [3]. Such systems can be either grid-connected or stand-alone, and consist of conventional and renewable distributed generation, power conditioning equipment and energy storage devices [4][6].

This work focuses on the techno-economic feasibility of developing a hybrid power system to meet the electrical power needs of Umuokpo Amumara, a rural community in the eastern region of Nigeria. Till date, from literatures reviewed on the renewable energy possibilities in this geographical area, the energy system proposed in this paper has never been considered and as such can be novel with respect to the geographical zone. Specifically, the work contributes the following:

- Proposing a standalone hybrid renewable energy system to provide power to a rural village in Nigeria
- Studying the feasibility of the proposed system to meet the electrical need of the community

The proposed system is chosen to combine solar, conventional diesel generator and battery storage. The feasibility simulation is carried out on HOMER (a tool developed by the National Renewable energy Laboratory USA [7]) for optimum sizing and cost analysis of renewable energy systems. HOMER is chosen as the best optimizing tool for the research as it is renowned for its ability to give accurate optimization results being that it already contains a lot of information on the geographical area of interest. This information includes mainly the abundant renewable energy resources and an almost accurate cost of the employed components. HOMER can provide cost optimization of hybrid power systems based on the Net Present Cost (NPC) method [8].

2.2 System Description

The proposed hybrid power system consists of 1) a solar photovoltaic (PV) array, 2) a diesel generator, and 3) a battery storage system. The diesel generator and the battery storage are intended to supply power when the solar power production is insufficient to meet the demand. The aim of the proposed system is to satisfy electricity needs of the Umuokpo community mainly by renewable energy sources with a very low dependence on the diesel generators.

2.2.1 Description of Umuokpo and Load Profile

Umuokpo is a remote settlement in Eastern Nigeria. It is one of the numerous rural areas in the world without any source of electricity due to its distance from the main cities, making grid connectivity cost prohibitive. There are about 8,000 inhabitants, 800 households, several community centers such as schools, churches, and town hall in the village. Most villagers leave the house in the morning and return in the evenings. Being in Nigeria, Umuokpo only has two dominant seasons, rainy and dry seasons. Each season lasts about six months each. The cooking and heating energy demands are not dependent on electricity. Therefore, the load profile of the village effectively remains similar throughout the year. A breakdown of the various types of electrical loads are tabulated in Table 2.1.

Table 2. 1: Electrical consumers in Umuokpo

Installations	**Number in Village**
Houses	800
Schools	2
Churches	3
Town hall	1
Small Shops	20
Village Water Pumping System	1

In this study, it is assumed that each house consists of a living room, four bedrooms, a kitchen, a bathroom, and a balcony. Typical appliances and installations of a house are shown in Table 2.2 as obtaines by readily available fittings in the market. Each house has a peak load of 1.42 kW, which amounts to 1.136 MW for 800 houses. In addition to the houses, the village also has some public installations. The public installations include a central water pumping system, three churches, two schools, a town hall and 20 shops. Considering these

public installations, the peak load is about 7.3 kW. Further breakdown of the electrical loads for each installation is shown in Table 2.3.

Table 2. 2: Electrical load of each house

Installation	**Electrical features**	**Load rating (W)**	**Hours of operation**	**Energy (Wh/day)**
4 bedrooms	4 * 100 W bulbs	400	6	2400
Sitting room	2* 100 W bulbs	200	6	1200
Kitchen	100 W bulb	100	6	600
Bathroom	100 W Bulb	100	6	600
Balcony	100 W bulb	100	6	600
Television	150 W	150	10	1500
Stereo	50 W	50	4	200
Ceiling Fan	120 W	120	5	600
Refrigerator	200 W	200	20	4000
Total		**1,420**		**11,700**

Table 2. 3: Electrical load for public installations

Installation	**Electrical features**	**Load rating(W)**	**Hours of operation**	**Energy (Wh/day)**
Schools (2)	2*(10*60 W bulbs) + (2*80 W bulbs)	1360	6	8160
Churches (3)	3*(10*100 W bulbs)	3000	4	36000
Town hall	4*60 W bulbs	240	3	720
Small shops (20)	20*60 W bulbs	1200	12	14400

water Pumping (1)	1500 W	1500	2	3000
Total		**7,300**		**62,280**

The total peak load of the village is a sum of the power from all the residential appliances and the public installations, which is calculated as follows:

$$\text{Peak load} = \text{House Peak} + \text{Community Peak} \quad (2.1)$$

For the considered Umuokpo village, the peak load is equal to 1,136 kW + 7.3 kW = 1,143 kW. Heating and cooking demands are met either through kerosene, propane gas or firewood. Therefore, these are not considered in the load profile.

In a conventional Nigerian home, the peak usage of power occurs in the evenings from 1600 -2200 hours - the morning and the afternoon power consumption being low. The village has a total energy consumption of 9.422 MWh/day. The daily, monthly and seasonal load variations are shown in Figures 2.1, 2.2 and 2.3, respectively.

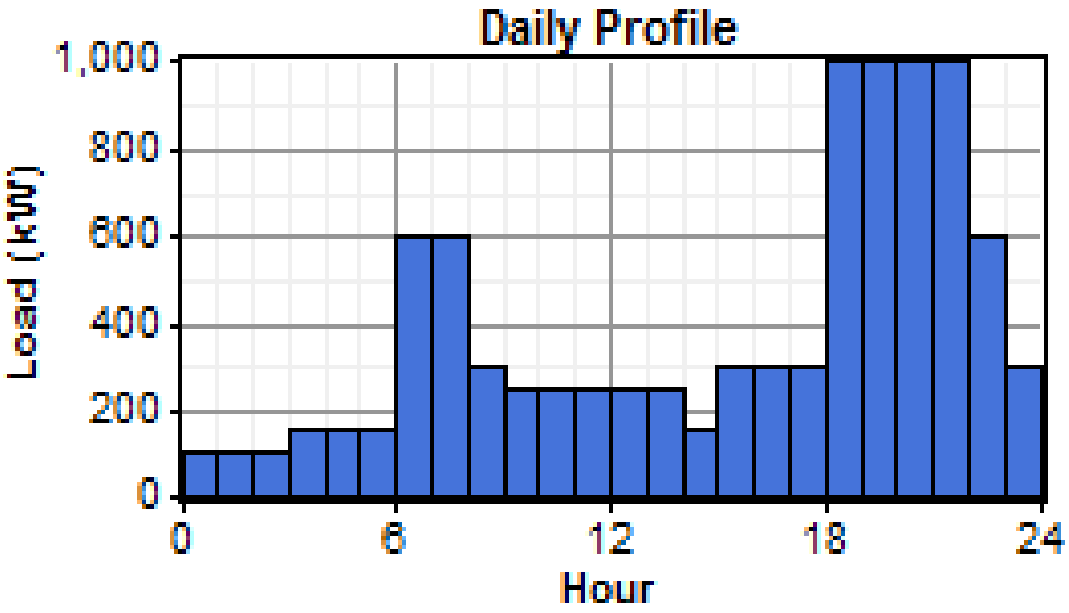

Figure 2. 1. Umuokpo daily load profile

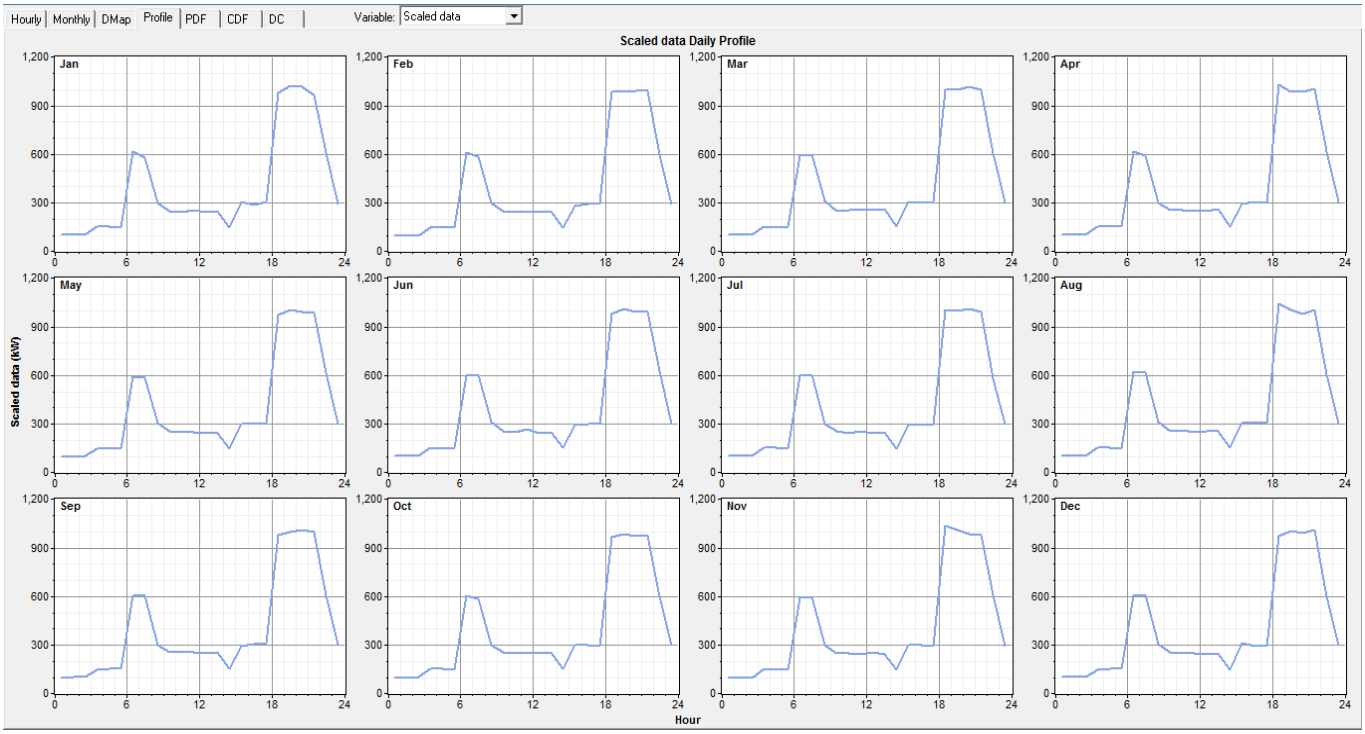

Figure 2. 2. Umuokpo monthly load profile

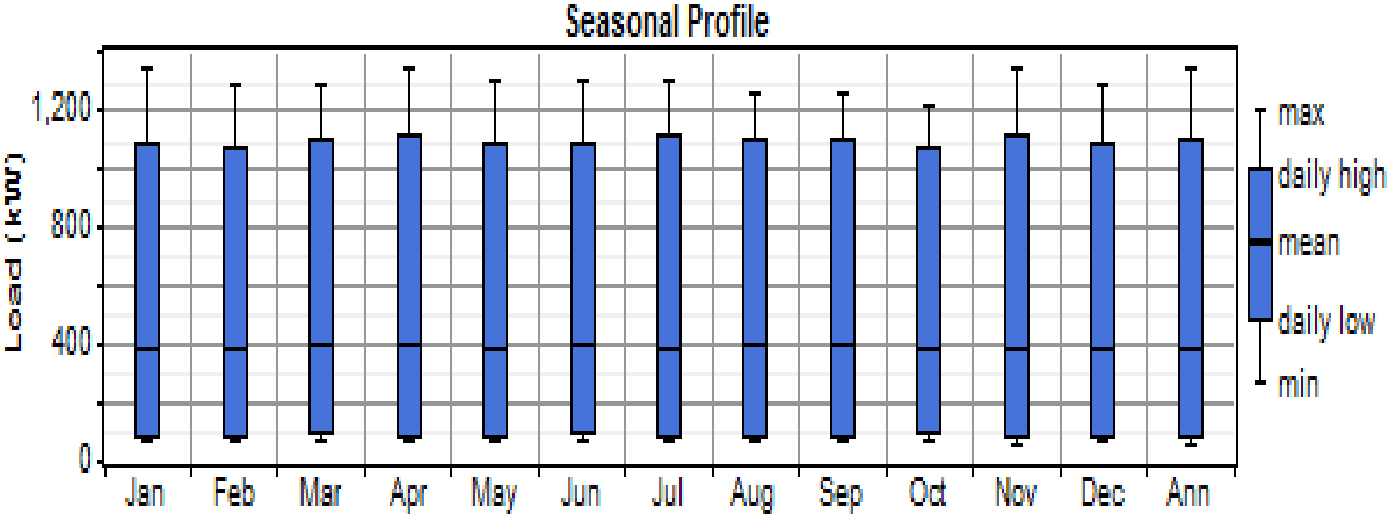

Figure 2. 3. Umuokpo seasonal load variation

2.2.2 Evaluation of Renewable Energy Potentials

The village of Umuokpo is situated down the hill with good exposure of solar irradiation and low wind speed. Both solar and wind power generation capacity is evaluated in this paper, the latter capacity being understandably low.

2.2.2.1 Solar Potential

The monthly solar radiation and clearness index of the village was obtained from the NASA surface meteorology and solar energy website [9] as shown in Table 2.4. From the table, the clearness index is higher in the dry season. The village has an average solar irradiation of 4.71 kWh/m^2/d, which indicates a high potential of electricity generation from solar.

Table 2. 4: Monthly solar irradiation and clearness index of Umuokpo Village [9]

Month	Clearness Index	Daily Radiation (kWh/m^2/d)
January	0.533	5.035
February	0.506	5.047
March	0.480	4.991
April	0.446	4.647
May	0.434	4.390
June	0.397	3.917
July	0.366	3.633
August	0.398	4.072
September	0.410	4238
October	0.430	4.318
November	0.498	4.747
December	0.540	4.488
Average	0.452	4.699

2.2.2.2 Wind Energy Potential

Data obtained from NASA [9] states that Umuokpo has an average wind speed of 2.70 m/s at an anemometer height of 50 m. Wind speeds during a 12-month period based on NASA data are plotted in Figure 2.4.

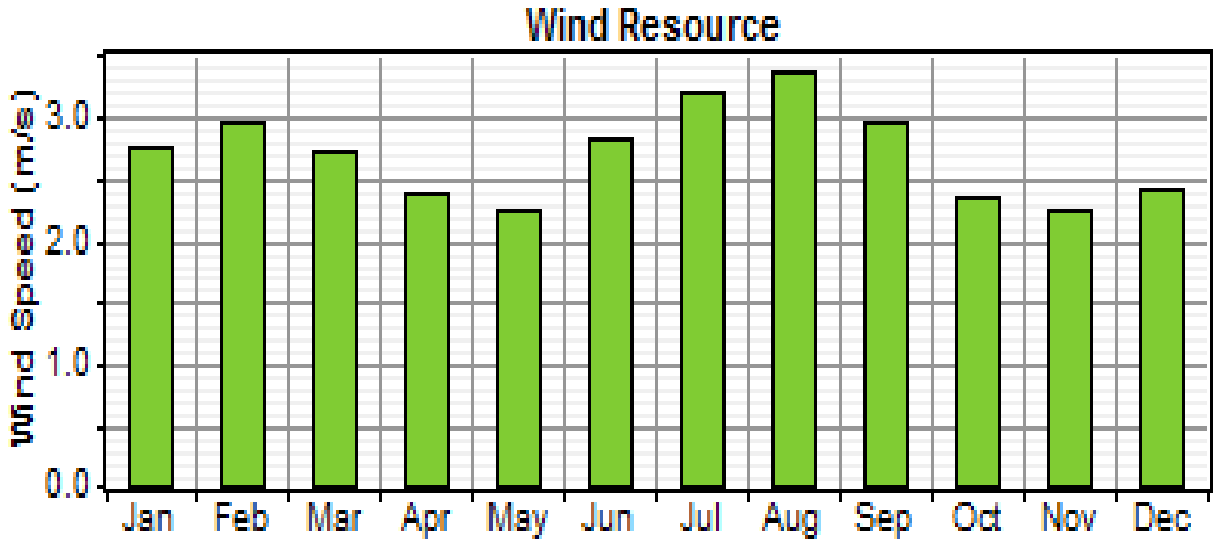

Figure 2. 4. Plot of the monthly wind speed

From the wind data, it is observed that at a hub height of 50 m the wind speed in the village is very low owing to the valley-like location of the village. In this case, the following wind speed conversion between different heights can be used, which is also known as the power-law wind speed model [12]:

$$U_Z = U_{Zr}(\frac{Z}{Z_r})^{\alpha} \qquad (2.2)$$

Where, Z, Z_r are the proposed height above the ground and reference height, respectively; U_Z, U_{zr} are wind speed at the proposed height and known wind speed, respectively; and α is the wind shear coefficient (0.2).

Since only 3.0 m/s speed can be attained at an impractical height of 84 m, inclusion of wind turbines in the design is cost prohibitive.

2.3 The Proposed Hybrid Power System Description

The considered hybrid system is consists of PV arrays, a diesel generator serving as back up, and a battery storage system as shown in Figure. 2.5.

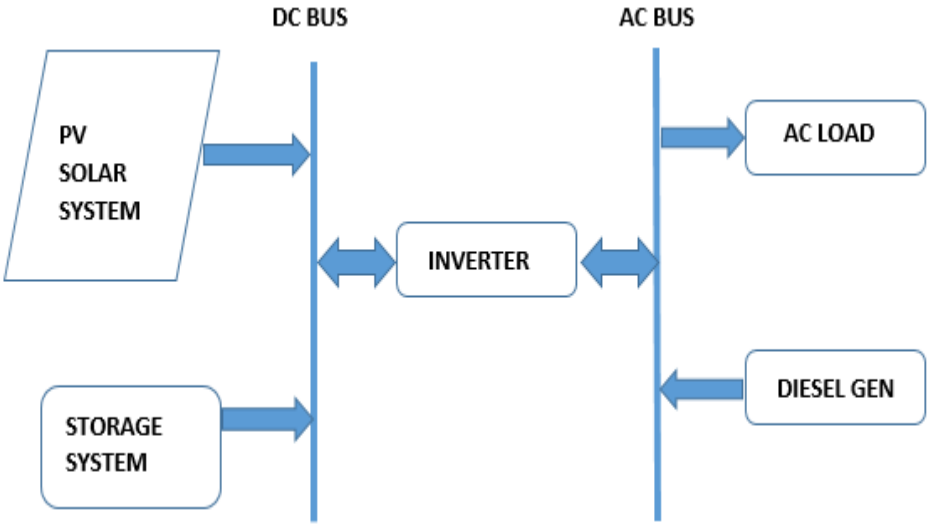

Figure 2. 5. The proposed hybrid system configuration

2.4 Homer Optimization

The simulations to identify the most feasible system for the village electrification was carried out on HOMER. A total of 5,292 simulations were carried out. In Nigeria, the current prices of petroleum products are quite high. The diesel price used in this study is assumed to be $0.69 per liter. The influence of the diesel price variations is evaluated in the sensitivity study. Three system configurations are considered in this study: 1) Diesel generator with the battery; 2) diesel generator alone, and 3) the proposed hybrid system.

2.4.1 Configuration 1 - Diesel Generator with the Battery

This system has a 1,500 kW diesel generator unit, and 2,500 units of battery storage (12V, 200Ah). The diesel generator is in operation for 2,292 hours of the entire year with a yearly production of 4.3 GWh/yr. Its surplus

energy is used to charge the battery, which in turn supplies power during the generator's shut-off time. Figure 2.6 shows a plot of the AC load, Generator power and the state of charge of the battery system in relation to the shut-off time of the generator.

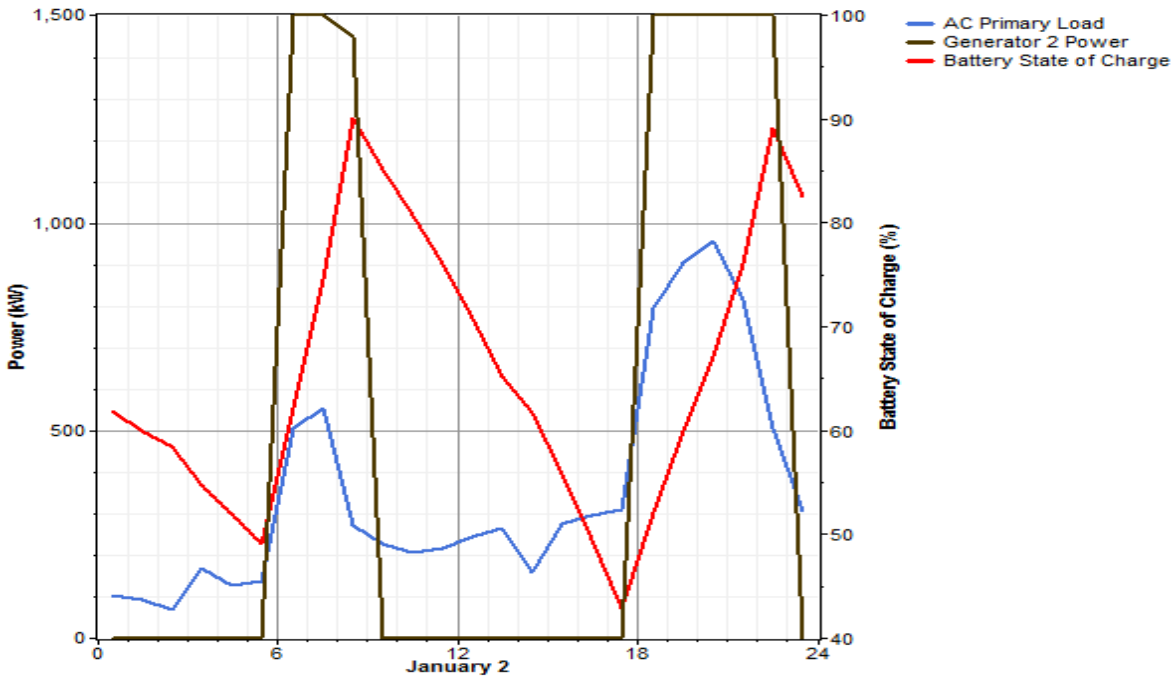

Figure 2. 6. Battery State of Charge meeting the load demand during the diesel generator off time

Figure 2.6 shows that the generator meets the community load demand and at the same time charges the battery. The battery begins to discharge at the point the generator power falls at or below the load demand. This continuous cycle of the battery charging, and discharging has a negative effect on the lifespan of the battery, which makes this system unattractive. The Net present cost of this configuration is $156,293,424 with an operating cost of $12,019,834. The cost itself makes the system very uneconomic. The continuous operation of the generator also will reduce the lifespan of the system.

2.4.2 Configuration 2 - Diesel Generator Alone

This configuration is solely made up of a 1,500 kW diesel generator unit, which runs for 8,760 hours in a year to meet the load demand of the community. This system has an excess energy production of 1.5 GWh/yr. Figure 2.7 shows the diesel generator power generation profile.

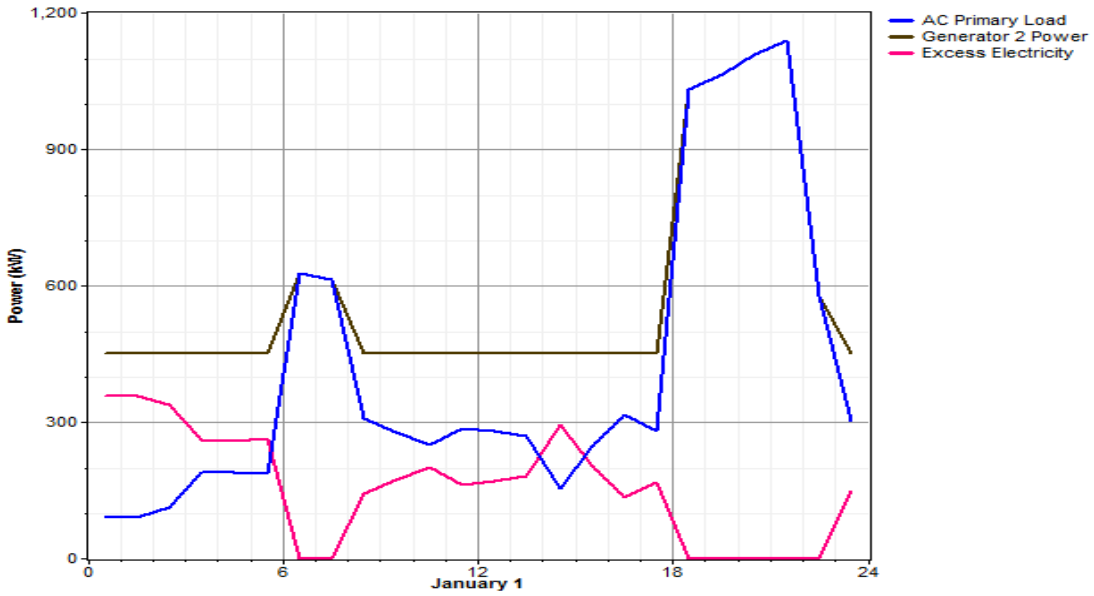

Figure 2. 7. Plot of the electrical production and load demand of the diesel generator alone.

2.4.3 Configuration 3 – The Proposed Hybrid PV/Diesel/Battery System

This configuration is the proposed hybrid system. It has an optimal configuration based on both cost and capacity to serve the load. The system consists of a 2,750 kW PV array, a 1,500 kW diesel generator as backup, and 15,000 units of battery system (12V, 200Ah) for energy storage. During the operation of the system, the PV is the main source of energy, while the generator and battery system are used to meet the power demand for the conditions without enough solar power. The configuration is a shown in Figure. 2.8 and the details of the proposed system components are shown in Table 2.5.

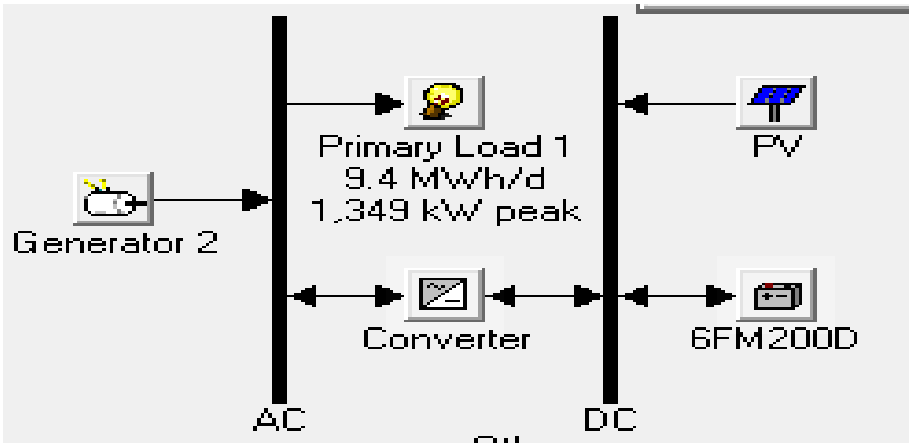

Figure 2. 8. Configuration for the optimal proposed system

Table 2. 5: Electrical Details of the components of the Proposed Hybrid system

Battery	
Nominal Capacity	36,000 kWh
Usable Nominal Capacity	21,600 kWh
Autonomy	55 hrs
Lifetime throughput	13,755,000 kWh
String Size	50
Strings in parallel	300
Total number of battery units	15,000
Energy in	2,970,676 kWh/yr
Energy out	2,391,040 kWh/yr
Expected Life	5.15 yrs
SOLAR PV SYSTEM	
Rated Capacity	2,750kW
Mean Output	415 kW
Mean Output	9,916 kWh/d
Capacity Factor	15.1%
Maximum Output	2,649 kW
PV penetration	106 %
Total Production	3,635,785 kWh/yr
DIESEL GENERATOR	
Rated Capacity	1,500 kW
Mean Electrical Output	1,000 kW
Operational Life	15.6 yrs
Capacity Factor	10.9 %

This system achieved 79% renewable energy fraction with the generated power of 3.6 GWh/yr from the PV array as shown in Figure 2.9. The diesel generator is in 'on' state for just 959 hours in the whole year, which is equivalent to about 3 hours daily. The battery system is charged with the excess electricity produced during the PV operational hours. During the nights when the PV systems cannot produce power, the battery feeds the grid with the stored electricity. The battery system has a nominal capacity of 36,000 kWh with an

autonomy time of 55 hrs. This in turn means that the battery can meet the energy needs of the mini grid to a period of three days.

From Table 2.6, it is observed that the power from the PV system can adequately meet the load demand while the diesel generator serves as the back-up. Also, the excess energy is channeled to the charging of the battery system. Thus, an excess energy of 3.12% (of the generated energy) is achieved in a rather balanced system.

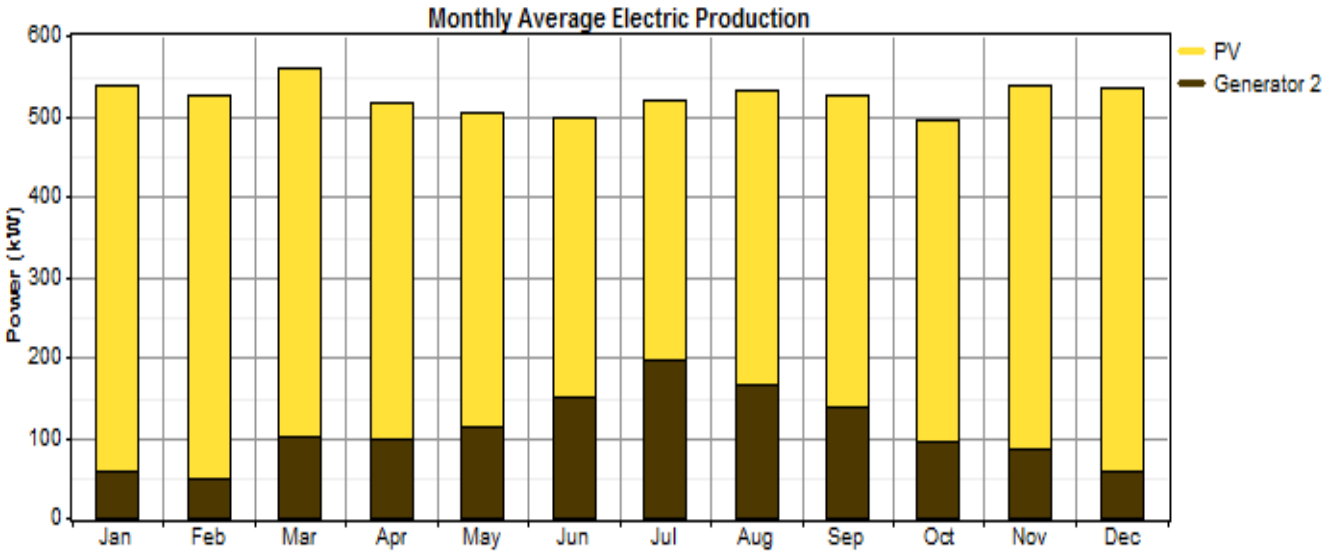

Figure 2. 9. Electrical power production of the optimal configuration

Table 2. 6: Summary of energy production and consumption of the system

Production	**kWh/yr**	**% Production**
PV array	3,635,785	79
Generator 2	959,000	21
Total	4,594,785	100
Consumption	**kWh/yr**	**% Consumption**
AC primary Load	3,439,031	100
Quantity	**kWh/yr**	**%**
Excess electricity	143,164	3.12
Unmet electric load	0.00237	0
Capacity shortage	42.2	0
Renewable Fraction		79

Figure 2.10 depicts the power generation and consumption of the system over a day. This shows that the PV system only generates power from 9.00 hours, and goes low at 15.00 hours, which is evident from the area on the map when the power from the PV is greater than the load curve. During the hours of low PV power, the battery begins to discharge, which indicates that the battery system supports the PV system to meet the load requirements. At night between 18.00 to 6.00 hours, the battery system alone meets the power requirements of the load, hence the drop in the battery's state of charge showing battery discharge. The power characteristics of the system for a period of three days are displayed in Figure. 2.11.

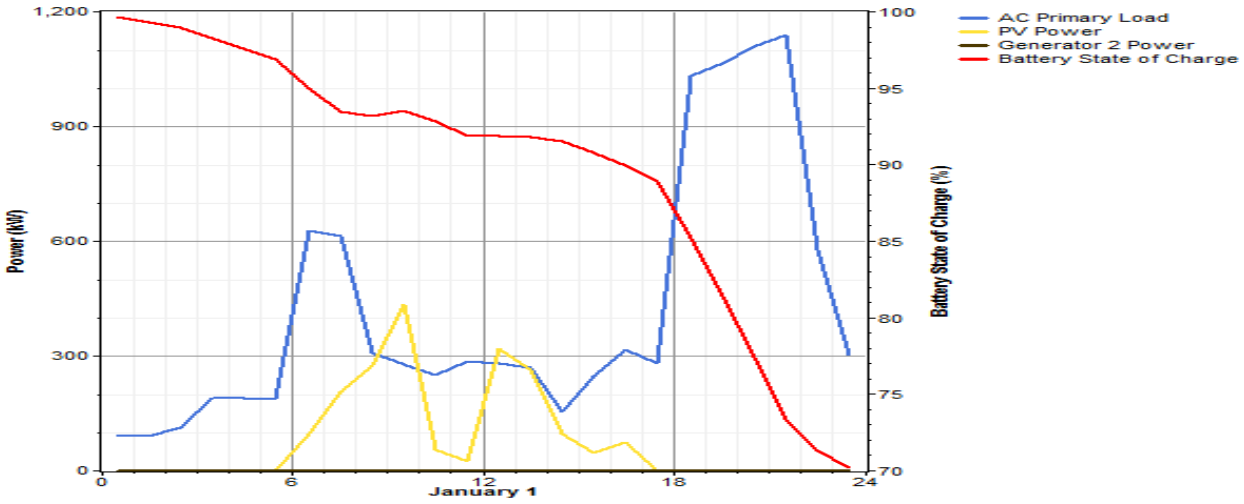

Figure 2. 10. Plot of daily electrical power production

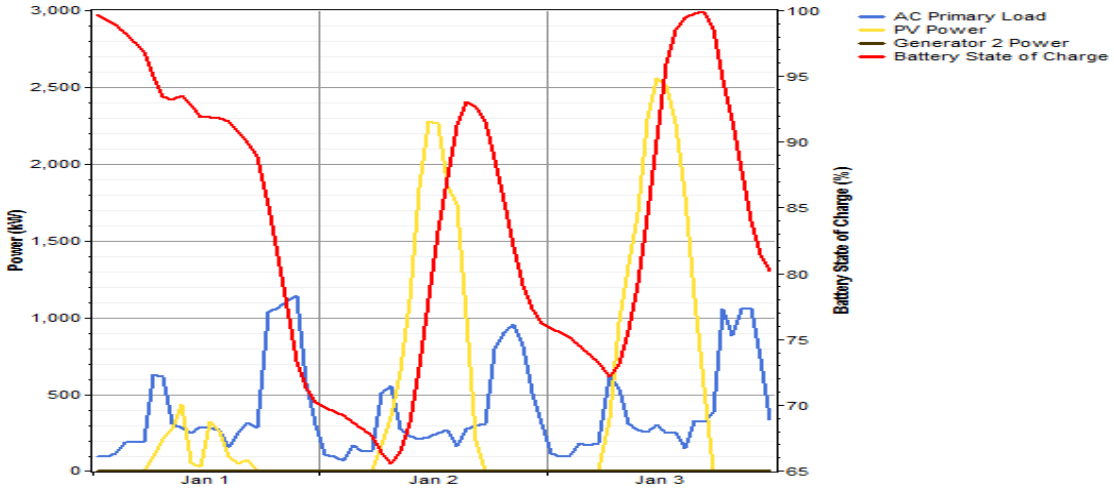

Figure 2. 11. Plot of system electrical characteristics for three days

In Figure 2.11, with special reference to Jan. 2, the battery state of charge curve begins to rise in the same graph with excess PV power. This means that during the day when there is good supply of sunlight, the PV system provides power for use to the load and at the same time charges the battery system. Recall that the aim of the battery system is to store energy when there is good sunlight supply and then supply energy to the load in periods of low sunlight when the PV system is not able to supply enough power. Also, it is noted that the generator production during this period is on the zero-line depicting that the PV array together with the battery system can meet the load demand with low dependence on the diesel generator.

2.4.4 Sensitivity Analysis

A sensitivity analysis is carried out for the system to evaluate the influence of the parameter variations. The parameters considered are the community load and the renewable energy resources. The load is varied between 10,000 kWh and 11,000kWh to observe the behavior of the system for an increased load demand. Since the solar irradiation varies significantly, a variability of 3.0 kWh/m^2/d to 5.0 kWh/m^2/d is considered for low and high irradiation conditions, respectively. The sensitivity results are shown in Figure 2.12.

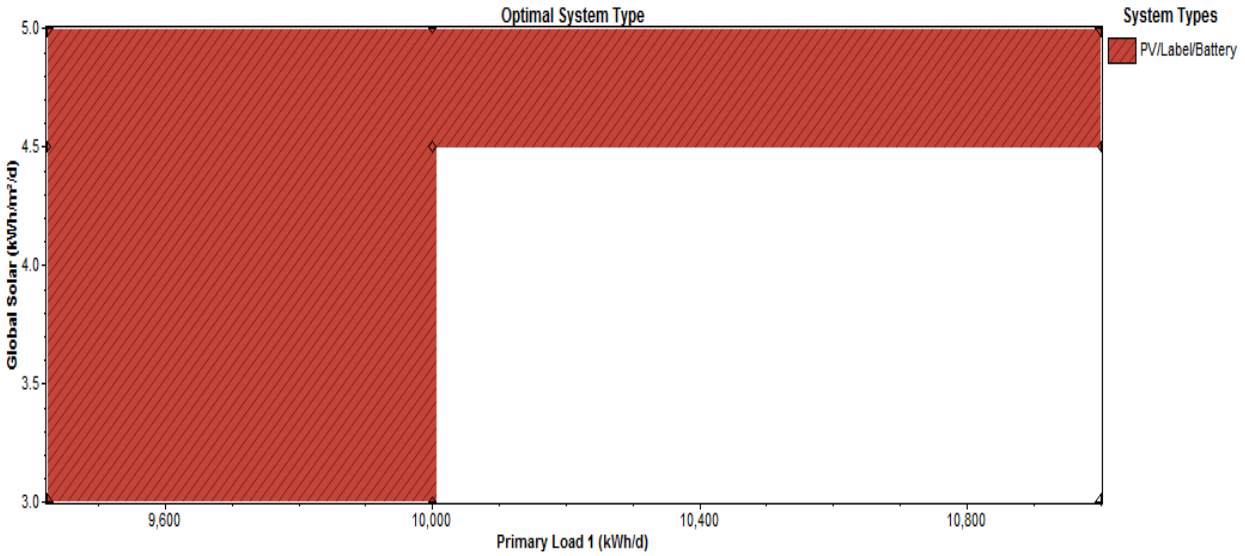

Figure 2. 12. Plot of system sensitivity analysis

It is observed in Figure 2.12 that even in the events of variation in load and renewable energy resources, the system can meet the load demands of the community. However, the plot shows that for solar irradiations less than 4.5 kWh/m^2/d, and load variations above 10,000 kWh/d the load demands will not be met.

2.4.5 Cost Summary

The cost aspects of the proposed system are discussed in this section. With 959 annual hours of operation for the diesel generator, the proposed system has low operational cost for running the diesel generator. The Net Present Cost of the system from HOMER is $54,496,420 with an annual operating cost of $3,279,261. The cost breakdown of the system is shown in Table 2.7.

Table 2. 7: Cost breakdown of the proposed system

Component	Capital ($)	Replacement ($)	O&M ($)	Fuel ($)	Salvage ($)	Total ($)
PV	3,492,064	952,738	111,601	0	-533,956	4,022,445
Diesel Gen.	220,000	72,353	29,422,188	2,427,331	-16846	32,125,024
Battery	7,200,000	8,991780	287,626	0	-148,153	16,331,256
Converter	1,664,400	434,123	0	0	-80,804	2,017,719
System	12,576,464	10,450,994	29,821,416	2,427,331	-7,7975,954	54,496,452

The cost of the proposed hybrid system is low compared to Configurations 1 and 2. Configuration 1 with the generator and battery system has a net present cost (NPC) of $156,293,424 and an operating cost of $12,019,834 annually. Configuration 2 with the diesel generator only, has the highest NPC value of $422.842.368 and an annual operation cost of $33,051,756.

The proposed system has the lowest Cost of Energy (COE) with a value of $1.240 /kWh while the others have $3.56 /kWh for Configuration 1 and $9.618 /kWh for Configuration 2. The COE of the proposed system is on the high side, but with critical look on the fact that the community has been off the grid for a long while, it is a critical investment to improve the quality of life for the community. The summary of the comparison

between the cost of the optimal hybrid system configuration and the other configurations are shown in Table 2.8.

Table 2. 8: Comparison of the optimal and non-optimal systems from HOMER

Item	Optimal system	Configuration 2	Configuration 1
PV capacity (kW)	2,750	-	-
Diesel Gen. Capacity(kW)	1,500	1500	1,500
Number of Batteries	15,000	-	2,500
Gen Operating hours	959	8760	2,292
Inverter Capacity(VA)	1500	-	1000
Total Cost $	54,496,420	422,842,560	156,293,280

2.5 Conclusion

The main objective of the paper is to evaluate the feasibility of a hybrid renewable energy system design with solar and battery as energy storage. Also, the system had a diesel generator which was used as back up. The cost optimization method in HOMER, the NPC method, is used to obtain the optimal case of the system design, where the total system cost is minimized.

A case study is conducted using the proposed hybrid system assuming to be implemented in Umuokpo Amumara, southeastern Nigeria. Heating needs of the community was not considered in the study because due to its tropical location, the heating is not considered a very important need of the community. Two additional configurations for power supply to the community were analyzed in the work.

The proposed renewable system fully met the power needs of the community. Solar resource was considered in this area as it is more abundant than the wind resource. The proposed system achieved 79% renewable fraction and produced a total energy of 4,594,785kWh/yr which comfortably meets the total energy need of the community of 3,439,031kWh/yr. It can therefore be deduced that the system will be self-sufficient as a

standalone system. The proposed system also depicted good energy storage as the stored power in the batteries was observed to supply the community with power over a good period with low power from the PV system. The proposed system is also the cheapest with a COE of $1.240 /kWh.

From the results obtained from the study, the proposed standalone hybrid power system is suitable for use in rural settlements with good renewable energy resources.

2.6 References

[1] T. Ma, H. Yang and L. Lu, "A feasibility study of a stand-alone hybrid solar–wind–battery system for a remote island", *Applied Energy*, vol. 121, pp. 149-158, 2014.

[2] P. Díaz, C. Arias, R. Peña and D. Sandoval, "FAR from the grid: A rural electrification field study", *Renewable Energy*, vol. 35, no. 12, pp. 2829-2834, 2010.

[3] P. Bajpai and V. Dash, "Hybrid renewable energy systems for power generation in stand-alone applications: A review", *Renewable and Sustainable Energy Reviews*, vol. 16, no. 5, pp. 2926-2939, 2012.

[4] S. Upadhyay and M. Sharma, "A review on configurations, control and sizing methodologies of hybrid energy systems", *Renewable and Sustainable Energy Reviews*, vol. 38, pp. 47-63, 2014.

[5] E. Hrayshat, "Techno-economic analysis of autonomous hybrid photovoltaic-diesel-battery system", *Energy for Sustainable Development*, vol. 13, no. 3, pp. 143-150, 2009.

[6] A. Al Busaidi, H. Kazem, A. Al-Badi and M. Farooq Khan, "A review of optimum sizing of hybrid PV–Wind renewable energy systems in oman", *Renewable and Sustainable Energy Reviews*, vol. 53, pp. 185-193, 2016.

[7] "HOMER Pro - Microgrid Software for Designing Optimized Hybrid Microgrids", *Homerenergy.com*, 2016. [Online]. Available: https://www.homerenergy.com/products/pro/index.html.

[8] D. Connolly, H. Lund, B. Mathiesen and M. Leahy, "A review of computer tools for analysing the integration of renewable energy into various energy systems", *Applied Energy*, vol. 87, no. 4, pp. 1059-1082, 2010.

[9] "ASDC | Projects | SSE (Surface meteorology and solar energy)", *Eosweb.larc.nasa.gov*, 2022. [Online]. Available: http://eosweb.larc.nasa.gov/sse/.

[10] S. Kalogirou, *Solar energy engineering- Processes and Systems*, 2nd ed. Amsterdam: Elsevier, 2014.

[11] M. Engin, "Sizing and Simulation of PV-Wind Hybrid Power System", *International Journal of Photoenergy*, vol. 2013, pp. 1-10, 2013.

[12] V. Quaschning, *Renewable energy and climate change*, 1st ed. John Wiley & Sons, Ltd, 2010, pp. 85-190.

Chapter 3

Sizing And Dynamic Modelling and Simulation of a Standalone PV Based DC Microgrid with Battery Storage System for A Remote Community in Nigeria

Co-authorship Statement

The work in Chapter 3 is a follow up on the AC microgrid designed and developed in Chapter 2. The work in chapter 3 focuses on the sizing of a DC microgrid for the same community in Chapter 2. This work was carried out to observe the best microgrid that will be suited for the community. The sizing indicated that a DC microgrid will be more suitable for the Umuokpo community as they are normally farmers and civil servants. Furthermore, the DC microgrid was then simulated in Matlab/Simulink to observe the dynamic performance of the proposed DC microgrid by transferring the system sizing obtained from the Homer Pro Simulation. The simulation results showed that the system meet the energy requirements of the community and at the same time operated at a stable condition.

I (Ndukwe Cherechi Izuchukwu) am the principal author and contributed to Conceptualization, Methodology, Software Investigation, Writing- Original Draft and Editing of this chapter. Dr. Tariq Iqbal contributed to the conceptualization and methodology of the research. Dr. Tariq Iqbal supervised the entire chapter, reviewed and corrected the research manuscript. The work in this Chapter has been published in the **Journal of Energy Systems** Volume 3, Issue 2, 2019; Pages 67-85, DOI: 10.30521/jes.544710.

Abstract

In this paper, a solar PV powered DC microgrid is proposed and designed for Umuokpo Amumara in Nigeria with 800 households and a number of community installations which include churches, schools, shops, and a water pumping system. The appropriate sizes of system components are determined to meet the all-time load

demand. A techno-economic feasibility study was carried out in Homer Pro to determine the energy needs of the community and as well the system size and configuration that best suits the community. The energy requirement of the community was obtained to be 3.16MWh/day. The battery storage system was also sized in this work and a battery system capacity of 21,944Ah was able to meet the community energy requirement for up to a day without renewable energy supply. The dynamic model of the proposed microgrid was simulated in MATLAB/SIMULINK to observe the system's dynamic response in view of the power quality, load impact, and battery storage charging. The results obtained from the simulation depicted a stand-alone DC microgrid that can meet the daily electrical energy requirements of the system with good voltage stability. The PV system used in the system could function at maximum power conditions even with variation in the weather conditions. This was achieved by employing the Incremental Conductance MPPT system.

3.1 Introduction

Most rural areas in Nigeria have been with no electrical supply from the national grid. This is mainly attributed to lack of access to these areas, which therefore translates to the high cost of grid installations. Worldwide, there is an estimation of above 1.5 billion people who lack access to electricity [1]. These communities have therefore resorted to the use of local methods to meet their lighting, heating, and cooking needs. This, in turn, has a detrimental effect on their economic stabilities. Most times, these areas have abundant renewable energy resources such as wind, solar, and hydro that are sources of cheap and clean energy. It is, therefore, recommended that these sources of energy be explored to provide electricity for these rural areas.

Microgrids can be of two types, which are the AC microgrid and the DC microgrid. For this community, a DC microgrid was proposed with the following reasons ; easy integration with renewable energy sources and storage [1,2], availability of most DC loads [3,4], loss reduction due to lower number of conversion stages [5], low cost of distribution and low system complexity [6].

Due to the absence of grid in Umuokpo Amumara and the very high availability of solar energy resource that can be harnessed for isolated microgrid, a Solar PV based DC microgrid will be an efficient way to generate stable and cheap electricity for the community.

This paper focuses on the sizing and dynamic modeling of a standalone solar PV based DC microgrid for electrification of Umuokpo Amumara. To the best of the authors' knowledge, a DC microgrid has never been proposed in existing literature for this geographical area. Therefore, this can be considered novel for the geographical area. Specifically, the contributions of this paper include:

- Development of a DC microgrid to provide power to the rural settlement.
- Feasibility study of the proposed DC microgrid to meet the electrical needs of the community.
- Dynamic modeling and simulation of the proposed DC microgrid including Maximum Power Point Tracking and DC Voltage Control.

3.2 Literature Review

DC microgrid is an attractive technology in modern electrical grid system because of its natural interfacing with the existing renewable energy sources [2]. The DC microgrid system is made up of mostly renewable energy sources and delivers the energy to the components of the microgrid in direct current form. Here the components of the microgrid are connected directly to the sources through the system bus and as a result, there is no need for conversion of the power. Figure 3.1 shows the block diagram and architecture of a DC microgrid.

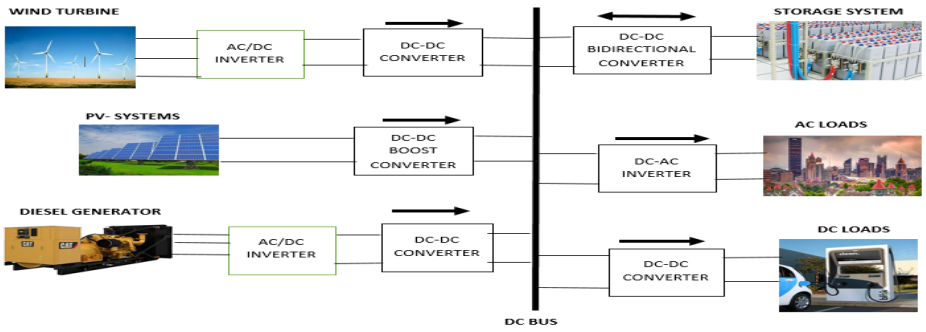

Figure 3. 1. Schematic Diagram of a Stand-alone DC microgrid

A DC microgrid conventionally consists of the renewable energy Source, the DC bus, the storage system and the loads, which may be either AC or DC. As earlier mentioned, the main advantage of the DC microgrid is the elimination of the high number of power conversion stages that lead to many losses. A PV-Wind energy-based DC microgrid, which incorporates a battery bank for storage, was proposed in [7]. The paper stated the importance of an optimal mix of renewable resources and storage to obtain a balanced system. Also, the system saw the incorporation of DC-AC converters to feed the AC loads in the telecommunication system. NSGA II optimization technique was employed for the sizing of the system. Cost of energy generation and high reliability were the justifications given by [8] for the shift in paradigm from the conventional AC energy generation to DC generation. The paper stated its focus as the rural area considering the low accessibility to electricity. The paper also stated that the orientation of the rural settlement has a very large effect on the configuration of the system, which in turn affects the efficiency of the system. Linear and clustered arrangements are the two forms of arrangements that are normally aligned with the rural settlements. The work employed Newton-Raphson's method modified for DC power flow to analyze the overall system losses. A DC microgrid was designed in [9], and the system did not employ the usual battery stack for energy storage but instead employed a variation of super-capacitors assisted regulators uninterrupted power supply. This energy bank has the advantage of fast transient time and low noise during its operation. Light dimming and air conditioning control systems were incorporated into the design to achieve optimal energy usage and low electricity consumption. The design of a DC microgrid for a residential building was carried out in [10]. This design was carried out for a microgrid with two DC voltage levels 380VDC and 24 VDC. The higher voltage was to feed the high-power appliances in the building such as the refrigerators and dryers while the lower voltage value was for the low power devices. From simulations in SIMULINK AND PSIM, the design was validated, and a conclusion reached that the 380/24VDC microgrid is more economical than the AC counterpart. A self-reliant DC microgrid was sized and experimented in [11]. The paper presented the sources of energy as PV photovoltaic system and fuel cells. Super-capacitors and electrolyzer systems were combined in the system as hybrid storage. The Adaptive Dynamic Power Management Strategy (ADPMS) is employed

in the sizing to solve the normal impediments of DC microgrids which include variation in sources and load, fuel starvation phenomenon of the fuel cell and the state of Charge (SoC) of the super-capacitor. The study was validated using a laboratory scale DC microgrid test bed. DC microgrids have been known overtime for high efficiency and reliability while having no frequency and reactive power issues [12]. Various operational controls have been studied by different researchers on the system and some of these control systems include centralized control [13], master-slave control [14], multi-agent control [15], distributed autonomous control [16]. From most research results, it is observed that the distributed control system is mostly used due to its advantage of more autonomous and flexible control configuration.

3.3 System Sizing

In power generation and distribution, the accurate supply of power to customers is paramount. Thus, the need for a power system that meets the energy requirement of the consumers. This research entails the design and simulation of a DC microgrid that will supply power to 800 houses in a remote part of the eastern region of Nigeria. This section of the research will depict the following details.

1. Accurate measurement of the load profile of the community.
2. A study of the available renewable energy resources in the community.
3. Optimal sizing of the power system.
4. Community load profile.

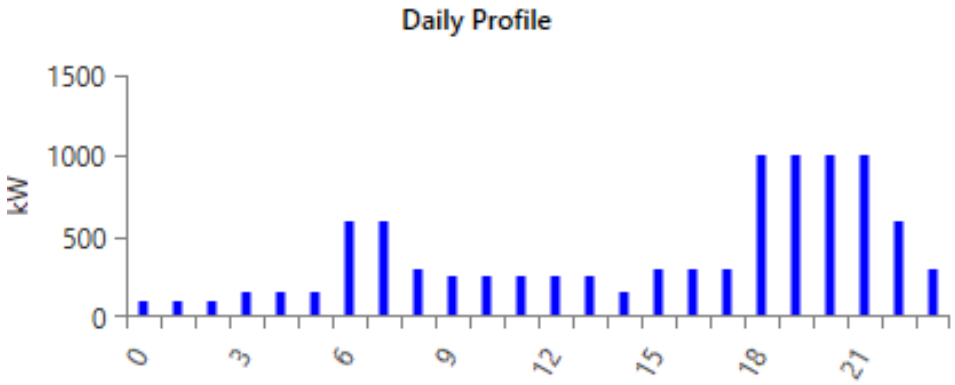

Figure 3. 2. Umuokpo Daily Load Profile

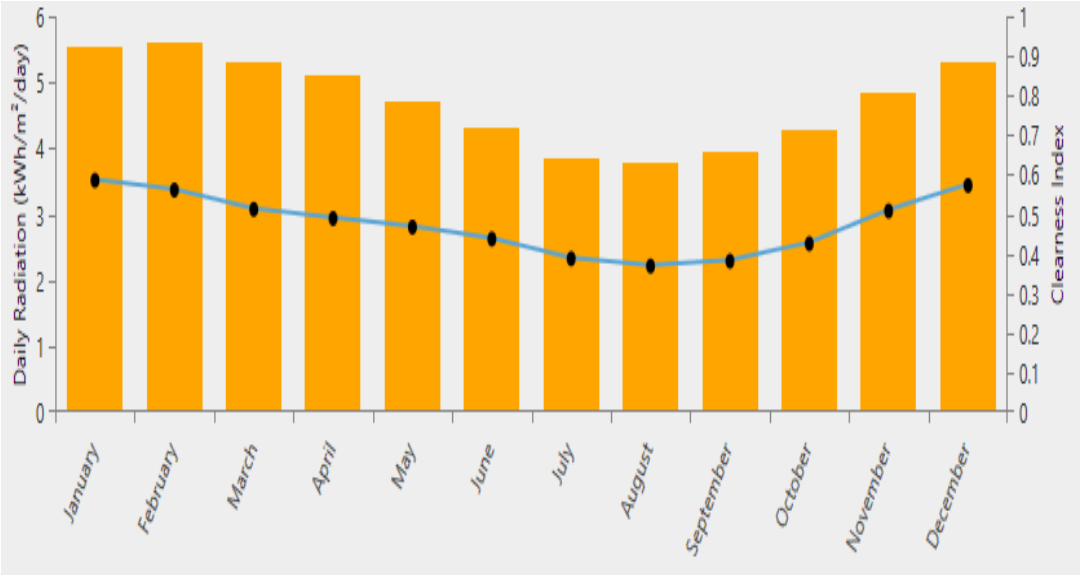

Figure 3. 3. The Plot of solar irradiation

The village consists of about 8,000 inhabitants with 800 houses and some community centers such as the schools, churches, and town hall. The village is a working-class village where inhabitants have various jobs and leave the house in the morning to return in the evenings. Nigeria has just two seasons in the year, which are the rainy and dry seasons. Figures 3.2 and 3.3 show the community daily load profile and the solar irradiation respectively. The installations and basic electrical needs of the community are shown in Tables 3.1, 3.2, and 3.3.

Table 3. 1: Electrical Installations in Umuokpo Community

Installations	**Number in Village**
Houses	800
Schools	2
Churches	3
Townhall	1
Small Shops	20
Village Water Pumping System	1

Table 3. 2: DC Electrical load of Each House

Installation	DC Electrical features	Load rating(W)	Hours of operation	Energy (Wh/day)
4 bedrooms	4*8.5W bulbs	34	6	204
Sitting room	2* 8.5W bulbs	17	6	102
Kitchen	8.5W bulb	8.5	6	51
Bathroom	8.5W	8.5	6	51
Balcony	14W	14	6	84
Television	30W	30	10	300
Stereo	20W	20	4	80
Ceiling Fan	15W	15	5	75
Refrigerator	150W	150	20	3000
Total		**297**		**3,947**

Table 3. 3: DC Electrical load for public installations

Installation	Electrical features	Load rating(W)	Hours of operation	Energy (Wh/day)
Schools (2)	2*(10*8.5W bulbs) + (2*8.5Wbulbs)	187	6	1122
Churches (3)	3*(10*8.5W bulbs)	255	4	1020
Town hall	4*8.5W bulbs	34	3	102
Small shops (20)	20*8.5W bulbs	170	12	2040
Village water Pumping system (1)	1000W	1000	2	2000
Total		**1,646**		**6,284**

From Table 3.2, it is observed that each house has a peak load of **0.30kW**, which amounts to only **238kW** when the 800 houses are considered. In addition to the houses, the village also has some public installations. The total peak load of the village is a sum of the power from all the house appliances and the public installations. This is calculated as shown below:

House Peak + Community Peak= Global Village Consumption (3.1)

238kW + 1.64kW= 239.7kW

Heating and cooking are not included in the load profile as the village employs traditional methods for heating and cooking. In a conventional Nigerian home, the peak usage of power occurs in the evenings from 16.00 - 22.00 as the community is at full capacity during this period. As a result, power usage will be low in the morning and afternoon hours. The village has a total energy consumption of **3.16MWh/day**. The village has an average solar irradiation of 4.7kWh/m^2/d, which depicts the possibility of good energy from the solar resources available in the area.

3.3.1. Battery Sizing

The storage system is very important in a microgrid. This system is employed to store excess energy generated by the generation system and then supplies the microgrid in days of low production. The battery capacity is obtained by:

$$E_{total} = \frac{E_{day}}{Inverter\ eff} \tag{3.2}$$

E_{day} is the energy need of the community for a day

$$E_{total} = \frac{3160kWh}{0.95} = 3326kWh$$

The battery capacity is calculated as:

$$Batt\ Cap = \frac{E_{total} \times Autonomy\ Days}{Bus\ Voltage \times Batt\ EFF \times \%DOD} \tag{3.3}$$

$$= \frac{3160000\ \times 1}{360 \times 0.8 \times 0.5} = 21{,}944Ah$$

Therefore, number of batteries in series:

$$N_S = \frac{Bus\ Voltage}{Battery\ Nominal\ Voltage} \tag{3.4}$$

$$Number\ of\ Strings = \frac{360}{12} = 30\ batteries$$

Number of batteries in parallel:

$$N_p = \frac{Total\ Battery\ Size}{Rating\ of\ Battery} \quad (3.5)$$

3.4 Homer Sizing Results

The simulations to pick the most feasible system for the village electrification was carried out in HOMER software. From the simulation, the most feasible system was selected based on the Net Present Cost (NPC) analysis, which highlights the system that meets the load demand at the lowest reasonable cost.

The optimal system consists of a 1,000kW PV array, a 630kW Diesel generator as backup and 4,680 units of battery system for energy storage. The PV is the main source of energy, while the generator and battery system are used to meet energy needs when the PV system is lower than the demand.

The optimal system achieved 88.6% renewable energy fraction with electrical production of 1.38GWh/yr from the PV array. The generator also, which is used as back up is ON only for just 616 hours in the whole year. This amounts to about 1.6 hours daily. The battery system is charged with the excess electricity produced during the PV operational hours. During the nights when the PV systems cannot produce power, the battery feeds the grid with stored power as can be observed in Figure 3.4. The battery system has a nominal capacity of 7,857kWh with an autonomy time of 29.8 hours.

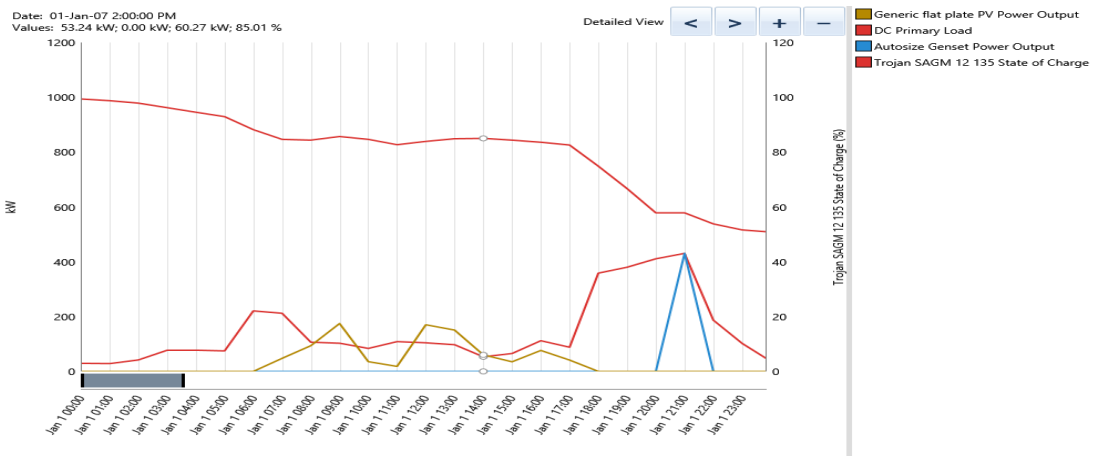

Figure 3. 4. Plot of daily Electrical component activities

From the sizing, the PV system comfortably meets the load power requirements and therefore makes the generator system strictly for back up. Also, the system depicts that the excess energy is applied to the charging of the battery system and thus the low value of excess energy to 15% of the generated energy. The low value of the excess energy depicts a very balanced electrical system.

3.5 System Overview and Description

The Proposed DC Microgrid power system consists of the following:

- A PV array for trapping energy from the sun
- A battery storage system to supply needed power in days of low renewable resources
- Boost converter
- Buck converter

The aim of the proposed system is to supply and satisfy the electrical requirement of the Umuokpo community with a high penetration of the renewable energy source and the battery storage system. Considering that a standard has not been specified for the DC voltage levels, a 360V DC bus voltage for the power distribution in the system was employed. This choice was made after thorough studies which indicated much usage of the 360VDC as it is ideal for long community distance distribution and suites the high amount of power that will be distributed through the community while meeting the safety level required as well. The system employed 24VLDC in-house distribution line, which is safe for residential usage and a 48VLDC for the community water pumping system.

The block diagram of the proposed DC microgrid is shown in figure 3.5.

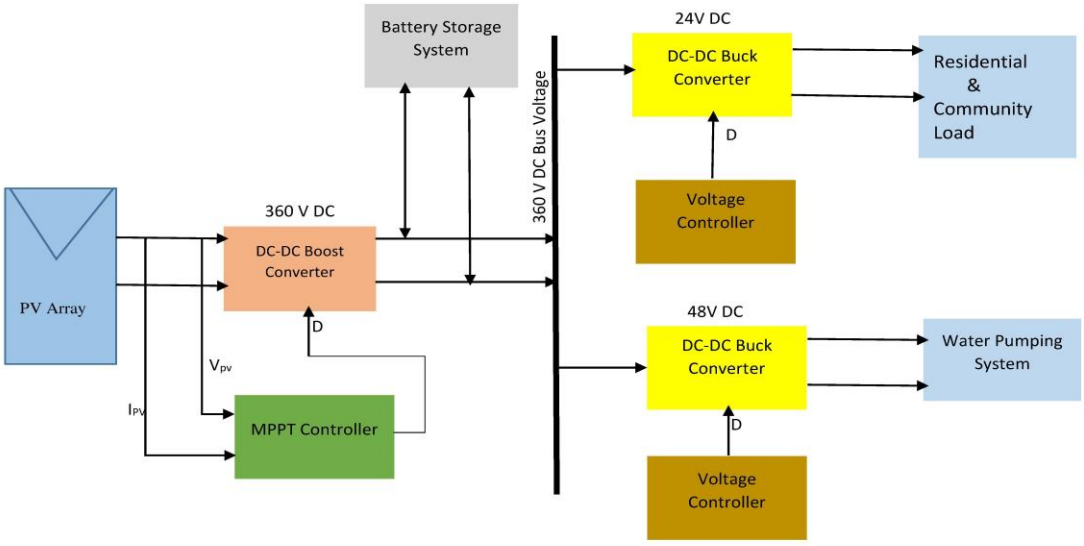

Figure 3. 5. Block Diagram of the proposed DC microgrid

3.5.1 Solar PV Model

The sample model of the PV module comprises a photocurrent source, a diode and some internal resistance connected as shown in Figure 3.6.

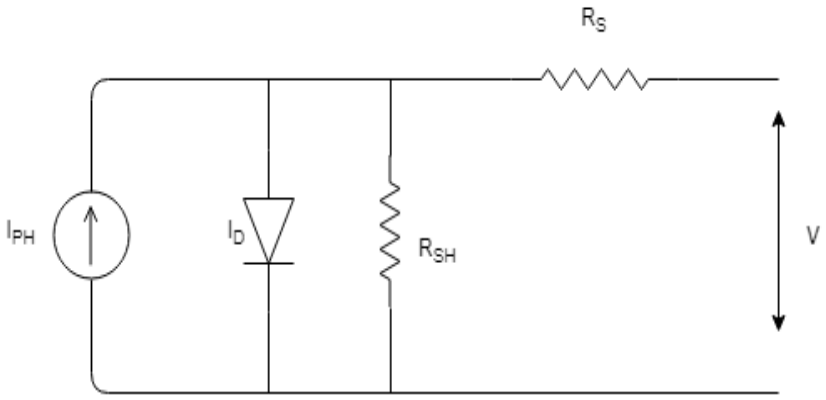

Figure 3. 6. Model of a Solar PV module

The current obtained from the PV module is given by:

$$I = I_{PH} - I_D = I_{PH} - I_O\left(exp\left[\frac{e(V+IR_S)}{KT_C}\right] - 1\right) - \frac{V+IR_S}{R_{SH}} \qquad (3.6)$$

Also, for low internal power dissipation, it is important to note that shunt or parallel resistors will be of larger value that the load resistance [2] which therefore can lead to the negligence of the two resistances to obtain the current (I) as the difference between the photo current (I_{PH}) and the diode current I_D as shown in equation 3.7.

$$I = I_{PH} - I_D = I_{PH} - I_O\left(exp\left[\frac{eV}{KT_O}\right] - 1\right) \quad (3.7)$$

Where: k= Boltzman Constant, T_c= Absolute Cell Temperature, e= electronic charge, V= Voltage across cell, I_O= Dark saturation current.

The fixed PV array has a minimum array size of 6.84kW. This PV array consists of 416 modules per string connected in series and 8 strings in parallel, resulting in 24 modules per array. Each 300W solar panel contains 72 PV cells connected in series. The parameters of the solar module employed in this study are shown in Table 3.4.

Table 3. 4: PV Module Electrical Specification

Electrical Specification	**Value**
Cells Per Module	72
Module Efficiency	15.21%
Power Output Tolerance	0/+3%
Maximum Power Voltage	37.5V
Maximum Power Current	8.00A
Open Circuit Voltage - V_{oc}	46V
Short Circuit Current	8.44A
Peak Power Watts - Pmax	300W

The I-V curve and P-V curves of the BOSH ENERGY c-Si M72 NA41126 300Wp panel under 400, 600, 800, and 1000 W/m^2 solar radiation are presented in Figure 3.7.

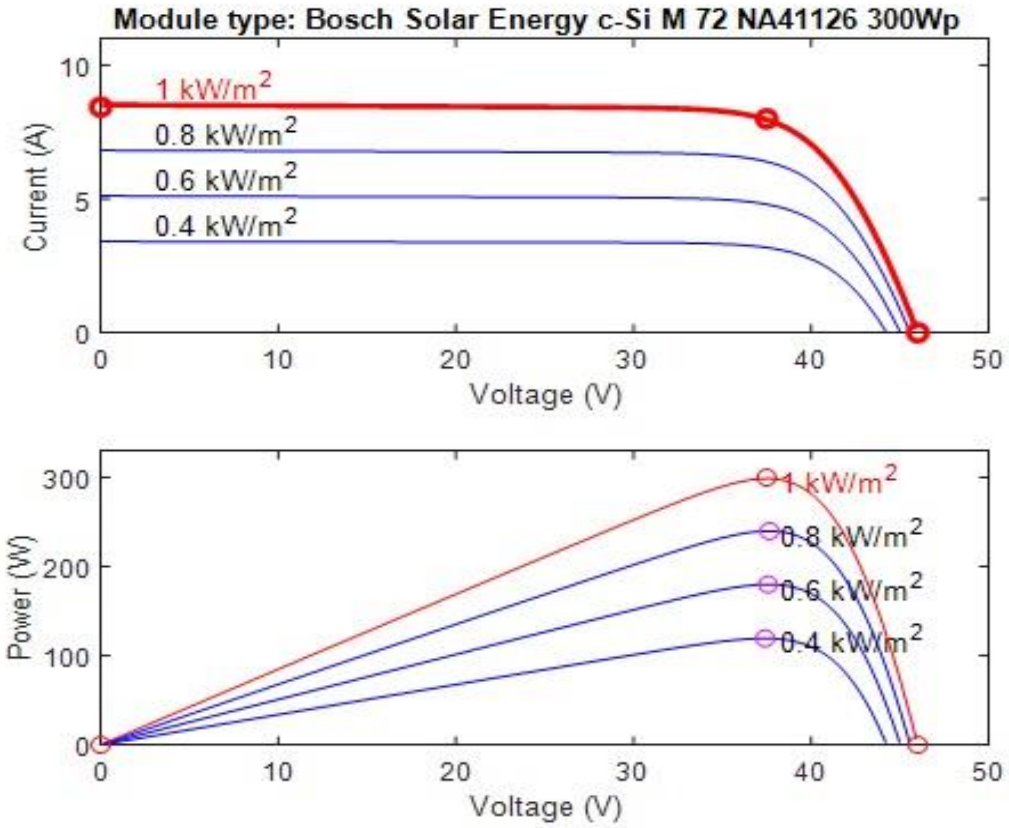

Figure 3. 7. I-V and PV curve of the 300W PV module

3.5.2 Battery Storage Design

The rate of discharge, depth of discharge, and temperature are the main factors that determine the life span and capacity of a battery storage system. In this paper, the Lead-Acid battery system is employed due to its simplicity and availability in the African market. Also, the Lead-Acid battery is more temperature tolerant and as a result, will function well in the hot temperature in Africa. Generally, in microgrids, battery systems are normally employed to supply energy needs to the loads at times of low energy generation from renewable energy sources. The battery storage system is also employed to smoothen voltage variations which occur as a result of the intermittent nature of the renewable energy sources. The specifications for the battery storage system are tabulated in Table 3.5.

Table 3. 5: DC microgrid Battery Storage Parameters

Electrical Specification	Value
Nominal Voltage (V)	360 V
Rated Capacity (Ah)	21,944 Ah
Maximum Capacity (Ah)	22,858.3 Ah
Initial state of Charge (%)	70%
Cut off Voltage (V)	270 V
Capacity at Nominal Voltage (Ah)	6,808.7Ah

3.5.3 DC-DC Boost Converter

The DC-DC boost converter has the function of stabilization and step up (boost) of the unregulated voltage that is obtained from the PV system. In this microgrid, the DC-DC boost converter steps up the PV voltage to the 360V bus voltage as needed for transmission and to charge the battery system. The equivalent circuit diagram of the boost converter is shown in Figure 3.8. As observed from the circuit diagram, the output voltage and current of the converter can be obtained from equations (3.8) and (3.9) respectively. From the stated mathematical expressions, it can be vividly observed that the converter output is affected by the duty cycle, D and the input. As a result, by variation of the duty cycle with the input being fixed, the output can be controlled.

$$V_O = \frac{1}{1-D} \times V_i \quad (3.8)$$

$$I_O = \frac{1}{1-D} \times I_i \quad (3.9)$$

Where: D = Converter duty Cycle, V_o = Output Voltage, V_i = Input Voltage, I_o and I_i = Currents

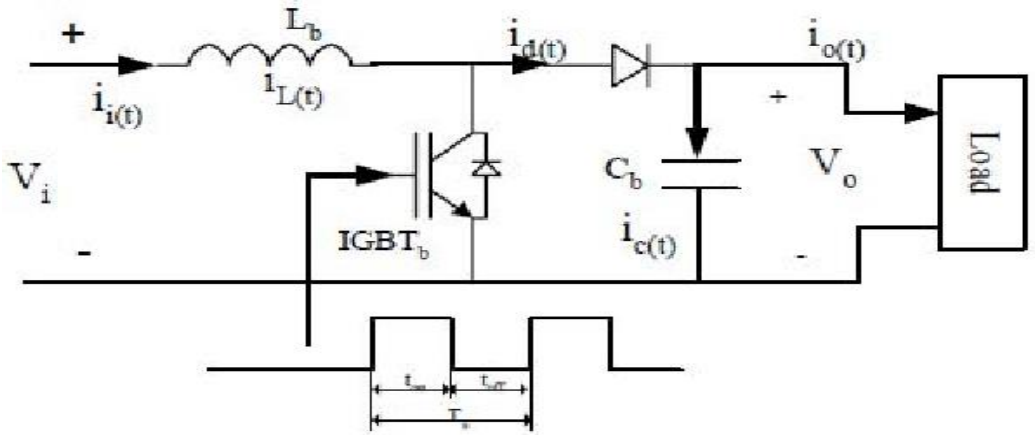

Figure 3. 8. DC-DC Boost Converter Circuit Diagram

3.5.4 DC-DC Buck Converter

The DC microgrid had different levels of voltage required for use at the load end, such as the residential buildings and the water pumping system. The DC-DC buck converter was employed to step down the voltage from the bus voltage to low voltages of 24VDC and 48VDC which are then fed to the homes and water pumping system respectively. The circuit diagram for the buck converter is shown in Figure 3.9.

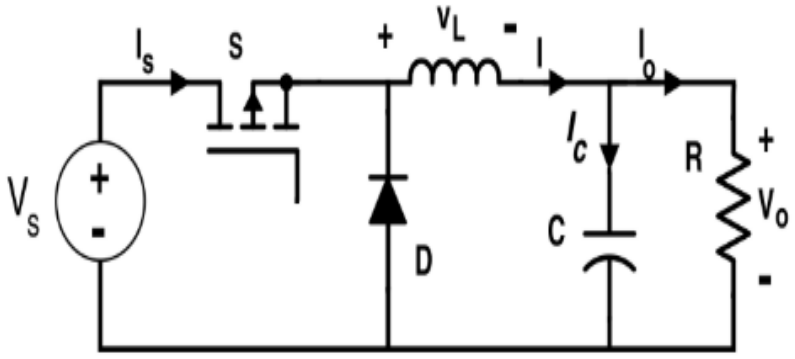

Figure 3. 9. DC-DC Buck converter

The output voltage of the DC-DC buck converter can be obtained using equations (5). Also, the buck converter is known to increase the current while stepping down the voltage.

$$V_O = D \times V_s \qquad (3.10)$$

Where: D = Converter duty Cycle, V_o = Output Voltage, V_s = Input Voltage.

3.5.5 MPPT Controller

The PV system works as shown on the I-V characteristics at every point an Operating Point (OP) which is highly dependent on the existing irradiance and temperature and this in turn affects the amount of power that can be extracted from the PV module. This, therefore, means that without any external control, the PV module will produce power only with direct effect from the variation in irradiance and temperature. Hence the intermittent nature of the power produced. Given the need to maintain maximum operating point at all times without effect from varying geographical conditions, an external system which is capable of tracking the various maximum points in the I-V characteristic curve will have to be employed. This system is defined as the Maximum Power Tracking System. Maximum Power Tracking can be achieved using various algorithms. In this paper, the Incremental Conductance MPPT algorithm is employed because of its efficiency and high level of accuracy over the usual Perturb and Observe algorithm [17]. The algorithm makes use of the voltage and current from the PV array as input to generate pulses which in turn are used to control DC-DC Boost converter duty cycle D. The Incremental Conductance algorithm is not affected by the solar module characteristics. This algorithm is illustrated by equations (3.11) and (3.12) and shown in Figure 3.10. The flowchart of the incremental Conductance MPPT algorithm is shown in Figure 3.11.

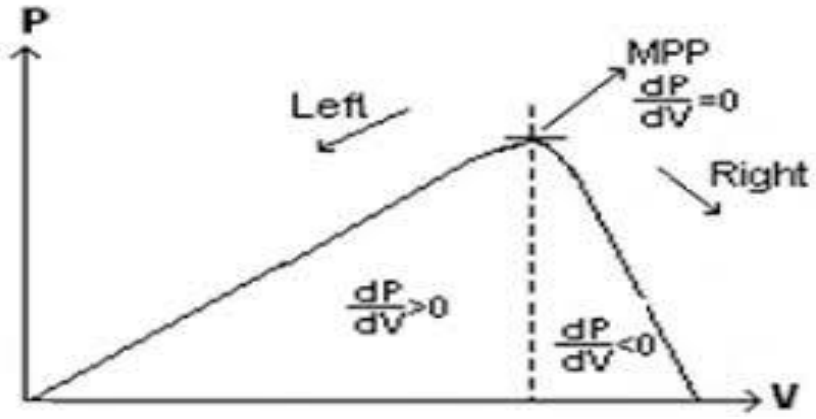

Figure 3. 10. Incremental Conductance MPPT

$$P = V \times I \tag{3.11}$$

$$\frac{dP}{dV} = \frac{d(V \times I)}{dV} = V \times \frac{dI}{dV} + I \tag{3.12}$$

Where: P= Power, V= Voltage, I= Current, dI/dV = Conductance. At MPPT, dI/dV or dP/dV must be equal to zero (0).

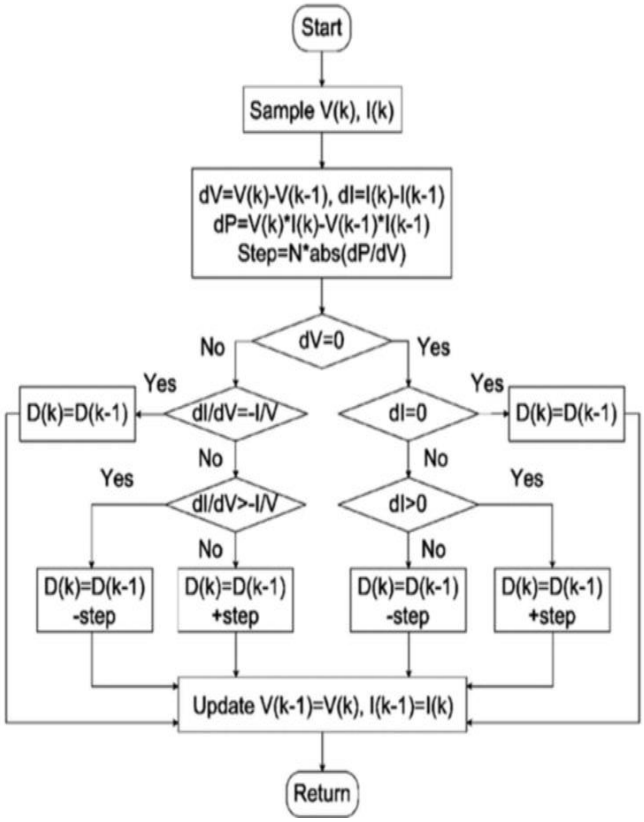

Figure 3. 11. Incremental Conductance MPPT Flow Chat

3.5.6 Voltage Mode Controller

The buck converter output voltage can be quite easily affected by variations from the system parameters [18]. Hence, the need for a control system which can maintain constant voltage notwithstanding any system distortion. In this paper, the voltage mode controller was applied to the proposed system. This is due to the robustness of the system and its ease of application [18]. The voltage mode controller is shown in Figure 3.12. Here, the DC voltage from the Boost Converter is detected and compared with the set reference voltage. Any

observed error is sent back to the PI controller as feedback which is applied to produce a constant voltage that is very close to the reference voltage. The voltage controller carries out this function continuously, to keep the DC voltage constant.

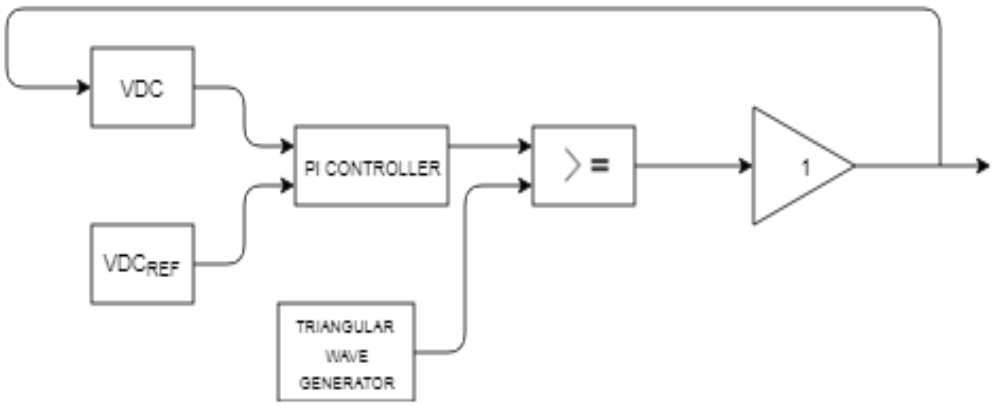

Figure 3. 12. The Voltage Control Block

3.6 Dynamic Simulation of The Proposed DC Microgrid on Simulink

Dynamic simulation is a very important step in the design and optimization of any system. For power systems, the dynamic simulation is carried out to observe the instantaneous and timely behavior of the system under study. This is to observe the dynamic behavior of the proposed system given the power quality, voltage stability, and load variation effects. The proposed DC microgrid was simulated in MATLAB/SIMULINK under various geographic and electrical conditions which are particular to the Umuokpo community. Parameters for the simulation were obtained from the various datasheets of the selected components. Due to the high number of homes in the community, it will not be very feasible to simulate 800 houses on the software. Therefore, for clarity, all houses were assumed to have the same power requirements. Three houses were simulated on SIMULINK and the water pumping system, which was operating on a different voltage level was also modeled in a different branch. The rest of the community load was also simulated on another branch. The loads were represented in SIMULINK with resistor values that correspond to the power requirement of each load, and hence the current behavior was also observed. Although the last branch which

is a combination of all other load had a very large amount of current, it was included for simulation purposes only, but will be separated accordingly during physical development.

The overall MATLAB/SIMULINK model of the DC microgrid is shown in the Appendix C.

3.6.1 Dynamic Simulation Results

The overall Simulink model of the proposed DC microgrid was simulated on MATLAB/SIMULINK for 1 minute, and the following important results were observed as shown from Figures 3.13 to 3.17.

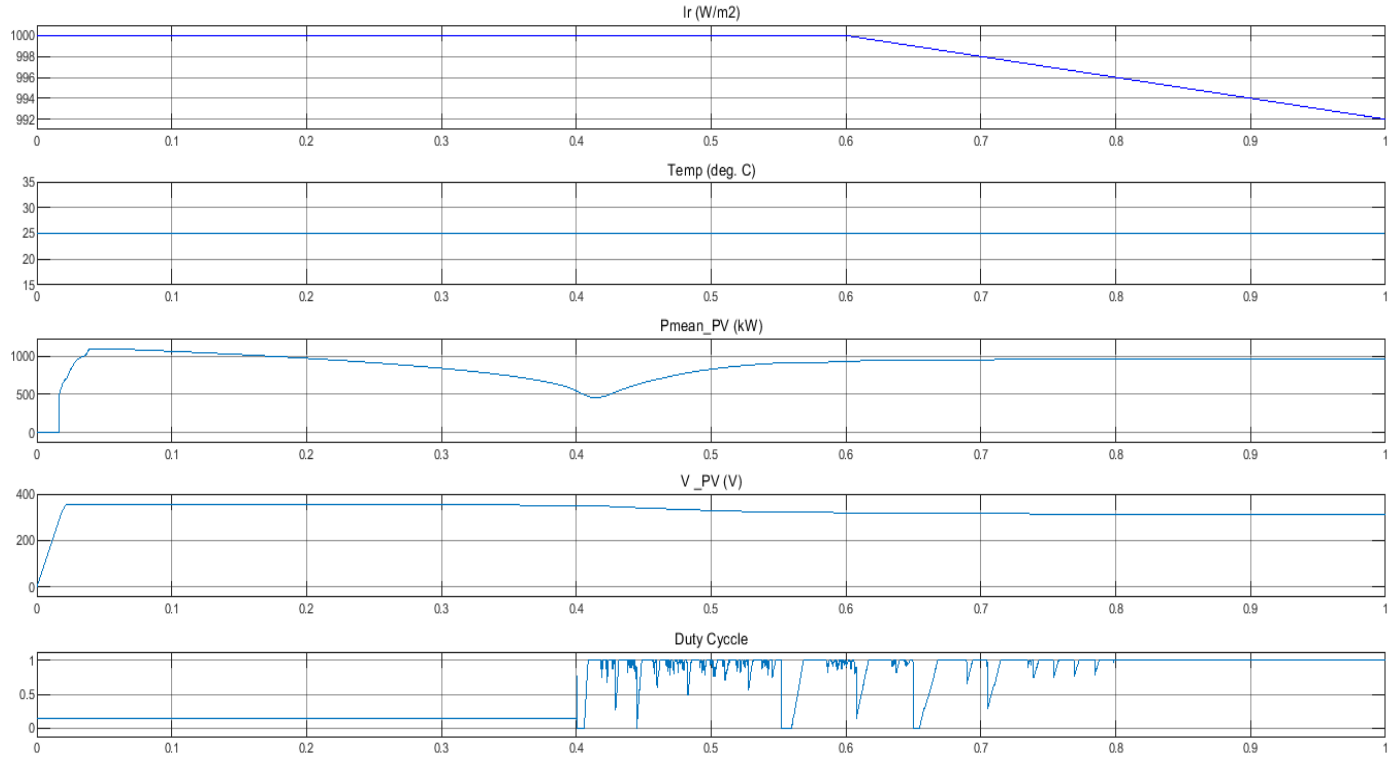

Figure 3. 13. Solar Irradiance, Temperature, Generated Power,Voltage and Duty Cycle of DC microgrid

Figure 3.13 shows the solar irradiance and temperature at which the PV system is being operated. Also, the figure shows the PV generated power, which shows its value as very close to the power of 1000kW. Furthermore, it depicts the continuous production of maximum power even with a decrease in the irradiance conditions, and this can be seen from the duty cycle plot with fluctuations. These fluctuations show that the MPPT control works continuously to keep power production at the maximum point. Figure 3.14 displays the

DC-DC boost converter output voltage. It shows that the output voltage from the PV system has been boosted to the system proposed 360VDC as bus voltage.

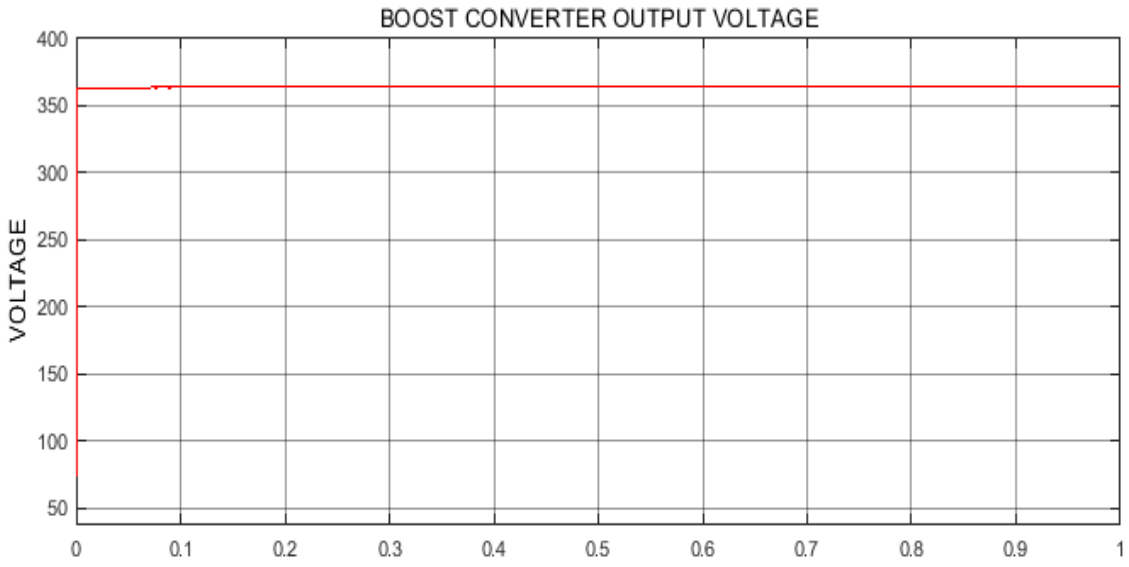

Figure 3. 14. DC-DC Boost Converter Output Voltage

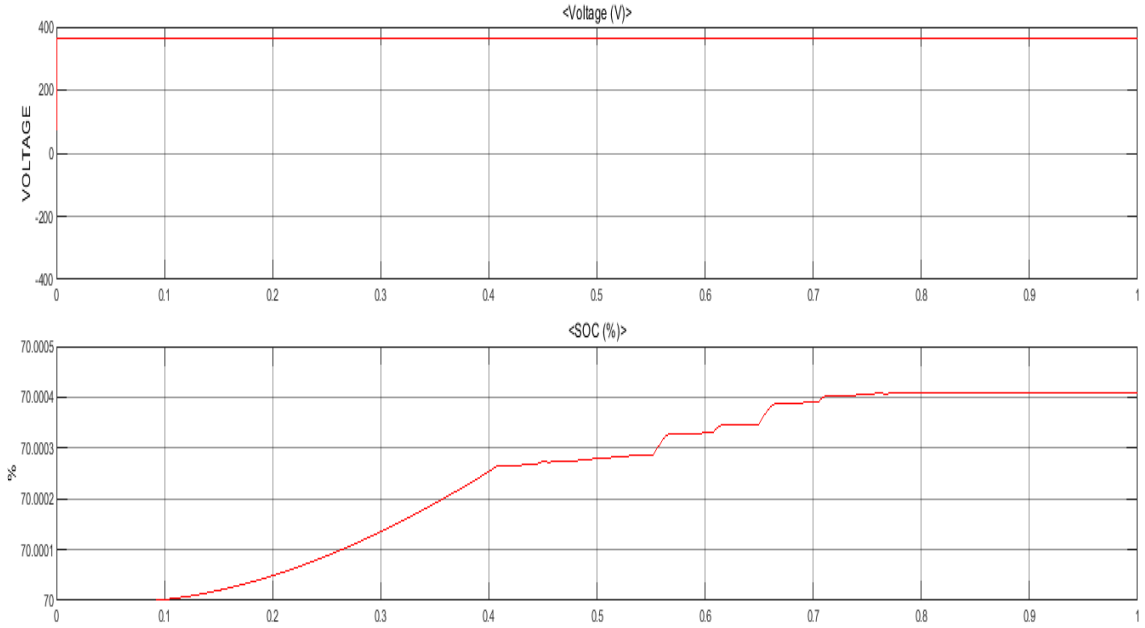

Figure 3. 15. Battery Voltage and State of Charge

Figure 3.15 depicts the battery storage system voltage, which is shown as 360V. This means that the battery system can supply power to the system with the system bus voltage. Also, the state of Charge of the battery

system is shown in the figure as it increases from an initial state of charge of 70% as stipulated in the simulation. This increase in the state of charge shows that the battery system is also being charged during the PV operation during the period of good irradiance.

Two load plots have been displayed in this work, as shown in Figures 3.16 and 3.17. Figure 3.16 depicts the load as connected to one residential home with voltage stepped down to 24V by the buck converter for domestic use. Also, the current was shown as displayed. The 24V was proposed for domestic use to accommodate even some high voltage devices in the home. Figure 3.17 shows the display of the community water pumping system, which had its voltage stepped down to 48VDC to satisfy the voltage requirement of the chosen water pumping device. The current was also shown in the display.

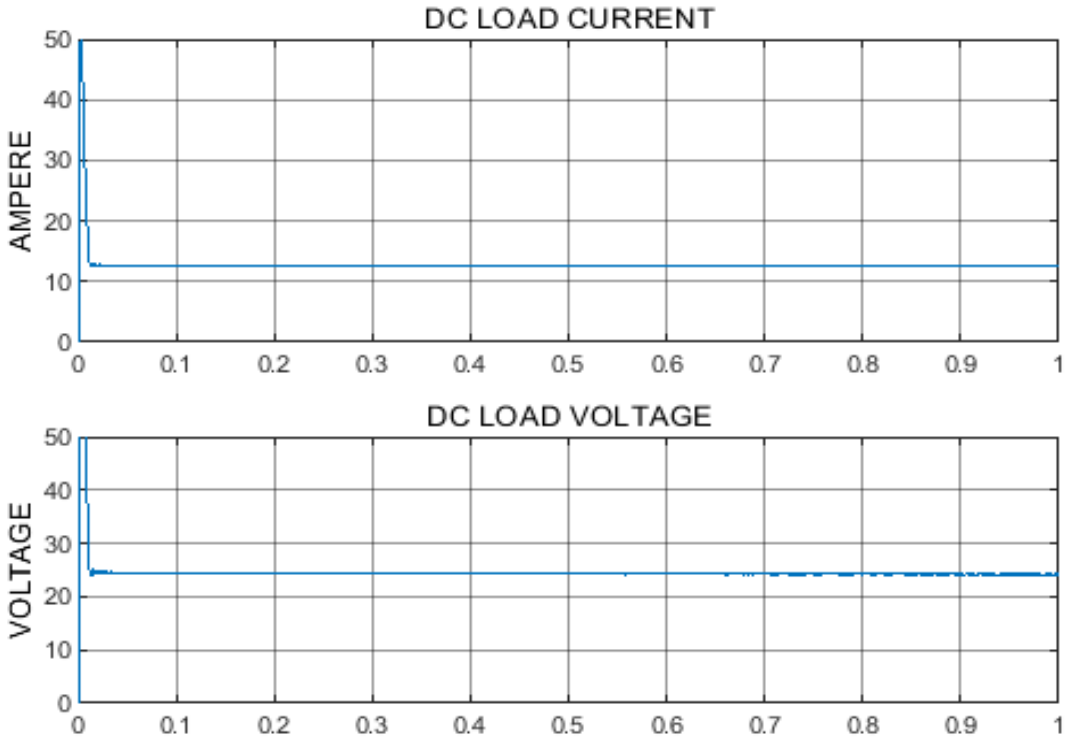

Figure 3. 16. Voltage and Current output for Residential house

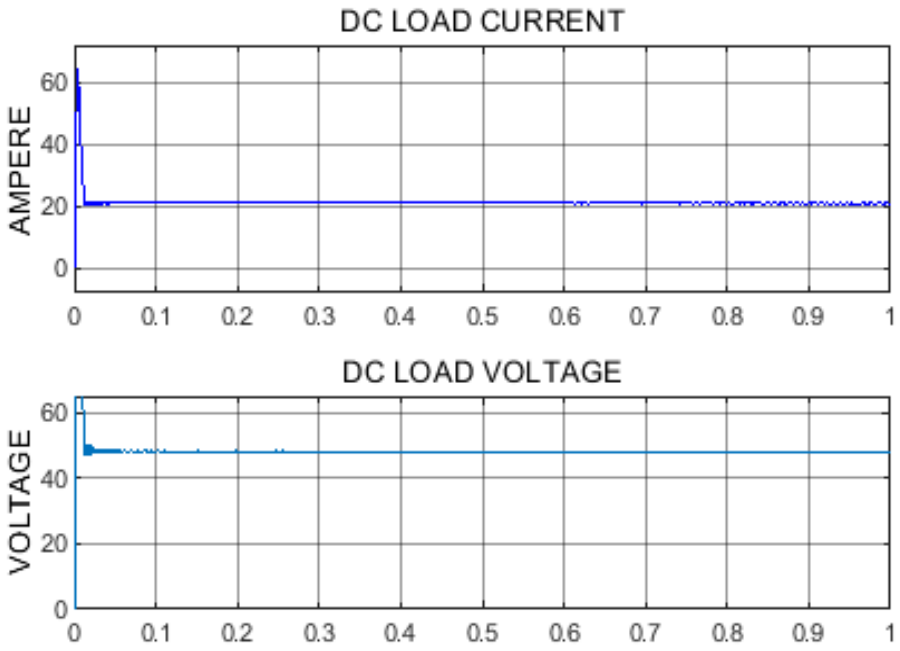

Figure 3. 17. The Voltage and Current Output for Water pumping facility

From all voltage displays, it will be observed that the voltages were of constant value, which depicts the proper functioning of the voltage mode controller to keep the load voltages at the desired voltage levels irrespective of any impact from the loads.

3.7 Future Work

In future, a comparison of the existing storage system which is Lead-acid battery and a storage system based on Ultra-capacitors can be carried out to observe the difference in behavior and ascertain which storage system is more suitable for the DC microgrid. Furthermore, a test-bed experiment will be carried out to observe the physical behavior of the systems for real-life testing.

3.8 Conclusion

This paper carried out the optimal modeling of a DC microgrid for Umuokpo Amumara, a remote community in Eastern Nigeria following the absence of grid electricity in the area since its existence. The optimal techno-economic modeling was carried out on HOMER Pro, considering the size of the community, location, and the

different facilities that exist in the community that require electrical energy as these parameters are of importance when proposing a power system for a specified location. Having known the energy requirements of the community **(3.16MWh/day),** the optimal power system which can meet the energy requirements of the community was obtained from HOMER Pro. To achieve this, the daily load profile of the community, solar and wind resource availability, the various components needed for the project such as the PV, wind turbine, and battery system were all imported into HOMER. In Homer, various simulations were run; to carry out the techno-economic feasibility of the system and this considered factors such as the system size and configuration, availability of the renewable energy resources and some economic factors such as life cycle of the system, net present cost, maintenance cost and annual operating cost for the system. The optimum system as proposed by the Homer simulation comprises of the PV, diesel generator that is strictly for backup and a battery storage system. To observe the near real-life behavior of the system with regards to transient reactions, the optimal system obtained from HOMER was simulated in MATLAB/SIMULINK. In the simulation, the power quality, voltage stability, and load impact were observed. The outputs obtained from the simulation such as the constant voltage, the maximum power operation and charging of the battery system depicted a very functional and feasibly independent power system that can stand as a solution to the long period the community has existed without electricity as it can comfortably meet its energy requirements.

3.9 References

[1] L. SHAVER, "Implementation of a DC Microgrid", Master of Science, University of Wisconsin-Madison, 2017.

[2] A. Elsayed, A. Mohamed and O. Mohammed, "DC microgrids and distribution systems: An overview", *Electric Power Systems Research*, vol. 119, pp. 407-417, 2015.

[3] S. -H. Ryu, J. -H. Ahn, B. -K. Lee and K. -S. Cho, "Single-switch ZVZCS quasi-resonant CLL isolated DC-DC converter for low-power 32″ LCD TV," *2013 IEEE Energy Conversion Congress and Exposition*, 2013, pp. 4887-4893.

[4] B. A. Thomas, "Edison revisited: Impact of DC distribution on the cost of LED lighting and distributed generation," *2010 Twenty-Fifth Annual IEEE Applied Power Electronics Conference and Exposition (APEC)*, 2010, pp. 588-593, doi: 10.1109/APEC.2010.5433612.

[5] K. Vijayaragavan, "Feasibility of DC Microgrids for Rural Electrification", Masters, Dalarna University Solar Energy Engineering, 2017.

[6] D. Kumar, F. Zare and A. Ghosh, "DC Microgrid Technology: System Architectures, AC Grid Interfaces, Grounding Schemes, Power Quality, Communication Networks, Applications, and Standardizations Aspects," in *IEEE Access*, vol. 5, pp. 12230-12256, 2017.

[7] R. Kaur, V. Krishnasamy and N. Kandasamy, "Optimal sizing of wind–PV-based DC microgrid for telecom power supply in remote areas", *IET Renewable Power Generation*, vol. 12, no. 7, pp. 859-866, 2018.

[8] M. Hamza, M. Shehroz, S. Fazal, M. Nasir and H. Khan, "Design and analysis of solar PV based low-power low-voltage DC microgrid architectures for rural electrification", *2017 IEEE Power & Energy Society General Meeting*, 2017.

[9] H. De Zoysa, P. Guruge, S. Kalingamudali, N. Kularatna and G. Kanishka, "Designing and constructing a DC microgrid with uninterrupted power supply capability and optimizing its energy usage by smart controlling system", *2018 IEEE International Conference on Industrial Electronics for Sustainable Energy Systems (IESES)*, 2018.

[10] V. Webb, "Design of a 380 V/24 V DC Micro-Grid for Residential DC Distribution", Master's Degree, The University of Toledo, 2013.

[11] B. Ramesh Naidu, G. Panda and P. Siano, "A Self-Reliant DC microgrid: Sizing, Control, Adaptive Dynamic Power Management and Experimental Analysis", *IEEE Transactions on Industrial Informatics*, pp. 1-1, 2017.

[12] Z. Shuai, J. Fang, F. Ning and Z. Shen, "Hierarchical structure and bus voltage control of DC microgrid", *Renewable and Sustainable Energy Reviews*, vol. 82, pp. 3670-3682, 2018.

[13] T. Zhou and B. Francois, "Energy Management and Power Control of a Hybrid Active Wind Generator for Distributed Power Generation and Grid Integration," in *IEEE Transactions on Industrial Electronics*, vol. 58, no. 1, pp. 95-104, Jan. 2011.

[14] Y. Panov, J. Rajagopalan and F. C. Lee, "Analysis and design of N paralleled DC-DC converters with master-slave current-sharing control," *Proceedings of APEC 97 - Applied Power Electronics Conference*, 1997, pp. 436-442 vol.1.

[15] C. Li, J. C. Vasquez and J. M. Guerrero, "Multiagent-based distributed control for operation cost minimization of droop-controlled DC microgrid using incremental cost consensus," *IECON 2015 - 41st Annual Conference of the IEEE Industrial Electronics Society*, 2015, pp. 005202-005205.

[16] G. Zhang, C. Li, D. Qi and H. Xin, "Distributed Estimation and Secondary Control of Autonomous Microgrid," in *IEEE Transactions on Power Systems*, vol. 32, no. 2, pp. 989-998, March 2017.

[17] S. Peake, *Renewable Energy*, 4th ed. Milton Keynes: Oxford University Press, 2017.

[18] K. Dubey and M. T. Shah, "Design and simulation of Solar PV system," *2016 International Conference on Automatic Control and Dynamic Optimization Techniques (ICACDOT)*, 2016, pp. 568-573.

Chapter 4

LoRa-based communication system for data transfer in microgrids

Co-authorship Statement

Chapter 4 presents the proposal of LoRa communication technology for data transfer within the microgrid. This work focused on the employment of LoRa for secondary level data transfer in hierarchical microgrids. The proposed system in this work focuses on the communication between the microgrid local controllers and the central controller for control purposes. The work showcased a proof-of-concept testbed experiment illustrating a one-way communication ability of LoRa to send measurements between the LoRa nodes and the gateway. This work also showed data coverage range of LoRa showing experimentally that LoRa has a good data coverage.

I (Ndukwe Cherechi Izuchukwu) am the principal author and contributed to Conceptualization, Methodology, Software Investigation, Writing- Original Draft and Editing of this chapter. Lawrence Aghenta contributed to the Experimental Setup of the work. Dr. Tariq Iqbal, Dr X. Liang and Dr. Jahangir Khan also contributed to the conceptualization and methodology of the research. The supervisors supervised the entire chapter, reviewed and corrected the research manuscript.

The work in this Chapter has been published in the **AIMS Electronics and Electrical Engineering,** 4(3): Pages 303–325. DOI: 10.3934/ElectrEng.2020.3.303.

Abstract

This paper proposes a LoRa-based wireless communication system for data transfer in microgrids. The proposed system allows connection of multiple sensors to the LoRa transceivers and enables data collection from various units within a microgrid. The proposed system focuses on communications at the secondary

communication level of the microgrid between local controllers of each distributed generation (DG) unit and the microgrid central controller due to the possibility of applying low-bandwidth communication systems at this level. In a proof-of-concept test bed setup, the data collected by the sensors are sent to the LoRa gateway, which serves as the central monitoring system from which control messages are sent to various microgrid components through their local controllers such as DG units, storage systems and load. In this work, to improve communication security, a private server has been developed using Node-Red instead of cloud servers that are currently used in most Internet-of-Things (IoT) monitoring systems. A range test of the proposed system is carried out to observe the rate of data delivery. It demonstrated over 90% data delivery at 4 km. Finally, a test bed experiment is conducted to validate key features of the proposed system by achieving one-directional data transfer in a grid monitoring system.

Keywords: communication system; data transfer; Internet of Things (IoT); LoRa technology; microgrids; Node-Red; private server

4.1 Introduction

Renewable energy-based microgrids with distributed energy resources (DERs), such as wind and solar generation, can operate at either grid-connected or islanded mode [1,2]. In the grid-connected mode, the grid defines the microgrid's voltage and frequency, hence the DERs are controlled to produce the desired amount of power [2]. In the islanded mode, the DERs are not only required to supply the microgrid's load demand, but also to regulate the distribution feeder's voltage and frequency within acceptable limits [3,4]. Isolated microgrids without grid connection in remote communities permanently operate in islanded mode. To achieve proper control and operation of a microgrid, each DG unit should be updated with information pertaining to the microgrid's operating mode [5]. This entails real-time power measurement of the grid, loads, and DGs as well as the state of charge (SoC) of battery storage systems [6]. The RMS value, phase angle, and frequency of the voltage, active and reactive power at specific points in the microgrid can also

serve as monitoring signals for the microgrid control systems [7]. Furthermore, instantaneous values of voltages at the DG terminals and the feeder are needed for synchronizing DG units within the microgrid [8]. It is expected that in the near future automated operation of microgrids can be achieved [9,10] by monitoring the system through various sensors, analyzing the collected sensor data and integrating the results into an advanced control scheme, and passing the control commands back to the nodes [11]. To achieve automation, a fast and reliable communication system for data and command transfer within the microgrid is a fundamental requirement [12]. Figure 4.1 shows a typical microgrid with advanced communication flow.

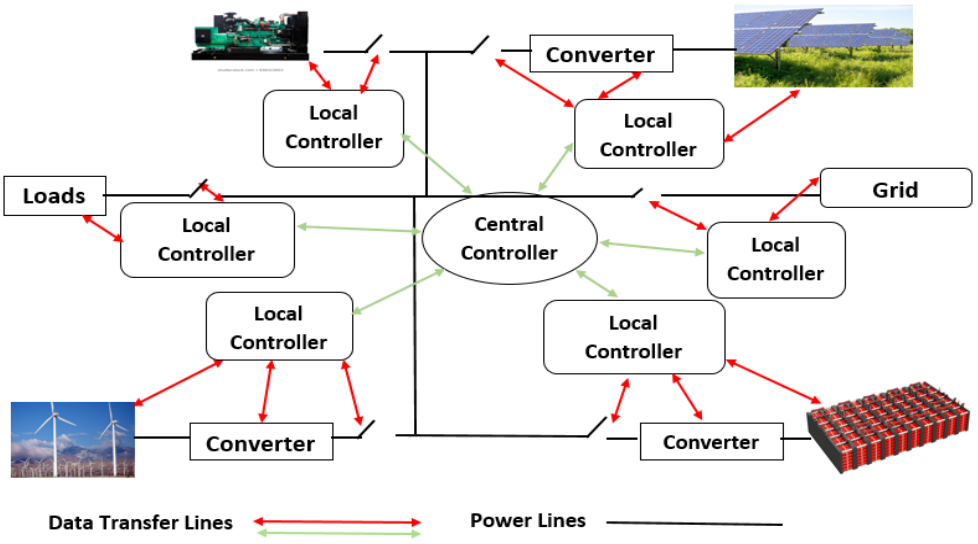

Figure 4. 1. A typical microgrid with advanced communication flow.

Communication technologies for microgrids can be categorized into wired and wireless: 1) the wired communication for data transfer within microgrids include ModBus, ProfiBus, power line communication and the Ethernet; 2) the major wireless communication technologies currently in use include Zig-Bee, Wi-Fi , WiMax and cellular. Table 1 shows the wireless communication systems currently employed for microgrid communication.

Table 4. 1: Wireless communication systems presently employed in microgrids.

Family	Data rate	Coverage	Advantages	Disadvantages
Zigbee	256 kbps	10-50 m	• Very low power consumption • Low cost equipment • Suitable for SCADA systems	• Low bandwidth • Do not scale to large networks
WiFi	Up to 54 Mbps	300m outdoors	• Low cost network deployments • High flexibility, suitable for different use cases	• High interference • High power consumption • Simple quality-of-service
WiMAX	Up to 100 Mbps	0-10 km	• Suitable for thousands of simultaneous users • Longer distance than Wi-Fi	• Complex network management • High cost of terminal equipment • Use of licensed spectrum
Cellular	14.4 Mbps – 500 Mbps	Up to 50 km	• Able to support tens of millions of devices • Low power consumption of terminal equipment • High flexibility suitable for different use cases. • Reduced interference	• High cost of usage (licensed spectrum) • High delay in transmission of data related to distance and number of users.

LoRa, also known as 'long-range' is an emerging communication technology, with applications in Internet of Things (IoT). Several examples of LoRa's application in various technical sectors are summarized as follows. In [13], a new architecture deploying LoRa was proposed for a large system monitoring, where the proposed system surpasses the need of existing gateways to enable much longer range of communication.

The application of LoRa in farming and agriculture was presented by researchers in [14], where LoRa devices were employed to transfer data from sensors used for monitoring cows to achieve better animal health and wellbeing. A LoRa-based sensor system is proposed in [15] for monitoring personnel in unfriendly work environments, and the sensor data are sent to the cloud through LoRa. This communication medium facilitates analysis and observation of the data and sends alerts when a problem is detected. In [16], a car diagnostic system is proposed using LoRa to communicate sensor data to a cloud for vehicle fault diagnosis. Ref. [17] presents LoRa's use in monitoring patients with mental health issues.

The works reviewed above demonstrate various systems where LoRa technology has been applied for communication and data transfer. However, to date, to the best of the authors' knowledge, LoRa communication has not been applied for data transfer within microgrids. This paper is the first to apply LoRa for microgrid communication.

The motivations for proposing the LoRa-based communication system include: 1) low cost, 2) acceptable communication range, 3) low energy consumption, and 4) high possibility of using in remote areas where other forms of communication, such as the internet and cellular networks, do not exist.

The main objective of the proposed LoRa-based communication system in this paper is to achieve data transfer from the nodes to the private server through the gateway, which is a one-directional data transfer for the grid monitoring function.

The main contributions of this paper include:

1) Proposal, design and development of a novel LoRa-based data communication system for microgrids,
2) Range testing of the proposed communication system,
3) Hardware test bed implementation of the proposed communication system.

This paper is organized as follows: Section 2 presents a literature review; Section 3 reviews LoRa technology for use in microgrids; Section 4 presents the proposed LoRa based microgrid communication system; Section 5 describes the system implementation; Section 6 presents the experimental set-up and range test; Section 7

presents the results. Key features of the proposed system and discussions on the achieved results are presented in Section 8. Main conclusions and directions for future work are presented in Section 9.

4.2 Literature Review

4.2.1 Microgrid Communication Schemes and layers

Predominantly, two types of data communication schemes are presently applied in microgrids: (a) centralized (also known as hierarchical), and (b) distributed. In the centralized scheme, all data from DGs, energy storage systems (ESSs), and loads are transmitted to the microgrid central controller, where the data are processed, and control commands are then transmitted back to the DGs and ESSs. In a distributed scheme, the data from DGs, ESSs, and loads are transmitted to other DGs and ESSs, where the data are received and processed [18,19]. The centralized scheme is easy to implement and maintain [20,21]. However, it has drawback in scalability, requires complex communication networks, and is more prone to communication failure [21]. The distributed scheme offers more flexibility and is more robust from communication failure [22]. On the other hand, it requires a complex algorithm and a longer processing time, has less precision and a higher possibility of data collision [23]. Most communication technologies (wired or wireless) can be employed in centralized or distributed data schemes [24]. Simplified illustrations of centralized and distributed data communication schemes are shown in Figure 4.2.

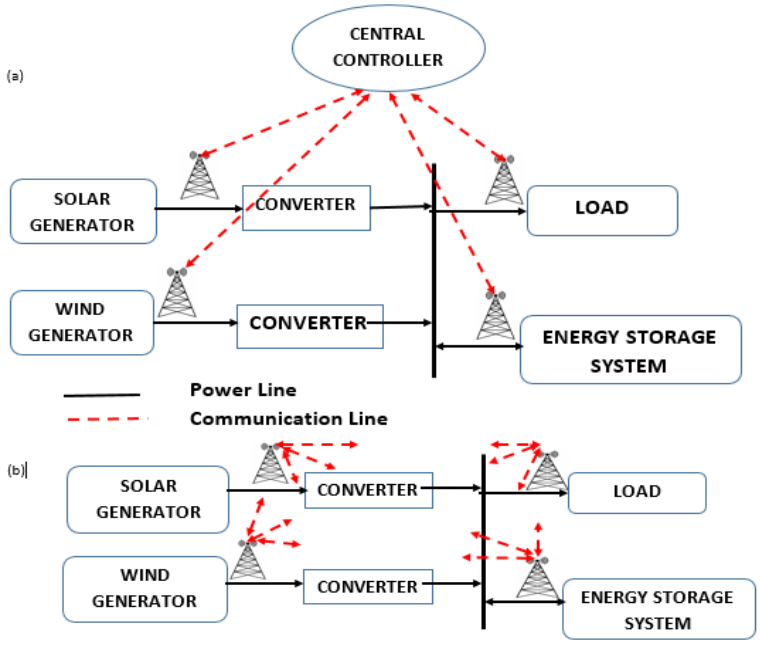

Figure 4. 2. Data communication schemes in microgrids: (a) centralized, and (b) distributed.

With full automation of microgrids in view, which would involve large number of sensors and actuators applied for monitoring and control, the microgrid communication can be classified into three levels [25] as shown in Figure 4.3.

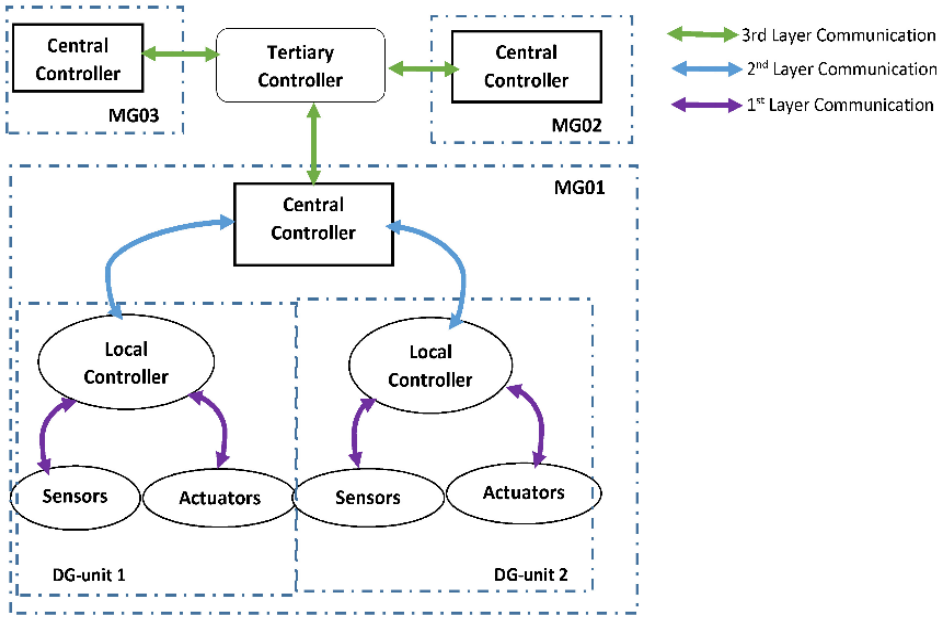

Figure 4. 3. Communication levels in a microgrid.

At the first (primary) level, the sensors are connected to a DG unit to be monitored and are also connected to the local controller for data collection through serial connection. This is feasible due to the proximity of the sensors, the local controller and the monitored DG units, ESSs and interfacing converters [25]. The second (secondary) level involves the communication between various local controllers situated in the DG units and the microgrid central controller. The secondary communication level is the main communication level of a microgrid [25]. At the secondary communication level, the communication requirement is primarily to send the sensor data (voltage and frequency), which are obtained from the sensors by local DG controllers, to the microgrid central controller. Control signals are sent from the microgrid central controller back to the DG unit's local controller for voltage and frequency control and stabilization. The microgrid circuit breaker status is also sent to the microgrid central controller during grid connection and isolation processes. Data to be transferred at the secondary communication layer can be formatted into packets that are generally in the bits size, and thus, the use of a reliable low-bandwidth communication system can handle the communication needs at this level. A bandwidth value of 1–100 kbps would be ideal for data transfer at the secondary communication level [44]. A detailed description of data transfer is shown in Figure 4.4, where the green and red dotted lines depict the status and control command communications, respectively, between the microgrid central controller and DG unit's local controllers. The third (tertiary) level for communication between networked microgrids requires higher data rates.

In this study, the proposed LoRa-based communication system is designed for the second control/communication level of the microgrids, transferring data between the local controllers on each DG unit and the central controller of microgrids, which enables parameter updates and control command signal transfer.

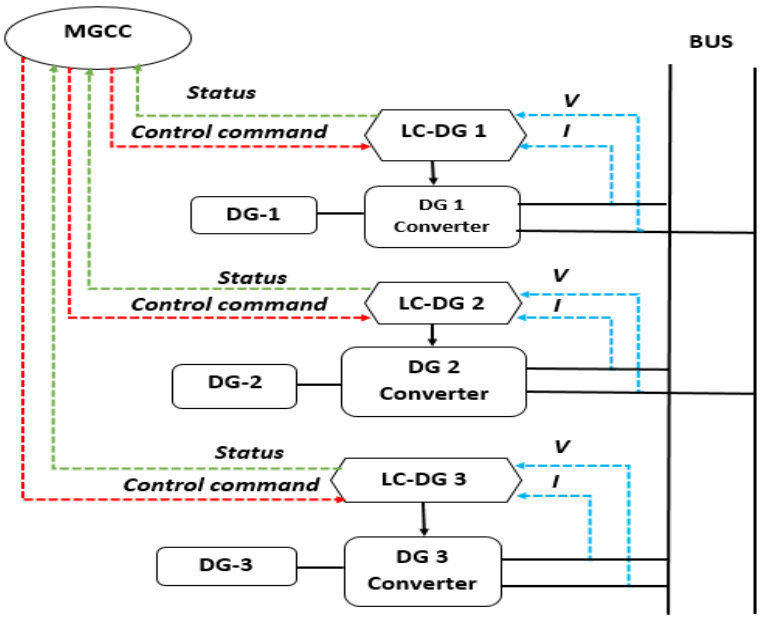

Figure 4. 4. Typical Description of the secondary communication layer of a microgrid.

4.2.2 LoRaWAN and LoRa Technology

The LoRaWAN protocol is a low power wide area network (LPWAN) designed for wireless connection of equipment to the internet [26] to achieve bi-directional communication between nodes and servers. A typical LoRaWAN architecture consists of various end-nodes connected to sensors, one or more gateways, and a minimum of one network server as shown in Figure 4.5. LoRaWAN is deployed in a star of stars topology where various nodes are connected to the gateway via LoRa links, and the gateway is connected to the network servers by IP networks [43].

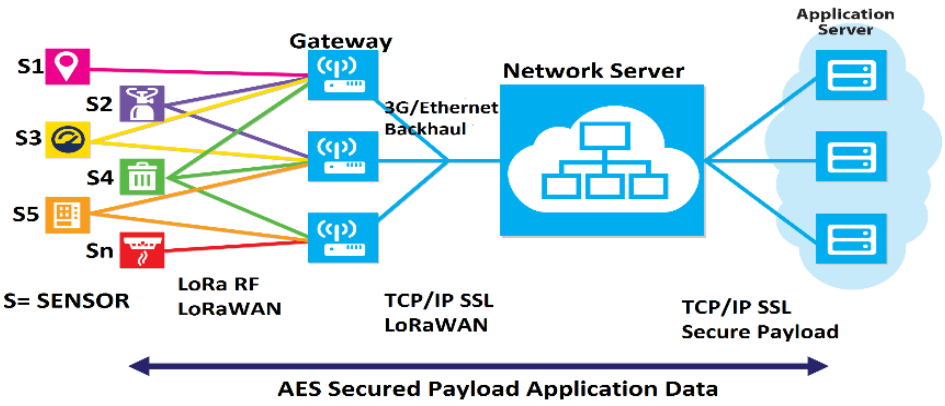

Figure 4. 5. Illustration of a typical LoRaWAN architecture [26].

The communication between nodes and the gateway is achieved by the Physical Layer LoRa communication system. The gateway functions more like a router that relays the data received from various nodes to the Server (Figure 4.5). A comparison of the LoRaWAN protocol to the Open System Interconnection (OSI) reference as shown in Figure 4.6 can serve as a better explanation of the LoRaWAN protocol.

LoRaWAN networks are differentiated from the classical TCP/IP communication through gateways and end-nodes [43]. The network server operates over the Transport Layer and controls the Media Access Control layer functions of the network [43]. LoRa, a physical layer technology, operates on the "Physical" layer L1 in Figure 6 with its main function as the "Application" layer L7 data transmission to the medium [43]. The OSI model's "Data link" layer L2 matches the LoRaWAN protocol, which defines secure medium access and end-node management strategies [43]. The end-nodes also have a function of energy conservation, which is at the "Application" layer L7 in the OSI model. Therefore, the end-nodes conduct functions at L1, L2, and L7 of the OSI model [43]. More details on LoRaWAN can be found in [26].

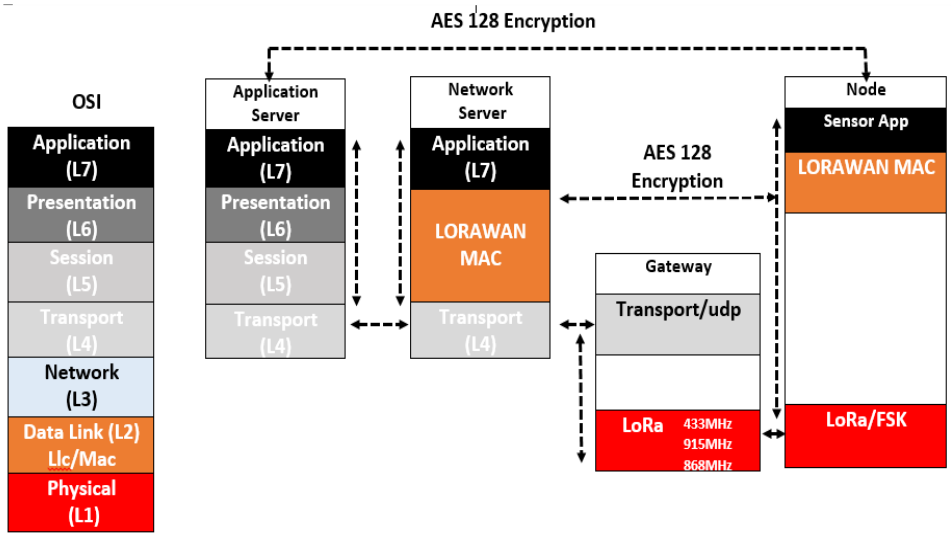

Figure 4. 6. Comparison of LoRaWAN to OSI model.

4.2.2.1 LoRa Physical Layer Communication

LoRa is the physical layer, or the wireless modulation used in creating a long-range communication link [26]. Most of the known wireless communication technologies use frequency shift keying (FSK) modulation at the physical layer [26] to achieve low power communication. LoRa, on the other hand, makes use of the Chirp Spread Spectrum Modulation (CSS) technique, which can achieve both low power and long-range communication. The chirp spread spectrum for message modulation works with chirps whose frequencies increase or decrease linearly over a certain amount of time [27]. LoRa operates in the free spectrum band (ISM), for example, at 868 MHz and 915 MHz band for Europe and USA, respectively [28]. It has a low data rate of up to 50 kbps [28], and bandwidth capabilities of 125 KHz, 250 KHz, and 500 KHz [29]. Conventionally, it uses a sweep tone, which increases (up chirp) or decreases (down chirp) in frequency over time for message encoding instead of the pseudorandom binary sequence used by the well-known direct sequence spread spectrum (DSSS) [30]. The modulation technique employed in LoRa spreads the message (signal) over a wide bandwidth, which makes it less affected by noise and interference [30]. Other low power communication systems do not have this feature by default. A LoRa transceiver can decode transmission 20 dB below the noise floor, making very long-distance communication at low power consumption possible.

Four important parameters control LoRa communication, which need to be well adjustable to achieve peak communication. These parameters are: 1) Transmission Power: is typically between 2 dBm and 14 dBm although it can be adjusted between –4 dBm and 20 dBm. This parameter has a direct impact on the system energy consumption and the range of the signal coverage [30]. 2) Spreading Factor (SF): is concerned with how many bits are encoded in each symbol, which can be set from 6 to 12. The range of signal and signal-to-noise-ratio are both increased by an increased spreading factor. However, it has a reducing effect on the transmission rate when the energy consumption is increased. 3) Bandwidth (BW): LoRa operates on the bandwidths of 125 KHz, 250 KHz and 500 KHz. 4) Coding Rate (CR): is the amount of forward error correction (FEC) that is applied to the message for protection against interference [30]. Therefore, an equation that states the transmission rate of the LoRa system is stated as follows:

$$TR = SF \times \frac{BW}{2^{SF}} \times CR \quad (4.1)$$

where, TR is Transmission Rate, SF is Spreading Factor, BW is Bandwidth, and CR is Coding Rate.

Ref [31] is the only literature that has investigated the enhancement of the Physical Layer scheme to solve the LoRa collision problems. Here an interleaved chirp spreading LoRa was devised to address LoRa's capacity limitations. In [32], a decoding algorithm to alleviate the impact of collision on the LoRa communication system is developed by employing a slight de-synchronization of the superimposed signals and specific features of the LoRa network. A full Media Access Control (MAC) protocol for collision resolution was also designed. The performance of LoRa was improved, which indicates that LoRa can be applied to even higher collision scenarios without any complications. The operation of the LoRa communication system was observed under Doppler effects in an experiment carried out in [33]. It showed that the LoRa modulation had high immunity to Doppler effects and can be used in satellite communication systems in orbits above 550 km with little or no restrictions. Ref. [34] proposes that LoRa's performance can be enhanced by applying message replication and using LoRa gateways with more diversified antennas. Furthermore, [35] states that the mass produced LoRa kits have also reduced the communication strength of the LoRa system. Therefore, a customized LoRa transceiver should be designed in order to achieve improved characteristics, such as increased sensitivity and improved immunity to interference. In the recent past the improvement in LoRa's scalability has been closely dependent on the variation of the Spreading Factor (SF) as mentioned in [36–39].

4.2.2.2 LoRa Software Implementation

LoRa communication is implemented on the software platform using open-source codes available on GitHub. Various forms of software codes are made available in GitHub for easy design of automation systems. This alone contributes greatly to the low-cost feature of the LoRa technology. The nodes are configured with various programming languages, such as C, C++ and Python. The nodes send processed sensor data to the gateway, through which the data can be forwarded to a network server.

4.3 LoRa Communication in Microgrids

LoRa is a fast-rising wireless communication technology. Its advantages over the existing wireless technologies make LoRa a suitable choice for communication applications in microgrids. Table 4.2 shows a comparison of the LoRa technology with other technologies already being used in microgrids. LoRa can be the most attractive technology for microgrid communication applications particularly in remote areas. For a complete LoRa communication system design, the three components (node, gateway and server) are important, which are briefly explained in the following subsections.

Table 4. 2: A comparison of LoRa and other wireless communication techniques for use in microgrids.

Specification	**LoRa**	**ZigBee**	**WiMAX**	**Bluetooth**	**Cellular**	**Wi-Fi**
Low cost of system components	X	X		X		
High interference immunity	X					
Long distance coverage	X					
Low power consumption	X	X		X		
Multipoint connection	X	X	X		X	X
High security	X	X	X			X
Sensor direct connectivity	X	X		X		
Expansion capability	X	X		X		X

4.3.1 LoRa Node

LoRa nodes are basically Semtech SX1276 transceivers that operate at the ISM frequency bands (868, 915, 433 MHz) of various regions of the globe. The nodes can send and receive data over the frequencies with capabilities to directly connect with sensors through microcontrollers, which makes them very reliable for communication. LoRa nodes can connect to many sensors, which are employed to measure various physical data such as voltage, current, temperature and pressure. There is one limitation that the LoRa node can only

communicate with a node that is set to the same frequency. In microgrids, the LoRa node will basically fit into the end-nodes that are connected to various DG units for data acquisition through sensors and microcontrollers. The acquired data is then sent out at a fixed frequency. A LoRa node has the capability to operate with open-source microcontrollers such as the Arduino Uno, Arduino Mega or ESP 32 to process the acquired data. There are three classes of LoRa nodes (Class A, B, and C) based on their capability of enabling bi-directional communication. Class C allows for a seamless bi-directional communication [26]. In this paper, this class of LoRa node is employed. The whole process of data acquisition and transmitting can be programmed on the end-node on the Arduino Integrated Development Environment (IDE) by coding.

4.3.2 LoRa Gateway

A LoRa gateway comprises a concentrator board with the capability to receive and forward LoRa packets (data received from the nodes) to the server. It also allows reverse communication from the server to the nodes for control purposes. A LoRa gateway can be described as a bridge between the sensors and the server. There are two types of LoRa gateways: single-channel and multi-channel. The multi-channel gateway has the ability to receive data at different frequencies. It is applied mostly to systems that require high amount of nodes operating at different frequencies. In microgrids, the LoRa gateway can be located at the microgrid central controller, where it can obtain the data sent in by various nodes connected to different DG units. Although the gateway has no data processing capabilities, it can collect all the data received from the nodes, and then relay to the server for processing.

4.3.3 LoRa Server

A server is a database with a user interface where the acquired data can be stored, processed and displayed to the user. In microgrids, the server serves as the central controller where the received data is processed, and control messages are sent back to the DG units.

4.4 The LoRa proposed communication system

In this paper, the proposed LoRa-based communication system consists of an IoT approach for transfer data. This involves the interaction between the LoRa communication devices and the sensors that are connected to various microgrid components for monitoring and transferring data. The sensors are programmed to obtain data from the monitored components. The data are processed and then sent by the LoRa nodes to the gateway. The gateway forwards these data to the server for processing. As stated earlier, the proposed system belongs to the second communication level. Figure 4.7 shows the full configuration of the proposed LoRa-based communication system for microgrid monitoring.

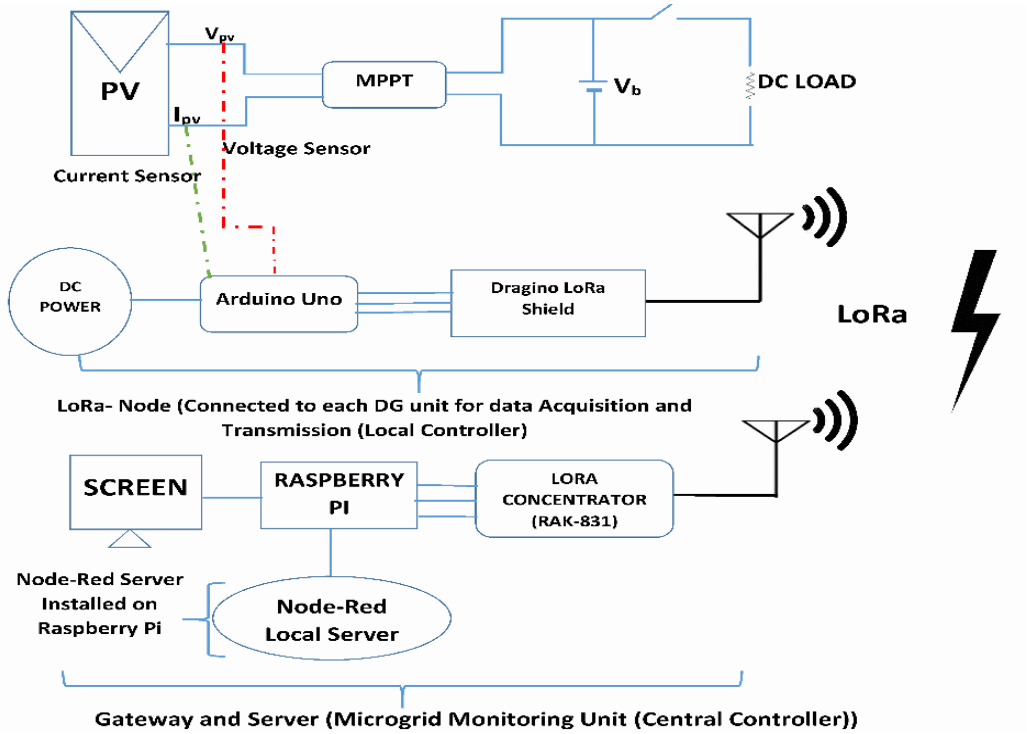

Figure 4. 7. Configuration of the proposed LoRa-based communication system.

In a practical microgrid, LoRa nodes can be connected to various local controllers. The system operation data for DG units, circuit breakers and battery storage are available at the local controllers. Such data can be transmitted by LoRa to the central controller of the microgrid. Command signals can also be sent back from the central controller to the local controllers using the proposed LoRa-based communication system.

4.5 Proposed system implementation methodology

To implement the proposed LoRa-based microgrid communication system, the sensors are connected to the Arduino Uno. The Arduino Uno unit is connected to the LoRa shield for data transmission. On initialization, the sensors read the monitored data, and the data are accessed by the Arduino through the connection pins, which are processed using modified open-source Arduino codes from the open-source coding platform (GitHub). The processed data is displayed on the serial monitor of the Arduino IDE. At this point, the values of the sensor readings are shown to confirm if the sensors had measured the correct values from the DG units. After the display and confirmation, the data is converted to LoRa packets for transmission using codes that are also integrated into the main processing program and uploaded to the board. The illustration of how a measured data is converted into LoRa packet format for transmission is shown in sub-section 4.5.2. The format for transmitting the data over LoRa is in Base64 format. Once in this format, the data can be transmitted to the gateway at the fixed allotted frequency for the sub-unit. This process is repeated continuously if the system is connected to the DG unit and is powered 'ON'. The flowchart for the operations for the node connected to the DG unit is shown in Figure 4.8.

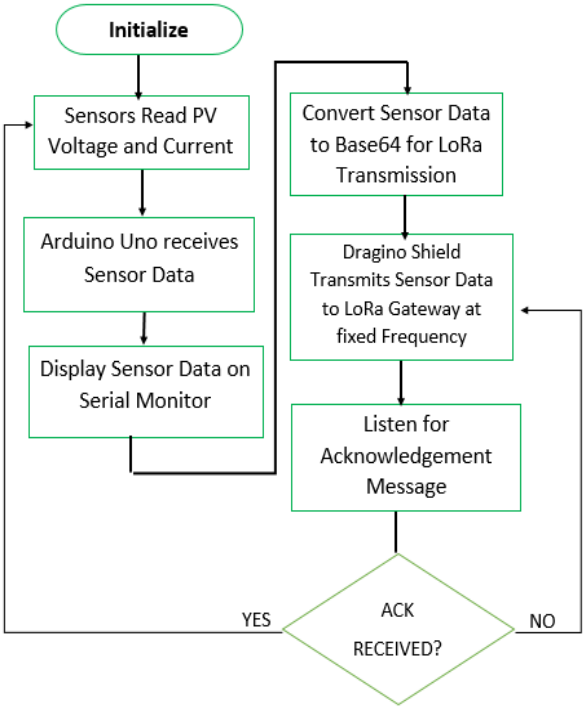

Figure 4. 8. LoRa node operation flow chart.

The gateway consists of a RAK831 concentrator module with multi-channel (8 channels) capabilities connected by the General-Purpose Input/Output (GPIO) pins to the Raspberry Pi that houses the local server. Once data arrives at the concentrator, it is forwarded to the server for processing. As stated earlier, the concentrator has no processing abilities but can pick up data that are sent by only designated nodes through a method called “frequency selection”. The RAK 831 concentrator is programmed to accept data packets arriving from devices that have been locked to its range of frequencies. The flow chart of the operation of the LoRa concentrator is shown in Figure 4.9.

The accepted data is then forwarded to the server through a designated port on the Raspberry Pi. Conventionally, in most IoT applications, web-based clouds, such as the Things Network, Thinger IO, Adafruit and LoRa Server, are used for monitoring. This requires monitoring from internet-enabled devices. This means that the data cannot be monitored without internet. Furthermore, the data is at a lower security level. In this work, the server was developed using Node-Red that was installed on the Raspberry Pi. This can be managed and viewed locally by authorized users. The main difference between the private server proposed in the paper and the cloud-based server is the absence of internet for data access in the private server. The advantage of the proposed private server is the data security. The private server is hosted on a hardware, which allows verification before someone can have access to the data received at the server. This makes the private server applicable to any system that requires a high level of data privacy.

At the server, the data is accessed at a designated port using the TCDUMP protocol. A java function code is written in the function node to extract the data, which contains the Base64 data. This node is also followed by a frequency dissection node (switching node) where the data is classified according to their frequencies. The data in each frequency is passed through a JSON block, where the data is changed to Base64 object. Then through a Base64 node, the data is converted back to human readable values. These values are then displayed on the server using the debug tool and can be further displayed on gauges and charts as shown in Figure 4.10. The Node-Red flows to attain this function is shown in Figure 4.11.

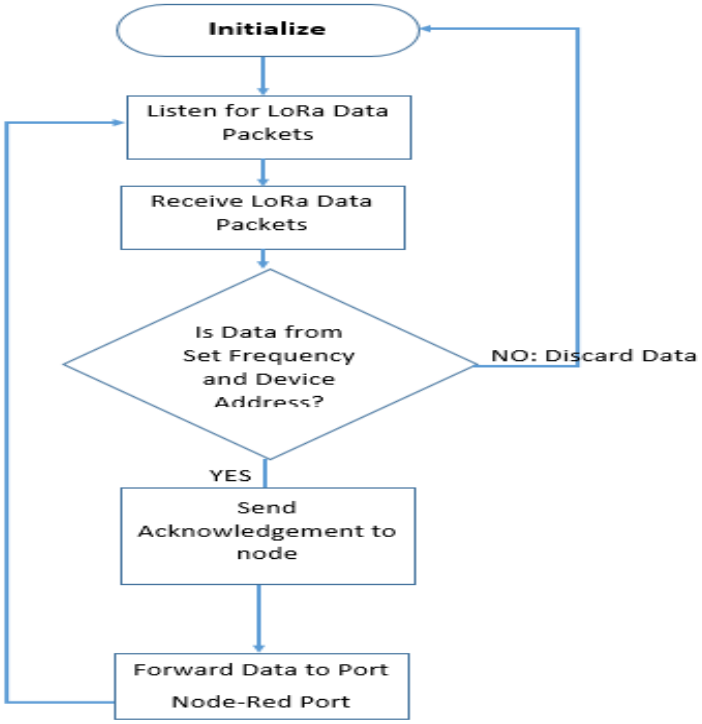

Figure 4. 9. LoRa gateway concentrator operational flow chart.

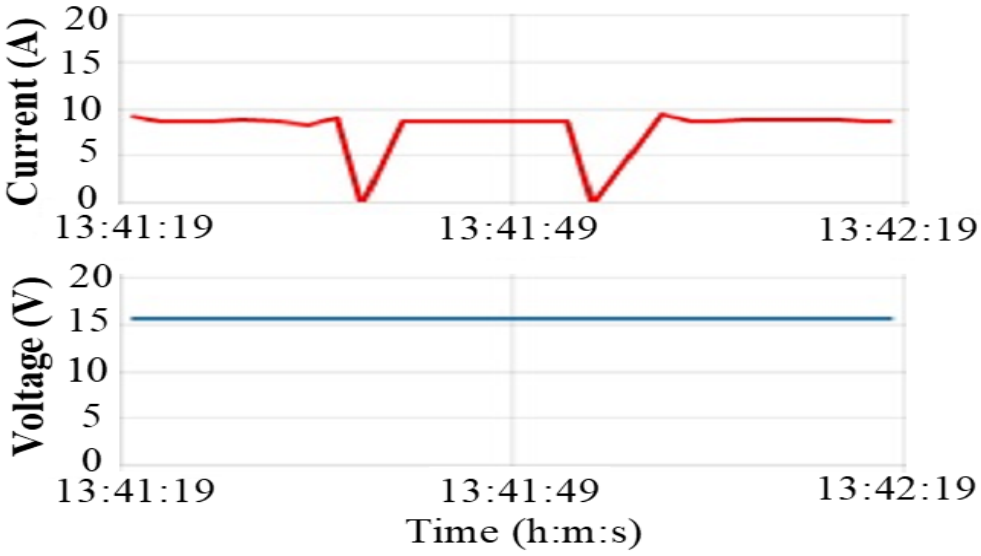

Figure 4. 10. Node-Red charts.

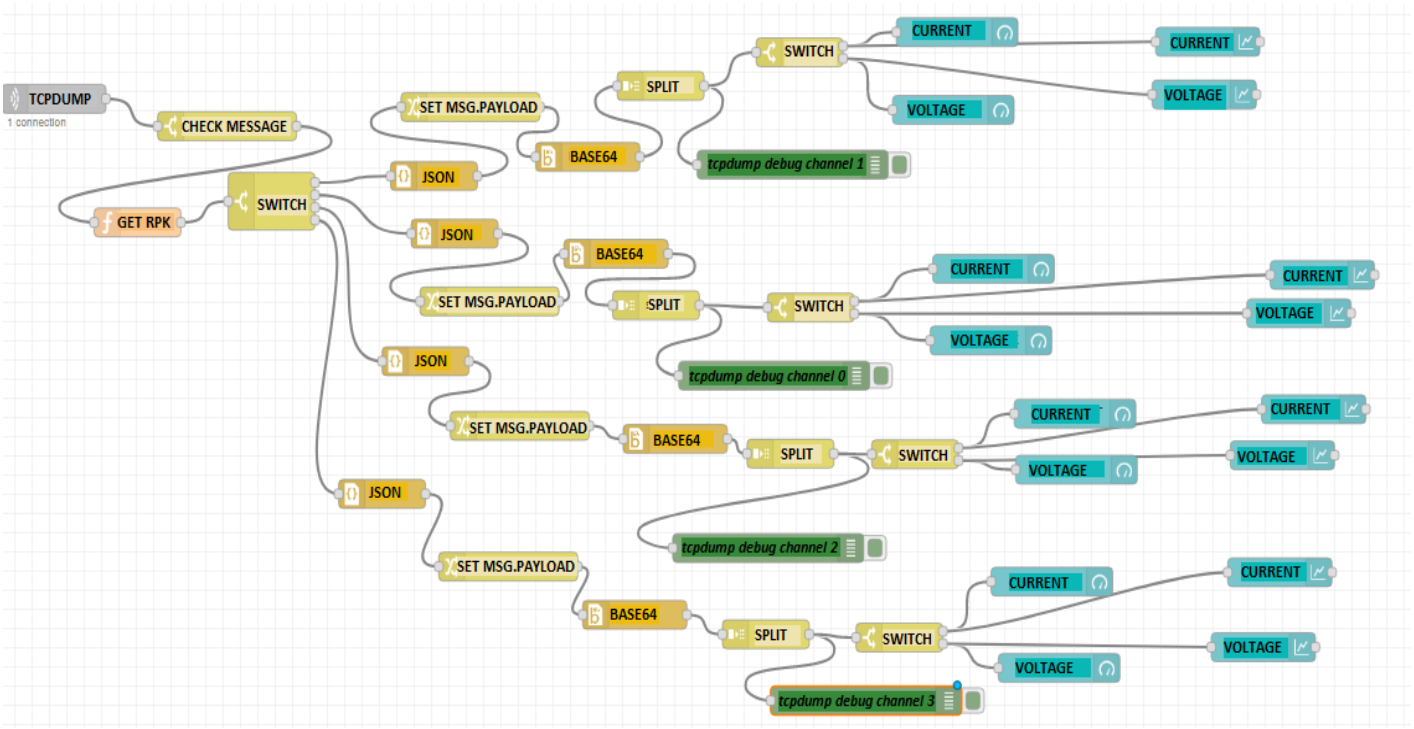

Figure 4. 11. Node-Red microgrid server flows.

4.5.1 LoRa data processing algorithm

The sensor data are transmitted using LoRa communication to the gateway terminal. The data being transmitted must be processed into the LoRa acceptable format before transmission. This format must conform to the required length and data size for appropriate transmission. LoRa uses the chirp spread spectrum as its mode of data modulation [26]. LoRa transfers the data in the Base64 format and the structure of a basic LoRa data frame is shown in Figure 4.12.

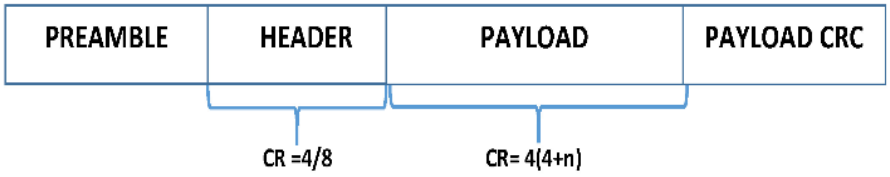

Figure 4. 12. Structure of a LoRa frame.

4.5.2 Base 64 encoding of a measured sensor value

Prior to transmission, the measured data are formatted into a LoRa transmittable data packet as illustrated using two examples. To encode the data in Base64, the following steps are followed:

1. The data is prepared in ASCII text format
2. The data is converted to ASCII binary format for each letter of the ASCII text
3. The binary codes obtained from Step 2) with 8-bits are joined together
4. The data is split into groups of 6-bit binary codes
5. The groups of six bits are converted back to decimal
6. Each obtained decimal value is matched with a Base64 symbol on the Base64 table where each decimal value between 0-63 has a matching symbol.

As an example, the steps of data conversion for a voltage sensor value of 210 V (as measured and converted for transmission), are shown in Figure 4.13.

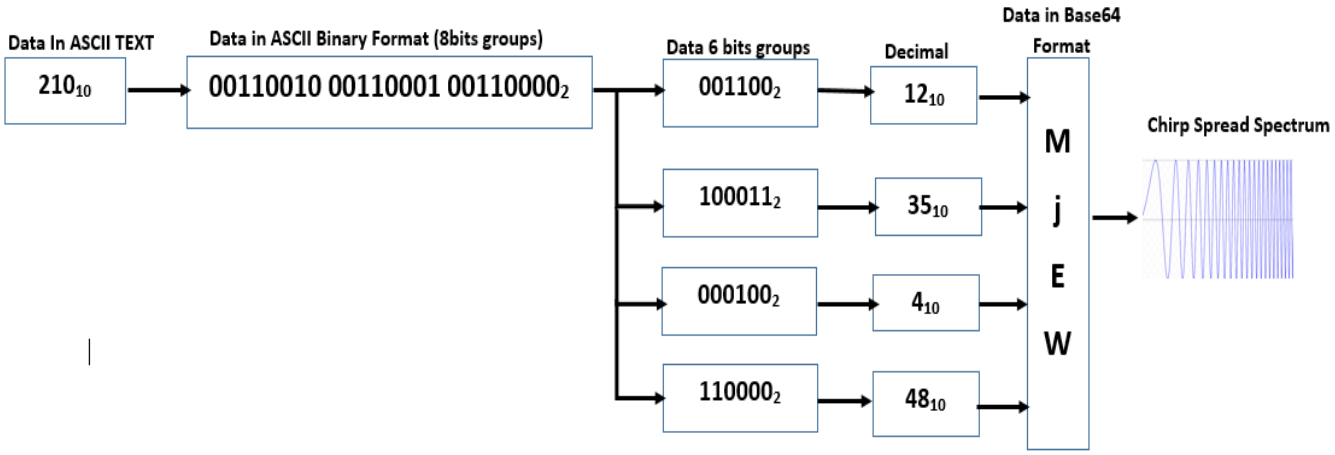

Figure 4. 13. Steps involved in encoding sensor value of 210 V in Base 64.

As shown in Figure 4.13, the voltage value of 210 V is transmitted over LoRa as a Base64 Symbol '**MjEw'.** Correspondingly, if the data is to be sent as a value specifically from a device on a particular DG unit, with specific details such as a voltage sensor connected to DG unit 2 on Channel 2 with device number 2, and measured voltage value of 210 V, the data to be transmitted is shown in Figure 4.14.

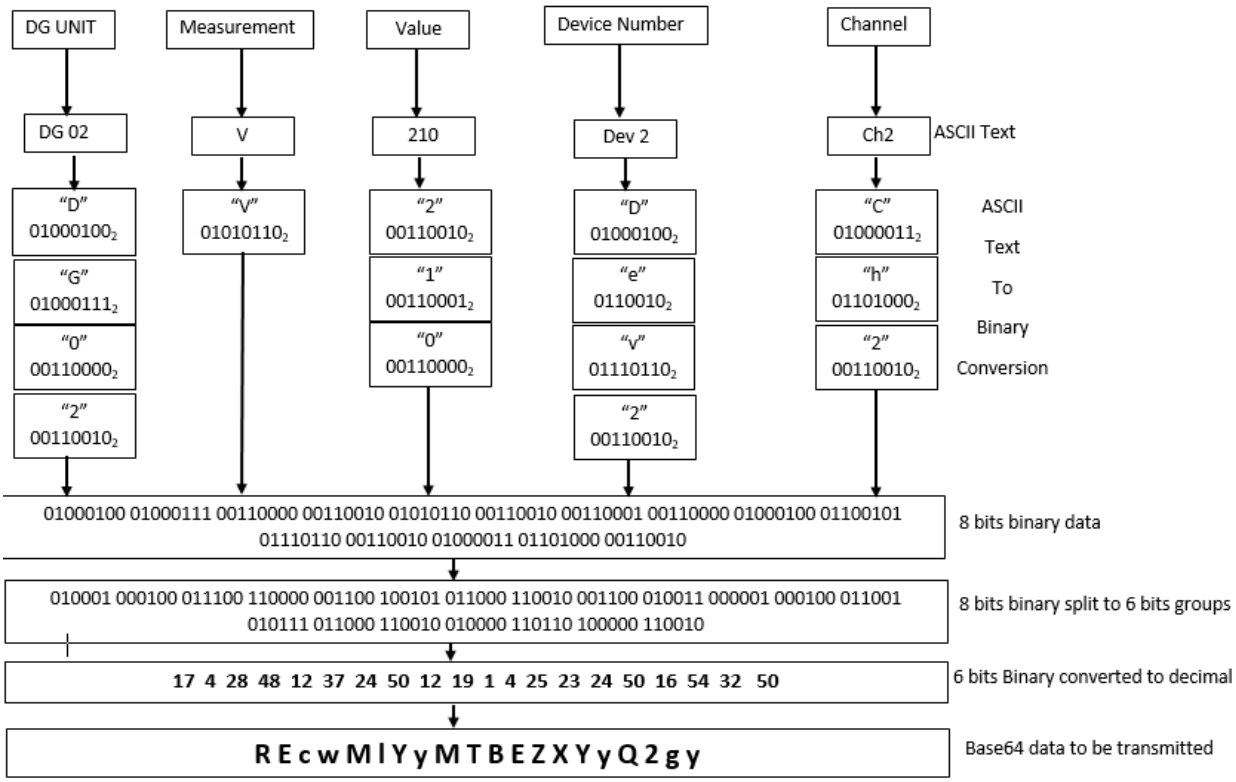

Figure 4. 14. Steps involved in encoding sensor value from a specific device in the microgrid.

The length of the data in Base64 format can be obtained by a relationship from the character length of the ASCII format. This is given as:

$$M_{L(BASE\ 64)} = \frac{4n}{3} \tag{4.2}$$

where, M_L is the Base64 message length, N is the length of ASCII text message. For instance, our data above in ASCII TEXT [DG02V210DEV2Ch2] has a length of 15 bytes.

$$M_{L(BASE\ 64)} = \frac{4\times15}{3} = 20\ bytes$$

Therefore, the Base64 encoded message will have 20 characters using the equation (4.2).

4.6 Experimental Test bed Setup

The proposed communication system was validated with a range test to confirm its maximum distance and accuracy of data transmission and reception. In this experiment, the LoRa gateway was placed at the top-most window on the Memorial University of Newfoundland (MUN) engineering building and kept stationary with power 'ON'. The node on the other hand was moved around in a car. Packet delivery was monitored at various distances as shown on the map in Figure 4.15.

Also, a test bed was set up in the Electrical Engineering Laboratory of MUN to observe the physical implementation of the proposed system. The laboratory houses a photovoltaic (PV) semi-microgrid consisting of 12 solar panels, which produces 130 W with 7.6 A at each panel. Two PV modules are connected in parallel to obtain 6 sets of PV systems with 260 W at about 14 A with a storage system. The system has a Maximum Power Point Tracking (MPPT) controller, which ensures maximum power production even during periods of unfavorable weather conditions.

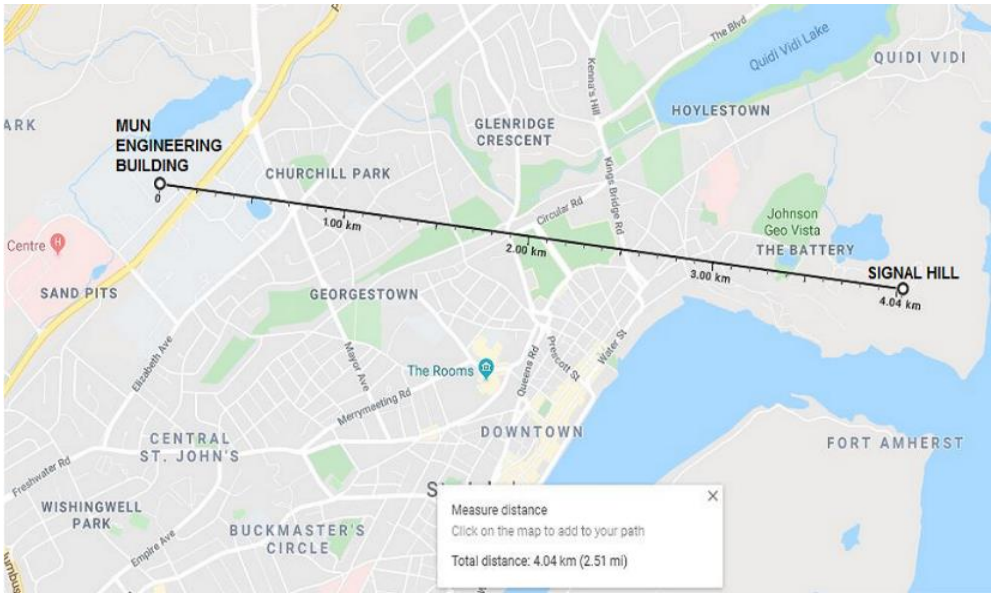

Figure 4. 15. Range test Distances in St. John's, NL, Canada.

During experiments, the voltage and current values of four sets of PV systems were monitored using four LoRa nodes. This setup was developed as a proof of concept, which can be scaled up to a larger number of nodes as required. Each node set-up is made up of an Arduino Uno microcontroller [48], a Dragino LoRa

shield [49], ACS712 Hall effect current sensor [50], and a voltage sensor as shown in Figure 4.16. Each PV unit's maximum voltage output is 16 V and the maximum current extraction is 30 A. This governs the choice of voltage and current sensors employed in the experiment. The wiring was sized to meet the voltage and current ratings. The voltage sensor was built using a resistive voltage divider to not overload on the Arduino microcontroller. This was scaled back up after data processing using the original voltage division ratio. These values were processed by the nodes and were sent to the gateway located in another part of the laboratory about 10 meters apart. At this location, their values were received, processed and displayed on the gauges and chats for observation. The gateway is comprised of a RAK831 LoRa concentrator [51], a Raspberry Pi 3 B+ model [52] and a monitor connected using HDMI. The experimental test bed setup is shown in Figure 4.17 with the LoRa nodes circled in green. These nodes were connected to various PV systems for data acquisition and transmission. The features and the mode of operation of the hardware components in the experiments are explained in references [48–52].

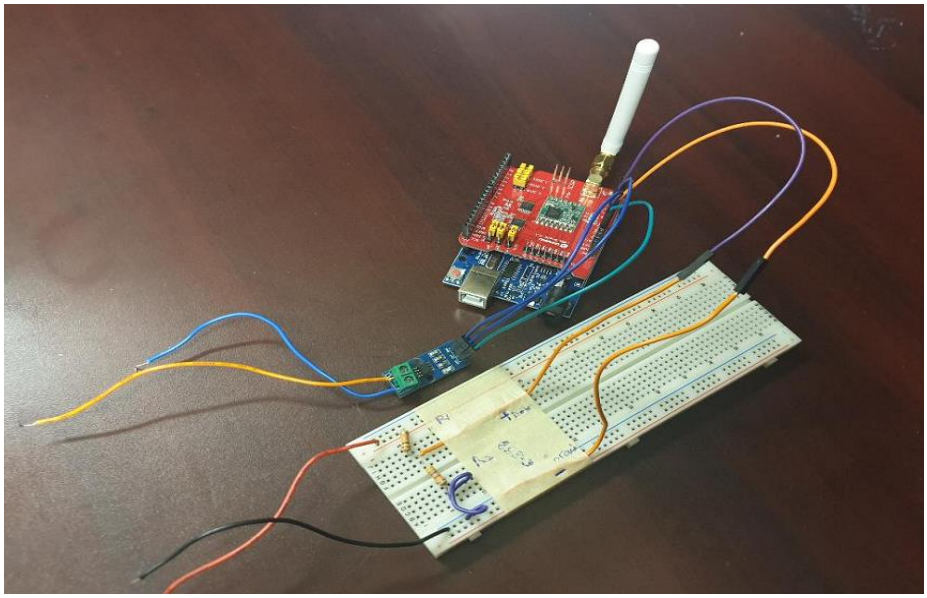

Figure 4. 16. LoRa node with voltage and current sensor.

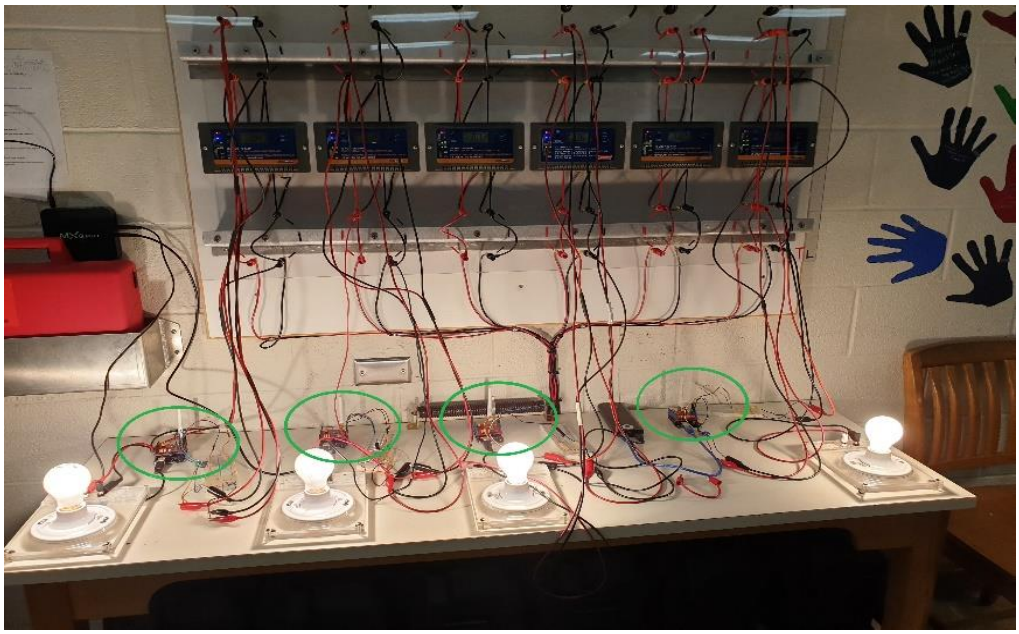

Figure 4. 17. Experimental setup with LoRa nodes circled in green.

4.7 Test Results

4.7.1 Range Test Results

The results obtained from the LoRa range test are shown in Table 4.3. Table 4.3 shows the packet delivery ratio (PDR) of the LoRa node at various distances from the gateway. The nodes sent data at the spreading factor of 7, coding rate of 4/5, and bandwidth of 125 kHz.

Table 4. 3: LoRa range test results.

Distance (km)	Number of Packets Transmitted	Packets Received	Packet Delivery Ratio (PDR)%
1	100	100	100%
2	100	100	100%
2.5	100	98	98%
3.48	100	93	93%
4	100	90	90%

Table 4.3 shows up to 4 km where a PDR of up to 90% was obtained. A PDR lower than 90% can reduce the fidelity of the data being transferred due to packet losses. Although not shown in Table 4.3, the experiment

was performed up to 7 km. However, after 4 km, the rate of packet delivery reduced drastically. This is caused by various forms of obstructions in the urban test area. LoRa can achieve data delivery to almost 15 km in rural areas that have very low number of obstructions. A data transfer range of 5 km maximum can be achieved in urban areas due to the presence of buildings and other structures [40–42].

The results from the range test show the packet delivery ratios for data transfer distances at a fixed Spreading Factor of 7. In reality, LoRa devices have the capability to automatically switch between Spreading Factors 7 and 12 to achieve better system performance in terms of transmission distance and data rate.

4.7.2 Experimental Test Bed Results

The proposed communication system was set up within the electrical laboratory about 10 meters apart from the sensors node and the gateway. Data transfer between the DG units and the central control system was achieved using LoRa communication technology to attain 100% data delivery and accuracy. As presented in Table 4.3, a range test was carried out to confirm the maximum distance at which the nodes (end devices) could send data to the gateway without packet losses. The sensors measured voltages and currents, which are displayed on the charts at the server end. This confirmed that the data were acquired, processed and transmitted using the LoRa communication technology without any disruption.

Figure 4.18 shows the measured data arriving at the RAK 831 LoRa gateway in the Base64 format. The data packet circled in yellow are the actual data to be monitored. The data is comprised of the DG unit device number, monitored value and channel number, which are decoded before they are displayed. The data obtained at the gateway is forwarded to the local node-red server through the TCPDump port for decoding, separation and display as shown in Figure 4.11. Figure 4.19 shows the measured voltage and current values from each node displayed on the Node-red gauges as devices 1 to 4. The values in Figure 4.19 are instantaneous screenshots of the voltage and current values obtained from each unit of the PV system. Figure 4.20 shows the measured voltage and current over a period, which demonstrates their real-time fluctuations. The stochastic nature of the current in Figure 4.20 is due to the intermittent nature of the renewable energy

source (PV) as the measurements were taken before the MPPT. The measured values conformed to the values displayed on the PV system boards. This verifies that the data are transferred and displayed in real-time.

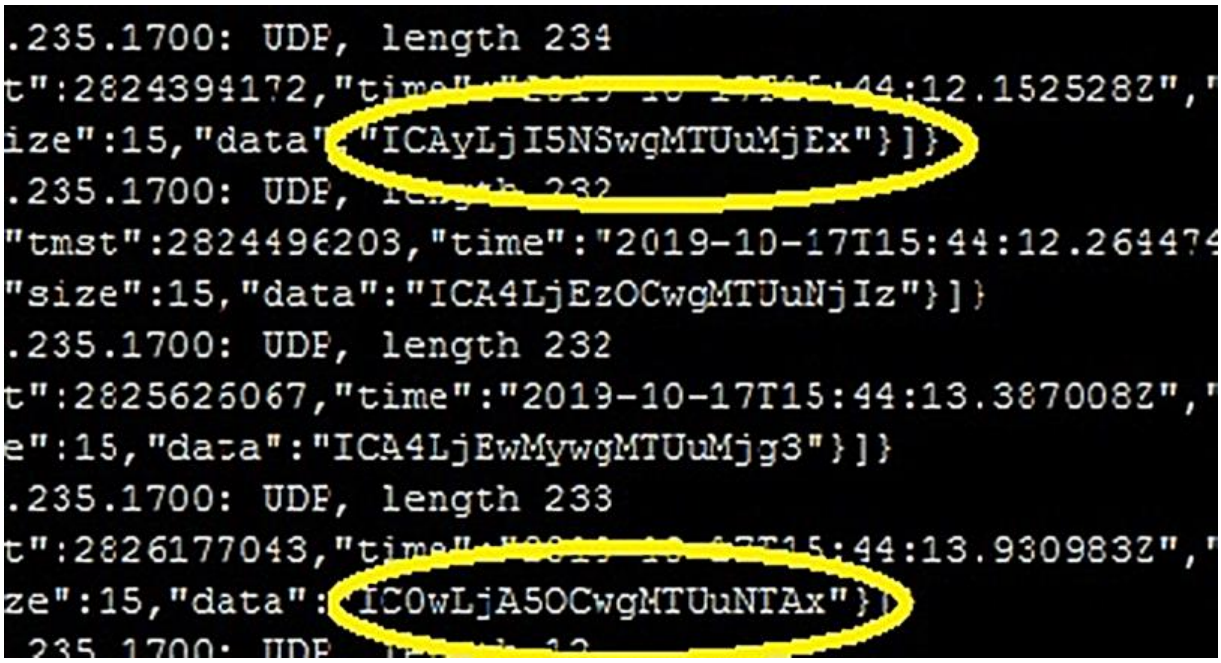

Figure 4. 18. LoRa Packets arriving at the RAK 831 concentrator.

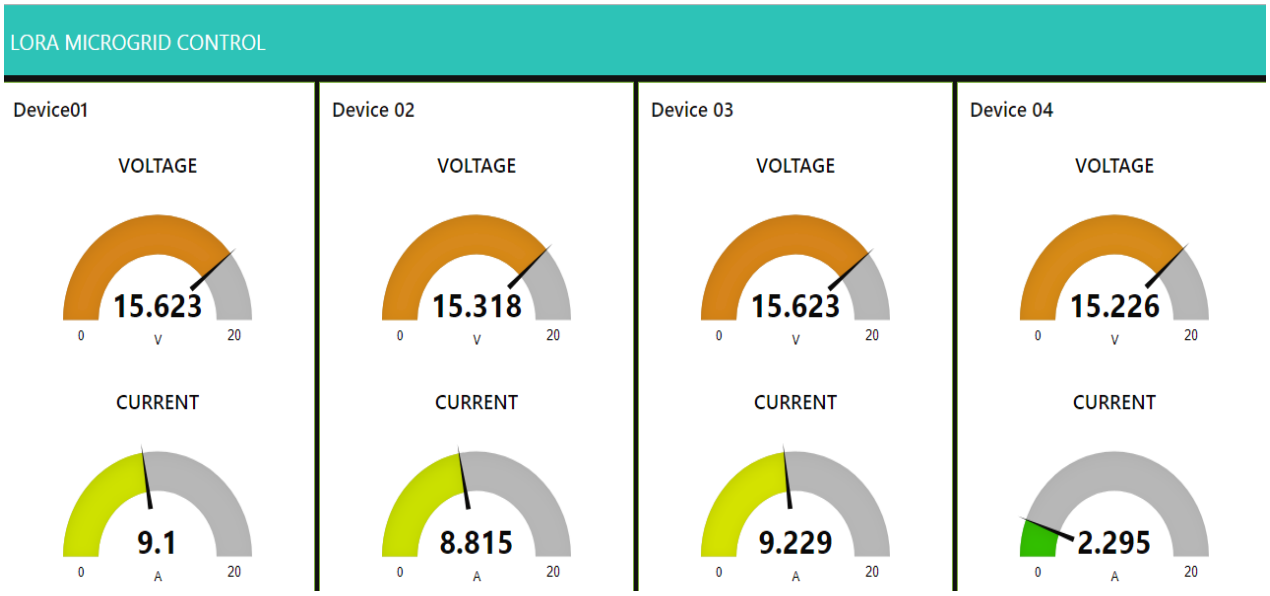

Figure 4. 19. Device sensor values displayed on the server gauges.

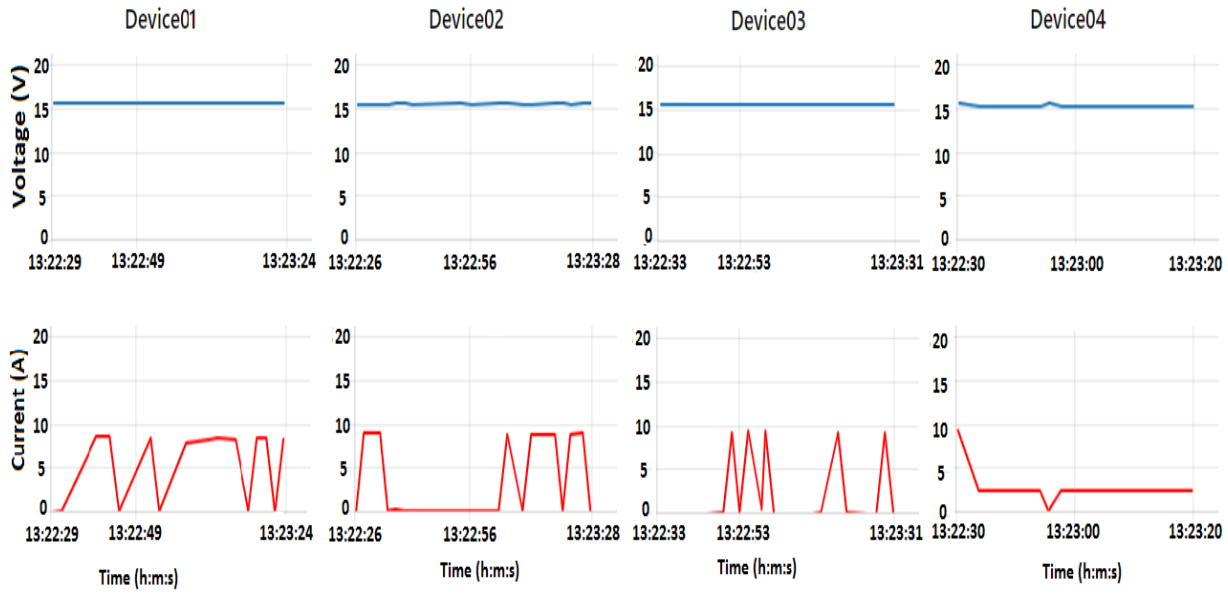

Figure 4. 20. Sensor values displayed on the server chart.

4.8 Discussions

This paper presents the design and development of a LoRa-based communication system for data transfer in microgrids for remote area applications. The features of the proposed system are summarized as follows:

- **Long Range Communication**: A data transmission range of 4 km was achieved. Table 4.1 shows the distances of data coverage of the existing wireless communication systems. Although LoRa cannot achieve data coverage distance compared with Cellular and WiMAX, LoRa is more advantageous from other perspective such as low cost and low power consumption, which are critical factors for remote application. Research activities are on-going to determine approaches through which range of data transfer can be extended in LoRa.
- **Low Cost**: The components for the proposed systems are readily available and inexpensive. Table 4.4 shows a bill of materials of the components used in the prototype.

Table 4. 4: Bill of materials.

S/N	Component	Qty.	Cost (CAD)
1	Raspberry Pi 3B	1	48.88
2	RAK 831 LoRa Concentrator	1	172
3	Dragino LoRa Shield	4	112
4	Arduino Uno Microcontroller	4	100
5	Current Sensor	4	20
6	Voltage Sensor	4	40
7	8GB SD Card	1	12.66
8	Miscellaneous (Resistors, wires etc.)	1	50
	Total		**555.54**

LoRa is an open-source system with no continual charges as compared with WIMAX and Cellular communication.

- **Low Power Consumption**: Table 4.5 shows the power requirements of the various existing wireless communication systems currently being used in microgrids. The study was carried out in real-time where the actual power requirements of the routers were used. The power requirement values were obtained from the datasheets of the devices for each communication system [45–47].

Table 4. 5: Power requirement comparison for various wireless communication systems.

Communication System	Power Consumption (W)
Zigbee	3.7
Wi-Fi	4.9
WIMAX	72
Cellular	28.8
LoRa	4.2

The results in Table 4.5 were obtained for data transfer between two devices of each wireless communication system. This approach reduced the complexity of the study since expanding the network would subsequently increase the power consumption. LoRa communications system still shows one of the lowest power consumptions.

- **Multi-sensor Connection Capabilities**: The proposed system allows the connection of a high number of sensors, which is a highly desirable feature for IoT application in microgrids. The system has the capability to monitor multiple parameters simultaneously. This advantage is demonstrated in our experiment where two sensors (voltage and current) have been connected to each node. Although only two sensors were connected in the setup, a node can accommodate multiple sensors if required.

4.9 Conclusion and Future Work

A LoRa-based communication system for data transfer within microgrids is proposed in this paper. The scheme can be employed to transfer measured data such as voltage, current, frequency and other parameters between the local controllers of DG units and the central controller of microgrids at the secondary level of control and communication. It features long-range data transfer up to 4 km, high interference immunity, low cost and low power consumption. The system can be deployed in areas where no internet or other form of communication exists, ideally for remote areas in developing countries. The proposed LoRa-based communication system was tested for one-directional communication where data was transferred from a DG unit's local controller represented by the LoRa nodes to the microgrid central controller housed by the LoRa gateway connected to the Raspberry Pi.

To achieve bi-directional communication, a reverse communication for command transmission is required. This will be explored in our future work. In this phase, the communication system will be set up to observe if DG units can be controlled from the server using LoRa. In addition, the delays caused by LoRa communication will be studied in future.

4.10 References

[1] E. Planas, J. Andreu, J. Gárate, I. Martínez de Alegría and E. Ibarra, "AC and DC technology in microgrids: A review", *Renewable and Sustainable Energy Reviews*, vol. 43, pp. 726-749, 2015.

[2] Zhao and F. Dörfler, "Distributed control and optimization in DC microgrids", *Automatica*, vol. 61, pp. 18-26, 2015.

[3] K. Das, A. Nitsas, M. Altin, A. D. Hansen and P. E. Sørensen, "Improved Load-Shedding Scheme Considering Distributed Generation," in *IEEE Transactions on Power Delivery*, vol. 32, no. 1, pp. 515-524, Feb. 2017.

[4] Y. Kim, E. Kim and S. Moon, "Distributed Generation Control Method for Active Power Sharing and Self-Frequency Recovery in an Islanded Microgrid," in *IEEE Transactions on Power Systems*, vol. 32, no. 1, pp. 544-551, Jan. 2017.

[5] K. Gia Ing, J. Jamian, H. Mokhlis and H. Illias, "Optimum distribution network operation considering distributed generation mode of operations and safety margin", *IET Renewable Power Generation*, vol. 10, no. 8, pp. 1049-1058, 2016.

[6] M. Mahfouz and M. El-Sayed, "Smart grid fault detection and classification with multi-distributed generation based on current signals approach", *IET Generation, Transmission & Distribution*, vol. 10, no. 16, pp. 4040-4047, 2016.

[7] J. Lin, W. Yu, N. Zhang, X. Yang, H. Zhang and W. Zhao, "A Survey on Internet of Things: Architecture, Enabling Technologies, Security and Privacy, and Applications," in *IEEE Internet of Things Journal*, vol. 4, no. 5, pp. 1125-1142, Oct. 2017.

[8] S. A. Saleh, E. Ozkop and A. S. Aljankawey, "The Development of a Coordinated Anti-Islanding Protection for Collector Systems with Multiple Distributed Generation Units," in *IEEE Transactions on Industry Applications*, vol. 52, no. 6, pp. 4656-4667, Nov.-Dec. 2016.

[9] Y. Xiao, *Communication and networking in smart grids*, 1st ed. Boca Ratón: CRC Press, 2012, pp. 241–275.

[10] B. Risteska Stojkoska and K. Trivodaliev, "A review of Internet of Things for smart home: Challenges and solutions", *Journal of Cleaner Production*, vol. 140, pp. 1454-1464, 2017.

[11] Z. Liu, C. Su, H. K. Høidalen and Z. Chen, "A Multiagent System-Based Protection and Control Scheme for Distribution System with Distributed-Generation Integration," in *IEEE Transactions on Power Delivery*, vol. 32, no. 1, pp. 536-545, Feb. 2017.

[12] S. Moayedi and A. Davoudi, "Distributed Tertiary Control of DC Microgrid Clusters," in *IEEE Transactions on Power Electronics*, vol. 31, no. 2, pp. 1717-1733, Feb. 2016.

[13] H. Lee and K. Ke, "Monitoring of Large-Area IoT Sensors Using a LoRa Wireless Mesh Network System: Design and Evaluation," in *IEEE Transactions on Instrumentation and Measurement*, vol. 67, no. 9, pp. 2177-2187, Sept. 2018.

[14] S. Benaissa et al., "Internet of animals: characterisation of LoRa sub-GHz off-body wireless channel in dairy barns", *Electronics Letters*, vol. 53, no. 18, pp. 1281-1283, 2017.

[15] F. Wu, J. Redouté and M. R. Yuce, "WE-Safe: A Self-Powered Wearable IoT Sensor Network for Safety Applications Based on LoRa," in *IEEE Access*, vol. 6, pp. 40846-40853, 2018.

[16] Y. Chou *et al*., "i-Car system: A LoRa-based low power wide area networks vehicle diagnostic system for driving safety," *2017 International Conference on Applied System Innovation (ICASI)*, 2017, pp. 789-791.

[17] A. T. Nugraha, R. Wibowo, M. Suryanegara and N. Hayati, "An IoT-LoRa System for Tracking a Patient with a Mental Disorder: Correlation between Battery Capacity and Speed of Movement," *2018 7th International Conference on Computer and Communication Engineering (ICCCE)*, 2018, pp. 198-201.

[18] S. Moayedi and A. Davoudi, "Distributed Tertiary Control of DC Microgrid Clusters," in *IEEE Transactions on Power Electronics*, vol. 31, no. 2, pp. 1717-1733, Feb. 2016.

[19] V. Nasirian, S. Moayedi, A. Davoudi and F. L. Lewis, "Distributed Cooperative Control of DC Microgrids," in *IEEE Transactions on Power Electronics*, vol. 30, no. 4, pp. 2288-2303, April 2015.

[20] B. Wang, M. Sechilariu and F. Locment, "Intelligent DC Microgrid With Smart Grid Communications: Control Strategy Consideration and Design," in *IEEE Transactions on Smart Grid*, vol. 3, no. 4, pp. 2148-2156, Dec. 2012.

[21] Q. Shafiee, T. Dragičević, J. C. Vasquez and J. M. Guerrero, "Hierarchical Control for Multiple DC-Microgrids Clusters," in *IEEE Transactions on Energy Conversion*, vol. 29, no. 4, pp. 922-933, Dec. 2014.

[22] P. García, P. Arboleya, B. Mohamed and A. A. C. Vega, "Implementation of a Hybrid Distributed/Centralized Real-Time Monitoring System for a DC/AC Microgrid With Energy Storage Capabilities," in *IEEE Transactions on Industrial Informatics*, vol. 12, no. 5, pp. 1900-1909, Oct. 2016.

[23] Zhao and F. Dörfler, "Distributed control and optimization in DC microgrids", *Automatica*, vol. 61, pp. 18-26, 2015.

[24] A. Khorsandi, M. Ashourloo and H. Mokhtari, "A Decentralized Control Method for a Low-Voltage DC Microgrid," in *IEEE Transactions on Energy Conversion*, vol. 29, no. 4, pp. 793-801, Dec. 2014.

[25] M. A. Setiawan, F. Shahnia, S. Rajakaruna and A. Ghosh, "ZigBee-Based Communication System for Data Transfer Within Future Microgrids," in *IEEE Transactions on Smart Grid*, vol. 6, no. 5, pp. 2343-2355, Sept. 2015.

[26] J. Haxhibeqiri, E. De Poorter, I. Moerman and J. Hoebeke, "A Survey of LoRaWAN for IoT: From Technology to Application", *Sensors*, vol. 18, no. 11, p. 3995, 2018.

[27] G. Pasolini et al., "Smart City Pilot Projects Using LoRa and IEEE802.15.4 Technologies", *Sensors*, vol. 18, no. 4, p. 1118, 2018.

[28] F. Aoudia, M. Gautier, M. Magno, M. Gentil, O. Berder and L. Benini, "Long-short range communication network leveraging LoRa™ and wake-up receiver", *Microprocessors and Microsystems*, vol. 56, pp. 184-192, 2018.

[29] J. Petäjäjärvi, K. Mikhaylov, M. Pettissalo, J. Janhunen and J. Iinatti, "Performance of a low-power wide-area network based on LoRa technology: Doppler robustness, scalability, and coverage", *International Journal of Distributed Sensor Networks*, vol. 13, no. 3, p. 155014771769941, 2017.

[30] T. Voigt, M. Bor, U. Roedig and J. Alonso, "Mitigating Inter-Network Interference in LoRa Networks", in *(EWSN) 2017 International Conference on Embedded Wireless Systems and Networks*, 2017, pp. 323-328.

[31] T. Elshabrawy and J. Robert, "Interleaved Chirp Spreading LoRa-Based Modulation," in *IEEE Internet of Things Journal*, vol. 6, no. 2, pp. 3855-3863, April 2019.

[32] N. El Rachkidy, A. Guitton and M. Kaneko, "Collision Resolution Protocol for Delay and Energy Efficient LoRa Networks," in *IEEE Transactions on Green Communications and Networking*, vol. 3, no. 2, pp. 535-551, June 2019.

[33] A. A. Doroshkin, A. M. Zadorozhny, O. N. Kus, V. Y. Prokopyev and Y. M. Prokopyev, "Experimental Study of LoRa Modulation Immunity to Doppler Effect in CubeSat Radio Communications," in *IEEE Access*, vol. 7, pp. 75721-75731, 2019.

[34] A. Hoeller, R. D. Souza, O. L. Alcaraz López, H. Alves, M. de Noronha Neto and G. Brante, "Analysis and Performance Optimization of LoRa Networks with Time and Antenna Diversity," in *IEEE Access*, vol. 6, pp. 32820-32829, 2018.

[35] N. Jovalekic, V. Drndarevic, I. Darby, M. Zennaro, E. Pietrosemoli and F. Ricciato, "LoRa Transceiver with Improved Characteristics," in *IEEE Wireless Communications Letters*, vol. 7, no. 6, pp. 1058-1061, Dec. 2018.

[36] B. Reynders, W. Meert and S. Pollin, "Power and spreading factor control in low power wide area networks," *2017 IEEE International Conference on Communications (ICC)*, 2017, pp. 1-6.

[37] F. Cuomo, M. Campo, A. Caponi, G. Bianchi, G. Rossini and P. Pisani, "EXPLoRa: Extending the performance of LoRa by suitable spreading factor allocations," *2017 IEEE 13th International Conference on Wireless and Mobile Computing, Networking and Communications (WiMob)*, 2017, pp. 1-8.

[38] M. Slabicki, G. Premsankar and M. Di Francesco, "Adaptive configuration of lora networks for dense IoT deployments," *NOMS 2018 - 2018 IEEE/IFIP Network Operations and Management Symposium*, 2018, pp. 1-9.

[39] K. Q. Abdelfadeel, V. Cionca and D. Pesch, "Fair Adaptive Data Rate Allocation and Power Control in LoRaWAN," *2018 IEEE 19th International Symposium on "A World of Wireless, Mobile and Multimedia Networks" (WoWMoM)*, 2018, pp. 14-15.

[40] R. Sanchez-Iborra, J. Sanchez-Gomez, J. Ballesta-Viñas, M. Cano and A. Skarmeta, "Performance Evaluation of LoRa Considering Scenario Conditions", *Sensors*, vol. 18, no. 3, p. 772, 2018.

[41] A. M. Yousuf, E. M. Rochester and M. Ghaderi, "A low-cost LoRaWAN testbed for IoT: Implementation and measurements," *2018 IEEE 4th World Forum on Internet of Things (WF-IoT)*, 2018, pp. 361-366.

[42] M. R. Seye, B. Ngom, B. Gueye and M. Diallo, "A Study of LoRa Coverage: Range Evaluation and Channel Attenuation Model," *2018 1st International Conference on Smart Cities and Communities (SCCIC)*, 2018, pp. 1-4.

[43] M. Ertürk, M. Aydın, M. Büyükakkaşlar and H. Evirgen, "A Survey on LoRaWAN Architecture, Protocol and Technologies", *Future Internet*, vol. 11, no. 10, p. 216, 2019.

[44] M. Saleh, Y. Esa, M. Hariri and A. Mohamed, "Impact of Information and Communication Technology Limitations on Microgrid Operation", *Energies*, vol. 12, no. 15, p. 2926, 2019.

[45] "XBee™ ZigBee®/802.15.4 Modules", *Digi.com*, 2017. [Online]. Available : https://www.digi.com/products/embedded-systems/digi-xbee/rf-modules/2-4-ghz-modules/xbee-zigbee#specifications.

[46] "DIR-462 WiMAX Router", *Dlink-me.com*, 2017. [Online]. Available: https://dlink-me.com/pdf/DIR-462.pdf.

[47] "Secure Industrial Cellular Routers", *Cellular Routers*, 2016. [Online]. Available: https://www.weidmuller.com/en/products/electronics/wireless_connectivity_solutions/wireless_solutions_overview/wireless_ethernet_cellular_modems/cellular_routers.jsp.

[48] "Current Sensor ICs", *Allegro Microsystems*, 2017. [Online]. Available: https://www.allegromicro.com/en/Products/Current-Sensor-ICs/Zero-To-Fifty-Amp-Integrated-Conductor-Sensor-ICs.aspx.

[49] "Arduino Uno for Beginners - Projects, Programming and Parts (Tutorial)", *Makerspaces.com*, 2016. [Online]. Available: https://www.makerspaces.com/arduino-uno-tutorial-beginners.

[50] "Arduino Shield featuring LoRa® technology", *Dragino.com*, 2014. [Online]. Available: http://www.dragino.com/products/lora/item/102-lora-shield.html.

[51] "RAK 831 LoRa Concentrator", *Downloads.rakwireless.com*, 2015. [Online]. Available: https://downloads.rakwireless.com/LoRa/RAK831-LoRa-Gateway/Hardware-Specification/RAK831%20Datasheet%20V1.3_RU.pdf.

[52] "Raspberry Pi 3 Model B+", *Static.raspberrypi.org*, 2015. [Online]. Available: https://static.raspberrypi.org/files/product-briefs/Raspberry-Pi-Model-Bplus-Product-Brief.pdf.

Chapter 5

An Open Source LoRa Based, Low-Cost IoT Platform for Renewable Energy Generation Unit Monitoring and Supervisory Control

Co-authorship Statement

Chapter 5 presents the design and development of an open source LoRa based, low-cost IoT platform for renewable energy generation unit monitoring and supervisory control. In this chapter, an IoT based SCADA system was designed and developed for monitoring and supervisory control of renewable energy systems. This system employed LoRa as the communication network. This therefore showed that the system did not depend on internet for data transfer which is one of the key features of the designed low-cost system. This makes the system able to be deployed to remote areas where there is no communication infrastructure in existence. Furthermore, for better system security, the proposed SCADA system has all its components hosted on one machine which eliminated the need for any cloud storage system and hence reducing the system vulnerability to attacks.

I (Ndukwe Cherechi Izuchukwu) am the principal author and contributed to Conceptualization, Methodology, Software Investigation, Writing- Original Draft and Editing of this chapter. The research in this chapter was supervised by Dr. Tariq Iqbal and Dr. Jahangir Khan. The supervisors also contributed to the conceptualization and Methodology of this chapter. They supervised the entire chapter, reviewed and corrected the research manuscript. The work in this Chapter has been published in the **Journal of Energy and Power Technology** 2022, volume 4, issue 1 doi:10.21926/jept.2201007.

Abstract

SCADA provides real-time system monitoring by constant communication and data exchange between various system devices to achieve data visualization and logging. Presently, in industrial systems, commercial SCADA systems are being used for data monitoring and control. These systems can be expensive, and as such can only be afforded by select industries. Even at these costs, the commercial SCADA systems face some challenges, which include interoperability and scalability issues. Research has shown that these problems can be solved by the introduction of low-cost materials and open-source software to achieve data monitoring for all levels of processes. This paper proposes an open source, low-cost Internet of Things (IoT)-based SCADA system that employs the IoT architecture for SCADA functions. The proposed system is an improvement to the existing IoT solutions by eliminating cloud based IoT platforms and introducing a single machine system. This solution increases the robustness of the system while reducing costs. The proposed system prototype consists of voltage and current sensors, Arduino Uno microcontroller and Raspberry Pi. The sensors acquire data from the monitored unit. The Arduino Uno receives the data and processes them for transmission to the Raspberry Pi using the LoRa communication technology. At the Raspberry Pi, the local Chirpstack platform processes the data and displays the measured data using the Grafana dashboard for real-time data monitoring, and the data is stored in an InfluxDB database. For system validation purposes, the prototype is designed, developed, and set up to monitor the panel voltage, current and battery voltage of a solar photovoltaic system. The results obtained from the experimental set-up are compared with the test data from physical digital multimeters. The system presented in this paper is a low-cost, open source, scalable and interoperable system. This, therefore, makes the proposed SCADA system an alternative for commercial SCADA systems, especially for select applications. The system proposed in this paper can be deployed to large industrial systems with appropriate upgrades and customization. The main contribution of this research is the design and development of a SCADA system that performs all the functions of a proprietary SCADA system at a very

low-cost with scalable and interoperability features which are the main limitations of the traditional SCADA systems.

Keywords

Internet of things; LoRa; open source; renewable energy systems; SCADA

5.1 Introduction

There is a lot of interest in renewable energy sources for power generation due to its environmental benefits such as greenhouse gas reduction and reduced dependence on fossil fuels for power generation. The renewable energy generation installation capacity in the world at the end of 2019 stands at 2,351GW [1]. This entails an increasing penetration of the renewable energy sources for power generation with possibly very high penetration in years to come both at the macro, mini and micro generation levels.

With the dispersed geographical distribution of the renewable energy generation units leading to a distributed structure, system monitoring, or supervision is very important for optimum performance. The continuous requirement for supervision, monitoring and control of the various units of the generation systems led to the development of the Supervisory Control and Data Acquisition (SCADA) systems. SCADA systems have been the core of industrial automation and control over the years [2]. An observation of the industrial automation pyramid shown in Figure 5.1 depicts that SCADA systems are responsible for monitoring and control of functional procedures among all devices while acting as an interface for human supervision from the downstream to upstream.

Figure 5. 1. Industrial automation pyramid [2].

Generally, a SCADA system is comprised of multiple sensors and actuators that make up the Field Instrumentation Devices controlled through the Remote Terminal Units (RTUs) [2]. The Communication Channel, Master Terminal Units (MTU) hosting the Human Machine Interface (HMI) are also important components of the SCADA system with functions that include data transfers between the RTUs and the MTU, data processing and display respectively. The MTU also allows the injection of controls from the HMI to the field instruments. The continuous increase in the sizes of the systems have also caused an increase in complexity hence a requirement for a more robust control system.

One of the very promising components of the shift in paradigm to the Industry 4.0 [2] is the Internet of Things (IoT) [3]. The IoT is a network architecture that was initially motivated by wireless communication for data exchange featuring low power consumption during data transfer [2]. In recent years, IoT has matured enough from field to server data communication [4-6].

IoT as a solution for industrial monitoring can be applied to distributed units of a renewable energy generation system. Due to the increased installed power capacity from renewable energy sources, there is an increasing need for more components. These systems can only be monitored and controlled by systems that allow for the connection of multiple sensors at very large distances for data collection, with good interoperability, low cost,

and low power consumption. Currently the industrial monitoring systems have mostly employed proprietary SCADA systems for data monitoring and remote control. These systems, however, face some challenges that include high cost of installation, operating and routine maintenance, high technical know-how requirement, and low level of interoperability. Furthermore, these proprietary SCADA systems face high scalability issues. To achieve a comprehensive solution to these challenges, a system for data acquisition, processing, transfer, and display will have to be developed for application at the macro, mini and micro processing levels. To this end, low-cost, open source IoT SCADA systems are being developed by various researchers.

This paper proposes the design and development of a low-cost, open-source SCADA system based on the IoT architecture for monitoring and supervision of the distributed renewable energy generation systems employing the LoRa communication Protocol as the communication channel for data transfer. LoRa communication has been employed in the work due to its features such as, low-cost, low power consumption, and the long range of data transfer. The proposed SCADA system brings a solution to many problems faced by the present-day commercial SCADA systems and an improvement to existing IoT solutions for system monitoring and supervisory control. As such, this can be applied to distributed renewable energy generation units.

The scope of this work is on the design, development and testing of the low-cost open-source SCADA system for the remote monitoring and supervisory control of energy generating systems. The remaining sections of the paper are organized as follows: Section 2 presents the review of traditional SCADA and the IoT SCADA systems. This section also reviews other research works that have been carried out to date. Section 3 describes the implementation of the proposed IoT SCADA system. Section 4 presents a detailed description of the components for the proposed system. Section 5 presents the implementation of the proposed prototype. Section 6 describes the design of the system prototype. The experimental setup of the proposed SCADA system is presented in Section 7. In Section 8, the results obtained from the prototype testing are presented. Section 9 discusses key features of the proposed SCADA system. The paper is concluded in Section 10.

5.2 Literature Review

5.2.1 Proprietary (Traditional) SCADA Systems

Over the years, SCADA systems have been an integral part of industrial systems which include the energy generation systems. The SCADA system is made up of the field instruments (sensors and actuators), Programmable Logic Controllers (PLCs: proprietary), communication channels (MODBUS, ProfiBus), industrial PCs that stand as the Master Terminal Unit (MTU) hosting the SCADA server and HMI.

A classification of the existing high end proprietary SCADA systems developed by the top companies are shown in Table 5.1.

Table 5. 1: Proprietary SCADA system classification.

SCADA System	Interoperability	Cost	Scalability	Security Requirements	Complexity
Simantic WinCC (Siemens)	No	High	Average	High	High
Clear SCADA (Schneider Electric)	No	High	Low	High	High
Ovation SCADA (Emerson)	No	High	Low	High	High
Micro SCADA (Allen Bradley)	No	High	Low	High	High
ABB Ability SCADA	No	High	Low	High	High
Experion SCADA (Honeywell)	No	High	Low	High	High
HMI SCADA (General Electric)	No	High	Low	High	High

Although to date, the SCADA systems have been continuously employed for monitoring and control in various industrial processes, it still faces some drawbacks which have affected its operation at all levels of process monitoring and control as shown in Table 5.1. These include:

1. *Interoperability*: Various companies such as Siemens, Allan Bradley, and Schneider Electric have developed Proprietary SCADA systems that can only operate with components from the same or participating manufacturers. Devices made by different manufacturers may not be easily integrated in one SCADA environment [7]. This also entails complications in troubleshooting where high level of expertise is needed.
2. *Scalability*: The commercial SCADA systems were originally developed with options to connect a fixed number of devices. Therefore, an increase in the number of components usually has a drastic degrading effect on the system performance [7].
3. *High security requirements*: Considering the exposure of the plant data to the internet due to its unavoidable application for data transfer, a lot of emphasis must be placed on development of strong security protocols to enhance data security.
4. *High cost*: Being an industrial work horse and considering the early mentioned drawbacks, to continue the usability of the traditional SCADA system, the cost of development, operating and maintenance will therefore be high. While large oil and gas companies, power producers, and other industries may afford it, smaller entities need to opt for more cost-effective solutions.

5.2.2 IoT Application for Industrial Systems Monitoring

With the advent of the Internet of Things (IoT), there is an extended improvement in the SCADA industry with better device monitoring, data visualization and device control being achieved with this shift in paradigm [8]. The IoT can be defined as a combination of diverse technologies to provide functional solutions to various industries. Although IoT solutions developed by various companies and researchers may differ at their various functions, attributes, and target industry, IoT solutions share the following core characteristics [8]:

1. *Data access*: This Characteristic deals with extraction of data from a particular monitored system. This is achieved by the employment of sensors.

2. *Data transfer*: The data must be transferred from the point of extraction to where it will be analyzed for efficiency purposes.
3. *Data management*: This deals with the conversion of the extracted data to useful information for analytic or control use.
4. *Data visualization*: For proper control decisions to be taken by either human personnel or machine controllers, the useful information which arises from data manipulation will have to be visualized.

A diagrammatic comparison of traditional SCADA architecture and the IoT solution architecture for a same plant scenario are displayed in Figure 5.2 and Figure 5.3.

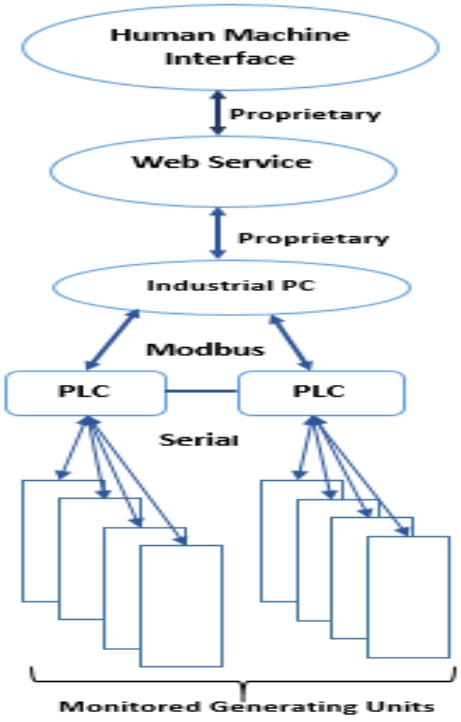

Figure 5. 2. Traditional SCADA architecture.

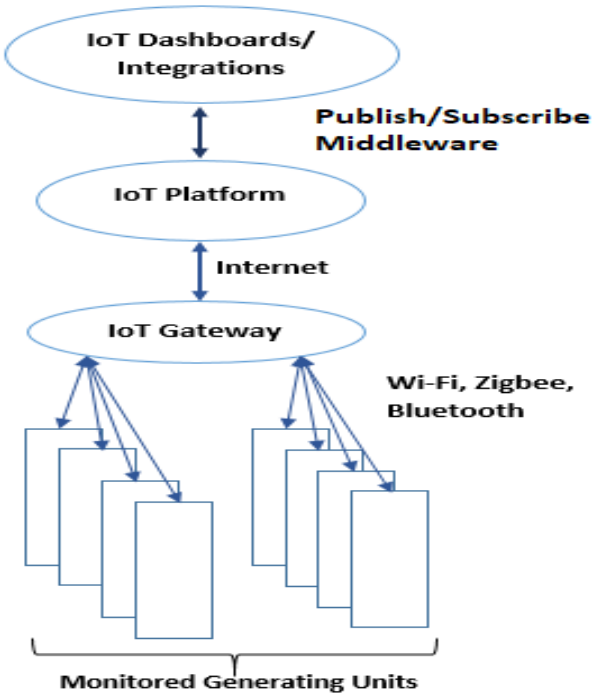

Figure 5. 3. IoT Solution architecture.

From Figure 5.2 and Figure 5.3, at the field instrumentation level, SCADA and IoT share the same manner of data extraction systems with sensors connected to the monitored system which depicts a level of relationship between SCADA and IoT. The communication channel is also another factor that may be considered in the relationship analysis. However, the Programmable Logic controllers and the Human-Machine interfaces in the SCADA systems are replaced with the IoT gateways and platforms respectively which depicts a significant shift to a system with a reduced number of components, hence less expensive, less power consuming but at the same time achieving same results as the traditional SCADA system. To better understand the application of IoT for SCADA solutions, the functionalities of the two replacement components in the IoT architecture that has facilitated the shift are explained.

5.2.2.1 IoT Gateway

An IoT gateway is basically a solution to enable the communication of various IoT components for data transfer [2]. There has been a continuous development and deployment of different types of IoT gateways

with very vast features for industrial applications [2]. In all the differences, there are some very important features that must be possessed by every IoT gateway which are explained as follows:

1. *Data management and handling*: An IoT gateway for industrial application should have a full ability to acquire and process data. This feature is a must have feature for an IoT gateway.
2. *Event management*: With industrial systems tending more towards event driven control, an IoT gateway to be applied to industrial applications is supposed to have a very strong event management feature for proper and seamless control of the process plant.
3. *Real-Time response*: This is a very important IoT gateway feature considering the criticality of real-time data exchange and control in industrial systems for performance evaluation.
4. *Scalability*: Expansion is very continuous in industrial systems. Therefore, a good IoT gateway will be highly scalable without any negative effect to its host system.
5. *Reliability and robustness*: This feature is a must have for any IoT gateway for industrial application. This is due to the very harsh environment to which most of these gateways are deployed.
6. *Security*: The IoT gateway should be able to reject unauthorized access to the system for security purposes.

5.2.2.2 IoT Platform

An IoT platform is defined as a middleware and infrastructure that allows interaction between end users and the edge devices [2]. With the increase in the diversity of the IoT devices, the IoT platform has become of high necessity for data retrieval and further processing. The IoT platform over the years have been observed to possess the following very important features:

1. *Monitoring capability*: The IoT platform can monitor the operating status of the various devices that are connected in the system.
2. *Software management*: Continuous downloading and updating of the device software

3. *Data centralization*: Data from the IoT devices are centralized by the IoT platform with the use of brokers through IoT protocols.
4. *Data processing*: The presence of algorithms for data processing. For instance, performing arithmetic operations of received data to provide another data.
5. *Security*: The IoT platform has the feature for communication authentication and encryption for data integrity.

5.2.3 Review of Previous IoT SCADA Research Designs

Several IoT based SCADA systems have been designed and developed by researchers aiming at achieving better monitoring at lower costs compared to those of the commercial SCADA systems. In [9], the authors proposed a low-cost, open-source SCADA system for solar photovoltaic system monitoring. The system consists of sensors to measure electrical parameters off a photovoltaic system, and the data is transferred to a locally installed EMMON CMS server for monitoring and control. The work has an advantage of reduced overall system cost for deployment and operation and low power consumption. However, the system employs internet for data exchange. This employment of internet for data transfer could be a drawback when considering the system for deployment to remote areas for monitoring purposes. The work in [10] implemented a web-based monitoring and control system for real-time electrical data measurement of a hybrid power system using web-based in-Touch system as the graphical user interface. Although the work also highlights a very high solution for the challenges faced by the traditional SCADA systems, it still faces the challenges of being prone to high cyber-attacks because it is a web-based system and the IoT platform is hosted in the cloud requiring internet for data transfer which therefore incurs more cost. The functions of a LoRa-based SCADA system were emphasized in [11]. The work focused majorly on the security of the communication system employed such as data encryption algorithm and security in the context of communication in microgrids. Ref [12] featured a low-cost SCADA system for CO_2 enhanced oil recovery. This system uses sensors and actuators connected to the wellhead, and the data is stored in MYSQL DBMS

database and presented on a graphical user interface. The proposed system has the advantage of very high-level data acquisition and logging but has a drawback with the communication Zigbee which cannot be employed for long distance industrial systems. The work highlighted in [13] designed and developed a low-cost, open source IoT-based SCADA system using Thinger.IO and the ESP32 microcontroller board. This system acquires electrical parameters and transfers to the IoT platform via the gateway. Although this work seemed to meet all the criteria, it employed a cloud based IoT platform and therefore required Wi-Fi for data transfer. This, therefore, affects its robustness for full integration as an autonomous system for data monitoring.

Recently, researchers in [14-17] have highlighted various designs of IoT solutions for data monitoring using the IoT architecture.

A review of the previous works shows that the main communication channels for data transfer in the systems are Wi-Fi and internet. Furthermore, none of the reported works have considered a remote initiated supervisory control of the monitored units. They have focused mostly on accurate monitoring of the system parameters for control decisions.

In this research work, a LoRa-based low-cost IoT SCADA system is designed and developed to monitor distributed renewable energy generation units. The proposed low-cost SCADA system employs LoRa communication for data transfer. This system includes a remote supervisory control functionality which has not been considered by previous research works done on the development of low-cost SCADA solutions. Employing LoRa for data transfer in this work depicts the system's ability to be deployed to areas without the existence of any communication infrastructure such as cellular and internet.

5.3 Proposed IoT SCADA System Implementation

The proposed low-cost, open-source SCADA system is based on the internet of things infrastructure. The proposed system is expected to meet all the criteria of the proprietary SCADA systems with more features

that mitigate the challenges of the traditional SCADA system. The criteria considered for full integration of the proposed IoT SCADA system into the energy generation systems include:

1. *Latency*: For real-time data exchange, the project considered a maximum data and command transfer time of 1 second. This level of latency is assumed very good for the data transfer at the supervisory level.
2. *Reliability*: Considering the distributed nature of the various components of the generating system which most times are in very harsh environments, the system components are supposed to be reliable enough to perform the monitoring function. The reliability of the communication channel is also of very high importance to ensure accurate and timely data delivery at every level.
3. *Low-cost and open source*: The proposed system should be of low cost and at the same time meet the monitoring requirements of the plant. The low cost will be achieved by the employment of low-cost materials and as well open source IoT platforms.
4. *Interoperability*: The components of the proposed system will be highly interoperable and as such will mitigate the interoperability challenges faced by the traditional SCADA system. This feature is achieved by the employment of materials from different manufacturers put together to achieve the proposed system.
5. *Scalability*: Scalability is very important in the current energy system as there are numerous improvements with the addition of more components and therefore the proposed system will have to be highly scalable to accommodate the continuous growth in components of the energy generation unit.
6. *Low power consumption*: One of the main advantages of IoT systems is the low power consumption. Therefore, the proposed system has also been designed to have an overall low power consumption capability.
7. *Robustness for remote area application*: The proposed system has been considered for application and deployment to remote areas for data acquisition and supervisory control. For this system, the LoRa

communication protocol is chosen as the communication channel. This makes the system totally internet independent and can therefore be deployed to remote areas without any existing communication infrastructure.

8. *Long range of data transfer*: The proposed system will have to achieve long range of data transfer. The application of LoRa as the communication channel depicts that the proposed system will achieve long range of data transfer. LoRa has been shown in various research to achieve data transfer distances of up to 15km especially in remote areas with little or no obstructions.
9. *Supervisory control*: Supervisory control is also a very important feature which the proposed system featured. This feature was considered a very important factor to achieving a complete SCADA system. This control feature can be either event driven, or personnel applied.

The architecture of the IoT SCADA solution proposed in this paper is shown in Figure 5.4.

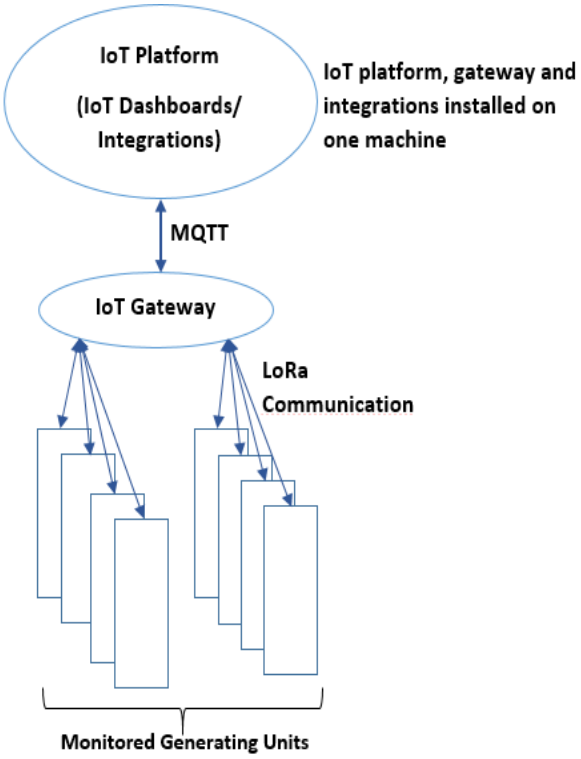

Figure 5. 4. Proposed IoT SCADA solution architecture.

Figure 5.4 shows that in the proposed IoT SCADA solution, the IoT platform, IoT gateway and the integrations are installed on a single host machine. This therefore eliminates the cloud hosted IoT platform in previous works and therefore internet is not required for data transfer. This makes the proposed system an independent and autonomous system which can be deployed to any area, especially remote areas without the need for any other communication infrastructure. This architecture also allows for the security and integrity of data as only authorized personnel can have access to data being transferred. Furthermore, being that only LoRa is used for data transfer, data encryption can also be carried out easily at the sensor level before data is transferred over the LoRa communication protocol. Additionally, the schematic diagram of the proposed SCADA prototype is shown in Figure 5.5.

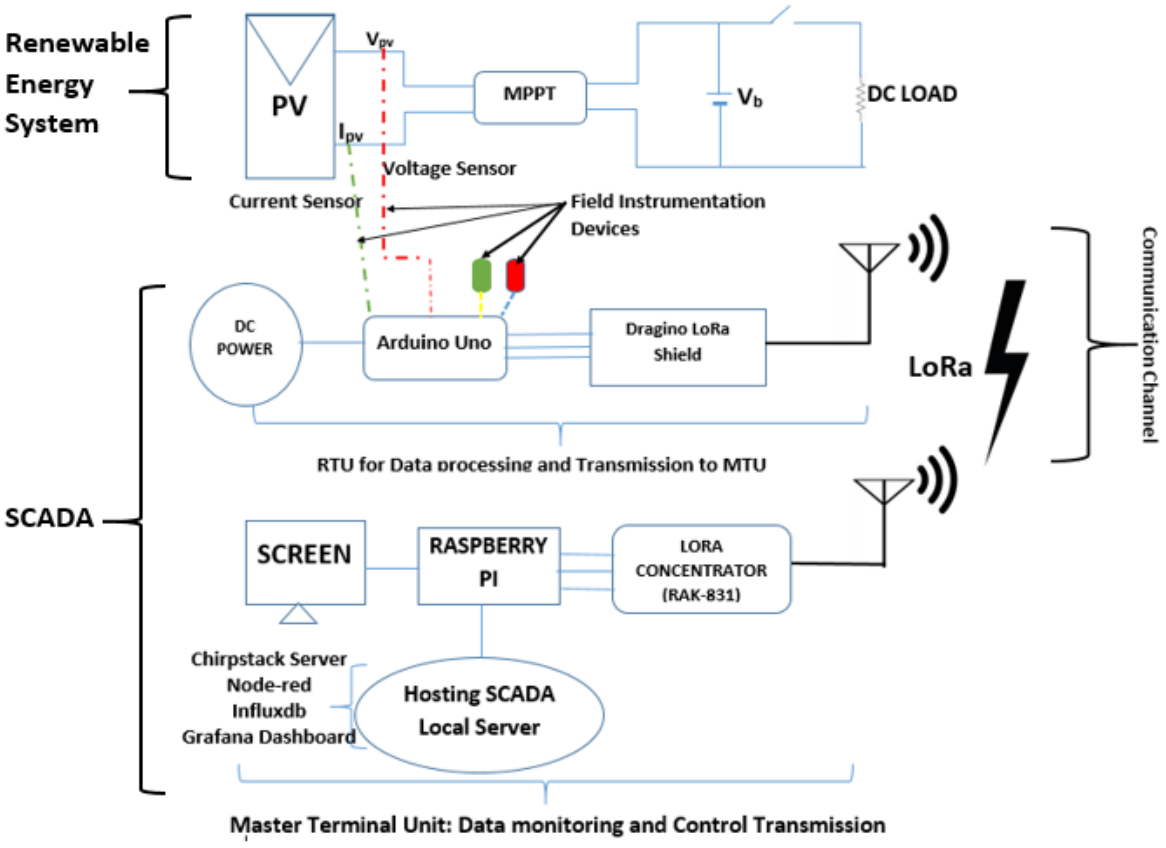

Figure 5. 5. Schematic configuration of the proposed SCADA system.

5.4. Components of the Proposed IoT Scada System Prototype

The proposed SCADA system was designed to meet the implementation criteria which have been enumerated in section 3. The software employed in this prototype include: Chirpstack IoT platform, Node-Red programming tool, InfluxDB database and Grafana IoT dashboard for data display. On the other hand, the hardware employed include voltage and current sensors, Arduino Uno microcontroller (RTU) and the Raspberry pi model 3B+ (MTU). Each of these components is described in detail below:

5.4.1 Software

5.4.1.1 Chirpstack IoT Platform

Chirpstack is an open source LoRaWAN Network Server stack [18]. This platform is a cost-effective network platform for the design of low-cost IoT experiments and projects. The Chirpstack IoT platform is made up of the following services: The Bridge, network server and the application server. The Chirpstack gateway bridge is a service responsible for the conversion of LoRa packet forwarder protocols into a Chirpstack network server common data-format (JSON and Protobuf). The network server is an open source LoRaWAN server with the responsibility of de-duplication of the received data frames [18]. The application server handles functions such as the join-request and encryption of the application payloads [18]. Furthermore, the application server offers a web interface for device management with a gRPC and RESTful API for integration with external services [18]. The main feature for data transfer across the components of the Chirpstack platform is the MQ Telemetry Transport (MQTT). The Chirpstack architecture is shown in Figure 5.6. This IoT platform was chosen due to its proven level of stability, data processing and high-level integration with LoRa communication which include data decoding and encoding, decryption, storage, and display. Moreover, this platform was compared with other IoT platforms such as the Things box, Things network, and Things speak that require cloud hosting. The Chirpstack IoT platform applied for the proposed system can be installed locally on a single machine with all its dependencies thereby increasing the compatibility of the system for various applications.

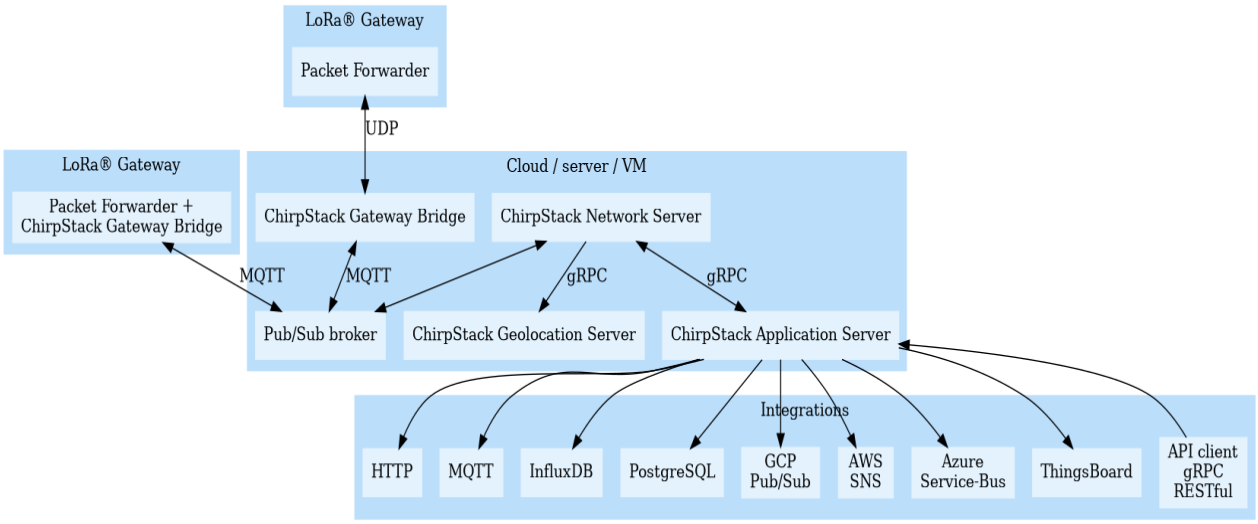

Figure 5. 6. ChirpStack IoT platform architecture [18].

5.4.1.2 InfluxDB Database

InfluxDB is an open-source time series database developed by InfluxData [19]. The InfluxDB is written in the Go programming language and optimized to handle time series data. The open-source version provides a full time series database platform with various other services. InfluxDB can either be run on the cloud or locally on a device. InfluxDB was compared with other IoT databases such as CrateDB, MongoDB, RethinkDB, SQLite. InfluxDB database being a time-series database has the following advantages over the above-mentioned databases.

- Very high speed of data recovery.
- Very large data storage comparison.
- Possess an SQL-like query language.
- Provides a built-in linear interpolation for missing data.
- Supports automatic data down sampling.
- Supports uninterrupted requests to compute aggregates.
- High integration capabilities with IoT platforms.

The schematic representation of the InfluxDB database architecture is shown in Figure 5.7.

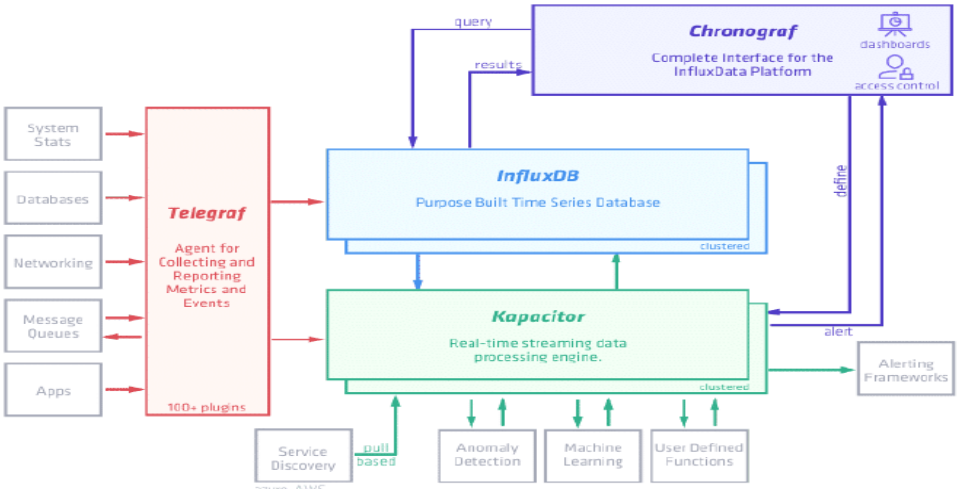

Figure 5. 7. InfluxDB architecture showing the components of the database [19].

5.4.1.3 Grafana IoT Dashboard

Grafana is a web-based data visualization platform that allows for interactive data analysis by employing various charts and graphs [20]. This dashboard has the capabilities to be integrated with various databases for data visualization. Recently, Grafana has gained increased usage in IoT applications for real-time monitoring of systems due to the following important features; dynamic display, alert systems, downlink plugins for system control, security system, ability to mix data sources and display on same graph, an-notation capabilities [20].

5.4.1.4 Node-Red Programming Tool

Node-Red is an open-source visual editor for connecting and communicating within IoT elements invented by IBM [21]. Node-Red is an easy-to-use tool as it eliminates the bulky programming function, involving a lot of code writing for connection of various project components for monitoring [21]. This tool is made up of various components known as “Nodes” that simply look like icons that can be dragged and dropped in the Editor Interface and wired together [21]. These different nodes offer different functions that range from simple debugging to more complicated flow operations [21]. Node-Red can be installed on a PC or microcomputer

for system monitoring where various nodes can be connected to form a flow for data acquisition and node control.

5.4.2 Hardware

5.4.2.1 Voltage Sensor

The voltage sensor employed in this design was built using the voltage divider principle. The sensor consists of a series connection of two resistors. The voltage sensor's output pin is connected to the pin the Arduino Uno microcontroller and the acquired data is drawn from this pin. Furthermore, the ground is connected to the Arduino Uno ground pin. In this sensor, the voltage drop across the second resistor is measured to scale down the voltage to a value under 5V which the microcontroller can handle. During processing, it is scaled up with the expression shown in equation (5.1) and the value of the Arduino ADC to obtain the proportional and accurate voltage value.

$$V_{in} = V_{out}\left(\frac{R_2}{R_1+R_2}\right) \qquad (5.1)$$

Where,

$$V_{out} = Sensor\ Measured\ Value\ \times V_{pp} \qquad (5.2)$$

$$V_{pp} = Arduino\ ADC\ Value = \frac{5.0}{1024.0} \qquad (5.3)$$

5.4.2.2 ACS 712 Hall-Effect Current Sensor

The ACS712 Hall-effect current sensor manufactured and distributed by the allegro micro-systems is employed to measure the line current. The sensor is a low-cost, Hall-effect based linear current sensor with 2.1 KV Rms isolation with a low-resistant current conductor [13]. The sensor allows up to 5 V of power supply [22]. The magnetic field inside the sensor is converted to a proportional voltage by the Hall IC, which is fused into the sensor system. The voltage obtained at the output is proportional to the measured current [22]. Three classes of the current sensor (30A, 20A and X5B) were employed for this work. These classes of

current sensors measure current values, which correspond to 2.5V to 5V. The values of the current sensors are collected from the data pin of the sensor, which is connected to the A0 pin of the Arduino Uno. The Vcc and Ground are connected accordingly. These pin connections are also duly considered while programming the systems.

5.4.2.3 Arduino Uno Microcontroller

Arduino Uno is a microcontroller board employed for various IoT applications because it is very cheap and as well requires a low amount of power [23]. Arduino employs a simplified version of C++, which makes programming easier [23]. The Arduino Uno is the most popular member of the Arduino family. The Arduino Uno allows a maximum voltage of 5V [23]. Figure 5.8 shows the Arduino Uno pin distribution.

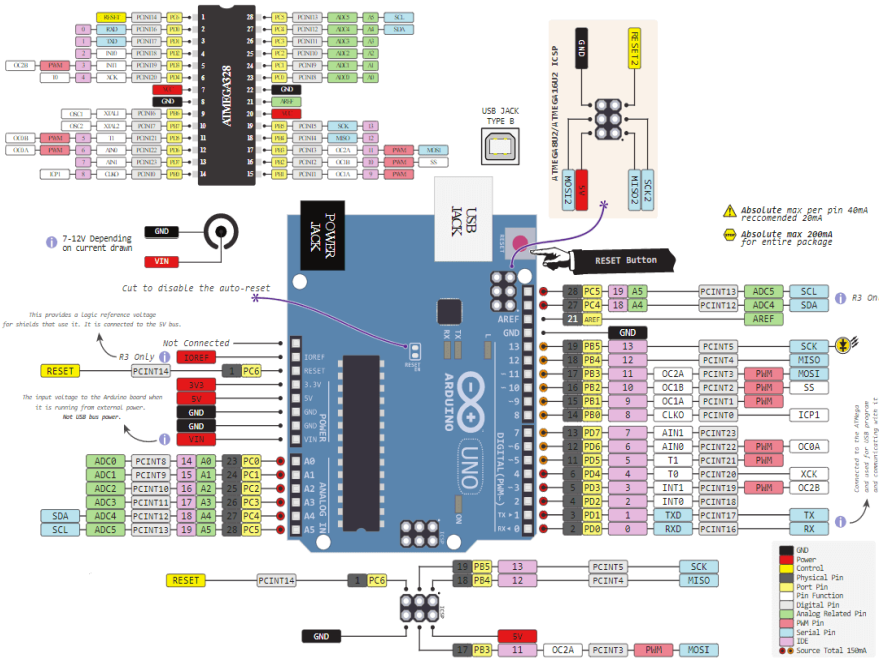

Figure 5. 8. Arduino Uno board specification summary [23].

5.4.2.4 Dragino LoRa Shield (V 1.3)

The LoRa shield is a single channel transceiver module that attains long distance communication in low data rates ranges. This module employs LoRa communication technology for data transfer [24]. The module is

based on the Semtech SX1276/SX1278 chip and has been instrumental to the enormous growth in low-cost IoT applications [24]. The Dragino shield has a sensitivity of over -148 dBm and +20 dBm power which has enabled it to achieve a very high link budget of 168 dBm [24]. LoRa shields are generally very suitable for robust and long-range IoT projects [24]. Figure 5.9 shows the Dragino LoRa shield. For this prototype implementation, three (3) LoRa shields are interfaced with the Arduino Uno to transmit data as LoRa Packets from the RTU to the MTU.

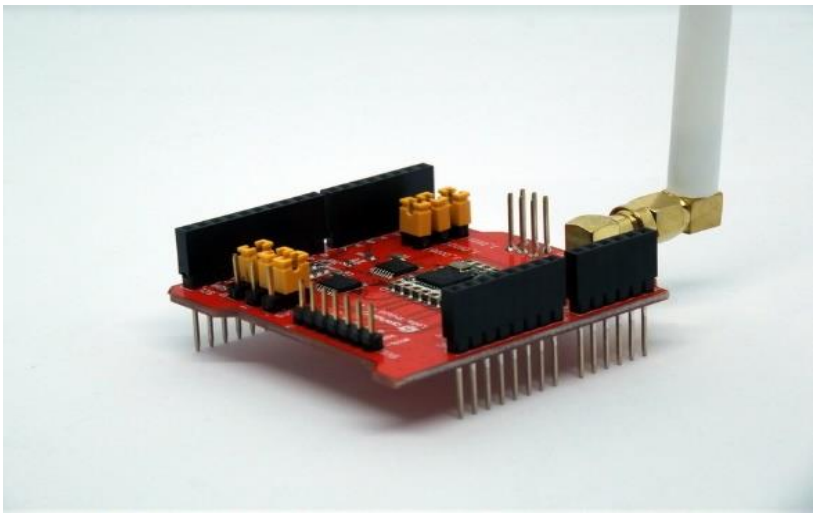

Figure 5. 9. Dragino LoRa shield [24].

5.4.2.5 RAK 831 LoRa Concentrator

The RAK 831 high-performance transceiver module [25] is employed in this work as the LoRa gateway. The concentrator is based on the Semtech SX1301, half-duplex gateway module, and supports up to 10 channels, 8 downlinks, 1 uplink and 1 FSK channel [25]. The Industrial Scientific and Medical (ISM) bands supports these channels for various regions. This module is typically employed to receive LoRa data packets from the end nodes which is also its function in this work. The RAK 831 is connected to a host machine and forwards the received data to the IoT platform hosted on the machine. A block diagram of the SX1301 base-band chip system is shown in Figure 5.10.

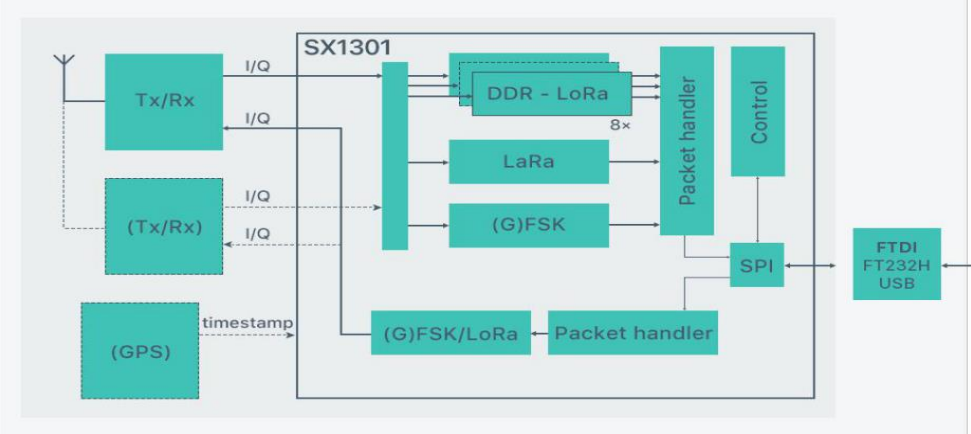

Figure 5. 10. SX1301 block diagram [25].

5.4.2.6 Raspberry Pi Micro-computer

The Raspberry Pi 3 model B+ was employed in this work. This is a single board micro-computer that operates on the Broadcom BCM283730, Cortex-A53 (ARMV8) 64-BIT SoC processor with a 1.4 GHz clock frequency [25]. The Raspberry Pi hosts the Chirpstack IoT platform and its dependences acting as the Master Terminal Unit. The features enumerated below make the Raspberry Pi suitable for application in the prototype of the proposed IoT SCADA system:

- 1GB LPDDR2 SDRAM.
- 2.4 GHz AND 5GHz IEEE 802.11.b/g/n/ac wireless LAN, Bluetooth 4.2.
- Gigabit Ethernet over USB 2.0.
- Extended 40-pin GPIO header.
- Full-size HDMI.
- Micro SD slot.
- 4 USB ports.
- 5V/2.5 DC power input.

5.4.2.7 MUN Electrical Engineering Laboratory Solar PV System

The Memorial University of Newfoundland (MUN) Electrical Engineering Laboratory houses a solar photovoltaic system which is made up of 12 solar panels that produce about 130 W at 7.6 A each. Two

photovoltaic modules are connected in parallel to make six sets of panels producing 260 W of power and about 14 A of current per set. The system also employs a Maximum Power Point Tracking (MPPT) system for maximum power capturing in all operating conditions. A battery (lead acid) storage system is also connected to the system for energy storage.

In this work, the system prototype is set up to acquire the PV voltage, PV current, PV power and the Battery voltage for remote monitoring and supervisory control.

5.5. Proposed System Prototype Implementation Methodology

To implement the proposed low-cost IoT SCADA system prototype, a voltage sensor and a current sensor are connected to the PV panels before the MPPT controller to measure the actual current and voltage being produced by the solar panels. A second voltage sensor is connected to the battery system to always monitor the battery voltage level. This process was set on three sets of modules. A 12V DC bulb was also connected to each system to represent the load. The load was in ON state all through the test period to allow for constant flow of current. The Arduino Uno is programmed on the Arduino IDE to process the sensor data, display on the IDE serial monitor and transmit the data via LoRa to the IoT gateway and platform installed on the Raspberry Pi. On arrival on the Raspberry Pi (MTU) through the LoRa gateway, the data is further processed by NodeRed and stored in the InfluxDB database. A Grafana dashboard is installed on the MTU to display data from the database. Subsequently, there is need for either personnel or automatic control of the unit being monitored, LEDs are connected to each Arduino Uno (RTU) to represent actuators, which could be switches, motors, relays etc. In this prototype, the LEDs (Green and Red) are controlled (ON and OFF) from the Grafana dashboard. As earlier mentioned, the LEDs used in this prototype can be re-placed by actual electrical actuators when being applied to full scale generation systems.

5.6. Prototype Design

The described hardware and software components were employed to develop a prototype of the proposed low-cost solution as shown in Figure 5.11. Here, three sensors are connected to the Arduino Uno

microcontroller. A Dragino LoRa shield (transceiver) is connected to the Arduino Uno for transmission of the acquired data over the LoRa communication technology. The sensors and the LoRa shields are powered by the 5V pin of the microcontroller. The MTU setup on the Raspberry Pi as shown in Figure 5.12 is located a distance away from the RTU setup. The MTU setup is made up of the Raspberry Pi, RAK 831 LoRa concentrator, a screen, and other accessories. The Chirpstack IoT server and the other integrations such as the InfluxDB database, Node-Red programming tool and Grafana dashboard are hosted on the Raspberry Pi. Although the components of the prototype system were placed close hence not showing the long-distance abilities of the LoRa communication system. Range tests for data delivery and packet delivery ratio analysis for LoRa communication have been already carried out by literatures such as [8] and [26] and therefore will not be repeated in this work.

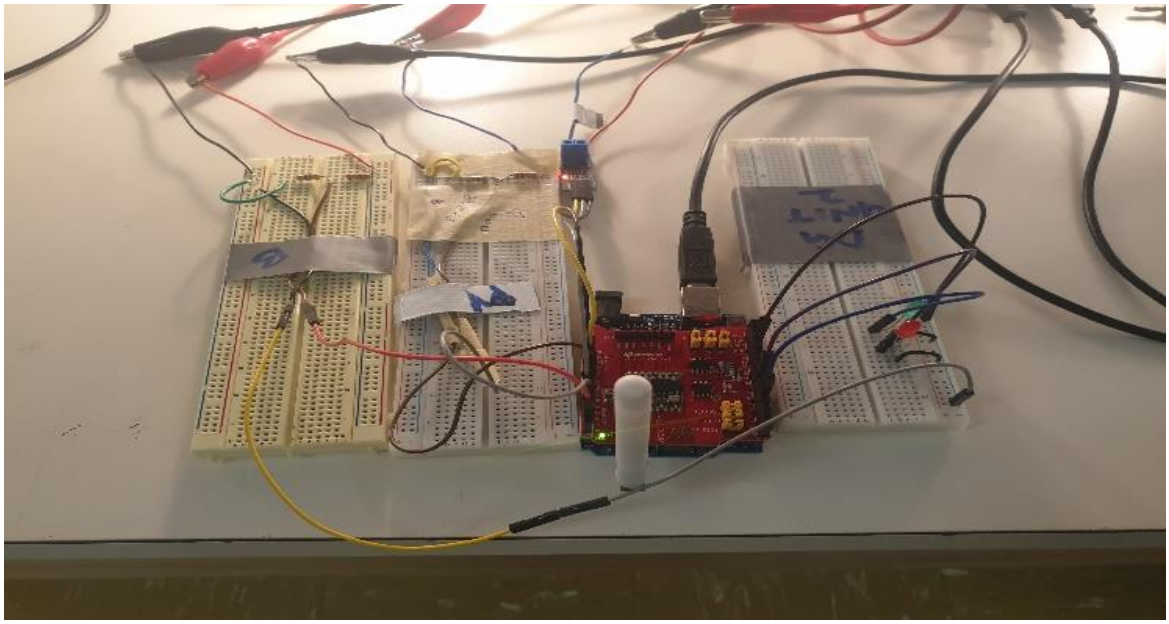

Figure 5. 11. Hardware implementation of the remote Terminal Unit.

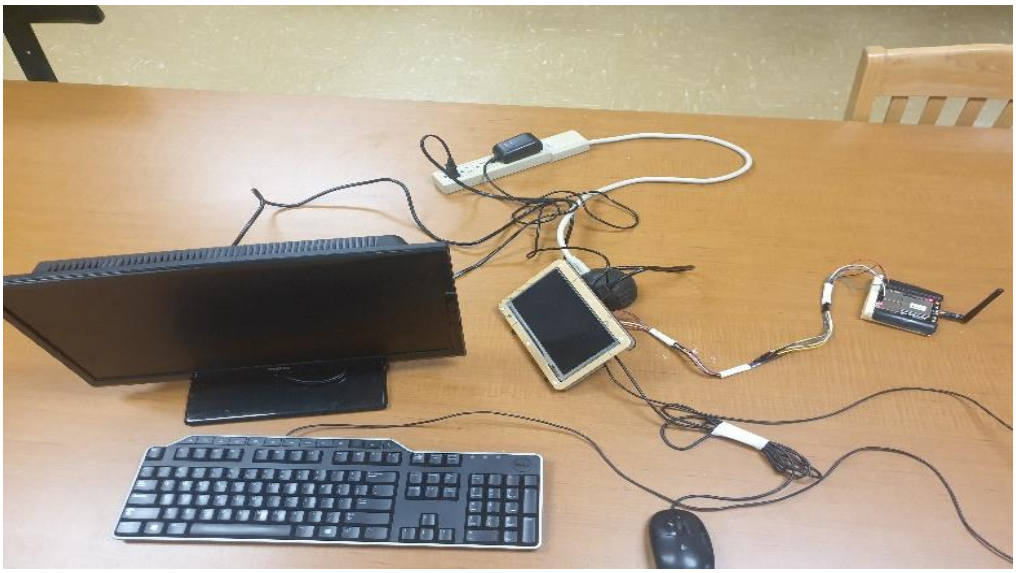

Figure 5. 12. Hardware implementation of the Master Terminal Unit.

5.7. Experimental Setup

Testing of the designed prototype was carried out by connecting the implemented hardware to the solar photovoltaic system at the Memorial University Electrical Engineering Laboratory as shown by the block diagram in Figure 5.13. Three units of the system were monitored using three RTUs, which acquire and transmit data to the MTU. On each RTU, there are two voltage sensors and a current sensor that collect the PV voltage, battery voltage and PV current respectively. The sensor data are acquired by the Arduino Uno through cable connection to the analog pins of the microcontroller. The data acquired is processed and transmitted to the MTU through the LoRa transceivers that are connected to the Arduino Uno microcontrollers. The experimental setup is shown in Figure 5.14.

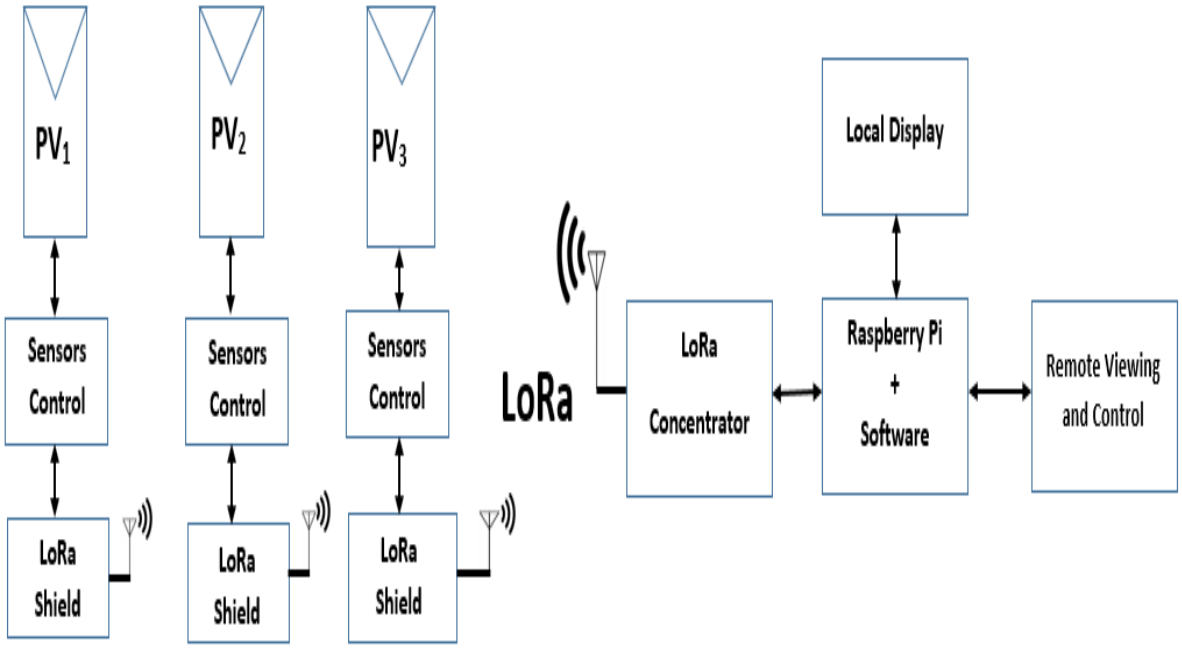

Figure 5. 13. The system prototype block diagram.

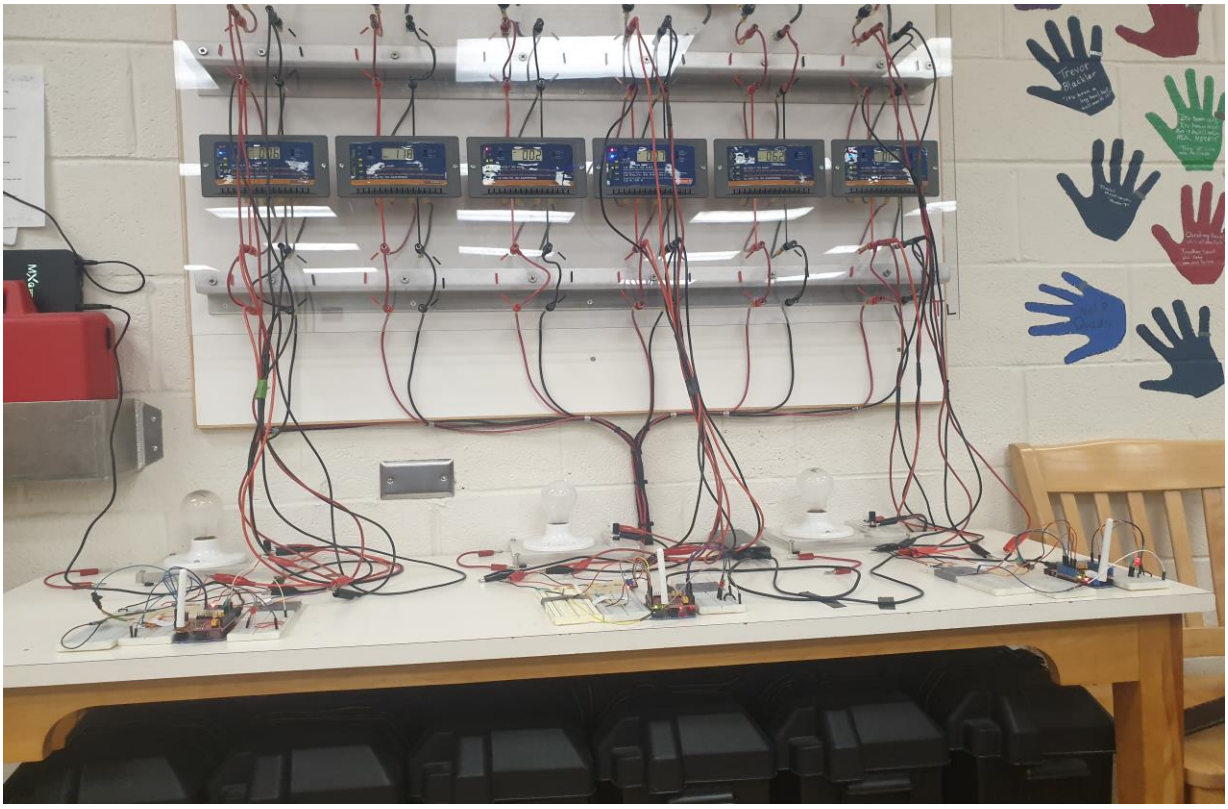

Figure 5. 14. Experimental setup of the proposed SCADA system including RTUs connected to PV system.

5.8. Results

The flowcharts in Figure 5.15 and Figure 5.16 depict the process of data acquisition at the RTUs and the data processing as it is performed at the MTU before being displayed at the Grafana dashboard for visualization.

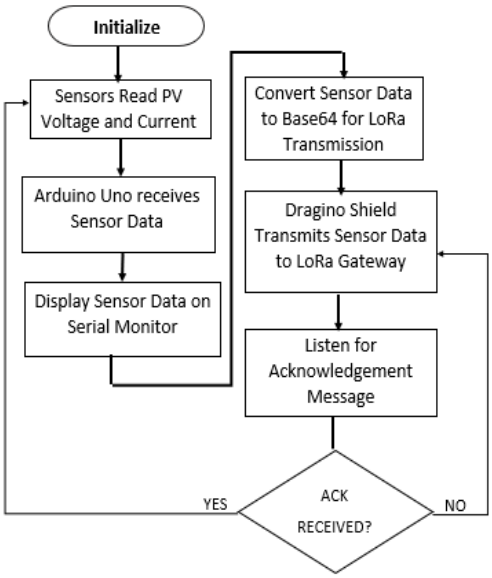

Figure 5. 15. Remote Terminal Unit flowchart.

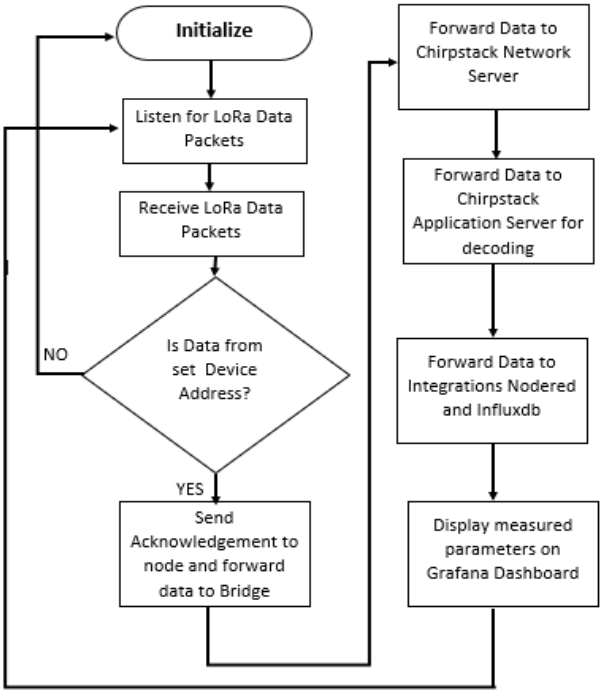

Figure 5. 16. Master Terminal Unit flowchart.

The sensor data were acquired from the units being monitored and transmitted to the IoT platform using the LoRa communication technology and posted on the Chirpstack platform console through the device profiles created on the platform as shown in Figure 5.17. On reception of the data, they are logged in the InfluxDB database and displayed on the Grafana dashboard for remote monitoring and supervisory control. The prototype of the proposed SCADA system was tested for a period of 3 weeks with series of disconnection and connections for system reliability check. During the test a load (12V DC bulb) was connected to the battery storage system to discharge the battery system and as such allow the continuous flow of a substantial amount of current to charge the battery. A Grafana dashboard with the data measurements was created and displayed the PV voltages, current and power of each unit as shown in Figure 5.18. The power of each PV unit was calculated as a product of the PV voltage and PV current measured from the system. The battery voltage level for the storage units were also monitored and displayed on the dashboard. To test the accuracy of the prototype, digital multimeters were connected to each of the measurement points of each unit to compare the multimeter values to those displayed on the IoT dashboard. The values from the dashboard and the multimeter readings matched with very minimal deviations, which indicates that the programming of the SCADA system was accurately carried out and the data being displayed are very accurate. The proposed SCADA solution has a data sampling time of 1 second depicting a very high and reliable data transfer speed. This, therefore, is suitable even in systems that require high speed data resolution. The LEDs connected to the RTUs were used to represent various forms of actuators that can be used in electrical generation systems such as relays, isolators, and switches. The LEDs were connected to the Arduino Uno microcontroller and programmed on the Arduino IDE to be controlled from the IoT platform either automatically or by the personnel on site.

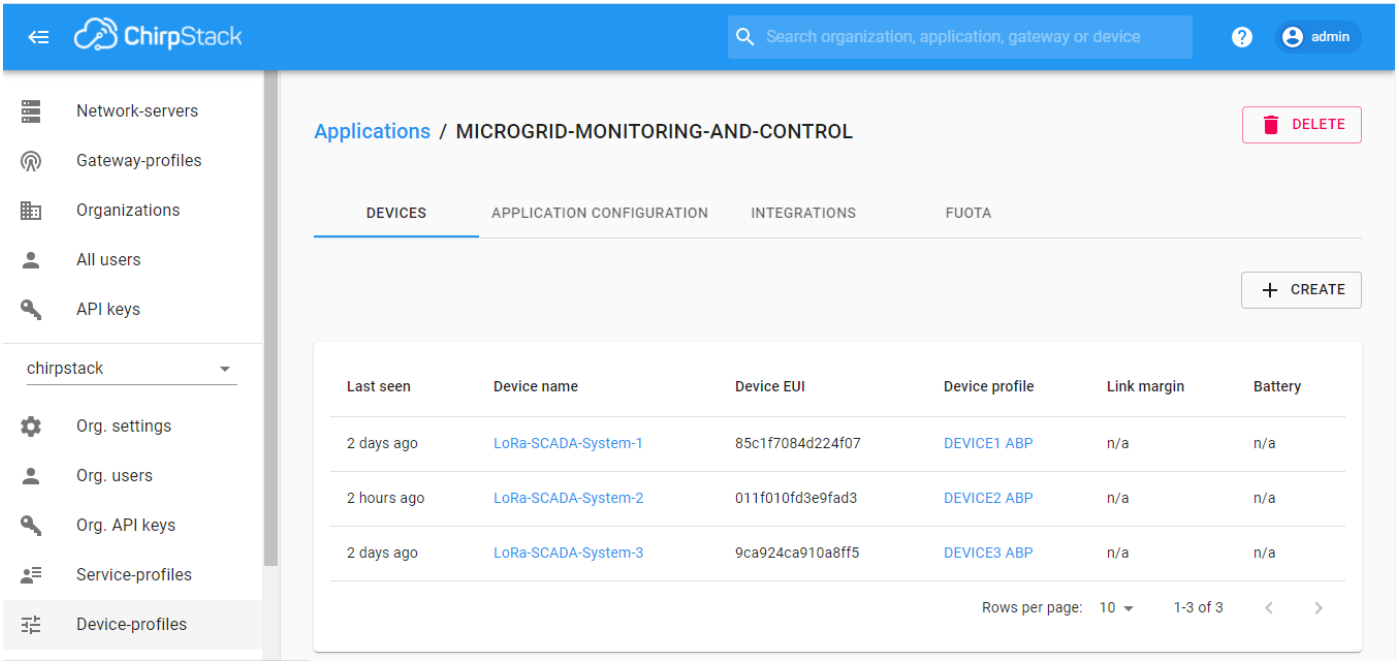

Figure 5. 17. The device profiles shown on the Chirpstack application server console.

Figure 5. 18. Real-time data measurement displayed on Grafana dashboard.

Two supervisory control scenarios were considered with the proposed SCADA solution. Firstly, a scenario with an operator watching the dashboard and observing the measured data, who can send a supervisory control command to the RTUs in case of any anomalies. In this scenario, the commands carry out one or two of the functions: Turn ON the RED LED, Turn ON the GREEN LED, Turn ON both LEDs and Turn OFF both

LEDs. In another scenario, the LEDs were also set to turn ON and OFF automatically through programming carried out on Node-Red. In this case, when the PV current and voltage are below the threshold (in the evening), the Green LED is automatically turned OFF while the RED is turned ON to indicate that the bulbs (loads) connected to the battery system are discharging the batteries. In the morning, when the sun is rising and the PV voltage and current begins to charge the battery and the voltages go above the threshold, the RED LED is turned OFF while the GREEN is turned ON. The Node-Red flow for the process is shown in Figure 5.19.

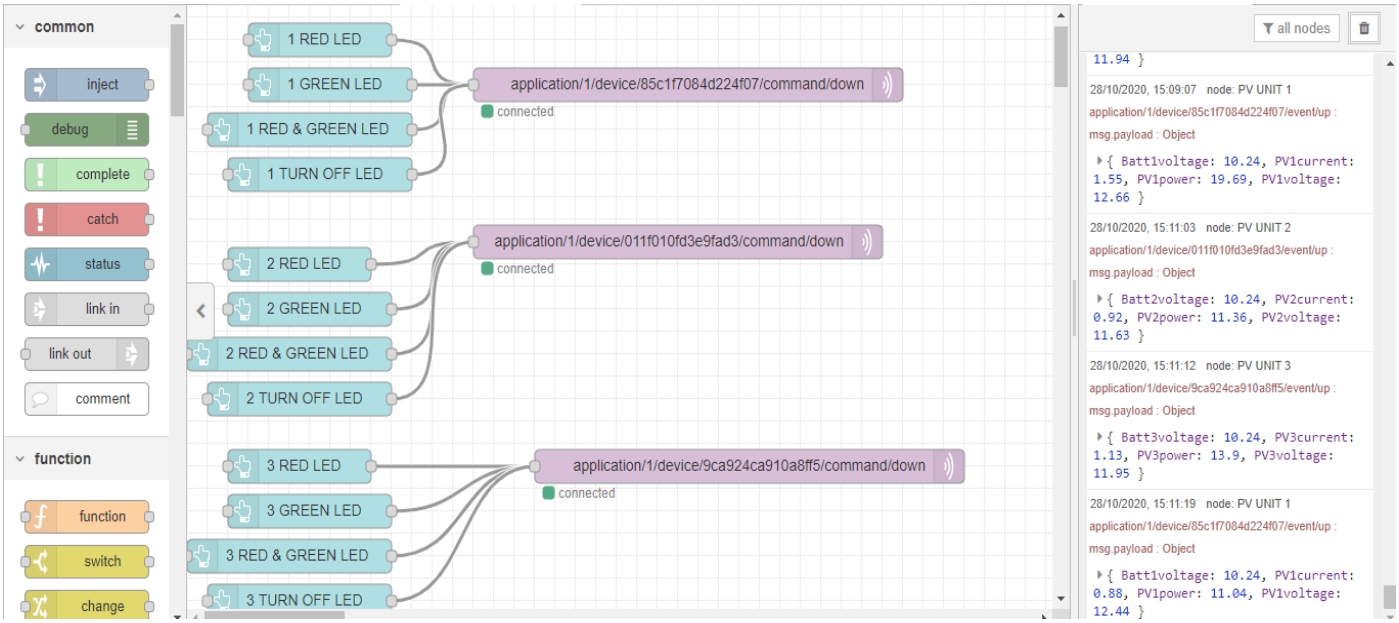

Figure 5. 19. Node-red flow for the supervisory control of the LEDs connected to the RTUs.

5.9. Discussion

The features of the low-cost open-source SCADA system proposed and designed in this work are aimed to mitigate the limitations of the conventional proprietary commercial SCADA systems. Some of the key characteristics of this proposed IoT SCADA solution are enumerated below:

- *Open Source and Interoperability*: The proposed system is made up of a mix of components from various vendors such as the Arduino Uno, Raspberry Pi and the Chirpstack IoT platform, InfluxDB,

Grafana and Node-Red. The programming of the systems is found in open-source sites such as the GitHub and Chirpstack forum. This indicates that the system is not tied to any proprietary vendor and troubleshooting, and resolution of the system does not require the service of an OEM.

- *System scalability*: The IoT concept allows connectivity of a very high number of sensors without any negative effect on the system. The proposed SCADA solution being built on the IoT architecture is robust enough to allow for a high level of scalability of the RTUs.
- *Robustness for remote area deployment*: The proposed system is an internet independent system. LoRa physical level communication protocol was employed for the data transfer in the system. This ensures that the proposed IoT SCADA solution can be deployed in remote areas with no internet or any other form of connectivity. The key components such as the Raspberry Pi and the Arduino can work in harsh conditions once they are well packaged.
- *Low-Cost*: The components employed in this design are cost effective. Table 5.2 shows the cost of each component and the overall cost of the system that consists of the sensors, three RTUs and the MTU as purchased from Amazon website. From the table, the overall cost of the system shows that the proposed SCADA system is relatively low cost when compared to the commercial SCADA systems when employed in the same system monitoring and control scenario.
- *User friendliness*: All the components ranging from the hardware to the software employed in the design and development of the system are easy to use. Most importantly, the Chirpstack IoT platform, InfluxDB database and the Grafana IoT dashboards are very user friendly.

Feasibility of deployment to large generation systems: The architecture of the pro-posed SCADA system is such that it can be applied for monitoring of large generation systems. It is anticipated that the proposed system can be deployed to large systems for monitoring with appropriate upgrade to the various hardware. This level of monitoring can be achieved with the key features such as the low-cost, scalability, interoperability and reliability still maintained as those of the IoT SCADA solution proposed in this work.

Table 5. 2: Bill of materials.

S/N	Components	Unit Cost (CAD)	Qty	Price (CAD)
1	Chirpstack.IO RPi image	0.00	1	0.00
2	Raspberry Pi 3 B	67.90	1	67.90
3	Arduino Uno Microcontroller	29.99	3	89.97
4	Dragino LoRa Shield	65.28	3	195.84
5	RAK 831 LoRa concentrator	170.00	1	170.00
6	ACS 712 Current Sensor	7.99	3	23.97
7	Voltage Sensor	0.00	6	0.00
8	Others (Resistors, Wires, LEDs etc.)	50.00	1	50.00
	Total:			$597.68

5.10. Conclusions

This work proposes a low-cost SCADA system developed for the monitoring of electrical parameters from distributed energy generation systems. The proposed system presents an IoT solution to the current challenges faced by the proprietary SCADA systems that causes them not to be applied for system monitoring at some levels. The proposed IoT system also presents a modification for the IoT solutions that have earlier been proposed by various researchers.

This modified system employed a system where the IoT platform, gateway and all integrations are hosted on a single machine thereby eliminating the need for cloud based IoT platform hosting and as a result remove the need for internet for communication with the cloud and at the same time increase system compactness. The reduction in components reduced the price of developing such system and increased the system's level of autonomy. This means that the proposed IoT SCADA solution in this work can be employed for system monitoring in areas with no existing communication infrastructure. Furthermore, the long-range capability of

LoRa has also made the proposed system suitable for data collection from distributed energy units up to distances of between 5 to 15 km especially in remote areas.

A prototype was designed using a combination of the hardware and software to achieve the IoT SCADA solution. To validate the system performance, the prototype was set up and tested at the Memorial University Electrical Engineering Laboratory. The system measured the PV voltage, PV current and battery voltage of photovoltaic units in the laboratory. For control purposes, LEDs were connected to the RTUs to represent actuators such as relays, switches, and pumps.

The results from the testing show that the system achieved SCADA functionalities, which include data retrieval, transmission, data management and display, and system control. The overall cost of the prototype to monitor the three solar PV units is about $600 CAD without any form of continuous subscriptions. The system has an IoT database from InfluxDB, which is a time-series database that allows the storage of all parameters over a very long period. The data presented on the IoT dashboard as measured by the system conformed to those measured using digital multimeters.

The whole solution was implemented as a local system where the server and all software elements were hosted on a single machine. This enhances security and data integrity as only authorized personnel can have access to the data as opposed to the cloud servers prone to cyber-attacks and makes the system robust for remote area applications in situations where there are no communication technologies. Although the prototype presented in this thesis cannot be deployed to large systems as it is, incorporating appropriate hardware upgrades and packaging with same proposed architecture will easily be deployed to large system for monitoring at a much lower cost and very high data monitoring standard.

5.11 References

[1] "Renewable Energy Now Accounts for a Third of Global Power Capacity", *Irena.org*, 2020. [Online]. Available : https://www.irena.org/newsroom/pressreleases/2019/Apr/Renewable-Energy-Now-Accounts-for-a-Third-of-Global-Power-Capacity.

[2] P. de Arquer Fernández, M. Fernández Fernández, J. Carús Candás and P. Arboleya Arboleya, "An IoT open-source platform for photovoltaic plants supervision", *International Journal of Electrical Power & Energy Systems*, vol. 125, p. 106540, 2021.

[3] E. Sisinni, A. Saifullah, S. Han, U. Jennehag and M. Gidlund, "Industrial Internet of Things: Challenges, Opportunities, and Directions," in *IEEE Transactions on Industrial Informatics*, vol. 14, no. 11, pp. 4724-4734, Nov. 2018.

[4] B. Chae, "The evolution of the Internet of Things (IoT): A computational text analysis", *Telecommunications Policy*, vol. 43, no. 10, p. 101848, 2019.

[5] B. Chae, "The evolution of the Internet of Things (IoT): A computational text analysis", *Telecommunications Policy*, vol. 43, no. 10, p. 101848, 2019.

[6] Y. Wang, Y. Xu and Y. Tang, "Distributed aggregation control of grid-interactive smart buildings for power system frequency support", *Applied Energy*, vol. 251, p. 113371, 2019.

[7] K. Rajeswar, “Industry 4.0 wave-relevance of SCADA in an IOT world and journey towards a true digital enterprise”. *IEEE India Info*, Vol 14: 78-88, 2019.

[8] H. Geng, *The Internet of things and data analytics handbook*, 2nd ed. New Jersey: John Wiley & Sons Inc, 2017, pp. 131-143.

[9] L. O. Aghenta and M. T. Iqbal, "Development of an IoT Based Open-Source SCADA System for PV System Monitoring," *2019 IEEE Canadian Conference of Electrical and Computer Engineering (CCECE)*, 2019, pp. 1-4.

[10] Li Wang and K. -H. Liu, "Implementation of a Web-Based Real-Time Monitoring and Control System for a Hybrid Wind-PV-Battery Renewable Energy System," *2007 International Conference on Intelligent Systems Applications to Power Systems*, 2007, pp. 1-6.

[11] A. Iqbal and T. Iqbal, "Low-cost and Secure Communication System for Remote Micro-grids using AES Cryptography on ESP32 with LoRa Module," *2018 IEEE Electrical Power and Energy Conference (EPEC)*, 2018, pp. 1-5.

[12] X. LU, "Supervisory Control and Data Acquisition System Design for CO2 Enhanced Oil Recovery", MASTER OF ENGINEERING, Electrical Engineering and Computer Sciences University of California at Berkeley, 2014.

[13] L. Aghenta and M. Iqbal, "Low-Cost, Open Source IoT-Based SCADA System Design Using Thinger.IO and ESP32 Thing", *Electronics*, vol. 8, no. 8, p. 822, 2019.

[14] N. P. Kumar and R. K. Jatoth, "Development of cloud based light intensity monitoring system using raspberry Pi," *2015 International Conference on Industrial Instrumentation and Control (ICIC)*, 2015, pp. 1356-1361.

[15] V. Sandeep, K. L. Gopal, S. Naveen, A. Amudhan and L. S. Kumar, "Globally accessible machine automation using Raspberry pi based on Internet of Things," *2015 International Conference on Advances in Computing, Communications and Informatics (ICACCI)*, 2015, pp. 1144-1147.

[16] S. Chanthakit and C. Rattanapoka, "MQTT Based Air Quality Monitoring System using Node MCU and Node-RED," *2018 Seventh ICT International Student Project Conference (ICT-ISPC)*, 2018, pp. 1-5.

[17] J. C. B. Lopez and H. M. Villaruz, "Low-cost weather monitoring system with online logging and data visualization," *2015 International Conference on Humanoid, Nanotechnology, Information Technology, Communication and Control, Environment and Management (HNICEM)*, 2015, pp. 1-6.

[18] B. Queté *et al*., "Understanding the tradeoffs of LoRaWAN for IoT-based Smart Irrigation," *2020 IEEE International Workshop on Metrology for Agriculture and Forestry (MetroAgriFor)*, 2020, pp. 73-77.

[19] M. Nasar and M. Kausar, "Suitability of Influxdb Database For Iot Applications", *VOLUME-8 ISSUE-10, AUGUST 2019, REGULAR ISSUE*, vol. 8, no. 10, pp. 1850-1857, 2019.

[20] S. Venkatramulu, M. Phridviraj, C. Srinivas and V. Rao, "Implementation of Grafana as open-source visualization and query processing platform for data scientists and researchers", *Materials Today: Proceedings*, 2021.

[21] M. Lekić and G. Gardašević, "IoT sensor integration to Node-RED platform," *2018 17th International Symposium INFOTEH-JAHORINA (INFOTEH)*, 2018, pp. 1-5.

[22] S. Singh, S. L. Arun and M. P. Selvan, "Regression based approach for measurement of current in single-phase smart energy meter," *2017 IEEE Region 10 Symposium (TENSYMP)*, 2017, pp. 1-5.

[23] Y. A. Badamasi, "The working principle of an Arduino," *2014 11th International Conference on Electronics, Computer and Computation (ICECCO)*, 2014, pp. 1-4.

[24] S. Bdiri, F. Derbel and O. Kanoun, "An 868 MHz 7.5 µW wake-up receiver with −60 dBm sensitivity", *Journal of Sensors and Sensor Systems*, vol. 5, no. 2, pp. 433-446, 2016.

[25] C. Ndukwe, M. Tariq Iqbal, X. Liang, J. Khan and L. Aghenta, "LoRa-based communication system for data transfer in microgrids", *AIMS Electronics and Electrical Engineering*, vol. 4, no. 3, pp. 303-325, 2020.

[26] M. R. Seye, B. Ngom, B. Gueye and M. Diallo, "A Study of LoRa Coverage: Range Evaluation and Channel Attenuation Model," *2018 1st International Conference on Smart Cities and Communities (SCCIC)*, 2018, pp. 1-4.

Chapter 6

Analysis of LoRa Transmission Delay on Dynamic Performance of Standalone DC Microgrids

Co-authorship Statement

This chapter analyzed the effect of employing LoRa for secondary control level data transfer in hierarchical DC microgrids. This simulation in this chapter was carried out in MATLAB/Simulink to observe the effects of LoRa transmission delay on the dynamic performance of the DC microgrid during system control. This study in this chapter considered the DC microgrid designed in Chapter 3. LoRa transmission delay were calculated for data and control signals that transmitted between the local controllers and the microgrid central controller. The calculated delays were included in the simulation as transport delays and the effects were observed on the DC bus voltage of the microgrid. To eliminate these variations, delay compensation techniques were proposed in the work to show that the system can still perform at near optimal capabilities even with the employment of a low bandwidth communication system such as LoRa.

I (Ndukwe Cherechi Izuchukwu) am the principal author and contributed to Conceptualization, Methodology, Software Investigation, Writing- Original Draft and Editing of this chapter. The research in this chapter was supervised by Dr. Tariq Iqbal, Dr. Jahangir Khan, and Dr. Jamil Mohsin. The supervisors contributed to the conceptualization and methodology of this chapter. They supervised the entire chapter, reviewed and corrected the research manuscript. A research manuscript was developed from the work in this chapter and has been published in Journal of Energy and Power Technology 2022, volume 4, issue 2 doi:10.21926/jept.2202022.

Abstract

One important aspect toward proper and stable functioning of a communication-based controlled microgrid is data transmission. Consequently, an analysis of the effect of data transmission delay is of significance for any chosen communication protocol. This paper focuses on the effect of employing LoRa for data transfer at the secondary control level of a standalone DC microgrid. It analyses the effect of LoRa transmission delay on the dynamic performance of DC microgrids. This paper simulates a community DC microgrid that operates in three modes: PV mode, battery mode and generator mode. This microgrid operates as a centralized communication-based controlled microgrid, with the secondary control level operating as an event-driven level. The system incorporates a hierarchical system where data is transferred between the various distributed energy resources (DERs) local controllers and the microgrid central controller (MGCC). Simulations for three scenarios are presented. In the first scenario, the microgrid is designed and simulated without a communication delay to observe the system behavior. Then LoRa transmission delay is calculated for the various signals transferred between the MGCC and the local controllers. This delay is introduced into the simulation as transport delays and the system exhibits a level of stability degradation. Subsequently, a time delay compensation system is incorporated into the system for more robust operation. The delay compensation is applied in two simulation scenarios. In the first scenario, the system inductor (L) and capacitor (C) components are re-calculated, and the system is re-simulated to get a stable system even with the applied communication delay. In the second scenario, the proportional integrator (PI) controller in the microgrid central controller is re-designed to a more robust form to compensate for the delay caused by the LoRa transmission. The results obtained from the two modified simulations realize a stable DC microgrid. This system modification allows for system stability again, similar to the simulation when the microgrid operated without any communication delay. This, therefore, demonstrates that with proper system design and implementation, low bandwidth communication systems such as LoRa can be effectively employed for data transfer in event-driven communication-based controlled DC microgrids.

Keywords
DC microgrid; microgrid control; LoRa communication; data transmission delay.

6.1 Introduction

Microgrids are important elements towards full realization of smart grids, which are already in existence in most developed countries. Such systems have the potential to attain higher grid resilience [1][2]. The United States Department of Energy has defined microgrid as an interconnection of distributed energy resources (DERs), energy storage systems (ESS) and groups of interconnected loads. Microgrids have been developed to either operate in grid-connected mode or in standalone (islanded) mode [3],[4]. The grid-connected microgrid is tied to a larger network and supported by the microgrid DERs in times of faults, blackouts etc. On the other hand, when the microgrid is directly supplying the loads with power generated by the DERs, it is referred to as islanded mode of operation.

Presently, microgrids are mainly classified as AC, DC, or hybrid AC/DC microgrids. This classification is mainly focused on the common voltage of the microgrid [5]. DC microgrids have shown to be more efficient due to the lower amount of internal conversion required for power transfer to the loads [5]. This is the reason, most of the DERs and ESSs are DC systems [5]. The main known challenges to date are around the design of efficient protection systems [6]-[8]. As such, the hybrid system has been developed with consideration of the advantages of both AC and DC systems. Note that in this research paper, only DC microgrid is considered.

DC microgrids can be operated in two primary control modes: (1) voltage-droop control and (2) communication-based control. In voltage-droop control, system stability is achieved by the application of a virtual resistor to the converter's voltage regulator [5]. This enables current/power-sharing. The main advantage of this control method is its total reliance on system parameters, and as such it does not require any communication system for data transfer [9], [10]. However, the droop control faces some challenges, which includes slow dynamic response and system voltage inaccuracies caused by circulation currents between the converters [11],[12]. This generally has a degrading effect on microgrid stability.

Communication-based control is based on continuous communication of various microgrid components for data transfer that facilitate control. Microgrids that are controlled using this method can be classified into centralized or decentralized systems [5]. In the centralized system, the main controller communicates with the local controllers of all components, which then sets various points and control actions based on the data obtained from the various controllers. On the other hand, a distributed system has no need for a central controller. As a result, it is immune to one of the main problems faced by the centralized system- a single point of failure. Understandably, the distributed control system is generally rather complex.

In recent times, research has focused on the employment of low bandwidth communication systems for data transfer within microgrids [13][14]. From literature, it has been observed that the benefit of such systems is in reduced number of parameters to be transferred. Even though various schemes are being investigated to date, these analyses are done on a general level.

LoRa has been proposed and successfully implemented in a wide variety of applications in various fields of engineering and technology. With more focus on microgrids, this has also been proposed for data transfer at the secondary control level [14].

From various research and to the best of authors knowledge, there has not been any specific work that covers the effect of LoRa transmission delay on the dynamic performance of a DC microgrid. As such, this research brings novelty to the knowledge base.

This paper presents an analysis of LoRa for data transfer in a centralized communication-based controlled DC microgrid and focuses on the effects of LoRa transmission delay on the dynamic performance of a standalone system.

The main contributions of this paper include:

1) Design and simulation of a DC microgrid with LoRa transmission delay to observe the effect of the LoRa transmission delay on the microgrid dynamic performance.
2) Demonstration of a stable DC microgrid with LoRa as the data transfer system by proper component selection and system redesign.

This paper is organized as follows: Section 2 presents a description of the communication-based DC microgrid; Section 3 describes the mathematical characterization of LoRa data transmission delay; Section 4 describes the DC microgrid being studied; Section 5 presents the simulation results; Section 6 discusses the results. Key conclusions and recommendations for future work are presented in Section 7.

6.2 Communication-Based DC Microgrid Control

Communication-based DC microgrid control can be defined as a microgrid control technique that depends substantially on constant communication between various microgrid components for real-time update of system parameters and control commands. This technique is either centralized or fully distributed. In centralized communication-based control, all sensor (i.e., field devices) data are measured and transmitted from various controllers to the microgrid central controller (MGCC). The received parameters are processed, and if parameter discrepancies exist, the central controller sends back control commands and operation set points to maintain system stability [5]. In most cases, this technique offers near optimal microgrid performance because the central microgrid controller constantly has real-time information of the microgrid resources. On the other hand, due to the total reliance of the microgrid reliability on the communication system, the system is susceptible to the single point of failure. This, therefore, emphasizes the importance of the reliable communication system for data transfer within microgrids employing this control technique.

In distributed communication-based control, the need for a central controller is not pressing as the local controllers have direct communication towards coordination and negotiation to achieve microgrid optimum stability [15]. This in turn, has an impact on system reliability. Furthermore, due to the distributed nature of this technique for microgrid control, it is immune to the single point of failure as with the centralized communication technique. However, system complexity of this technique has been the main limitation [16]. The centralized and distributed techniques are shown in Figure 6.1. In this research, a centralized communication-based microgrid control technique is employed for simplicity.

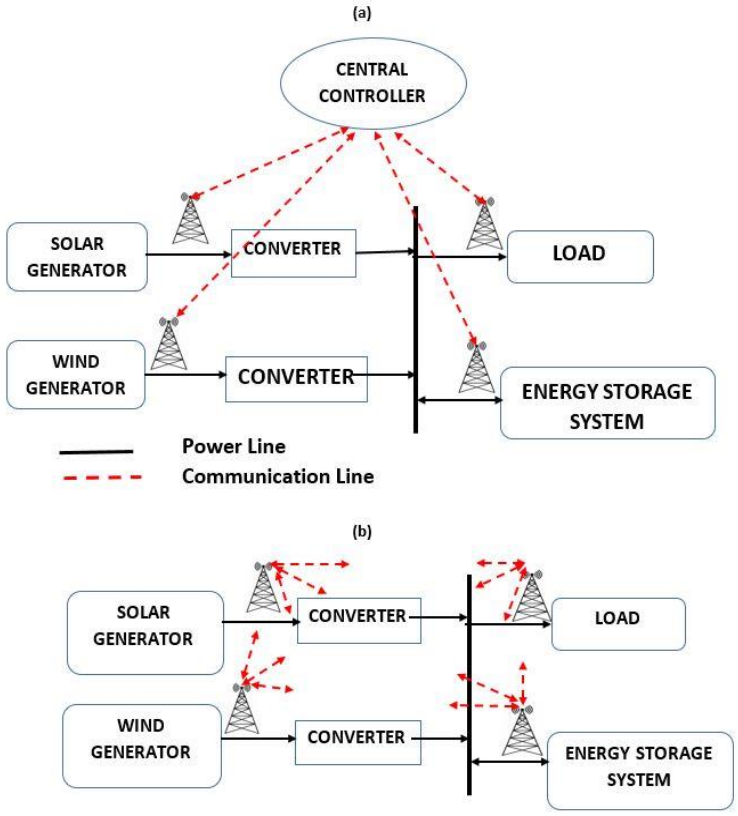

Figure 6. 1. (a) Centralized communication microgrid control (b) distributed communication microgrid control.

Data and control commands transfer within microgrids can be either "state-driven" or "event-driven". State-driven control is specifically based on continuous transfer of system state variables to the controller. These variables are constantly sampled and periodically transmitted. In the event-driven control, the controllers are only triggered by anomalies in the system. Hence, reducing the frequency of parameter transfer. Rather events trigger actions for system operation mode switch. This control, therefore, can function more with a low communication bandwidth than the state-driven control. The event-driven control presents some advantages such as low communication bandwidth requirements and low computational process, which in turn saves energy [17][18]. However, it is important to note that event-driven control requires a deep understanding of the system to increase system alertness thereby avoiding unexpected system events that might level to the system instability. State-driven control still dominates for microgrid control due to its already-existing experience and the possible difficulties involved in the development of event-driven control algorithm [17].

For state-driven control, system performance has been the focus, while event-driven control may be suitable for certain applications to balance between control performance and system efficiency. In microgrid control, as stated in [5], state-driven control is well employed in primary control between the sensors and the local controller sharing parameters such as gate pulses to the converters and electrical parameters. Furthermore, event driven control can be applied to secondary control levels where parameters such as event report, state changes, parameter reduction and command signals are transferred between the local controller and the central controller.

6.2.1 Microgrid event-driven control

A hierarchical microgrid control structure is employed in this research. The primary control layer is consisted of local controllers that communicate continuously with various sensors connected to the DERs. This control level functions in the state-driven mode. The local controllers continuously monitor and measure the state variables that are vital to maintain various modes and operating points. In the secondary control layer, the microgrid central controller communicates with the local controllers and assigns operating modes for stability with reference to the changed parameters it received from the local controllers. The secondary control layer is event controlled. The secondary control layer being event-controlled entails that it does not require continuous communication between the microgrid central controller, and the local controllers located at the various distributed generation (DG) units. This reduces the overall communication bandwidth requirements for data and command transfer.

The analysis in this paper strictly focuses on the dynamic performance of the secondary control level. The authors in [19] state that, in comparison, if the sampling frequency of a high bandwidth communication is f_s, then the low bandwidth communication protocol will have a sampling frequency of $\frac{f_S}{N}$ (meaning, there is a reduction of data amount to $\frac{1}{N}$ in low bandwidth communication), where N is the number of control periods.

This analogy allows for the employment of low-bandwidth communication systems for event-driven secondary level control data transfer.

In event-driven control, during normal operations, communication only happens with an event that also results to a control action. Therefore, if the total sampling time during the control process $T_S = \sum_0^{N_S} T_{NS}$ [17], where N_s is the number of samples sent through the communication network during the control process and T_{NS} is the sampling time of one sample of N_s. Assuming the same sample duration, high bandwidth communication T_S will be higher than low bandwidth communication T_S. In event driven control, $T_S|_e = \sum_0^{m-1} T_{NS}$, where m is the number of events triggered during the control process.

Considering that events do not occur frequently, the $T_S|_e$ is very much lower compared to T_S in high and low bandwidth communication. This work employs an event-driven communication-based secondary level microgrid control.

6.3 LoRa Data Transmission Delay Mathematical Characterization

LoRa has recently been developed as a physical layer communication technique known very well for its low power consumption and long-range data transfer capabilities. These features have facilitated its significant growth for industrial applications for which microgrids is not an exception. Due to the proprietary nature of this communication protocol, there has not been a detailed mathematical description of the system. This section focuses on mathematical characterization of LoRa transmission delay. LoRa is defined as a linear chirp signal because it corresponds to a waveform whose frequency increases or decreases linearly with time [20].

The following notations are used in the characterization, as shown in Table 6.1.

Table 6. 1: LoRa Modulation Notations

Notation	Description
f_c	Starting frequency of up-chirp
B_W	Bandwidth
SF	Spread factor used for modulation (usually, 7 to 12 in LoRa)
T	Data transfer period of chirp = $\frac{2^{SF}}{B_W}$
μ	+1 (up chirp)
	-1 (down chirp)
$\theta(t)$	Phase of the chirp signal
$c(t)$	Carrier signal
s(t)	Transmitted symbol waveform
$f(t)$	Instantaneous frequency of chirp signal

In LoRa modulation, the carrier signal, *c(t)*, is a linear up-chirp given by the expression[20]:

$$c(t) = f(x) = \begin{cases} \exp(j\theta(t)), & 0 \le t \le T \\ 0, & o.w. \end{cases} \quad (6.1)$$

The instantaneous accumulated phase of the chirp signal $\theta(t)$ and the instantaneous frequency as a function of time are given by[20]:

$$\theta(t) = 2\pi f_c + \pi\mu\frac{B_W}{T}t^2, \ 0 \le t \le T \quad (6.2)$$

$$f(t) = \frac{1}{2\pi}\frac{d\theta(t)}{dt} = f_c + \mu\frac{B_W}{T}t, \ 0 \le t \le T \quad (6.3)$$

Therefore, for a general case for symbol transmission, the transmitted symbol waveform s(t), is given by [20],

$$s(t) = \begin{cases} \exp(j\emptyset(t)), & 0 \le t \le T \\ 0, & o.w. \end{cases} \quad (6.4)$$

The instantaneous chirp frequency of the coded symbol is then defined as [20]:

$$f(t) = \begin{cases} f_c + \mu \frac{B_W}{T}\left(t - \frac{K}{B_W}\right) + B_W, \ 0 \le t \le \frac{K}{B_W} \\ f_c + \mu \frac{B_W}{T}\left(t - \frac{K}{B_W}\right) \quad , \ \frac{K}{B_W} \le t \le T \end{cases} \tag{6.5}$$

Furthermore, the instantaneous accumulated phase of the coded symbol is then defined as [20]:

$$\emptyset(t) = \begin{cases} 2\pi f_c t + 2\pi\mu \frac{B_w}{T}\left(\frac{t^2}{2} - \frac{K}{B_W}t\right) + 2\pi B_W t, \ 0 \le t \le \frac{K}{B_W} \\ 2\pi f_c t + 2\pi\mu \frac{B_w}{T}\left(\frac{t^2}{2} - \frac{K}{B_W}t\right) \quad , \ \frac{K}{B_W} \le t \le T \end{cases} \tag{6.6}$$

Traditionally, data is transmitted on LoRa communication technology as data packets in $BASE_{64}$ format. A detailed analysis of LoRa in the context of microgrid data transfer has been presented in [14] where the conversion is achieved in the following key steps:

1. Data preparation into ASCII text format.
2. Each letter of the ASCII text format is converted to ASCII binary format.
3. The binary codes obtained from the step above with 8 bits are joined together
4. The joined binary data is now split into 6-bit binary codes.
5. Each 6-bits is then converted to decimal value
6. Each decimal value is matched with a Base64 symbol on the Base64 table, where each decimal value from 0- 63 has a matching symbol.

To further illustrate the LoRa transfer format, the above-stated steps are shown in Figure 6.2 for a measured 360 V (possible microgrid bus voltage).

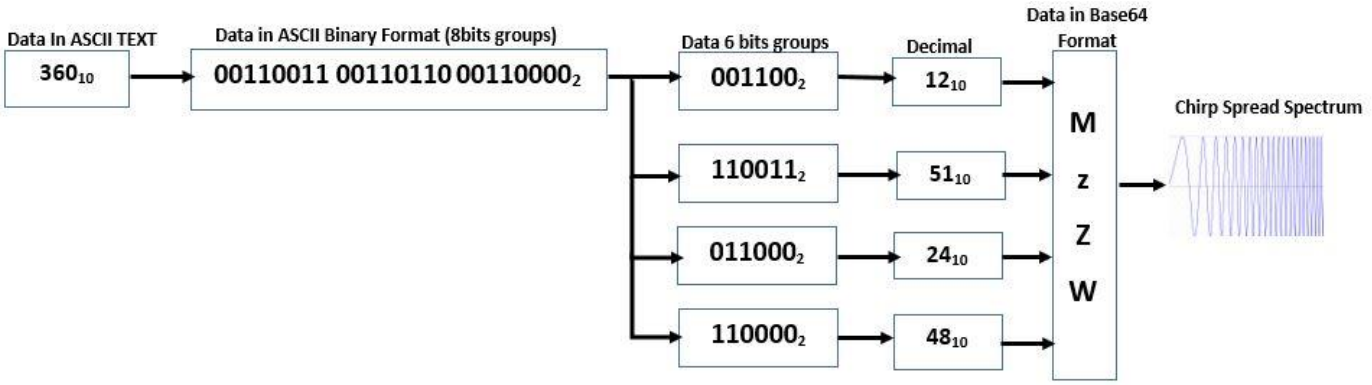

Figure 6. 2. Representation of LoRa data formatting before transmission

The structure of a basic LoRa data frame is shown in Figure 6.3.

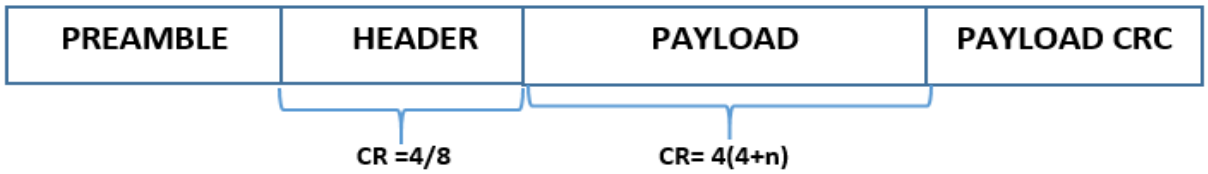

Figure 6. 3. Structure of a LoRa frame.

The time to transfer each chip by a LoRa device depends on the bandwidth. This time is calculated as:

$$T_{chip} = \frac{1}{Bandwidth} \qquad (6.7)$$

In LoRa communication, there are three statutory bandwidths through which data can be transmitted. These are: 125 kHz, 250 kHz, and 500 kHz [20]. The bandwidth can also be defined as the chip rate, which is the number of vibrations or wave cycles per second. Hence,

$$BW = R_C = Chip\ Rate \qquad (6.8)$$

For a bandwidth of 125 KHz, the chip rate is 125000 chips/sec. Therefore,

$$T_{chip} = \frac{1}{125{,}000} = 0.000008\ sec$$

T_{chip} for the 125 kHz, 250 kHz and 500 kHz are 8µs, 4µs and 2µs respectively. This shows that with increased bandwidth there is a reduction in transmission time. The transmission time for a LoRa symbol T_{symbol} is calculated as:

$$T_{symbol} = \frac{2^{SF}}{BW} \quad (6.9)$$

Where, SF is the spreading factor, and BW is the bandwidth.

From Equation (6.9), the time to transfer a symbol with the existing spreading factors (7 -12) and the bandwidths are shown in Table 6.2.

Table 6. 2: A comparison of LoRa transfer bandwidths delays

SF	T_{symbol} (µs) @ BW = 125 KHz	T_{symbol} (µs) @ BW = 250 KHz	T_{symbol} (µs) @ BW = 500 KHz
7	1,024	512	256
8	2,048	1,024	512
9	4,096	2,048	1024
10	8,192	4,096	2048
11	16,384	8,192	4096
12	32,768	16,384	8,192

Table 6.2 shows that an increase in bandwidth has a decreasing effect on the data transmission time. Furthermore, an increase in the spreading factor increases the transmission time. The transmission time doubles with a one-step increase in the spreading factor (SF).

The expressions for calculating the data transmission time for a LoRa frame is given by:

$$T_{frame} = T_{preamble} + T_{payload} \quad (6.10)$$

$$T_{payload} = n_{payload} + T_{symbol} \quad (6.11)$$

$$n_{payload} = 8 + \max\left(ceil\left[\frac{8PL - 4SF + 28 + 16CRC - 20IH}{4(SF - 2DE)}\right](CR + 4), 0\right) \quad (6.12)$$

$$T_{preamble} = (n_{preamble} + 4.25)T_{symbol} \quad (6.13)$$

Normally, $n_{preamble} = 8$ for LoRa

Where,

PL = number of bytes.

IH = Implicit header.

(If Header is enabled, IH =0 if Header is disabled, IH = 1).

DE = low data optimization

(DE = 1, enabled, 0 = disabled)

CR = Coding rate (default = 1)

CRC = 1 if enabled, 0 if disabled (default is 1)

6.4 Microgrid Case Study

The DC microgrid under study in this paper is shown in Figure 6.4. It is a community standalone DC microgrid that consists of a 1000 kW photovoltaic (PV) system connected to the DC bus through a DC/DC boost converter, a battery system integrated into the DC bus through a bidirectional DC/DC charger, a 630 kW diesel generator connected to the DC bus through a full-bridge rectifier. The microgrid bus voltage is 360 V DC, and the total DC community load of 300 kW. The values of the converter parameters as calculated for this simulation are shown in Table 6.3.

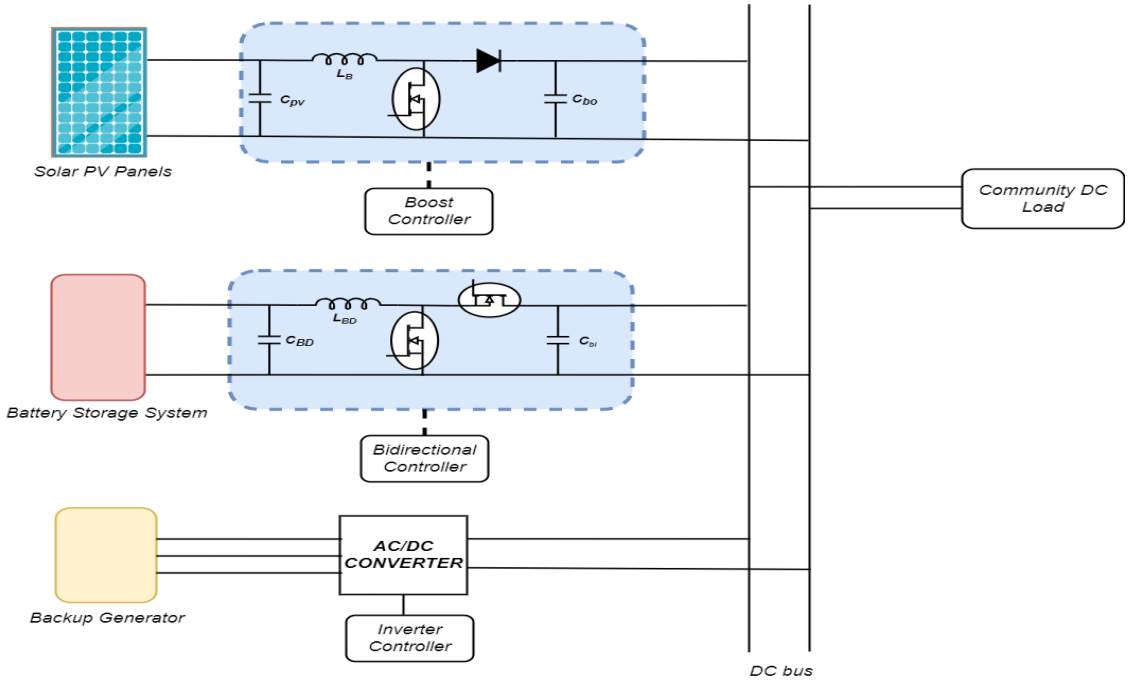

Figure 6. 4. Block Diagram of the studied DC Microgrid

Table 6. 3: DC microgrid converter parameters values

Unit	Component	Value
Bidirectional Converter	Inductor	13.38e-6 H
	Capacitor	38.5e-6F
Boost Converter	Inductor	7.5e-6 H
	Capacitor	1200e-6 F

The microgrid operates in three modes: photovoltaic (PV) mode, battery mode and generator mode. In the PV mode, the solar PV panels primarily supply the load, and the excess power is used to charge the battery. In this mode, the microgrid bus voltage is maintained by the bidirectional DC/DC converter controlled by the central microgrid controller, and the boost converter tracks the maximum power point (MPPT) of the PV system. When the power generated by the PV system goes lower than the load requirement, the battery system discharges to supply the load. At some point, if the PV power does not increase and the battery voltage falls

below the threshold selected, the diesel generator turns on to supply the load, and at the same time charges the battery to avoid damaging the battery. The system will return to the PV mode when the power produced by the solar PV system is enough to service the load and charge the battery back above the desired threshold.

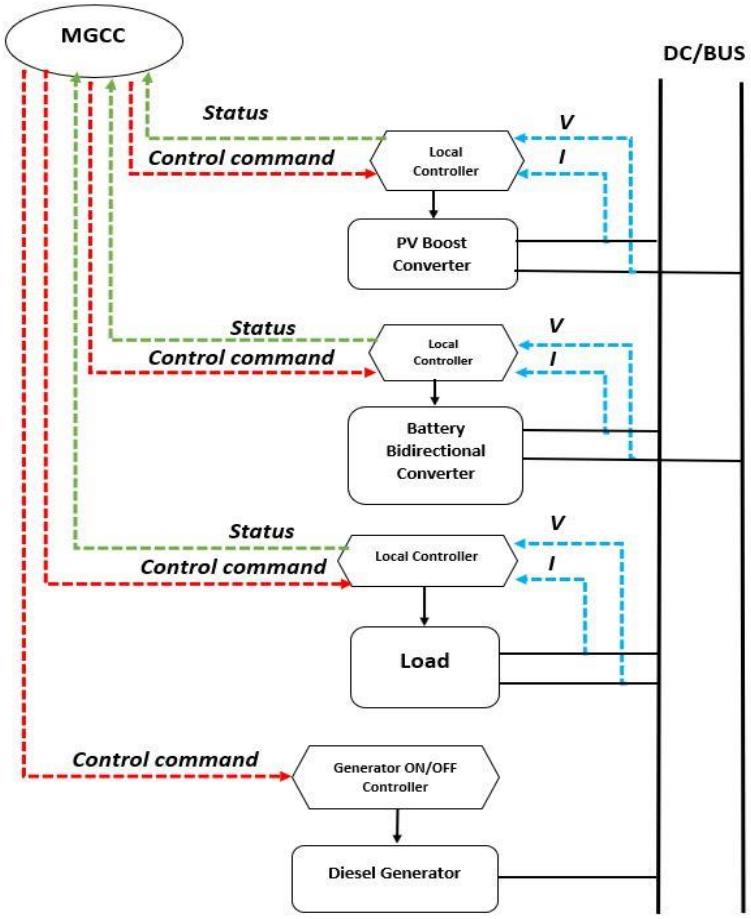

Figure 6. 5. Communication topology of DC microgrid

Figure 6.5 shows the communication topology of the DC microgrid. It can be observed that each converter has a local controller. The local controller sends and receives data from the microgrid central controller (MGCC) to coordinate their operations towards achieving system stability and optimum performance. In this study, the local controllers communicate with the central microgrid controller using the LoRa communication protocol. This is because this study is focused on analyzing the effect of employing LoRa communication for data transfer on microgrid performance.

The DC microgrid in the paper is controlled using the hierarchical, centralized control method, which is composed of the primary and secondary layers. In the primary layer, there is continuous communication between the sensors and the local controllers monitoring various parameters such as the input/output voltages and/or currents of the various converter depending on the control type as set by the MGCC. Furthermore, in the secondary control, the MGCC assigns the modes of operation depending on the parameter values received from the local controllers to maintain a reliable microgrid operation during the transition between the operation modes. A control logic is implemented within the microgrid central controller for the adopted control scheme to maintain a reliable and optimum operation.

In this study, the DC microgrid was simulated in Matlab/Simulink^{TM} to observe the dynamic performance when the calculated LoRa transmission delays were introduced. The LoRa transmission delay as calculated for the data sent and received is introduced into the communication between the bidirectional local controller and the MGCC. The effects on the dynamic performance of the microgrid are analyzed during the transition between various modes. These periods are taken into consideration as they are the main events that will trigger required control actions. The DC microgrid was simulated for a period of 4 seconds on Simulink. The switching from the PV mode to the battery mode occurs at t = 1 s, while the switching to the generator mode takes place whenever the battery voltage drops below the threshold and back to the PV mode at t = 3 s. The simulation is then completed at t = 4 s.

The MGCC maintains a normal operation while the load power is being supplied by the solar PV system to service the community load and as well charge the energy storage system. The microgrid DC bus voltage is maintained at 360 V by the DC/DC bidirectional converter controller while the boost converter is MPPT-controlled. When there is a discrepancy between the load power requirement and the power generated by the PV system, the load controller sends a signal (111) to the MGCC. The MGCC then transmits a control signal (000) to the bidirectional converter to switch from the charging mode to the discharging mode to supply the load power requirements. At this period, the DC bus voltage remains controlled by the DC/DC bidirectional

converter controller and the battery voltage is monitored. when the battery voltage drops below 322.6 V, which corresponds to 50% State of Charge (SOC), to avoid over-discharging of the battery, the MGCC transmits a signal (101) to switch ON the diesel generator to supply the load and at the same time charge the battery system. The diesel generator continues to run until normal conditions such as higher irradiance are restored and MGCC sends a signal (010) to turn OFF the diesel generator and return to the PV operational mode. This microgrid control scheme is shown in Figure 6.6.

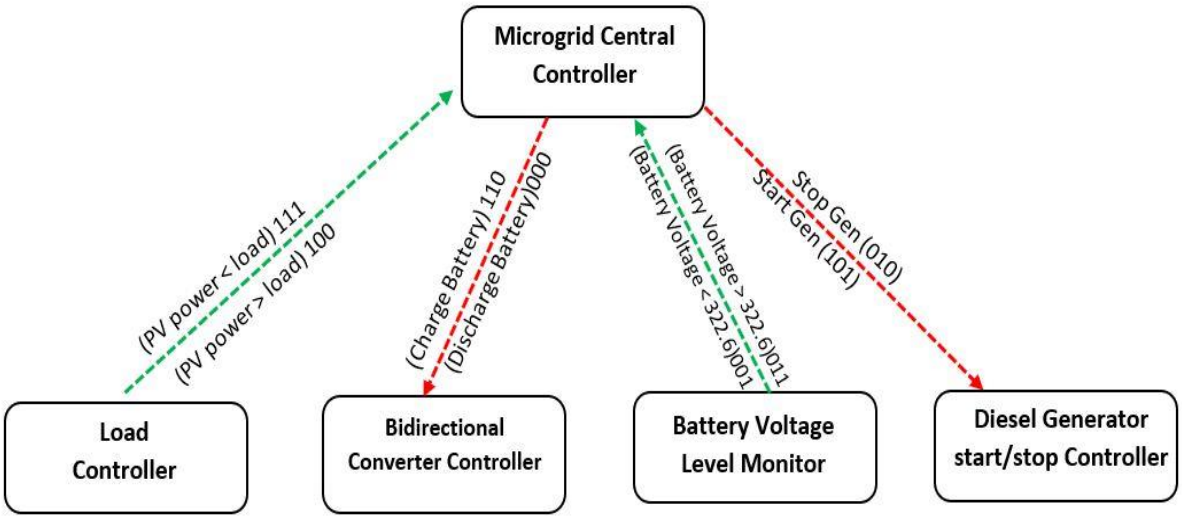

Figure 6. 6. Microgrid control scheme

6.5 Simulation Results

This section presents the simulation of the DC microgrid illustrating the switching into the various modes. This shows a normal system without transmission delays, as well as the impact of LoRa transmission delay on the DC bus voltage (V_{DC}), and the voltage across the DC/DC bidirectional converter switch. A transmission delay factor for the signals between the bidirectional local controller and the MGCC was calculated using equations (6.7) -(6.13) and introduced during communication between the local controllers and the MGCC for transition between the modes after the system control logic decisions have been made at the MGCC.

6.5.1 Microgrid normal operation (no transmission delay)

Figure 6.7 shows the microgrid DC bus voltage during transitions between the modes without communication delays.

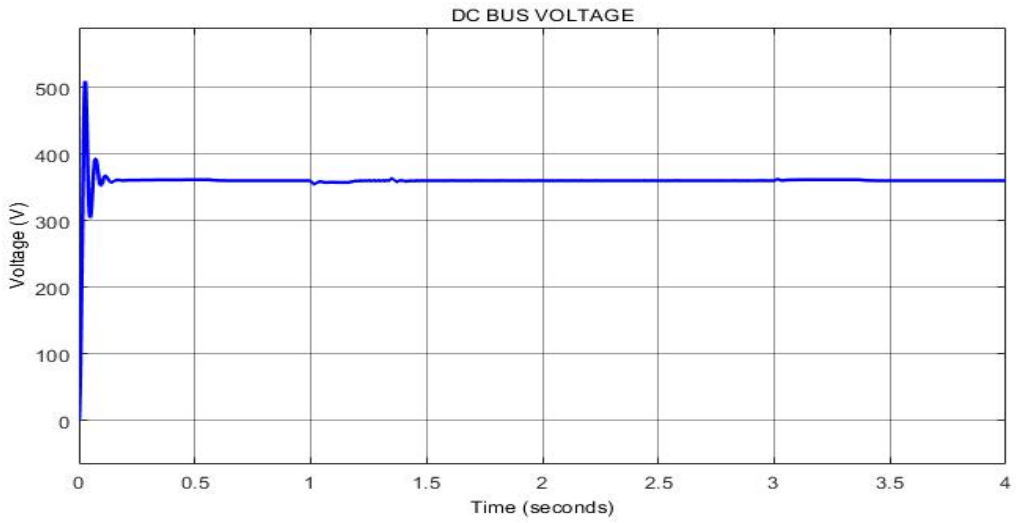

Figure 6. 7. Microgrid DC voltage for simulation without LoRa delay

Figure 6.7 shows the DC bus voltage during the simulation time. The figure depicts the stability of the DC bus voltage during the transmission times between the operation modes. The DC bus voltage was maintained at 360 V throughout the simulation time. The voltages of the bidirectional converter with no delays are as shown in Figure 6.8.

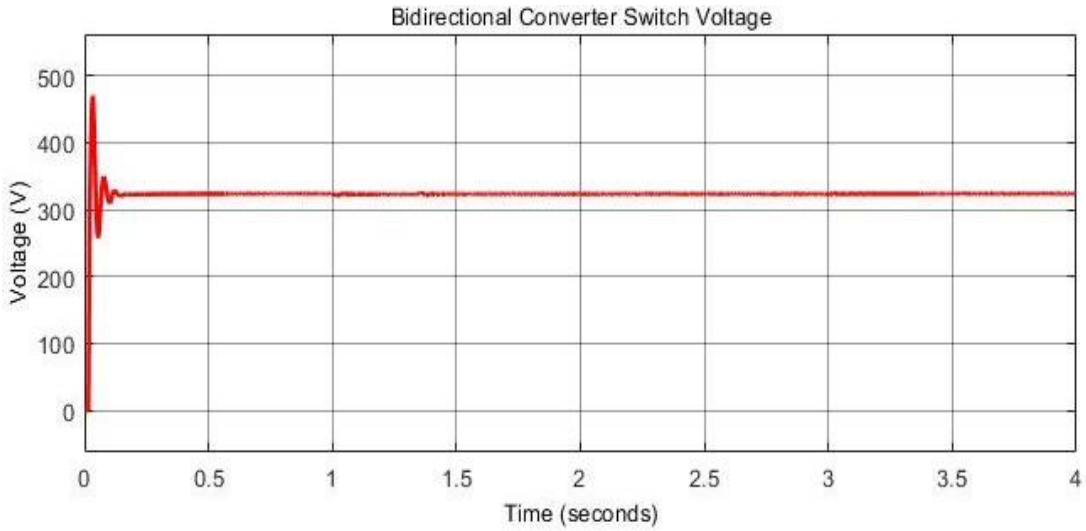

Figure 6. 8. Bidirectional converter switch voltage

During the operation of the DC microgrid, the battery was also being charged and discharged. Figure 6.9 shows the charging and discharging process of the energy storage system.

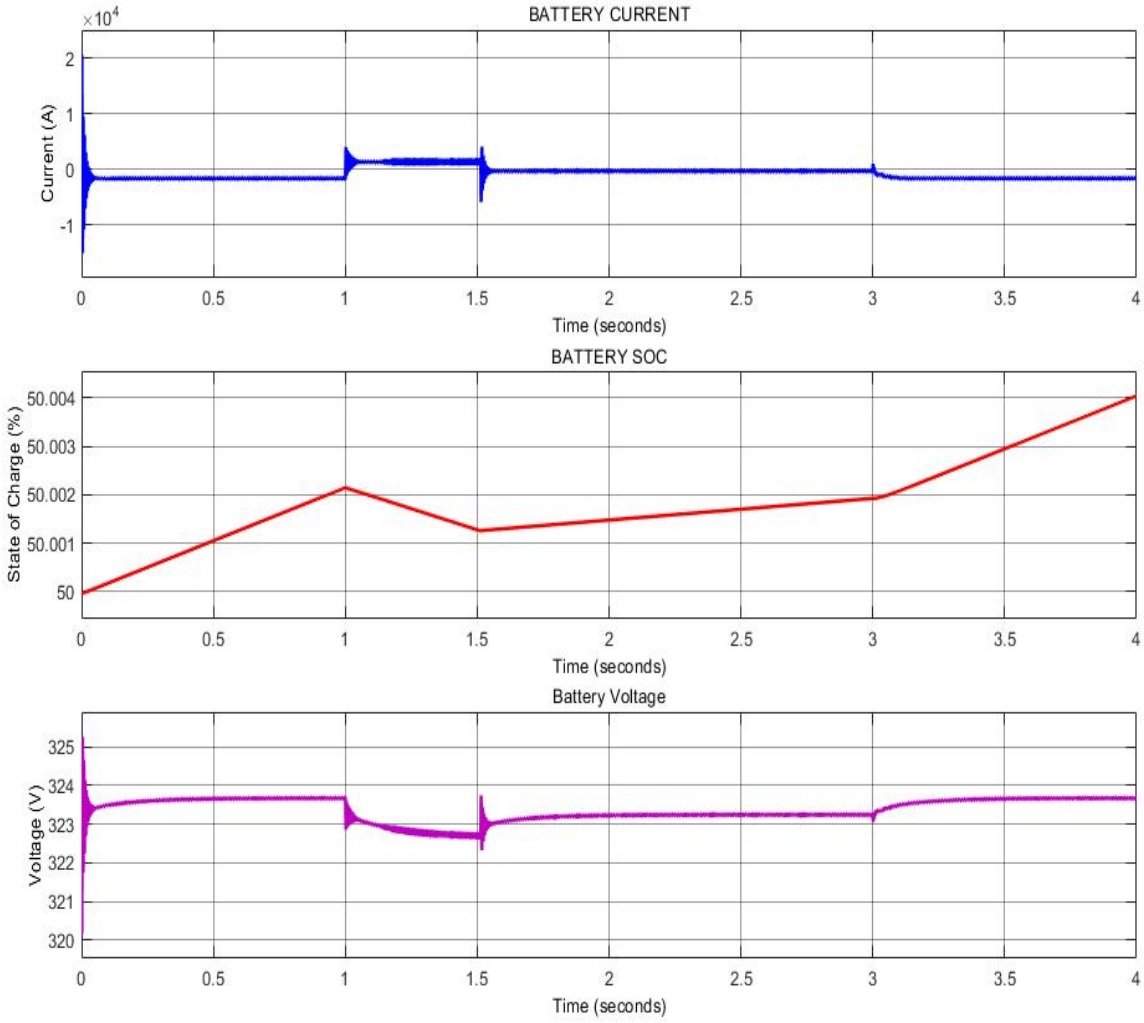

Figure 6. 9. DC microgrid battery parameters

All the key parameters in Figures 6.7 – 6.9 show that the system operated at optimum stability across the transition points. This is due to the absence of communication delay in the transmission of measured data and the required control command between the local controllers and the microgrid central controller.

6.5.2 Microgrid operation with LoRa data transmission delay

In the studied microgrid, LoRa was employed to send data from the local controllers of the distributed energy resources to the microgrid central controller, and for control commands from the central controller to the local

controllers. Therefore, the LoRa transmission delays for transferring each signal between the local controllers and the microgrid central controller using the LoRa communication system were calculated using equations 6.7 – 6.13 and shown in Table 6.4. For this research, the data was transferred using the highest LoRa bandwidth of 500 KHz. This is because in LoRa transmission, the higher the transmission bandwidth, the lower the transmission delay, as observed from table 6.1.

Table 6. 4: Signal Transmission Time

Signal	**Base64 Format**	**Transmission time (milliseconds)**
100	MTAw	10.88
110	MTEw	10.88
111	MTEx	10.88
000	MDAw	10.88
001	MDAx	10.88
011	MDEx	10.88

Therefore, for a complete control process to stabilize the system during the mode switching, a bidirectional data transfer must occur between the local controller and the MGCC. This means two signals must be transmitted. The delay of each signal during the transfer is added, and a total transmission delay of 21.76 ms was calculated and introduced into the system simulation during the mode switching events. The transmission delay was introduced as a transport delay in Simulink representing the data transmission between the local controller of the various microgrid components and the microgrid central controller and vice versa. In this study, the controller computational and processing time are neglected as the focus is on the data transmission time of LoRa communication during data transfer between the MGCC and the local controllers. Figures 6.10 and 6.11 show the effect of this transmission delay on the system performance.

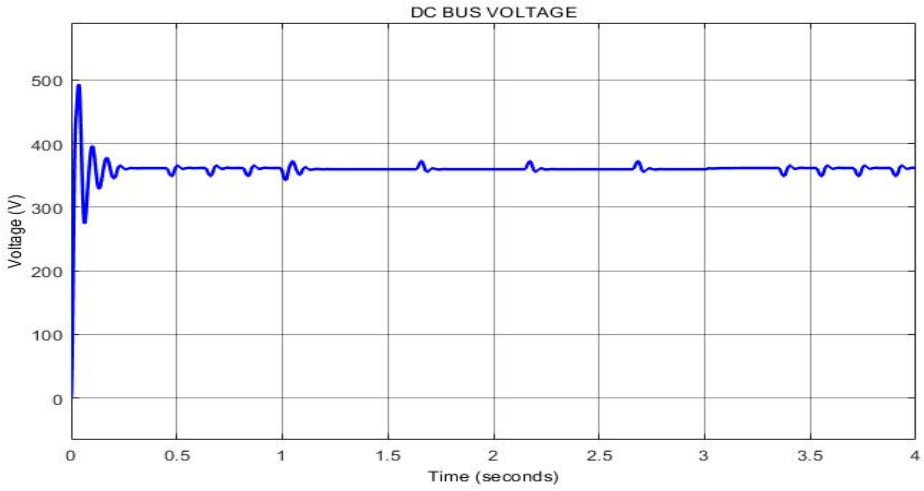

Figure 6. 10. Microgrid DC voltage for simulation with LoRa transmission delay

Figure 6. 11. Bidirectional converter switch voltage with delay

From Figure 6.10, the DC bus voltage shows variations at various points in the simulation time. The transmission delay increased the error between the reference voltage and the measured DC voltage at various instances. At the simulation time 1.19 seconds, the DC voltage spiked to 372.4 V which represents a 4% spike when the power source was switched from the PV source to the battery. We also observed voltage variations at 1.75 s, 2.27 s 2.82 s. furthermore, the DC bus voltage took a negative variation of about 3.8% at 3.325 s, 3.69 s and 3.880 s. This represents a system with a high level of instability. This instability results from the applied LoRa transmission delays imposed on variations DC bus voltage. Figure 6.11 also showed the

bidirectional converter switch voltage which also has a very large amount of voltage variations caused by the introduction of the LoRa communication delay.

6.5.3 Mitigating the effect of LoRa transmission delay on DC Bus Voltage

To eliminate the effect of delay on the DC microgrid stability, two system modification scenarios were considered.

6.5.3.1 Bidirectional Converter LC Component Recalculation

In this method, the DC microgrid bidirectional converter's LC components were re-calculated with consideration of the LoRa communication delay. To compensate for the variation in the bus voltage caused by the communication delay, the converter capacitor value was increased. This capacitor modification had a smoothening effect on the DC bus voltage. The new values of the components are shown in Table 6.5. The DC bus voltage and the bidirectional converter switch voltage obtained from the redesigned system's simulation are shown in Figures 6.12 and 6.13.

Table 6. 5: Signal Transmission Time

Unit	Component	Value
Bidirectional Converter	Inductor	13.38e-6 H
	Capacitor	45.8e-6 F
Boost Converter	Inductor	7.5e-6 H
	Capacitor	1200e-6 F

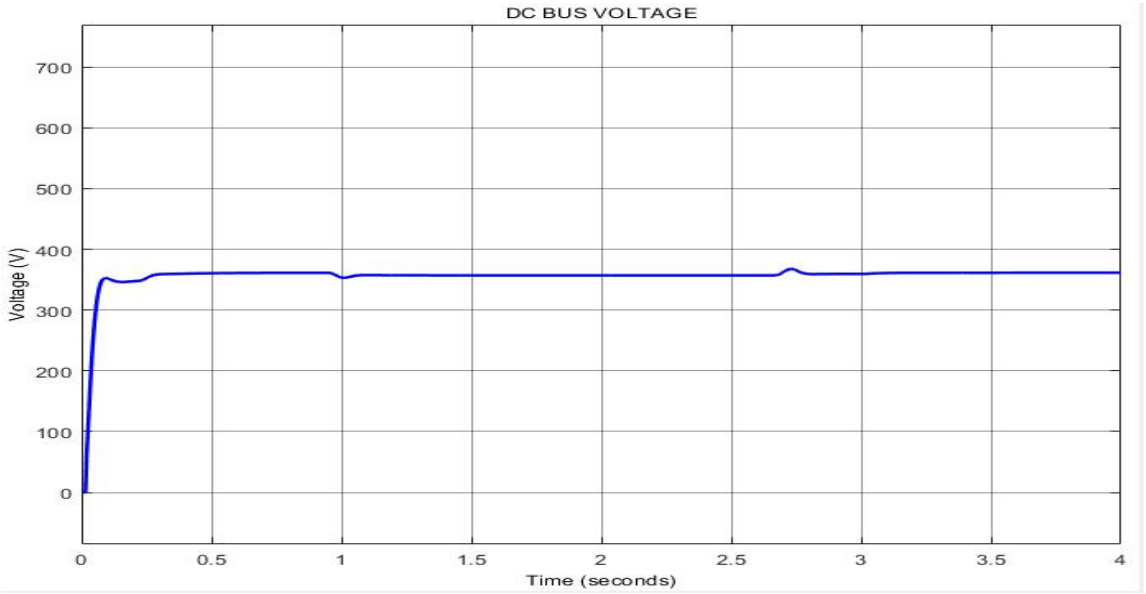

Figure 6. 12. DC bus voltage for redesigned microgrid with LoRa transmission delay

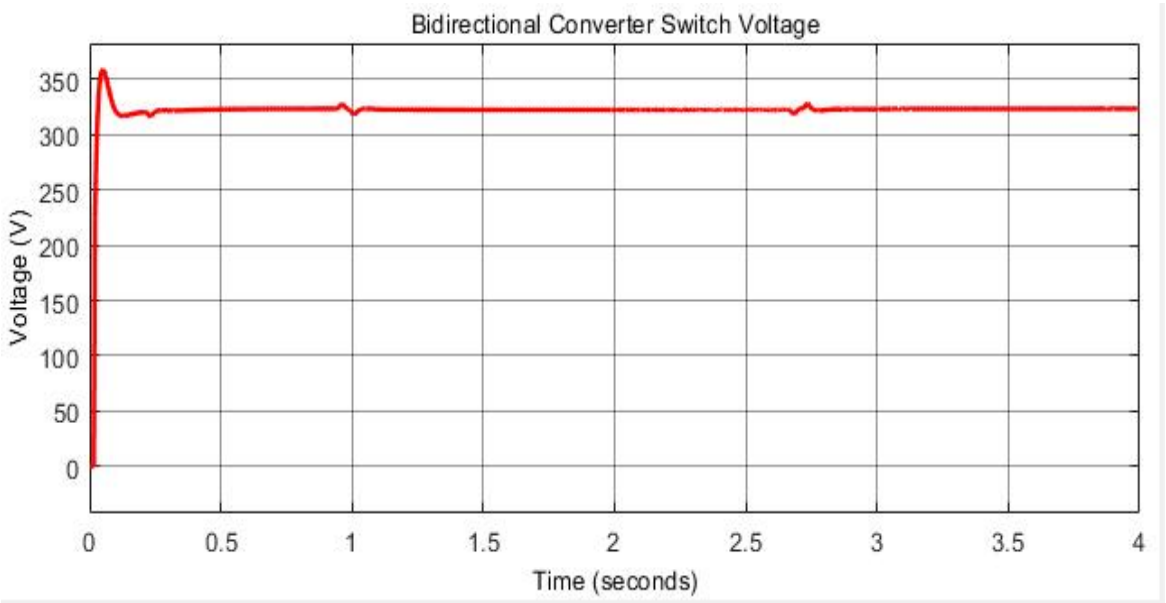

Figure 6. 13. Bidirectional converter switch voltage with modified parameters

From Figures 6.12 and 6.13, a more stable system is observed. The DC bus voltage presented in Figure 6.12 shows a voltage without much variations, which is almost similar to the DC bus voltage in Figure 6.7. The voltage in Figure 6.12 has variations of less than 1% at 1 s and 2.75 s of the simulation. These spikes are relatively small resulting from transitions from the PV mode to the generator mode. However, at 3 s when the microgrid returns to the PV mode due to increase in irradiation, there are no noticeable spikes in the DC bus

voltage. Figure 6.13 shows the bidirectional converter's switch voltage, which also follows the same pattern as the DC bus voltage with slight variations at the same simulations times as with the DC bus voltage.

6.5.3.2 Modification of the PI Controller for Better System Robustness

In DC microgrids, PI controllers have been used to address time delay effects such as DC bus voltage variations [22][23][24][25]. This method involves re-designing the PI controller parameters towards achieving a robust controller system that can maintain system stability even in various system degradation scenarios. After thorough investigation of the controller systems proposed in the literatures, the controller proposed in [25] was applied to the simulation. The proposed system employs a fuzzy-PI dual-mode controller for DC voltage regulation. This controller features speedy response, low overshoot, good robustness, and strong anti-interference under different working conditions allowing for DC voltage stability even with larger transmission delays when compared to results from the controllers proposed in the other literatures. The details on the design and simulation of the proposed technique are fully explained in the literature [25], and as such, not repeated in this paper. The schematic of the employed controller modification is shown in Figure 6.14. The DC bus voltage obtained from the simulation employing the new controller is shown in Figure 6.15.

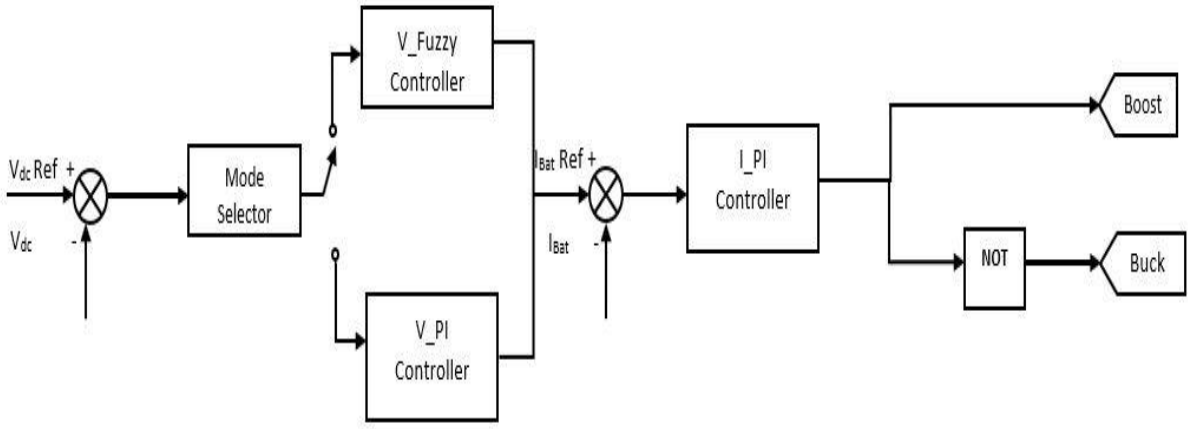

Figure 6. 14. Schematic of modified PI controller in MGCC

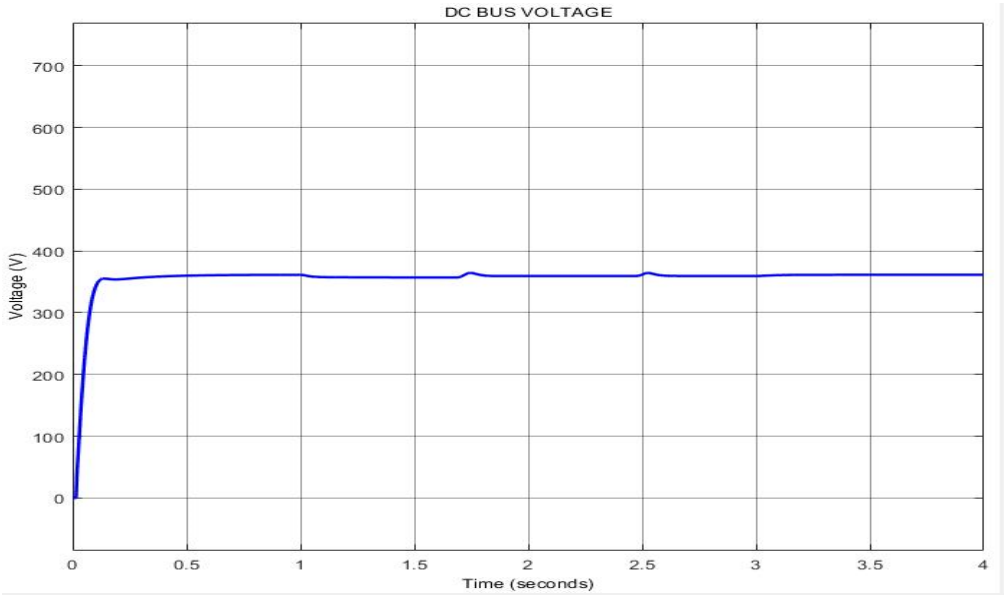

Figure 6. 15. DC microgrid DC bus voltage with modified controller

The DC bus voltage shown in Figure 6.15 presents a microgrid with a stable bus voltage even with the introduction of the LoRa communication system. The presented graph shows the presence of very small amount of voltage variations at 1.75 s representing system transition from battery to backup generator supply. There were no voltage variations at 1 s when transitioning from the PV system to the battery supply. Furthermore, another negligible voltage variation was observed at 2.5 s. these variations are minimal and demonstrate that the system still maintains a high level of stability even with the communication delay.

6.6 Discussion

The first simulation scenario involved a DC microgrid without communication delay. Various key system parameters observed in the results showed that the system operated in optimum stability. However, the introduction of LoRa transmission delay caused reduced system stability demonstrated by spikes in parameters especially while transitioning between various modes. This therefore entails that a stable DC microgrid with the LoRa transmission delay must be achieved. The DC microgrid was therefore simulated for a third scenario. The third simulation was carried out in two scenarios.

In the first mitigation simulation, only the LC components of the bidirectional converter were re-calculated and re-designed. The new component values were employed, and the system was re-simulated. The results obtained showed that the delay imposed on the system by LoRa was not large, and a simple re-calculation of the system parameters achieved a more stable performance.

In the second stability test, the PI controller was modified with additional functionalities to improve the robustness of the system in Matlab/Simulink™. The results also showed a DC voltage with reduced spikes. The PI controller modifications allowed for system stability even for a larger delay time.

The results obtained from the simulations in the delay mitigation section exhibit a stable system even during the transitions with the delays incorporated. This therefore confirms that with a refined system design, LoRa communication can be employed for data transfer and still achieve system stability.

Furthermore, the results also showed that the communication system to be employed for data transfer within a microgrid should be taken into consideration in the microgrid design stages especially if low bandwidth communication is to be employed.

6.7 Conclusion and future work

In this paper, the effects of LoRa transmission delay on the dynamic performance of a DC microgrid were analyzed. This analysis was carried out to observe how the microgrid would function when a low bandwidth communication system such as LoRa is employed for data transfer at the secondary control level. For a centralized communication-based controlled microgrid as presented in the paper, a very reliable communication structure is required. Data transmission delay is therefore a very important factor towards achieving a stable microgrid operation. To complete the analysis, a DC microgrid was simulated in Matlab/Simulink™. The microgrid operated in three modes: namely, PV mode, battery mode and generator mode. The system was simulated for three scenarios to understand system function without transmission delay, with LoRa transmission delay and with the system parameters re-calculated and re-designed to achieve

stability. Our analysis and simulations indicate that LoRa transmission delay can be compensated for within the systems controllers.

As a recommendation for future work, ways of extending LoRa communication range for its application to large area microgrids will be very important. This is because, microgrids have DERs at various distances, and the distance of LoRa coverage generally has a negative effect on the transmission delay. This will, in turn have a negative effect on microgrid stability.

6.8 References

[1] M. S. Saleh, A. Althaibani, Y. Esa, Y. Mhandi and A. A. Mohamed, "Impact of clustering microgrids on their stability and resilience during blackouts," *2015 International Conference on Smart Grid and Clean Energy Technologies (ICSGCE)*, 2015, pp. 195-200.

[2] M. Saleh, Y. Esa, Y. Mhandi, W. Brandauer and A. Mohamed, "Design and implementation of CCNY DC microgrid testbed," *2016 IEEE Industry Applications Society Annual Meeting*, 2016, pp. 1-7.

[3] D. Ton and M. Smith, "The U.S. Department of Energy's Microgrid Initiative", *The Electricity Journal*, vol. 25, no. 8, pp. 84-94, 2012.

[4] N. Hatziargyriou, *Microgrids: Architectures and Control*, 1st ed. New York, NY, USA: Wiley-IEEE Press, 2014, pp. 4-70.

[5] M. Saleh, Y. Esa and A. A. Mohamed, "Communication-Based Control for DC Microgrids," in *IEEE Transactions on Smart Grid*, vol. 10, no. 2, pp. 2180-2195, March 2019.

[6] E. Hossain, E. Kabalci, R. Bayindir and R. Perez, "Microgrid testbeds around the world: State of art", *Energy Conversion and Management*, vol. 86, pp. 132-153, 2014.

[7] Z. Liu, X. Xu, H. Abdelsalam and E. Makram, "Power System Harmonics Study for Unbalanced Microgrid System with PV Sources and Nonlinear Loads", *Journal of Power and Energy Engineering*, vol. 03, no. 05, pp. 43-55, 2015.

[8] S. Backhaus et al. “DC scoping study—Estimate of technical and economic benefit”, *Los Alamos Nat. Lab., Los Alamos*. Pp 1-94, 2015.

[9] D. Chen and L. Xu, "Autonomous DC Voltage Control of a DC Microgrid With Multiple Slack Terminals," in *IEEE Transactions on Power Systems*, vol. 27, no. 4, pp. 1897-1905, Nov. 2012.

[10] R.S. Balog, P.T. Krein, “Autonomous local control in distributed DC power systems”, *University of Illinois Urbana-Champaign*, 2006.

[11] Y. Ito, Y. Zhongqing and H. Akagi, "DC microgrid based distribution power generation system," *The 4th International Power Electronics and Motion Control Conference, 2004. IPEMC 2004.*, 2004, pp. 1740-1745.

[12] J. Lee, H. Kim and B. Han, "Operation Analysis of a Communication-Based DC Micro-Grid Using a Hardware Simulator", *Journal of Power Electronics*, vol. 13, no. 2, pp. 313-321, 2013.

[13] A. Pinomaa, J. Ahola and A. Kosonen, "Power-line communication-based network architecture for LVDC distribution system," *2011 IEEE International Symposium on Power Line Communications and Its Applications*, 2011, pp. 358-363.

[14] C. Ndukwe, M. Tariq Iqbal, X. Liang, J. Khan and L. Aghenta, "LoRa-based communication system for data transfer in microgrids", *AIMS Electronics and Electrical Engineering*, vol. 4, no. 3, pp. 303-325, 2020.

[15] J. Zhao and F. Dörfler, "Distributed control and optimization in DC microgrids", *Automatica*, vol. 61, pp. 18-26, 2015.

[16] A. Khorsandi, M. Ashourloo and H. Mokhtari, "A Decentralized Control Method for a Low-Voltage DC Microgrid," in *IEEE Transactions on Energy Conversion*, vol. 29, no. 4, pp. 793-801, Dec. 2014.

[17] W. Heemels, J. Sandee and P. Van Den Bosch, "Analysis of event-driven controllers for linear systems", *International Journal of Control*, vol. 81, no. 4, pp. 571-590, 2008.

[18] J. Sandee, W. Heemels and P. van den Bosch, "Case Studies in Event-Driven Control", *Hybrid Systems: Computation and Control*, pp. 762-765, 2007.

[19] X. Lu, J. M. Guerrero, K. Sun and J. C. Vasquez, "An Improved Droop Control Method for DC Microgrids Based on Low Bandwidth Communication with DC Bus Voltage Restoration and Enhanced Current Sharing Accuracy," in *IEEE Transactions on Power Electronics*, vol. 29, no. 4, pp. 1800-1812, April 2014.

[20] T. Haritsa, B. Yashu, U. Kumar and M. Suma, "Mathematical Characterization and Simulation of LoRa", *Wireless Personal Communications*, vol. 115, no. 2, pp. 1481-1506, 2020.

[21] J. Petäjäjärvi, K. Mikhaylov, M. Pettissalo, J. Janhunen and J. Iinatti, "Performance of a low-power wide-area network based on LoRa technology: Doppler robustness, scalability, and coverage", *International Journal of Distributed Sensor Networks*, vol. 13, no. 3, p. 155014771769941, 2017.

[22] W. Zhang, Y. Fang, R. Ye and Z. Wang, "Analysis and Design of a Double Fuzzy PI Controller of a Voltage Outer Loop in a Reversible Three-Phase PWM Converter", *Energies*, vol. 13, no. 15, p. 3778, 2020.

[23] A. Elnady, "PI Controller Based Operational Scheme to Stabilize Voltage in Microgrid," *2019 Advances in Science and Engineering Technology International Conferences (ASET)*, 2019, pp. 1-6.

[24] R. A. Barbosa, D. de Almeida Souza and A. P. da Nóbrega Tahim, "Adaptive Control of DC Microgrid Using PI Controller and Fuzzy Inference," *2019 IEEE PES Innovative Smart Grid Technologies Conference - Latin America (ISGT Latin America)*, 2019, pp. 1-6.

[25] Y. Zhang, S. Wei, J. Wang and L. Zhang, "Bus Voltage Stabilization Control of Photovoltaic DC Microgrid Based on Fuzzy-PI Dual-Mode Controller", *Journal of Electrical and Computer Engineering*, vol. 2020, pp. 1-10, 2020.

Chapter 7

Thesis Conclusions and Future Works

7.1 Conclusions

The recent increasing quest for a more human friendly (greener) environment has enhanced the continuous development of various microgrid around the globe. This classification of microgrids as AC, DC or hybrid results from the main bus supply voltage of the microgrid. The AC microgrid being the traditional way of power supply has been employed in microgrid for power generation and distribution. In recent times research showed that the DC microgrid can be employed for power generation and supply especially to remote communities with lower energy requirements and easy transition to DC devices. The DC microgrid has been mainly focused on these days due to the myriad of advantages which it has over the AC counterpart which include reduced energy loss due to lower amount of conversion stages, direction penetration of the renewable energy sources, low system complexity and low cost of energy distribution. This increased interest in the DC microgrid has led to various research aimed at continuous improvement of the DC microgrid.

For optimal function of the DC microgrid, continuous monitoring and control of the system is very important both for the operators and the customers, hence the importance of a robust and reliable communication system for effective data and control signal transfer within the microgrid. In the AC microgrid, which has a higher number of parameters to measure and control, the main high bandwidth communication systems such as the GSM and internet. have been employed for data transfer. However, with the reduction of parameters to be measured in the DC microgrid, research has shown that low bandwidth communication systems such as the Zigbee, Sigfox, and LoRa can be employed in a well-designed microgrid for data transfer.

LoRa is a Low Power communication system that has recently gained interest for data transfer in various industrial systems. The interest for LoRa application in various systems is due to the following features: low power consumption, long range of coverage, immunity to interference etc. LoRa is a low bandwidth

communication system, therefore its employment for data transfer with the microgrid has to be meticulously studied to avoid any negative effects on the operation of the microgrid.

This research focused on the sizing, design and simulation of the AC and DC microgrids and the employment of the LoRa communication system for data transfer at the various communication and control levels of the DC microgrid. LoRa was considered for this research because, it has not been considered for data transfer within the microgrid and as such the research is considered as novel.

7.2 Research Summary

The core research of this thesis is presented in Chapter 2 to Chapter 6. The summary of each chapter will be explained as follows.

Chapter 2 presented the sizing of an AC microgrid for a remoted community in eastern Nigeria. This chapter studied the energy needs of the community. Furthermore, the research also studied the renewable energy resources in the community. The results showed that the community is a small community with low energy requirements. The study also showed that solar energy was the only resource that was abundant in that area. A hybrid power system comprising of the PV solar system, an energy storage system and a backup generator was sized in HOMER software for the community to meet the energy requirements of the community. The most optimal system was selected based on, cost of installation, cost of operation, and the cost of energy.

Chapter 3 presented a similar study of the same community for the sizing of a DC microgrid. In this study, the AC devices which were employed for the calculations in Chapter 2 were replaced with DC appliances and the community energy requirements were recalculated. The results of the recalculation showed that by conversion of the community electrical installations to DC, the energy requirement of the community was reduced drastically with then further affected the size of the power generation system for the community. Furthermore, the sized power system was simulated in MATLAB/Simulink to observe the dynamic

performance of the system. The simulation results obtained showed that the designed DC microgrid operated at a stable and optimum capacity.

Chapter 4 presented the implementation of LoRa for data transfer at the secondary control level of the DC microgrid. In this chapter, a one-way proof of concept communication of the LoRa protocol was present to observe the range of communication and the time of data transfers. The results from the experimental setup of the system showed the possibility of the LoRa communication system for microgrid communication.

Chapter 5 presented the design and implementation of a LoRa based SCADA system for supervisory monitoring and control of renewable energy generation systems. The system designed in this chapter employed the various features of LoRa communication system to develop a low-cost IoT based SCADA systems which eliminated the exclusive requirements of the proprietary SCADA systems currently being employed in the industry. The designed system featured low-cost which comes from the fact that the materials employed for the design of the system were very cheap materials such as the Arduino Uno, Raspberry Pie and the various sensors employed for the design. Also, the system features high data security. This was shown because the system was designed as a compact system with no internet dependence. The system employed the LoRa Physical level communication for data transfer between the RTUs and the MTU. Furthermore, the data processing and remote control was carried out in all-in-one Linux machine which serves as MTU. The Linux machine hosts all the other components of the SCADA system such as the HMI for display and control purposes and the storage for data logging. This eliminated the need for any cloud service thereby enhancing the security of the transferred data. The elimination of the internet in this system design also showed that the system is robust enough to be employed in remote communities with no existing communication infrastructure.

To study the effect of employing LoRa communication for secondary level data transfer within the DC microgrid as presented in Chapter 4, Chapter 6 presented the analysis of LoRa transmission delay on the dynamic performance of the DC microgrid. In this chapter, the secondary communication level of the DC

microgrid control scheme was studied. The system considered in this chapter was the DC microgrid centralized communication-based control. This control scheme has very high dependence on the communication system employed for data transfer and as such a good study of the communication system is recommended before employment. The LoRa transmission delay for every data and signal transmitted between the local controller and the microgrid central controller was calculated. This calculated transmission delay was integrated into the Simulink model of the DC microgrid. This research observed the simulation of a DC microgrid in three scenarios which included simulation without communication delay, simulation with LoRa communication delay, and simulation of the DC microgrid with a delay compensation system. The employment of LoRa at this secondary control level of the DC microgrid control induced some level of system instability. However, this abnormality caused by the LoRa transmission delay was corrected by the proposed delay compensation schemes described in the chapter. This therefore shows that with proper component calculation and design, LoRa can be employed for DC microgrid secondary level data transfer.

7.3 Research Contributions

The Contributions of this research include:

- Sizing, development and design of both AC and DC microgrids for a remote community in Nigeria. The DC microgrid presented in chapter 3 showed lower operation cost and other financial implications. This therefore, showed that with conversion to DC appliances, the energy requirements of the community will be reduced, therefore having a reduced effect on the generation system. Furthermore, the sized DC microgrid was simulated in Simulink and the result depicted that the sizing was able to meet the energy needs of the community.
- Investigation of LoRa communication technology for data transfer at the secondary control level of the DC microgrid. This research covered a first design and range test of the LoRa communication technology. To ascertain its employability for data transfer at the secondary control level of DC microgrid, the effect of data transmission delay was investigated and solutions towards eliminating

the delay effect were proposed. This is considered novel because to the best of the authors knowledge there is no other research that covered this area.

- Design and development of a low-cost SCADA system based on the LoRa technology and other open-source components for renewable energy generation systems. The system designed in this part of the thesis is an internet-independent system which does not require internet or any other communication system for data and control transfer. The system designed is robust enough to be employed in geographical areas with no existing communication infrastructure.

7.4 Future Works

The work presented in this thesis opens new research directions for LoRa communication for employment in microgrid data transfer and the development of reliable, secure, low-cost IoT based SCADA systems for remote monitoring and supervisory control. However, there are in existence several knowledge gaps and research that could be conducted towards achieving better employment of LoRa for data transfer at various levels of industrial systems. Some of the recommendations for future works are summarized as follows:

- Since LoRa has proven to be very capable from research to be employed for data transfer and can achieve results like the other communication systems. research into how to extend the data coverage distance to allow for employment in larger renewable energy generation systems will be very important.
- Increased security in the designed SCADA system solution can be achieved through the development of reliable data encryption algorithms on the LoRa communication channel for safety and integrity of the transferred data.

7.5 Research Publications

This PhD research produced 5 journal papers and 1 conference paper. The research papers are as follows.

7.5.1 Journal Papers

1. C. Ndukwe, T. Iqbal, X. Liang and J. Khan, "Optimal Sizing and Analysis of a Small Hybrid Power System for Umuokpo Amumara in Eastern Nigeria", *International Journal of Photoenergy*, vol. 2019, pp. 1-8, 2019. Available: 10.1155/2019/6960191.

2. C. Ndukwe and T. Iqbal, "Sizing and dynamic modelling and simulation of a standalone PV based DC microgrid with battery storage system for a remote community in Nigeria", *Journal of Energy Systems*, pp. 67-85, 2019. Available: 10.30521/jes.544710.

3. C. Ndukwe, M. Tariq Iqbal, X. Liang, J. Khan and L. Aghenta, "LoRa-based communication system for data transfer in microgrids", *AIMS Electronics and Electrical Engineering*, vol. 4, no. 3, pp. 303-325, 2020. Available: 10.3934/electreng.2020.3.303.

4. C. Ndukwe, M. Iqbal and J. Khan, "An Open Source LoRa Based, Low-Cost IoT Platform for Renewable Energy Generation Unit Monitoring and Supervisory Control", *Journal of Energy and Power Technology*, vol. 4, no. 1, pp. 1-1, 2021. Available: 10.21926/jept.2201007.

5. C. Ndukwe, M. Iqbal, J. Khan and M. Jamil, "Analysis of LoRa Transmission Delay on Dynamic Performance of Standalone DC Microgrids", *Journal of Energy and Power Technology*, vol. 4, no. 2, pp. 1-1, 2022. Available: 10.21926/jept.2202022.

7.5.2 Conference Papers

1. C. Ndukwe, M. T. Iqbal and J. Khan, "Development of a Low-cost LoRa based SCADA system for Monitoring and Supervisory Control of Small Renewable Energy Generation Systems," 2020 11th IEEE Annual Information Technology, Electronics and Mobile Communication Conference (IEMCON), 2020, pp. 0479-0484, doi: 10.1109/IEMCON51383.2020.9284933.

Appendix A

Supporting Information for Chapter 4*

Arduino Code for LoRa One Way Data transfer

```
#include <lmic.h>
#include <hal/hal.h>
#include <SPI.h>

const float vpp = 0.004882813;
float sensitivity = 0.100;
const int analogInput = A0;
#ifdef COMPILE_REGRESSION_TEST
# define FILLMEIN 0
#else
# warning "You must replace the values marked FILLMEIN with real values from the TTN control panel!"
# define FILLMEIN (#dont edit this, edit the lines that use FILLMEIN)
#endif
static const PROGMEM u1_t NWKSKEY[16] = {0x32, 0xF8, 0xD5, 0x7D, 0x2A, 0x08, 0xE2, 0x4F, 0xED, 0x83, 0x14, 0x90, 0x0F, 0x1A, 0xE2, 0x62};
static const u1_t PROGMEM APPSKEY[16] = { 0xAB, 0x0A, 0xEE, 0xD3, 0xE9, 0xBB, 0x62, 0xE5, 0x3F, 0x95, 0xEE, 0x7C, 0x98, 0xEF, 0x57, 0xCD };
static const u4_t DEVADDR = 0x00BC3BBE ;

void os_getArtEui (u1_t* buf) { }
void os_getDevEui (u1_t* buf) { }
void os_getDevKey (u1_t* buf) { }

static uint8_t payload[5];
static osjob_t sendjob;
```

```
const unsigned TX_INTERVAL = 1;
const lmic_pinmap lmic_pins = {
    .nss = 10,
    .rxtx = LMIC_UNUSED_PIN,
    .rst = 9,
    .dio = {2, 6, 7}
};

void onEvent (ev_t ev) {
    Serial.print(os_getTime());
    Serial.print(": ");
    switch(ev) {
        case EV_SCAN_TIMEOUT:
            Serial.println(F("EV_SCAN_TIMEOUT"));
            break;
        case EV_BEACON_FOUND:
            Serial.println(F("EV_BEACON_FOUND"));
            break;
        case EV_BEACON_MISSED:
            Serial.println(F("EV_BEACON_MISSED"));
            break;
        case EV_BEACON_TRACKED:
            Serial.println(F("EV_BEACON_TRACKED"));
            break;
        case EV_JOINING:
            Serial.println(F("EV_JOINING"));
            break;
        case EV_JOINED:
            Serial.println(F("EV_JOINED"));
```

```
    break;
case EV_JOIN_FAILED:
    Serial.println(F("EV_JOIN_FAILED"));
    break;
case EV_REJOIN_FAILED:
    Serial.println(F("EV_REJOIN_FAILED"));
    break;
case EV_TXCOMPLETE:
    Serial.println(F("EV_TXCOMPLETE (includes waiting for RX windows)"));
    if (LMIC.txrxFlags & TXRX_ACK)
      Serial.println(F("Received ack"));
    if (LMIC.dataLen) {
      Serial.println(F("Received "));
      Serial.println(LMIC.dataLen);
      Serial.println(F(" bytes of payload"));
    }
    // Schedule next transmission
    os_setTimedCallback(&sendjob, os_getTime()+sec2osticks(TX_INTERVAL), do_send);
    break;
case EV_LOST_TSYNC:
    Serial.println(F("EV_LOST_TSYNC"));
    break;
case EV_RESET:
    Serial.println(F("EV_RESET"));
    break;
case EV_RXCOMPLETE
    Serial.println(F("EV_RXCOMPLETE"));
    break;
case EV_LINK_DEAD:
```

```
            Serial.println(F("EV_LINK_DEAD"));
            break;
        case EV_LINK_ALIVE:
            Serial.println(F("EV_LINK_ALIVE"));
            break;

        case EV_TXSTART:
            Serial.println(F("EV_TXSTART"));
            break;
        case EV_TXCANCELED:
            Serial.println(F("EV_TXCANCELED"));
            break;
        case EV_RXSTART:

            break;
        case EV_JOIN_TXCOMPLETE:
            Serial.println(F("EV_JOIN_TXCOMPLETE: no JoinAccept"));
            break;
        default:
            Serial.print(F("Unknown event: "));
            Serial.println((unsigned) ev);
            break;
    }
}

void do_send(osjob_t* j){

    if (LMIC.opmode & OP_TXRXPEND) {
        Serial.println(F("OP_TXRXPEND, not sending"));
```

```
    } else {
     float Current= 0;
      float value1= analogRead(analogInput);
      int counts = value1 ;
     float svoltage = counts * vpp;
      svoltage -=2.50;
      Current = svoltage/sensitivity;
      Serial.print   ( Current );

const float R1 = 10000.0;
     const float R2 = 4700.0;
     float value = analogRead(A2);
     float vout = value * vpp;
     float Voltage = vout / (R2/(R1+R2));
    Serial.print(Voltage);
      delay(1);
      }
        LMIC_setTxData2(1, payload, sizeof(payload)-1, 0);
       Serial.println(F("Packet queued"));
    }

void setup() {
    while (!Serial);
    Serial.begin(115200);
    delay(1);
    Serial.println(F("Starting"));
    #ifdef VCC_ENABLE
    pinMode(VCC_ENABLE, OUTPUT);
    digitalWrite(VCC_ENABLE, HIGH);
```

```
delay(1000);
#endif
os_init();
LMIC_reset();
uint8_t appskey[sizeof(APPSKEY)];
uint8_t nwkskey[sizeof(NWKSKEY)];
memcpy_P(appskey, APPSKEY, sizeof(APPSKEY));
memcpy_P(nwkskey, NWKSKEY, sizeof(NWKSKEY));
LMIC_setSession (0x13, DEVADDR, nwkskey, appskey);
for (int c = 0; c < 9; c++){
//  LMIC_disableChannel(c);
}
```

Appendix B

Supporting Information for Chapter 5*

Arduino Code for LoRa Bidirectional Communication for Remote Monitoring and Supervisory Control of the LoRa- Based SCADA System (for one RTU).

```
#include <lmic.h>
#include <hal/hal.h>
#include <SPI.h>

#ifdef COMPILE_REGRESSION_TEST
# define FILLMEIN 0
#else

# define FILLMEIN (#dont edit this, edit the lines that use FILLMEIN)
#endif

static const PROGMEM u1_t NWKSKEY[16] = {0x32, 0xF8, 0xD5, 0x7D, 0x2A, 0x08, 0xE2, 0x4F, 0xED, 0x83, 0x14, 0x90, 0x0F, 0x1A, 0xE2, 0x62};

static const u1_t PROGMEM APPSKEY[16] = { 0x27, 0x27, 0x9A,0x5F, 0x68,0x0A, 0x23, 0xA1, 0x1C, 0x84, 0x91, 0xBC, 0x74,  0xFE, 0X09, 0X0F};

static const u4_t DEVADDR = 0x00BC3BBE ;

void os_getArtEui (u1_t* buf) { }
void os_getDevEui (u1_t* buf) { }
void os_getDevKey (u1_t* buf) { }

static uint8_t mydata[] = "Hello, world!";
static osjob_t sendjob;
```

```
const unsigned TX_INTERVAL = 1;

const lmic_pinmap lmic_pins = {
    .nss = 10,
    .rxtx = LMIC_UNUSED_PIN,
    .rst = 9,
    .dio = {2, 6, 7},
};

#define LED_RED 8
#define LED_GREEN  5

void onEvent (ev_t ev) {
    Serial.print(os_getTime());
    Serial.print(": ");
    switch(ev) {
        case EV_SCAN_TIMEOUT:
            Serial.println(F("EV_SCAN_TIMEOUT"));
            break;
        case EV_BEACON_FOUND:
            Serial.println(F("EV_BEACON_FOUND"));
            break;
        case EV_BEACON_MISSED:
            Serial.println(F("EV_BEACON_MISSED"));
            break;
        case EV_BEACON_TRACKED:
            Serial.println(F("EV_BEACON_TRACKED"));
            break;
        case EV_JOINING:
            Serial.println(F("EV_JOINING"));
```

```
    break;
case EV_JOINED:
    Serial.println(F("EV_JOINED"));
    break;

case EV_JOIN_FAILED:
    Serial.println(F("EV_JOIN_FAILED"));
    break;
case EV_REJOIN_FAILED:
    Serial.println(F("EV_REJOIN_FAILED"));
    break;
case EV_TXCOMPLETE:
    Serial.println(F("EV_TXCOMPLETE (includes waiting for RX windows)"));
    if (LMIC.txrxFlags & TXRX_ACK)
      Serial.println(F("Received ack"));
    if (LMIC.dataLen) {
      Serial.println(F("Received "));
      Serial.println(LMIC.dataLen);
      Serial.println(F(" bytes of payload"));



      if (LMIC.dataLen == 1) {
        uint8_t result = LMIC.frame[LMIC.dataBeg + 0];
        if (result == 0)  {
          Serial.println("RESULT 0");
          digitalWrite(LED_RED, LOW);
          digitalWrite(LED_GREEN, LOW);
        }
        if (result == 1)  {
          Serial.println("RESULT 1");
```

```
        digitalWrite(LED_RED, HIGH);
        digitalWrite(LED_GREEN, LOW);
      }
      if (result == 2)  {
        Serial.println("RESULT 2");
        digitalWrite(LED_RED, LOW);
        digitalWrite(LED_GREEN, HIGH);
      }
      if (result == 3)  {
        Serial.println("RESULT 3");
        digitalWrite(LED_RED, HIGH);
        digitalWrite(LED_GREEN, HIGH);
      }
    }
    Serial.println();

  }

  os_setTimedCallback(&sendjob, os_getTime()+sec2osticks(TX_INTERVAL), do_send);
  break;
case EV_LOST_TSYNC:
  Serial.println(F("EV_LOST_TSYNC"));
  break;
case EV_RESET:
  Serial.println(F("EV_RESET"));
  break;
case EV_RXCOMPLETE:
  // data received in ping slot
  Serial.println(F("EV_RXCOMPLETE"));
  break;
```

```
        case EV_LINK_DEAD:
            Serial.println(F("EV_LINK_DEAD"));
            break;
        case EV_LINK_ALIVE:
            Serial.println(F("EV_LINK_ALIVE"));
            break;

        case EV_TXSTART:
            Serial.println(F("EV_TXSTART"));
            break;
        case EV_TXCANCELED:
            Serial.println(F("EV_TXCANCELED"));
            break;
        case EV_RXSTART:
            /* do not print anything -- it wrecks timing */
            break;
        case EV_JOIN_TXCOMPLETE:
            Serial.println(F("EV_JOIN_TXCOMPLETE: no JoinAccept"));
            break;
        default:
            Serial.print(F("Unknown event: "));
            Serial.println((unsigned) ev);
            break;
    }
}

void do_send(osjob_t* j){

    if (LMIC.opmode & OP_TXRXPEND) {
        Serial.println(F("OP_TXRXPEND, not sending"));
```

```
    } else {
        LMIC_setTxData2(1, mydata, sizeof(mydata)-1, 0);
        Serial.println(F("Packet queued"));
    }
}

void setup() {
    Serial.begin(115200);
    Serial.println(F("Starting"));

    pinMode(LED_RED, OUTPUT);
    pinMode(LED_GREEN, OUTPUT);

    #ifdef VCC_ENABLE
    // For Pinoccio Scout boards
    pinMode(VCC_ENABLE, OUTPUT);
    digitalWrite(VCC_ENABLE, HIGH);
    delay(1000);
    #endif

    os_init();
    LMIC_reset();

    #ifdef PROGMEM

    uint8_t appskey[sizeof(APPSKEY)];
    uint8_t nwkskey[sizeof(NWKSKEY)];
    memcpy_P(appskey, APPSKEY, sizeof(APPSKEY));
    memcpy_P(nwkskey, NWKSKEY, sizeof(NWKSKEY));
    LMIC_setSession (0x13, DEVADDR, nwkskey, appskey);
```

```
#else
LMIC_setSession (0x13, DEVADDR, NWKSKEY, APPSKEY);
#endif

#if defined(CFG_eu868)

LMIC_setupChannel(0, 868100000, DR_RANGE_MAP(DR_SF12, DR_SF7),  BAND_CENTI);      // g-band
LMIC_setupChannel(1, 868300000, DR_RANGE_MAP(DR_SF12, DR_SF7B), BAND_CENTI);      // g-band
LMIC_setupChannel(2, 868500000, DR_RANGE_MAP(DR_SF12, DR_SF7),  BAND_CENTI);      // g-band
LMIC_setupChannel(3, 867100000, DR_RANGE_MAP(DR_SF12, DR_SF7),  BAND_CENTI);      // g-band
LMIC_setupChannel(4, 867300000, DR_RANGE_MAP(DR_SF12, DR_SF7),  BAND_CENTI);      // g-band
LMIC_setupChannel(5, 867500000, DR_RANGE_MAP(DR_SF12, DR_SF7),  BAND_CENTI);      // g-band
LMIC_setupChannel(6, 867700000, DR_RANGE_MAP(DR_SF12, DR_SF7),  BAND_CENTI);      // g-band
LMIC_setupChannel(7, 867900000, DR_RANGE_MAP(DR_SF12, DR_SF7),  BAND_CENTI);      // g-band
LMIC_setupChannel(8, 868800000, DR_RANGE_MAP(DR_FSK,  DR_FSK),  BAND_MILLI);      // g2-band

#elif defined(CFG_us915) || defined(CFG_au915)

LMIC_selectSubBand(1);
#elif defined(CFG_as923)

#elif defined(CFG_kr920)

#elif defined(CFG_in866)

#else
# error Region not supported
#endif

LMIC_setLinkCheckMode(0);
```

```
    LMIC.dn2Dr = DR_SF9;
    LMIC_setDrTxpow(DR_SF7,14);
    do_send(&sendjob);
}
void loop() {
    os_runloop_once();
}
```

JavaScript Code to Extract Measured Parameter at the MTU

```
// Decode decodes an array of bytes into an object.
//  - fPort contains the LoRaWAN fPort number
//  - bytes is an array of bytes, e.g. [225, 230, 255, 0]
//  - variables contains the device variables e.g. {"calibration": "3.5"} (both the key / value are of type string)
// The function must return an object, e.g. {"temperature": 22.5}

function Decode(fPort, bytes) {
  var PVcurrent = (bytes[0]  <<8) | bytes[1];
  var PVvoltage = (bytes[2]  <<8) | bytes[3];
  var PVpower   = (bytes[4]  <<8) | bytes[5];
  var Battvoltage = (bytes[6] <<8) | bytes[7];

  return {PV3current: PVcurrent/100,
         PV3voltage: PVvoltage/100,
          PV3power: PVpower/100,
          Batt3voltage: Battvoltage/100

         };
```

Supporting Information for Chapter 6*

MATLAB/Simulink Model of the understudied DC Microgrid